INVESTIGATING THE GENETIC AND MECHANISTIC BASES OF PHOTOSYNTHESIS USING NATURAL VARIATION

By

Donghee Hoh

A DISSERTATION

Submitted to
Michigan State University
in partial fulfillment of the requirements
for the degree of

Cell and Molecular Biology—Doctor of Philosophy

2021

ABSTRACT

INVESTIGATING THE GENETIC AND MECHANISTIC BASES OF PHOTOSYNTHESIS USING NATURAL VARIATION

By

Donghee Hoh

To alleviate global food insecurity in the face of global climate change, many strategies have been proposed including the possibility of planting improved crops developed through molecular breeding by using natural genetic variations. Although photosynthesis directly contributes to yield, exploring natural variations in photosynthesis is a highly under-investigated approach for improving crop yield. The photosynthetic performance under adverse environmental conditions has large natural variations, so exploring these variations would be the way to improving the tolerance of crops as well as to uncovering mechanistic bases by elucidating natural strategies for adaptation of certain variants. By exploring natural variations in genetic diversity with more detailed photosynthetic phenotyping, a novel approach, which is available to test (support or reject) hypothetical models that can be used to identify the genetic and mechanistic bases, is proposed in this work, and tested, leading to major findings.

Firstly, I demonstrated this novel approach by exploring linkages between genetic polymorphisms and multiple, mechanistically-related phenotypes in a population of recombinant inbred lines (RILs) of cowpea (*Vigna unguiculata.* (L.) Walp.) generated from parent lines with significant differences in photosynthetic responses to chilling. The proposed co-association analysis showed mechanistic linkages among photosynthetic efficiency, photoprotection, photodamage and capture and feedback regulation by control of the thylakoid proton motive force, including with those for photosystem II (PSII)

quantum efficiency (Φ_{II}), nonphotochemical quenching (NPQ) in both the qE and qI forms, the redox state of Q_A (q_L), the redox states of photosystem I (PSI), the activity of the thylakoid ATP synthase (*g*H+,) and the light-driven thylakoid proton motive force (*pmf*). The follow-up biochemical/biophysical assays show that genetic variations impact low temperature tolerance/sensitivity by modulating: 1) redox states of Q_A; 2) the thylakoid *pmf*, through effects on cyclic electron flow, leading to differences in the rates of photodamage to PSII.

With the same approach, I observed variations in the relative compositions of the thylakoid-specific fatty acid and specifically, 16:1$^{\Delta 3\text{-trans}}$PG were strongly co-associated with the network of photosynthetic parameters, showing nearly linear dependence of PSII quantum efficiency (ΦII) across the RIL populations. These results suggest that the genetically determined variations in chilling responses of photosynthesis involve common, mechanistic or genetic linkages with 16:1$^{\Delta 3\text{-trans}}$PG composition. This correlation between lipid composition and photosynthetic responses at low temperature were qualitatively recapitulated in mutants or transgenic *Arabidopsis* lines with altered 16:1$^{\Delta 3\text{-trans}}$PG composition, suggesting that differential accumulation of 16:1$^{\Delta 3\text{-trans}}$PG leads to changes in photosynthetic responses at low temperature.

The outcome of this dissertation by exploring natural variations is enlightening to underlying mechanisms and readily applicable to molecular breeding to improve photosynthesis for higher, more climate-resilient productivity.

This dissertation is dedicated to my Umma and Appa.
Soli Deo Gloria.

TABLE OF CONTENTS

LIST OF TABLES

LIST OF FIGURES

KEY TO SYMBOLS AND ABBREVIATIONS

1Chl*	Excited chlorophyll state
1Chl*	Excited chlorophyll state
1O2	Singlet oxygen
1P	Singlet electron state of primary reaction center donor
3-PGA	3-phosphoglycerate
3Chl*	Triplet chlorophyll state
3P	Triplet electron state of primary reaction center donor
A	Net CO_2 assimilation
ADP	Adenosine diphosphate
CBB cycle	Calvin-Benson-Bassham cycle
*C*c	CO_2 concentration in chloroplast
CEF	Cyclic electron flow
CF_1F_o	Coupling factor 1 and O, indicating to the structure of ATP synthase
Chr	Chromosome
*C*i	Intercellular CO_2 concentration
CO_2	Carbon dioxide
Cys	Cysteines
DEPI	Dynamic environment photosynthesis imager
DGDG	Digalactosyldiacylglycerol
DIRK	Dark interval relaxation kinetics
DNA	Deoxyribonucleic acid

DTT	Dithiothreitol
ECS	Electrochromic shift
ER	Endoplasmic reticulum
ETR	Electron transport rate
Fd	Ferredoxin
FNR	Ferredoxin-NADP+ reductase
FTR	Ferredoxin thioredoxin reductase
GAP	Glyceraldehyde phosphate
*g*H+	Conductivity (inverse resistance) of the thylakoid membrane to proton flux
*g*m	Mesophyll conductance
*g*s	Stomatal conductance
H^+	Protons
H_2O_2	Hydrogen peroxide
HMP-PG	High-melting-point PG
LED	Light emitting diode
LEF	linear electron flux/flow
LHC	Light harvesting complex
LOD	Logarithm of the odds
LV	Latent variable
MDH	NADP- malate dehydrogenase
$Mg2^+$	Magnesium ion
MGDG	Monogalactosyldiacylglycerol

MPR	Mehler-peroxidase reaction
NADP+	Nicotinamide adenine dinucleotide phosphate, oxidized
NADPH	Nicotinamide adenine dinucleotide phosphate, reduced
NLM	Nyctinastic leaf movement
NPQ	Non-photochemical quenching
NPQ(T)	NPQ calculated using a theoretical (T) FV/FM value
NTRC	NADPH thioredoxin reductase C
O_2	Oxygen
OEC	Oxygen evolving complex
P	Primary reaction center donor
P680	Primary photosystem II chlorophyll electron donor
P700	Primary photosystem I chlorophyll electron donor
PAR	Photosynthetically active radiation
PC	Plastocyanin
PC	Phosphatidylcholine
PE	Phosphatidylethanolamine
PG	Phosphatidylglycerol
Pheo	Pheophytin
PI	Phosphatidylinositol
Pi	Inorganic phosphate
pmf	Proton motive force
ppm	Parts per million
PQ	Plastoquinone

PQH_2	Plastoquinol
Prx	Peroxiredoxin
PsbS	PSII subunit S protein
PSI	Photosystem I
PSII	Photosystem II
PTOX	Plastid terminal oxidase
PVE	Percent variance explained
ϕII	Quantum yield of the photosystem II
ϕNO	Quantum yield of unregulated energy dissipation
ϕNPQ	Quantum yield of non-photochemical quenching
QA	Photosystem II primary electron acceptor quinone
QB	Photosystem II secondary electron acceptor quinone
*q*E	Energy dependent quenching. The rapidly reversible component of NPQ (pH and energy dependent quenching component of NPQ)
*q*I	Photo-inhibitory quenching. The slowly relaxing component of NPQ (Irreversible long-lived component of NPQ)
*q*L	Fraction of photosystem II centers able to perform charge separation QTL quantitative trait locus
QTL	Quantitative trait locus
RC	Reaction center
RIL	Recombinant inbred line
ROS	Reactive oxygen species
RuBisCo	Ribulose-1,5-bisphosphate carboxylase-oxygenase
RuBP	Ribulose 1,5-bisphosphate
S1/ S2/ S3/ S0/ Sn	S-state of the oxygen-evolving complex

SNP	Single-nucleotide polymorphism
SPAD	Special products analysis division (of Minolta)
SQDG	Sulfoquinovosyldiacylglycerol
Trx	Thioredoxin
V(DE)	Violaxanthin (de-epoxidase)
*V*c.	Velocity of rubisco for carboxylation
VDE	Violaxanthin de-epoxidase
*v*H+	Rate of proton flux through the thylakoid membrane
*v*o	Velocity of rubisco for oxygenation
Yz	Photosystem II D1 protein tyrosine Z
Z	Zeaxanthin
ΔGATP	Free-energy of hydrolysis of ATP
ΔpH	Difference in pH across the thylakoid membrane
ΔμH+	Electrochemical potential of protons
Δψ	Difference in electric field across the thylakoid membrane

CHAPTER 1

USING NATURAL VARIATIONS TO EXPLORE REGULATORY MECHANISMS OF PHOTOSYNTHESIS

Donghee Hoh

1.1 Introduction

With the need to feed a growing world population in the face of global climate change, improving crop productivity is an imperative goal. Since photosynthesis directly contributes to crop yield (Long et al., 2006; Raines, 2011; Zelitch, 1982), understanding how it performs and is regulated under non-ideal conditions may be key to improving plant productivity. One strategy is to take advantage of natural variations in photosynthesis, combining extant or hidden traits, to improve in response to changing environments. However, such natural variations in photosynthesis have been relatively uninvestigated, in part because of the lack of high-throughput phenotyping tools to capture detailed, dynamic responses. By taking advantage of recent advances in genomics and high-throughput photosynthetic phenotyping tools, this dissertation aims to understand how plants survived in response to environmental changes and reveal additional mechanisms of adaptation. These findings can immediately help to guide the breeding and engineering of photosynthesis for more robust and climate-resilient productivity. The approach also gives important clues about the underlying, basic mechanisms of these variations of photosynthetic control.

Among abiotic stress, low temperature is a major constraint on photosynthesis, productivity, and geographical distribution of important cultivated crops (Ort, 2002). The global climate change, which induces not only warming but variations in temperatures, leads to unpredictable periods of increased and decreased growth temperatures, which cause transient chilling (sub-optimal, but non-freezing temperatures) (Gu et al., 2008), resulting in decreased photosynthesis and crop yields.

Grain legumes are one of the most important sources of protein to combat malnutrition and famine in developing countries on account of their tolerance to drought to low soil fertility (Muchero et al., 2009) and symbiotic N fixation. However, for example, cowpea (Vigna unguiculata L. Walp), warm-season annuals, are sensitive to chilling stress to the temperature range of 20 to 1°C (Ismail et al., 1997). Below certain critical temperatures within this range, the plants show a decreased rate of germination, photosynthesis, growth, and crop yield.

To better understand how photosynthesis responds, the process of photosynthesis will be described and a literature review on specific components of photosynthesis and their interactions with low temperature is followed. The last section will introduce an approach for exploring natural variations in plant photosynthesis.

1.2 Basic model of oxygenic photosynthesis

Photosynthesis is the process of using light energy to convert inorganic precursors (CO_2 and H_2O) to organic compounds (CH_2O). The process involves the capture of photons of photosynthetically active radiation (PAR), which drive a series of electron transfer steps that are coupled to biological reduction-oxidation (redox) chemistry and proton transfer reactions, leading to the storage of energy in ATP and NADPH, which are, in turn used to drive multi-step enzymatic pathways of carbon assimilation, photorespiration, and associated biosynthetic and cellular processes.

1.2.1 Light reactions.

The light reactions of photosynthesis take place in the chloroplast in eukaryotes, where photochemical reaction is localized in the thylakoid membrane, which embeds multiple photosynthetic complexes, including photosystems II (PSII) and I (PSI), cytochrome b_6f and the chloroplast ATP synthase. The light reactions of photosynthesis store energy from absorbed photons as chemical energy (bonds) in the forms of ATP and NADPH (Figure1.1) in a complex, multi-stage process.

The initial step of photochemical reaction is the light absorption by protein-embedded pigment molecules, mostly chlorophyll and carotenoids, forming the light-harvesting complexes (LHCs). When the chlorophyll pigments in the LHCs absorb light in the blue or red spectrum regions, they form excited singlet states, called “excitons”. Absorption of longer wavelength (red) photons directly produces the lowest energy excited state, S1 of the chlorophylls. Absorption of short wavelength (violet to blue) photons produces the S2 excited states, which rapidly decay by internal conversion to the S1 state. The S1 states can relax through several avenues: energy transfer to other LHCs or to the reaction centers, fluorescence, non-radiative decay (non-photochemical quenching) and intersystem crossing (formation of triplet states).

When excitons reach a PSI or PSII reaction center, they can excite special chlorophylls to excited states that can form energy-storing charge separated states. In PSII, the excited state, P680*, can reduce a series of electron carriers, resulting in transfer of electron to a pheophytin molecule (Pheo) to form P_{680}+Pheo-. On the electron donor side of PSII, $P680^+$ is re-reduced by the electrons ultimately obtained from the oxygen-evolving manganese cluster. On the electron acceptor side of PSII,

electron on Pheno is rapidly transferred to the primary electron quinone acceptor, Q_A, forming $P_{680}+Q_A-$. By sequent transport of electrons via PSII-associated pheophytin and the bound Q_B plastoquinone (PQ) molecule to reduce a second, exchangeable plastoquinol (PQH_2) at the Q_B site. Generation of Q_B-associated PQH_2 requires the transfer of two electrons, and concerted uptake of two protons from the stromal side of the thylakoid membrane. Plastoquinol diffuses from PSII to the cytochrome *b_6f* complex (cyt *b_6f*) with electron transfer coupled to proton translocation into the lumen through the cyt *b_6f*-associated Q-cycle mechanism, which operates an energy-conserving bifurcating electron transfer reaction at the site of PQ oxidation, generating reduced plastocyanin (the electron donor to photooxidised P700 in photosystem I (PSI)) and reduced PQ at the (PQ) reduction site of the *b_6f* complex. Photooxidation of P700 in PSI generates a reductant of sufficiently low potential to reduce stromal ferredoxin (Fd), which serves as an electron donor to $NADP^+$ (generating NADPH) catalyzed by ferredoxin $NADP^+$ reductase (FNR). This process is referred to as linear electron flow (LEF) (Baker et al., 2007). The transfer of two electrons from water to NADPH during LEF results in the transfer of six protons from the stromal side of the thylakoid membrane to the lumen (i.e 6H+/2e), establishing a proton gradient, with an associated proton motive force (*pmf*). The thylakoid *pmf* is composed of two components, a proton gradient between the thylakoid lumen and the chloroplast stroma (ΔpH) and an electric field generated across the thylakoid membrane (ΔΨ) (Kramer et al., 2004) and those are thermodynamically equivalent to drive ATP synthesis by rotation catalysis of ATP synthase. *Pmf* drives (energetically uphill) ATP synthesis by transporting protons through ATP synthase (Avenson et al., 2005) and can be equated as:

$$pmf = \Delta\psi(i{-}o) + \frac{2.3RT}{F}\Delta pH(o{-}i)$$

where R is the universal gas constant, F is Faraday's constant, and Δψ (i-o) and ΔpH (o-i) are the differences in electric field and pH calculated as the difference between the lumen (inside – i) and stroma (outside – o) respectively (Kramer et al., 2004). The ΔpH component of *pmf* has important roles in regulating electron transfer and light capture. Acidification of the thylakoid lumen, which accompanies the formation of ΔpH induces the so-called energy-dependent exciton quenching, qE, a rapidly-reversible form of nonphotochemical quenching (NPQ), the non-regulated dissipation of absorbed light energy. The qE mechanism involves two lumen pH-dependent processes, the xanthophyll cycle (i.e. the reversible de-epoxidation of violaxanthin to zeaxanthin) and protonation of PsbS (Brooks et al., 2014; Takizawa et al., 2008). This mechanism leads to conformational change or reorganization of PSII, so that antenna complexes dissipate excess energy to prevent overexcitation of chlorophyll and over-reduction of ETC. ΔpH can also limit electron flux to PSI through pH-dependent slowing quinol oxidation at cytb_6f, "photosynthetic control (PCON)" (Chow & Hope 2004; Takizawa et al. 2008). Another important characteristic of *pmf* is the associated electric field (ΔΨ) which influences the probability of PSII charge recombination and associated singlet oxygen production, a potential source of photodamage (Davis et al., 2016).

There have been reports that cyclic electron flow (CEF) and Mehler peroxidase reaction (MPR), also called the water-water cycle, regulate photosynthesis under stress conditions (Asada, 1999; Johnson, 2011). In cyclic electron flow (CEF), *pmf* (and ATP) is generated, but with no net reduction of NADPH (Joliot and Johnson, 2011) as stromal electrons are transferred back into the PQ pool through ferredoxin (Fd) and plastoquinol

reductase (PQR) enzymes such as proton gradient regulation (PGR) 5/1 (although the involvement of this complex in CEF enzymology is disputed) or the proton motive thylakoid NADPH dehydrogenase-like enzyme (NDH). Alternative electron sink pathways can also contribute to energy balancing. For example, the Mehler peroxidase reaction (MPR), involves the transfer of electrons from PSI to reduce O_2, forming superoxide O_2^-, which dismutates to H_2O_2 and dioxygen through the activity of superoxide dismutase (SOD). H_2O_2 is further reduced to water via ascorbate peroxidase (APX) by oxidizing ascorbic acid (AsA) to monodehydroascorbate (MDA). CEF and MPR would change NADPH/ATP ratio (decreased reducing equivalent and excessive ATP), leading to a metabolic imbalance if those reactions are not properly regulated.

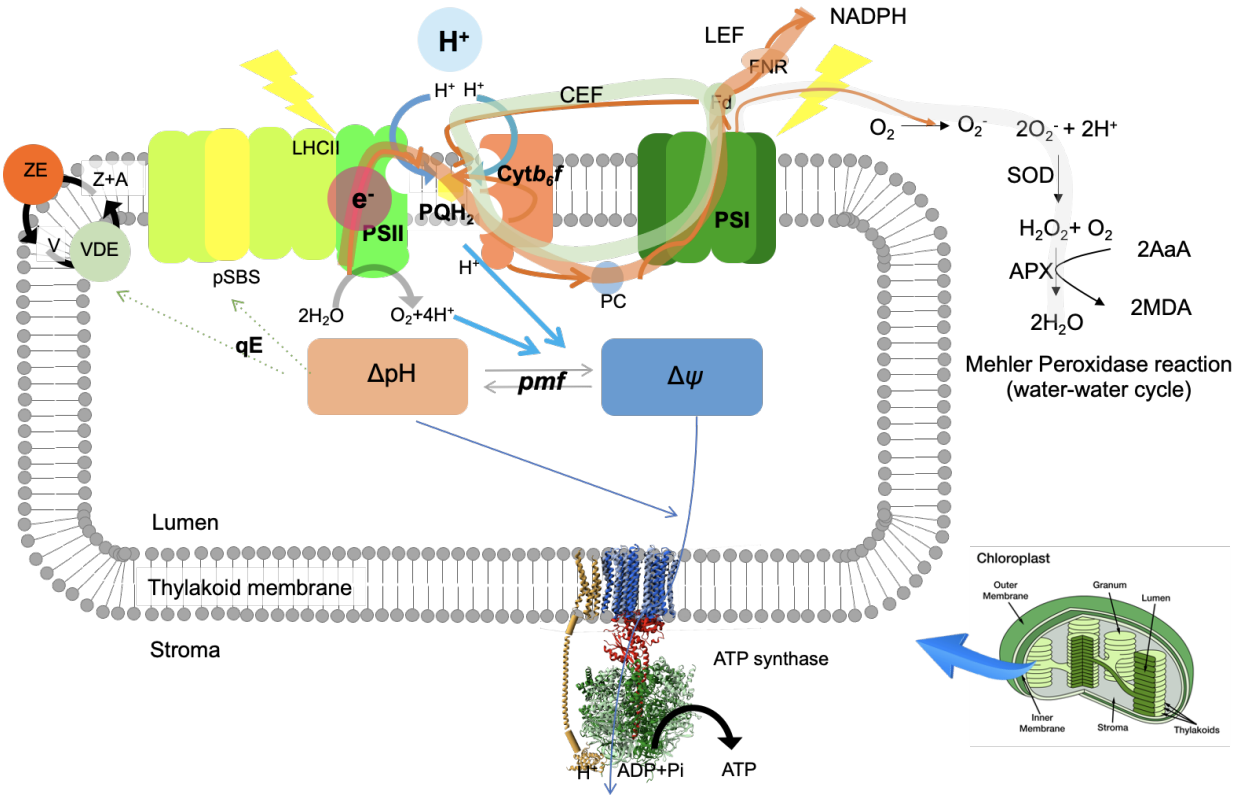

Figure 1.1 A basic model of photosynthetic electron transport and proton transfers.

This scheme represents the results of light absorption, photosynthetic electron transport (orange arrows), and proton transfers (blue arrows). Light absorbed by LHCII transferred to the photosystem reaction center leads to charge separation in photosystem II (PSII). Electrons reduce plastoquinone to plastoquinol at Q_B site. Plastoquinol transfers electrons to cytb_6f and those electrons and protons from stroma to lumen establish proton motive force (*pmf*). The electrons are transferred to photosystem I (PSI) by plastocyanin to reduce $NADP^+$. In PSII, $P680^+$ is re-reduced from electrons by water splitting at the oxygen-evolving complex (OEC). This process is linear electron flow (LEF, orange thick line) (Baker et al., 2007). In cyclic electron flow (CEF, green thick line), it also builds *pmf*, but no net reduction of NADPH (Joliot and Joliot, 2006). *Pmf* is composed of two components, proton gradient between the thylakoid lumen and the chloroplast stroma (ΔpH) and electric field generated across the thylakoid membrane (ΔΨ) (Kramer et al., 2004).*pmf* drives ATP synthesis by transporting protons through ATP synthase (Avenson et al., 2005). Also, *pmf* plays an important role for regulating electron transfer and light processing by inducing energy-dependent quenching qE. This mechanism is based on lumen acidification, inducing xanthophyll cycle and protonation of PsbS (Brooks et al., 2014; Takizawa et al., 2008).Mehler peroxidase reaction (MPR) is shown in a gray thick line. It is also called a water-water cycle which means electrons from water to make water. O_2 is reduced by electrons from PSI, forming superoxide O_2^-, which dismutates to H_2O_2 through superoxide dismutase (SOD). H_2O_2 is further reduced via ascorbate peroxidase (APX) by oxidizing ascorbic acid (AsA) to monodehydroascorbate (MDA).

Figure 1.1 (cont'd):
Abbreviations: PSII, photosystem II; PSI, Photosystem I; LHCII, Light harvesting complexes; PQH_2, plastoquinol; PC, plastocyanin; Fd, ferredoxin; FNR, Ferredoxin—$NADP^+$ reductase; V, violaxanthin; VDE, violaxanthin de-epoxidase; Z, zeaxanthin; ZE, zeaxanthin epoxidase; AsA, ascorbic acid; APX, ascorbate peroxidase; SOD, superoxide dismutase; MDA, monodehydroascorbate.
Note: lipid membrane was simplified. The source ATP synthase: James Hedberg is licensed under a Creative Commons Attribution-NonCommercial-ShareAlike 3.0 Unported License

1.2.2 Carbon assimilation.

Carbon assimilation, referred to as Calvin-Benson-Bassham (CBB) cycle, is the enzymatic process in the stroma for the assimilation of CO_2 in the atmosphere by utilizing energy sources, ATP and NADPH, from the light reaction. The CBB cycle process consists of 13 biochemical reactions (Figure 1.2) and can be categorized into three phases: carboxylation, reduction and regeneration. Carboxylation of Ribulose 1,5-bisphosphate (RuBP) is the first step of the CBB cycle. Ribulose-1,5-bisphosphate carboxylase-oxygenase (RuBisCo) committed this step from Ribulose 1,5-bisphosphate, CO_2 and H_2O to from 3-phosphoglycerate (3-PGA). The next phase, reduction of 3-PGA by employing products of light reactions, producing Glyceraldehyde phosphate (GAP). The last phase is the regeneration of RuBP for operating the CBB cycle continuously. Some intermediates in CBB cycles are precursors for the starch and sucrose in the chloroplast and cytosol respectively. When assimilation of carbon is limited by the ability to regenerate phosphate through the production of those end products of photosynthesis, triose phosphate utilization (TPU) was observed. The major limiting steps in CBB cycle are carboxylation (producing 3-PGA by RuBisCo), and RuBP regeneration and TPU limitation, and those are identified by A/Ci response curves through a model introduced by Sharkey (Sharkey et al., 2007) (Figure 1.3). TPU

limitation is known to be associated with *pmf* (Yang et al., 2016). The increases in *pmf* should lead to stronger lumen acidification, increased qE and slowing of electron transport (Kiirats et al., 2009; Neuhaus et al., 1989; Sharkey, 1985; Takizawa et al., 2008).

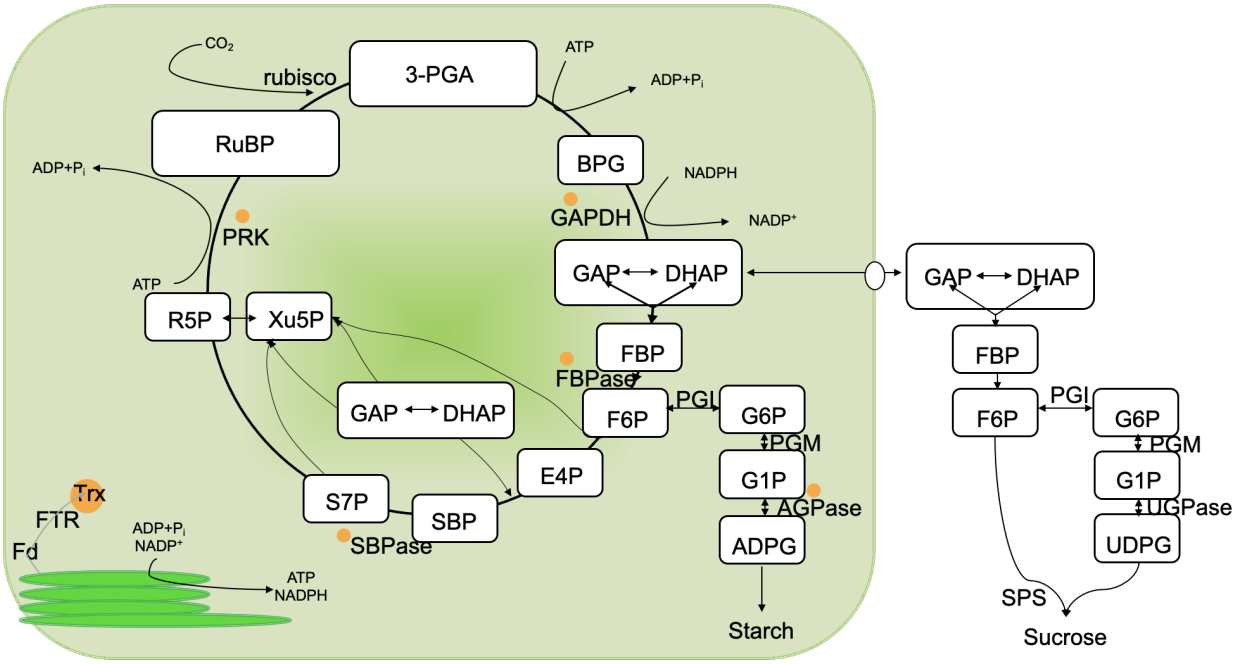

Figure 1.2 Calvin-Benson- Bassham (CBB) cycle, intermediates, and some enzymes are noted.
Thioredoxin and thioredoxin-regulated enzymes are shown in orange dots.

Abbreviations: AGPase, ADP glucose pyrophosphorylase; BPG, 1,3-bisphosphoglycerate; DHAP, Dihydroxyacetone phosphate; E4P, Erythritol 4-phosphate; F6P, Fructose 6-phosphate; FBP, Fructose 1,6-bisphosphate; FBPase, Fructose-1,6- bisphosphatase; Fd, Ferredoxin; FTR, ferredoxin-thioredoxin Reductase; G1,6BP, Glucose 1,6-bisphosphate; G6P, Glucose 6-phosphate; GAP, Glyceraldehyde 3-phosphate; GAPDH, glyceraldehyde- 3-phosphate dehydrogenase; 3-PGA, 3-phosphoglycerate; PGI, Phosphoglucose isomerase; PGM, Phosphoglucomutase; PRK, Phosphoribulokinase; R5P, Ribose 5-phosphate; Ru5P, Ribulose 5-phosphate; RuBP, Ribulose 1,5-bisphosphate; rubisco, bis-phosphate carboxylase/oxygenase; S7P, Sedoheptulose 7-phosphate; SBP, Sedoheptulose 1,7-bisphosphate; SBPase, Sedoheptulose-1,7-bisphosphatase; SPS, Sucrose-phosphate synthesis; Trx, thioredoxin; UGP, UTP-glucose-1-phosphate uridylyltransferase; Xu5P, Xylulose 5-phosphate

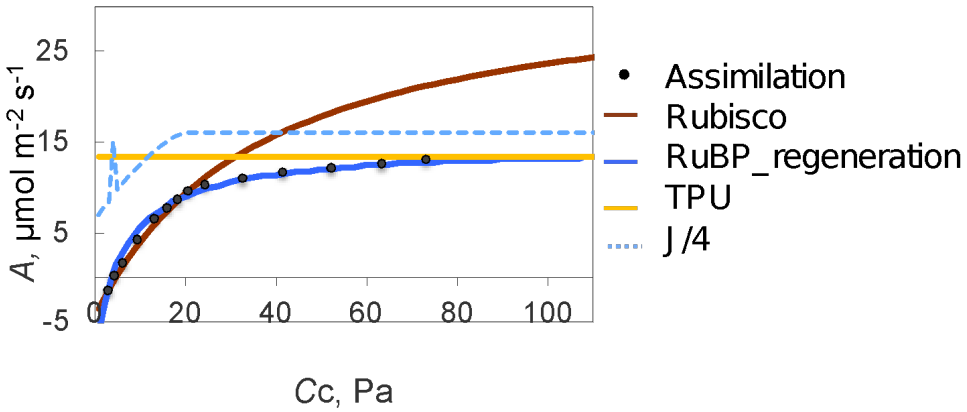

Figure 1.3 Three different types of limitation steps can be predicted by fitting CO_2 response curve.
We can distinguish limiting factors between CBC limitations (Rubisco or RuBP regeneration) or triose phosphate utilization. Presumed limiting factors by measuring assimilation rate at different external concentrations of CO_2. The sample data is shown in black dots, showing a hyperbolic curve in response to CO_2 concentrations. By using a mathematical model developed by (Sharkey et al., 2007), three possible limitations are predicted: rubisco limitation, RuBP regeneration and TPU limitation, shown as red, blue and yellow color, respectively.

1.3 Chloroplast redox regulation of photosynthesis

As described earlier, the photosynthetic reaction is a biological oxidation-reduction (redox) process, producing reduced metabolites from oxidized inorganic precursors. The intermediates, ATP and NADPH from LEF are utilized for the regeneration of RuBP in the CBB cycle, showing both reactions are dependent on light availability. Furthermore, in this process, potentially harmful reactive intermediates such as reactive oxygen species (ROS, i.e. singlet oxygen and superoxide) could be generated, requiring the fine-tuning of regulation systems to avoid deleterious side reactions (Apel and Hirt, 2004). We focus here on redox regulatory mechanisms, thioredoxin mediated disulfide-thiol exchange, which has been long considered as important regulation processes for photosynthetic reactions in response to light availability (Kaiser et al., 2015; Pearcy et al., 2004). Several enzymes are known as

regulated by light-dependent reductive activation, for example, the gamma subunit of chloroplast ATP synthase and several key enzymes in the CBB cycle such as FBPase, SBPase, Phosphoribulokinase (PRK), GAPDH, rubisco activase (Michelet et al., 2013), AGPase (Geigenberger, 2011) (Figure 1.2) The two current systems for the activation of redox regulation systems and an inactivation system recently discovered will be introduced (Figure 1.6).

1.3.1 Two thioredoxin systems, FTR and NTRC.

The first system is ferredoxin-thioredoxin reductase (FTR) regulatory system in plastid which was discovered in the 1970-80s (Buchanan, 1980) and is now recognized as a central regulatory system for photosynthesis, transferring information from thylakoid membrane to stroma for regulation of enzymes. Briefly, this reaction is followed by sequent electron transfer from PSI to ferredoxin (fdx), FTR and thioredoxin (trx) and target enzymes. Trx contains cysteine residues that are redox-active and reversibly transfer the reducing potentials from light reactions to thiol-regulated enzymes (Figure 1.4A). Initially, two forms of trx, f and m, were proposed (Buchanan, 1980) but later, more than 20 multiple isoforms of trx were found by sequencing of the *Arabidopsis thaliana* genome and categorized into several classes, trx f, m, x, y and z in the chloroplast (Collin et al., 2003; Geigenberger et al., 2017; Yoshida et al., 2014). They have conserved sequence motifs (WCGPC) to interact with target enzymes but react with different sets of target enzymes (Collin et al., 2003; Geigenberger et al., 2017; Schürmann and Jacquot, 2000, 2000; Yoshida et al., 2014).

The second redox regulation system (Schürmann and Jacquot, 2000) is NADPH-dependent thioredoxin reductase C (NTRC), which was discovered relatively recent as

a chloroplast thiol-regulatory system and found exclusively in oxygenic organisms (Pulido et al., 2010; Serrato et al., 2004) (Figure 1.6B). In contrast to the FTR system, NTRC uses NADPH as a reducing power to deliver electrons to target enzymes via trx. NADPH can be produced from either LEF or by the oxidative pentose phosphate pathway (OPPP) (Neuhaus and Emes, 2000). Interestingly, it was found that NTRC mainly functions under limited light conditions or in the dark, using NADPH generated from OPPP. Evidence has been presented for the involvement of NTRC activation for ATP synthase, ADP-glucose pyrophosphorylase, chlorophyll biosynthesis and 2-cys peroxiredoxin system (Carrillo et al., 2016; Cejudo et al., 2012; Lepistö et al., 2013; Michalska et al., 2009).

1.3.2 Oxidation system of 2-cys peroxiredoxin (2CP).

While the light-dependent reduction of regulatory thiols is well established, the mechanism of thiol oxidation is also important for determining the steady-state redox poise of the regulatory thiols (Ojeda et al., 2018; Vaseghi et al., 2018; Yoshida et al., 2018). The oxidative thiol modulation cascade was proposed in three different groups and commonly suggested that 2-Cys peroxiredoxins (2CP) are involved as an electron sink to oxidize reductively activated proteins in the dark (Figure 1.6C). The likely mediator for thiol oxidation of target proteins is Trx-like2 (TrxL2), which has a less negative redox potential than the thiols on typical regulatory proteins. TrxL2 transfers reducing power from redox-regulated proteins to 2CP and further, reduced peroxiredoxin reduces H2O2 to H2O. The protein-oxidizing activity of TrxL2 is strongly dependent on 2CP and H2O2(Ojeda et al., 2018; Vaseghi et al., 2018; Yoshida et al., 2018). Other forms of Prx, Prx IIE or Prx Q, showed no similar role of 2CP in the dark

transition, indicating that 2CP is specifically involved in oxidation cascade (Ojeda et al., 2018; Vaseghi et al., 2018; Yoshida et al., 2018)). Also, it was found that NTRC modulated 2CP to contribute to the control of chloroplast redox homeostasis (Pérez-Ruiz et al., 2017). Consistent with this role, overexpressing NTRC delayed dark-induced oxidation of FBPase and GAPDH, indicating that NTRC is one of the factors involved in this oxidation process (Ojeda et al., 2018; Vaseghi et al., 2018; Yoshida et al., 2018). Several thiol-regulated enzymes were revealed from those studies being oxidized by 2CP for instance, CF1-γ (Ojeda et al., 2018; Vaseghi et al., 2018; Yoshida et al., 2018), FBPase (Ojeda et al., 2018; Vaseghi et al., 2018; Yoshida et al., 2018), SBPase (Ojeda et al., 2018; Vaseghi et al., 2018; Yoshida et al., 2018), rca (Ojeda et al., 2018; Vaseghi et al., 2018; Yoshida et al., 2018) and NADP-MDH (Ojeda et al., 2018; Vaseghi et al., 2018; Yoshida et al., 2018).

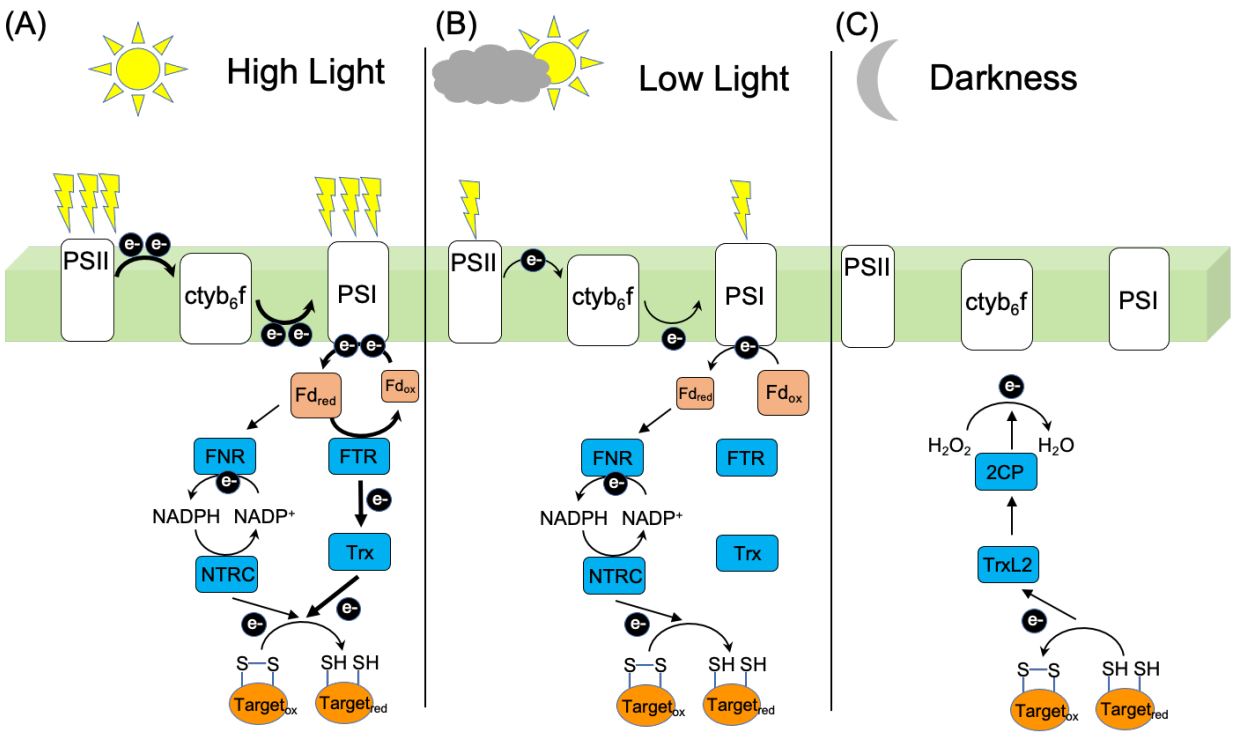

Figure 1.4 Scheme of chloroplast redox regulation.
Two activation systems (A and B) under different light availability and deactivation systems (C) under dark are shown. (A) Under high light intensity, ferredoxin-thioredoxin reductase (FTR) regulatory system is dominantly reduced thiol-regulated target enzymes. (B) Under limited light availability, the NADPH-dependent thioredoxin reductase C (NTRC) system mainly functions. (C) Under dark, 2CP mediates oxidizing the target enzymes. (Figure courtesy: John Froehlich, modified from Kaiser et al., 2019)

1.4 Lipid membrane and photosynthesis

The thylakoid membrane, which is highly conserved in oxygenic photosynthetic organisms, is composed of a set of lipids with fatty acids that are distinct from those of other cellular components (Hurlock et al., 2014). Also, as described earlier, the thylakoid membrane is the place for electron transport with embedded photosynthetic apparatus such as PSII, PSI, cyt*b*$_6$*f* and ATP synthase and diffused mobile electron transport carrier, such as PQH_2. Thereby, it is thought that membrane lipids may play important roles in maintaining photosynthesis (Boudière et al., 2014) as structural and functional components. Thylakoid membranes consist of uncharged galactolipids,

monogalactosyldiacylglycerol (MGDG) and digalactosyldiacylglycerol (DGDG), with anionic lipid, phosphatidylglycerol (PG) and sulfoquinovosyldiacylglycerol (SQDG).

Each lipid class has a specific role and structure depending on the nature of the head group and acyl chains. The shape of MGDG with a small galactose polar head is similar to the truncated cone shape forming an inverted hexagonal II phase. Different from MGDG, DGDG with two galactose moieties in the polar head group, accordingly, have a similar cross-sectional area with the hydrophobic region, forming bilayer lamellar phase without curvature feature. These neutral galactolipids constitute a bulk portion of the total thylakoid membrane about 60-80 mol%, thus the ratio of those lipids important for structural, functional of the membrane is thought to be important (Demé et al., 2014; Murphy, 1982), especially, it was reported that membrane remodeled in responses to stress conditions (Moellering and Benning, 2011; Moellering et al., 2010; Roston et al., 2014), and this will be more detailed in section 1.5. Different from neutral galactolipid, PG and SQDG with a negative charge in the head group at neutral pH, classified as acidic lipids and PG is the only phospholipid in the thylakoid membrane (Dorne et al., 1990; Wada and Murata, 2004) which has been extensively getting attention for roles in photosynthetic reactions.

1.4.1 Biosynthesis of membrane lipids.

Before emphasizing the functional and structural involvement of each lipid for photosynthetic reactions, general descriptions of biosynthesis will be overviewed (c.f. Figure 1.5 and 1.6). Fatty acid synthesis is localized in plastids (Bates et al., 2013) and further modifications take place in the plastid, ER and acetyl-CoA /PC-pool. The first committed enzyme for fatty acid biosynthesis is acetyl- CoA carboxylase (ACCase).

Malonyl-CoA is synthesized by ACCase from Acetyl-CoA and bicarbonate (Figure 1.5) and this step has been considered as key regulatory steps for the biosynthesis of fatty acids (Nikolau, Ohlrogge, & Wurtele, 2003). After that, acyl carrier protein (ACP) helps to convert from Malonyl-CoA to Malonyl-ACP. Fatty acids are from acetyl-coA as a starting unit and using malonyl-ACP as elongator over multiple cycles. Synthesized fatty acids can be modified unsaturated by enzymes in the plastid and transferred to either ER or acetyl-CoA/ PC-pool, and further modified in the ER. In the plastid, MGDG, MGDG, SQDG and PG are synthesized, whereas PG, PI, PE and PC are synthesized in the ER. The synthesized PC in ER is transferred to the PC pool and transferred to plastid. More details involved in glycerolipid synthesis are in Figure 1.6.

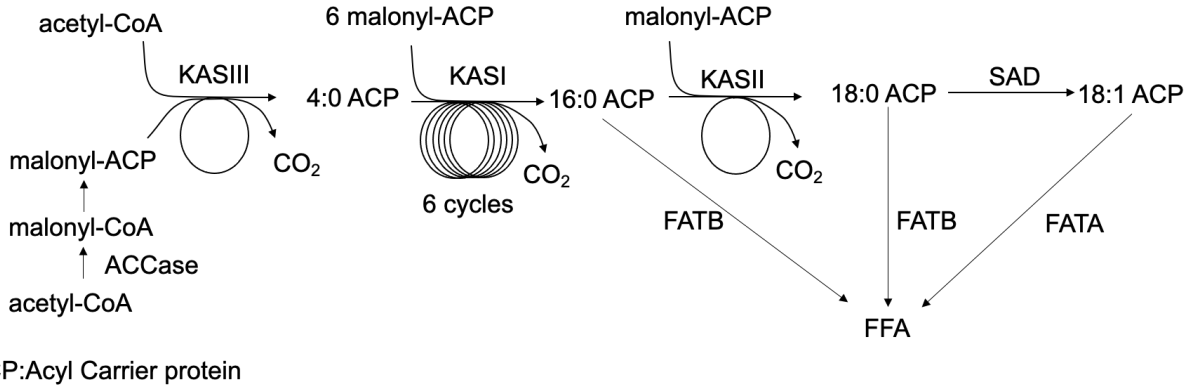

Figure 1.5 Overview of plastid fatty acids synthesis.
ACCase is the first committed step of enzyme for fatty acid synthesis, producing malonyl-CoA from acetyl-CoA and CO_2. Overall, the high oxidation state of substrates (carbohydrate) converted to highly reduced products by three different condensing enzymes (KASI, KASII and KASIII) with releasing CO_2 at each cycle**.**

Abbreviations: ACCase: Acetyl-CoA carboxylase, ACP: Acyl carrier protein, KAS: Ketoacyl-ACP reductase, FATA: acyl-ACP thioesterase A, FATB: acyl-ACP thioesterase, SAD: 18:0-ACP desaturase, FFA: free fatty acid. Modified from (Bates et al., 2013; Shamsi et al., 2012)

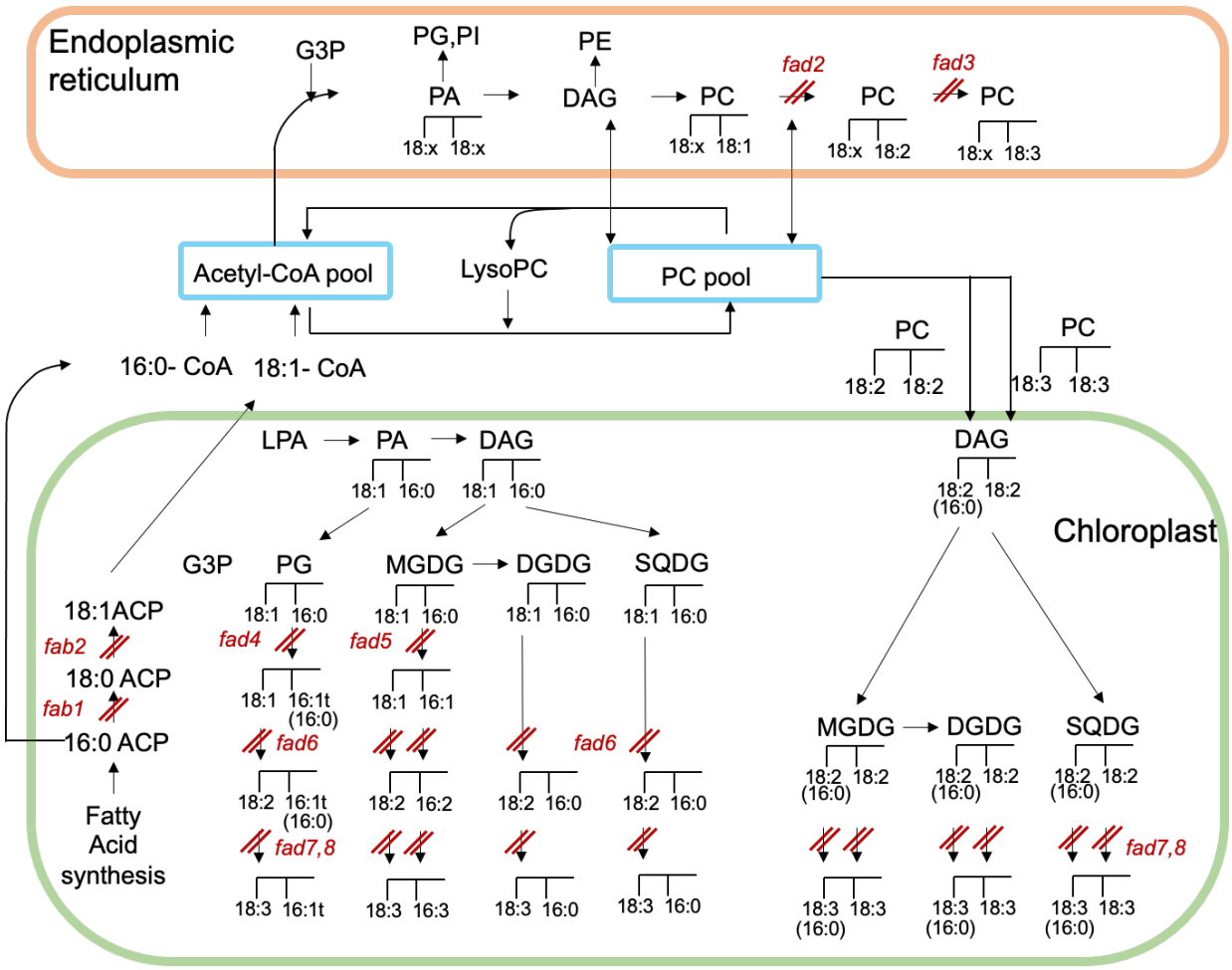

Figure 1.6 Overview of assembly of membrane glycerolipids synthesis.
The synthesis of glycerolipids in the chloroplast is called the prokaryotic pathway, and the endoplasmic reticulum (ER) is called the eukaryotic pathway. In leaves, both pathways are active simultaneously, making mainly galactolipids, sulfolipid and PG in the plastid pathway and PC, PE, PG, PI in the ER pathway. Each red line indicates steps blocked in mutants, which are shown in red italic letters. *fab*1 and 2 are involving fatty acid synthesis while fad2, 3, 4, 5, 6, 7 and 8 are desaturases, which add double bonds to fatty acids.

Abbreviations: fab: fatty acid biosynthesis, fad: fatty acid desaturase, DAG: diacylglycerol, LPA: lysophosphatidic acid, PA: phosphatidic acid, ACP: Acyl carrier protein, MGDG: monogalactosyl diacylglycerol, DGDG: digalactosyl diacylglycerol, PG: phosphatidylglycerol, SQDG: sulfoquinovosyl diacylglycerol, PC: phosphatidylcholine, PE: phosphatidylethanolamine, PI: phosphatidylinositol.
Modified from (Buchanan et al., 2015)

1.4.2 Functional and structural roles of membrane lipids in photosynthesis.

Each lipid class has specific effect on photosynthesis discovered by a set of mutants in photosynthesis that are summarized in Table 1.1-4. Hereafter, I am aiming to more focus on four lipid classes; MGDG, DGDG, PG and SQDG which are constitutes for thylakoid membrane, where photosynthesis takes place.

1.4.2.1 MGDG

MGDG is the main constituent of the thylakoid membrane and substrate of DGDG. MGDG synthesized from UDP-galactose to diacylglycerol and MGDG synthase gene, *mgd1*, 2 and 3, are found in *Arabidopsis thaliana*(Awai et al., 2001; Miège et al., 1999). MGD1 is the major isoform contributing to the synthesis of the bulk galactolipid in the chloroplast (Jarvis et al., 2000; Kobayashi et al., 2007) and MGD 2 and 3 has a marginal role, conditionally contribute DGDG synthesis when inorganic phosphate (Pi) deficiency condition (Kobayashi et al., 2009).

Table 1.1 Lipid mutants altered MGDG compositions.

Mutant	Enzyme blocked	Lipid phenotype	Physiological phenotype	References
mgd1-1	Knockdown MGD1 T-DNA insertion	75% of reduction of MGD1 expression, 42% less MGDG content compared to WT	* Maximal PSII efficiency (Fv/FM) similar to WT and no effects on intrinsic PSII activity (Aronsson et al. 2008) * But at high light intenssity, moderate defects wiith the leakage membrane was observed: increased conductivity, lower pmf, less acidification, less Z and more V due to decreased PH dependent Z cycle (from V to Z), less photoprotection, susceptible to photoinhibition (Aronsson et al. 2008).	Jarvis et al. 2000; Aronsson et al. 2008
mgd1-2	Knockout MGD1	98% loss of MGDG and dramatic decrease in DGDG content (negligible amounts of both MGDG and DGDG,)	* Severe disorder in PS complex and no ET, showing lethal phenotype under sufficient nutritional condition * Under P deficiency condition, mgd1-2 showed large accumulation of DGDG alternative (due to MGD2/MGD3 pathway was activated) , but still ET dysfunctional since LHC-PS complex, indicating the MGDG is major role for these complexes.	Kobayashi et al. 2007; Kobayashi et al., 2013
amiR-MGD1	knockdown MGD1 (dexamethasone (DEX)-inducible promoter)	showed 75% of MGD1 expression, variation of 25%- 85% reduction of MGDG	* Decreased intrinsic PSII activity. Decreased electron-accepting capacity of QA. * In addition, PSII efficiency decreased due to impaired electron transfer downstream of PSII under light. * Increased phiNO, non-regulated form of heat and fluorescence, decreased photoprotective capcity	Fujii et al. 2014
M18	toabcco knockdown MGD1	53% decreased MGDG	* Decreased Cyt b6/f complex levels and blocked electron transport * reduced photoprotective capacity leads cumulative photodamage under long-term exposure to high light	Wu et al. 2013

1.4.2.2 DGDG

DGDG synthesis is catalyzed by DGDG synthase (DGD), two homologous DGD1 and DGD2, which transfer galactose from UDP-galactose to MGDG (Kelly and Dörmann, 2002; Kelly et al., 2003).

Table 1.2 Lipid mutants altered DGDG compositions.

Mutant	Enzyme blocked	Lipid phenotype	Physiological phenotype	References
dgd1	point mutation in DGD1	90% decreased DGDG content	* Structural changes (pale green leaves, curved thylakoid membrane, dwarf phenotype). * Decreased quantum yield of photosynthesis. **PSII** * The level of LHCII to PSIII core proteins and carotenoids, which are involved in the xanthophyll cycle, is increased. * OEC activity was affected while the acceptor side of PSII was not that affected. * The laser flash fluorometer showed a deficiency of DGDG increased the probability of the dissipate recombination reaction between $P680^+$ and Q_{A^-}, probably due to slower electron donation to the OEC complex from water. **PSI** * PSI subunits such as PSaD and PsaE on the stromal side are less stable after treatment of chaotropic salts in vitro assay. * Protein analysis by using blue native polyacrylamide gel electrophoresis (BN-PAGE) analysis, LHCI and PsaD lacking in PSI supercomplex are observed. * Decreased PSI core proteins (PsbA and PsaB) with other subunits(PsaC, PsaL and PsaH). * PSI acceptor-side limitation, showing an increased capacity for CEF, increased reduction rate of PQ pool and decreased capacity for state transition, leading to increased susceptibility of PSI photoinhibition.	(Dörmann et al., 1995; Guo et al., 2005; Härtel et al., 1997; Ivanov et al., 2006; Reifarth et al., 1997; Steffen et al., 2005)
dgd2	T-DNA insertion DGD1	no significant decreased in DGDG content	* Normally grown. * No effect on quantum yield.	(Kelly et al., 2003)
dgd1/ dgd2	double mutant	has a very low content of DGDG, a negligible amount of DGDG	* Growth retardation compared to *dgd1* and decreased quantum yield (about 37% decreased) compared to WT * Transgenic expression of bacterial glucosylgalactosyldiacylglycerol (GlcGalDG) showed rescued the growth and chloroplast structure, however, photosynthesis reaction is not rescued (partly rescued), indicating that second galactose residue of DGDG has no specific function for growth and structural organization, but has a specific role for maintaining efficient photosynthetic machinery.	(Hölzl et al., 2006, 2009; Kelly et al., 2003).

1.4.2.3 PG

The phosphatidylglycerophosphate (PGP) synthase1 (PGP1) is essential for PG biosynthesis.

Table 1.3 Lipid mutants altered PG compositions.

Mutant	Enzyme blocked	Lipid phenotype	Physiological phenotype	References
pgp1	point mutation of PGP1	80% of decreased enzyme activity and 30 % of decreased PG content	* Pale green and slightly decreased capacity of photosynthesis.	(Xu et al., 2002)
null mutant *(pgp1-2).*	Knockout PGP1	more decreased PG content compared to *pgp1* (80% of reduction compared to WT)	* Pale yellow-green and unable to be grown under photoautotrophic condition, requiring sucrose. * Disturbed formation of PS-LHC complexes and ET. * Under Pi limitation, *pgp1-2* showed increased MGDG, DGDG and SQDG while decreasing PG content, showing completely abolished PSII photochemical reaction while Chls and PS proteins were observed, suggesting the importance of PG in photosynthesis reaction.	(Babiychuk et al., 2003; Hagio et al., 2002; Kobayashi et al., 2015)

1.4.2.4 SQDG

SQD2 gene transfers sulfoquinovose from UDP-sulfoquinovose to diacylglycerol, which is the final step of SQDG biosynthesis.

Table 1.4 Lipid mutants altered SQDG compositions.

Mutant	Enzyme blocked	Lipid phenotype	Physiological phenotype	References
sqd2	SQD2 T-DNA insertion mutants	completely lacked SQDG	* No outstanding effects under optimal conditions. * Fv/FM similarly, Φ_{II} is slightly decreased.	(Yu et al., 2002)
sqd2pgp1-1 double mutant	T-DNA insertion in SQD2 and point mutation in PGP1	reduced fraction of total anionic lipids by about one-third	* Strongly affected growth and photosynthetic capacity. * Chl content decreased, decreased PSII efficiency and a higher fraction of reduced Q_A.	(Yu and Benning, 2003)

1.5 Effects of low temperatures on photosynthesis

The low-temperature stress could be categorized into a freezing (<0 °C) and chilling (0–15 °C) stress (Miura and Furumoto, 2013). Chilling (or suboptimal) temperatures are often major constraints on photosynthesis, productivity, and geographical distribution of important cultivated crops (Allen & Ort 2001). Counterintuitively, with global climate change, which induces not only warming but variations in temperatures, transient chilling (sub-optimal, but non-freezing temperatures) can be a major problem (Gu et al. 2008).

Here, this section focuses on the primary components of photosynthesis affected by short chilling stress, mostly based on the knowledge introduced in the previous sections.

As reviewed by Allen & Ort, 2001 (Allen and Ort, 2001), several major components of photosynthesis can be affected by chilling, non-freezing temperature, including light reaction, carbon fixation, and stomatal conductance. Many of the light reaction processes have also been suggested to be affected by chilling stress, including thylakoid electron transport, photodamage and repair, photoprotection and downregulation of PSII and photosystem I (PSI) (Sonoike, 1996), activation of alternative electron sinks and oxidative stress. In particular, process of photodamage and repair has known as the most impacted factors among electron transport systems in chilling conditions (Aro et al., 1993).

1.5.1 Photodamage (chronic photoinhibition) and repair and its involvement of lipids.

Under adverse environmental conditions, the ability of photosynthetic protection exceeds capacity or fails, leading to induce qI, which is photoinhibitory quenching, photodamage, and it is rather a chronic photoinhibition. In PSII, plants evolved to amend this photodamage by repairing the main component of PSII, D1 protein.

At low temperatures, thylakoid membranes can be altered from the liquid crystal phase to the gel phase (Lyons, 1973; Raison, 1973) and this could, in turn, affect the diffusion of plastoquinone/ plastoquinol (PQ/PQH_2) (Clarke and Johnson, 2001) or turn-over of D1 protein (Moon et al., 1995). When the membrane becomes rigid, PQ/PQH_2 diffusion slows down and PQ pool becomes reduced, which increases the reduction of

Q_A, increasing the probability of ROS production (Khorobrykh and Ivanov, 2002) and subsequent photodamage. During oxidative damage to PSII, the D1 component in the PSII reaction center becomes damaged, necessitating induction of the repair mechanism to restore PSII function. The phosphorylated PSII core monomer migrates to stroma-exposed (non-appressed region) lamella for replacement of damaged D1 protein with a newly synthesized one (Figure 1.7). Antenna proteins detach from the core monomer and assemble again with the new D1 protein. This core monomer will then migrate to the grana stacks again (appressed region) (Kirchhoff, 2014). The replacement of D1 protein could be slowed down by altered membrane fluidity and increased unsaturated fatty acids enhance diffusion and accelerate repair (Moon et al., 1995).

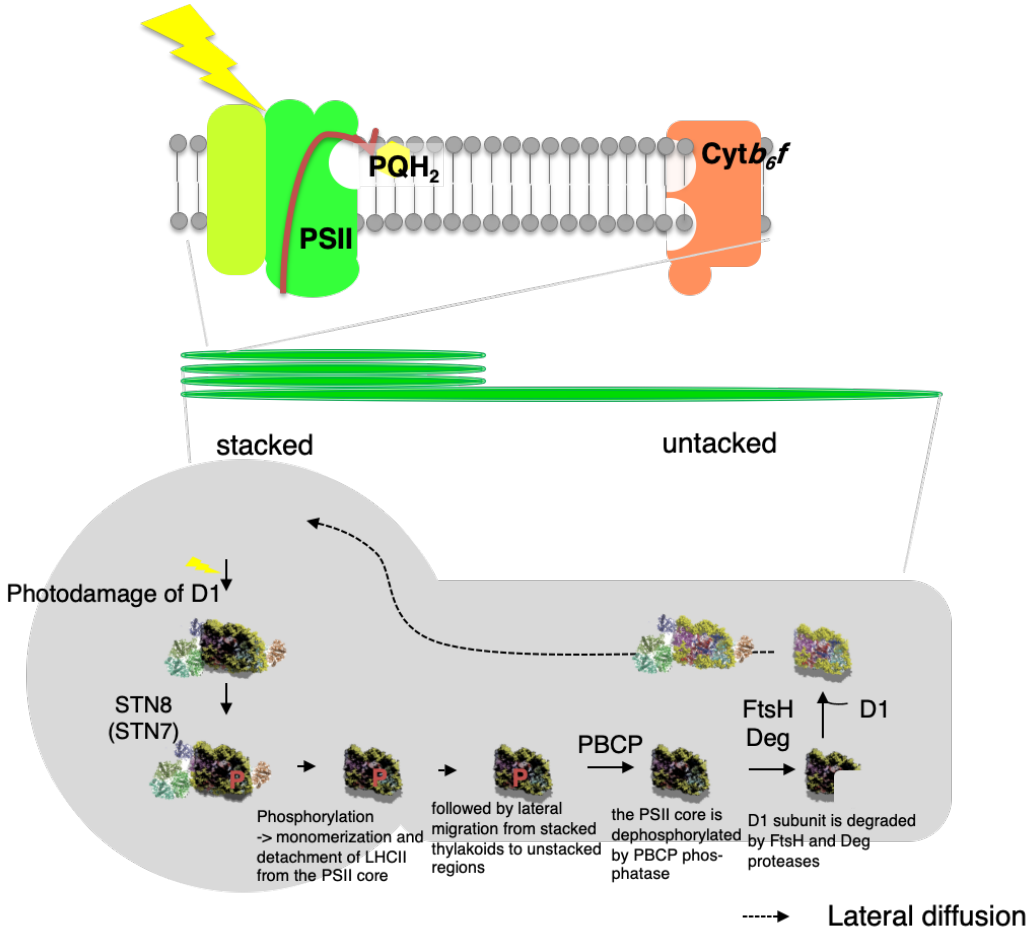

Figure 1.7 Overview of PSII repair cycle.
After light-induced photodamage of PSII, mainly in D1 protein, PSII complexes in stacked thylakoid region are phosphorylated, monomerized, detached from LHCII and further migrated to unstacked thylakoid region. Degraded damaged D1 protein substitute to new D1 protein, reassembling and migrating to stacked grana region. Image from (Wei et al., 2016) and Reconstitution figures from (Kirchhoff, 2014).

There have also been reports that changes in thylakoid lipid compositions influence the viability and photosynthetic capacity in response to chilling temperature. A series of mutant lines was isolated to test for roles of specific classes of fatty acids in response to chilling stress (Hugly and Somerville, 1992; Miquel et al., 1993; Wu et al., 1997). These kinds of studies demonstrated that the level of saturation or unsaturation of fatty acids is important in the tolerance to chilling stress balance of saturation and unsaturation level of fatty acid is important in the tolerance to chilling stress (e.g., *fad6*

and *fad2)*. However, there is also a counterexample, the plant with increased lipid saturation but showed improved photosynthetic performance at low temperature (Barkan et al., 2006).

An alternative hypothesis is that specific FAs species of PG, high- melting-point PG (HMP-PG), a combination of molecular species of saturated fatty acid (16:0 and 18:0) and16:1$^{\Delta 3\text{-trans}}$ (PG 16:1t), contribute chilling sensitivity. Wolter et al. showed that more than 50% of the PG molecules were HMP-PG in the plants, leading to chilling sensitivity (Wolter et al., 1992). However, contrary results have also been shown, exhibiting that an increased portion of HMP-PG species, *fab1* high PG 16:0 were unable to confer chilling sensitivity, concluding that the high-melting-point molecular species of PG cannot be the primary determinant of chilling sensitivity in this transgenic plant (Wu and Browse, 1995).

Despite considerable efforts, the contribution of specific species of fatty to the robustness of photosynthesis is unclear (Siegenthaler and Murata, 2006). One possible minor effect is that they only have a strong impact under specific sets of conditions that are not typically imposed in the lab. Another (non-exclusive) possibility is that these components contribute quantitatively to the robustness of the plant, through complex interactions with other biochemical/physiological interactions. These types of intertwined interactions are difficult to tease apart using conventional genetics, but it may be possible to approach by exploring natural variations, as described in the following section (section 1.6).

1.5.2 Carbohydrate metabolism and oxidative stress at low temperature.

It has been suggested that, at least under some conditions, carbohydrate metabolism (Figure 1.2) has greater sensitivity than other photosynthetic components in response to chilling stress (Leegood and Furbank, 1986). Both triose phosphate utilization (TPU) and end product consumption (sink strength) are more limiting than Rubisco and RuBP generation at low temperature (Cen and Sage, 2005; Loreto and Medrano, 2012; Mott et al., 1984; Sharkey and Bernacchi, 2012). Specifically, it has been shown that CO_2 assimilation is not increased even when CO_2 availability is high, if the ability of the plant to utilize TP is decreased, especially at low temperature and in plants with low capacities for starch synthesis or sucrose export (Sharkey, 1985; Yang et al., 2016).

Considering not only triose phosphate but also other metabolite pools of the Calvin- Benson cycle tend to change in response to chilling stress (Kobza and Edwards, 1987; Paul et al., 1990; Sassenrath et al., 1990), the multiple Calvin-Benson cycle enzymes are down-regulated, and the participation or additional regulatory networks must be invoked. Several key enzymes in carbon metabolism are regulated by light-dependent reductive activation through the thioredoxin (TR) and NADPH-thioredoxin reductase C (NTRC) systems. As the imbalance in the assimilatory force (AF) (Heber, 1989) with a relative deficit in energy stored in NADPH will lead to net oxidation of regulatory thiols, simultaneously shutting down CBB cycle at several points and/or starch synthesis. Sassenrath et al. showed that the FBPase and SBPase were inhibited under chilling and high light conditions, indicating that chilling induced photooxidation of thioredoxin-mediated activation of chloroplast enzymes (Sassenrath et al., 1990).

Provided that TR or NTRC is active, enzymes that have regulatory sulfhydryl groups with redox midpoint potentials within about 60 mV of -320 mV (at physiological pH between 7 and 8) should be modulated by changes in the redox state of the NADPH pool (Kramer et al., 1990; ORT, 2002; Stitt, 2004).

1.6 Natural variations of photosynthesis

As I stated in the introduction, the main goal of this dissertation is to understand and guide the way to improve photosynthesis by exploring natural variations in photosynthesis. Based on literature review research, previous sections (section 1.2-1.5) introduced the possible models that will be tested in this dissertation. In this section, a new conceptual approach to test those models will be introduced: natural genetic variation can be used to assess specific mechanisms that enable varieties of cowpea to tolerate environmental responses, further could be applied to breeding efforts.

1.6.1 Natural variations in photosynthesis are key to understanding how plants adapt to environments.

Natural variations in plants are strategies for the plants to improve in response to environmental stress, including gene drift, natural selection, adaptation of species to changing environments. Exploring natural variation is the way to improve crops but also the way to study how plants evolved. However, it is highly unexplored in photosynthesis research since it requires robust and high-throughput phenotyping tools. By taking advantage of recent advances of high-throughput photosynthetic phenotyping tools (Cruz *et al.* 2016; Kuhlgert*et al.* 2016), detailed, robust and reproducible, we are able to

explore multiple processes of photosynthetic responses in a large number of plants which have natural variations.

This approach is distinct from classic genetics. Because classical genetics approaches introduce (typically deleterious) mutations that are not commonly found in natural populations, it can miss variations that have evolved to adapt to specific environments. We propose to test hypotheses to seek to understand the underlying mechanisms of natural variations in photosynthetic responses by testing for potential co-linkages. Also, those findings could be directly applied to improving crops with identified genetic marker information.

To study this, one needs a population with genetic diversity for statistical analysis. The genetically diverse population for which polymorphisms--usually single nucleotide polymorphisms (SNPs)--have been mapped, to indicate how they differ from each other. These populations include recombinant inbred lines (RILs), or collections of divergent accessions collected in the field (for genome-wide association studies (GWAS), or various populations, including nested association mapping (NAM) population, multiparent advanced generation intercross (MAGIC) population (Rakshit et al., 2012) and so on. When these populations are exposed to specific conditions of interest, various phenotypes are recorded and quantitative or categorical phenotype parameters are then statistically compared to the occurrence of the polymorphisms.

Quantitative Trait Loci (QTL) is a range of genetic components that are statistically associated with the presence of a certain trait (Broman et al., 2003). Mapping/ Identifying QTL is the process to find the genomic locations that are associated with phenotypes. As a tool for exploring natural variations, we adapted QTL

mapping, proposing the “comparative QTL linkage” to determine possible mechanistic/ genetic linkage. QTL mapping has predominantly been used by plant breeders to identify genetic markers for desirable traits, that can be used to introgress multiple desirable traits into elite production lines (Boukar et al., 2016). In the past, most QTL analyses used bulk or aggregate phenotypes, such as yield or disease symptoms, partly because large numbers of measurements are required. However, the lack of specificity in these measurements makes it difficult to assess the contributions from individual processes. The proposed work takes advantage of high throughput phenotyping that measures multiple phenotypes simultaneously (Cruz et al., 2016; Kuhlgert et al., 2016), which will allow us to assess linkages between processes, and thus test specific hypothetical models. By comparing the QTL profiles for the different processes or phenotypes we can ask if, to a reasonable statistical level, the genetic diversity in one process is linked to that of another. By “linked” we mean that it is either controlled by the same genetic loci or is mechanistically related so that one process influences the other.

This “comparative QTL linkage” approach may allow us to assess the mechanistic bases of natural variations in plant responses. It is critical, though, that the limitations of the approach be carefully considered. For example, the observation that QTLs for two phenotypes do *not* overlap would strongly indicate that genetic diversity controlling these processes are not genetically or mechanistically linked, at least in this particular population, and at the experimental conditions and timeframe, i.e. a linkage *could* exist in another population or under different conditions. Therefore, care must be taken when generalizing findings because they may apply only to a particular population, and at the experimental conditions and timeframe. Observation of QTL overlaps must

also be considered with caution because each QTL may contain multiple genes, i.e. the observed “linkage” is to the entire region, not necessarily to any particular genes.An apparent linkage is not proof of a mechanism, which required subsequent experimentally tests. Lastly, observation of a potential linkage does not necessarily imply a particular cause-effect relationship, although in certain cases time-resolved QTL measurements can provide insights on mechanisms, e.g. a phenomenon related to the “cause” may appear at an earlier time than those associated with “effects.” However, it is also possible that a third (or more complex) factor controls any linkages. When we are aware of those caveats of this approach and appropriately employ it, the patterns of linkages give us clues about the mechanisms.

1.6.2 Some examples for chilling tolerance of photosynthetic QTLs.

There have been reported chilling tolerance photosynthetic QTL analysis in diverse crops such as maize (Fracheboud et al., 2002; Strigens et al., 2013), sorghum (Ortiz et al., 2017), barley (Tyrka et al., 2015). However, little is known of chilling tolerance QTL analysis in legumes.

In maize study (Fracheboud et al., 2002) for chilling tolerance under the constant light condition (400 μmol photons m^{-2} s^{-1}), 18 QTLs are found under optimal temperature and 19 QTLs are identified in the chilling conditions by phenotyping photosynthesis including chlorophyll fluorescence measurements and CO_2 exchange rate. In both conditions, only four QTLs are co-localized in the same traits, showing that genetic variance of controlling photosynthesis is different depending on temperature conditions. Also, Fracheboud et al. showed that biomass and carbon fixation rate was significantly involved in tolerance to photoinhibition, indicating that limited

photosynthetic capacity from photoinhibition is a key factor for tolerance of maize at low temperature.

In sorghum study (Ortiz et al., 2017), mapping with carbon assimilation and fluorescence measurement showed that generally high correlation with net assimilation and ΦII under chilling conditions and found co-localized QTL in transpiration rate and stomata conductance with ΦII (Ortiz, Hu, & Salas Fernandez, 2017). This indicates ΦII is a good representation for overall photosynthesis rate in chilling stress. Furthermore, these results give insights that we are able to get great insights on photosynthetic regulation if we can measure parameters over the time-course without destruction of plants. Also this study showed that stomatal conductance is not the only factor for limiting carbon assimilation, verifying previous research on maize (Fracheboud et al., 2002; Nie, 1992; Strigens et al., 2013). Although, Ortiz et al did not measure NPQ, qE and qI specifically, there is a possibility that decreased linear electron flow (LEF) due to the photosystem II damage contributes to the low carbon assimilation.

1.7 Aims of the Dissertation

Section 1.2-1.5 provides an overview of photosynthesis and related components of photosynthesis could be affected by chilling stress. Section 1.6 introduces a novel approach to explore those mechanisms by exploring natural variations. The subsequent chapters will present the applications of novel approach with major findings (Chapter 2 and 3).

Chapter 2 introduces a network of feedback regulatory processes of the light reactions at low temperature, “genetically-controlled responses to low temperature identify roles

for responses to thylakoid proton motive force, cyclic electron flow and the rates of photodamage and repair of photosystem II."

Chapter 3 focuses on the interaction with membrane lipids and photosynthesis reactions, "genetically-controlled variations in photosynthesis indicate new roles for fatty acid"

Overall, this dissertation will shed light on mechanistic linkages of light reactions, specific fatty acids at low temperatures by exploring natural variations. Further, we expect that an outcome of this research could be utilized to help improve the tolerance of crops in response to environmental stress.

BIBLIOGRAPHY

BIBLIOGRAPHY

1. Aklilu, E. (2021). Review on forward and reverse genetics in plant breeding. All Life *14*, 127–135.

2. Allen, D.J., and Ort, D.R. (2001). Impacts of chilling temperatures on photosynthesis in warm-climate plants. Trends Plant Sci. *6*, 36–42.

3. Apel, K., and Hirt, H. (2004). Reactive oxygen species: metabolism, oxidative stress, and signal transduction. Annu. Rev. Plant Biol. *55*, 373–399.

4. Aronsson, H., Schöttler, M.A., Kelly, A.A., Sundqvist, C., Dörmann, P., Karim, S., and Jarvis, P. (2008). Monogalactosyldiacylglycerol deficiency in Arabidopsis affects pigment composition in the prolamellar body and impairs thylakoid membrane energization and photoprotection in leaves. Plant Physiol. *148*, 580–592.

5. Aro, E.M., McCaffery, S., and Anderson, J.M. (1993). Photoinhibition and D1 protein degradation in peas acclimated to different growth irradiances. Plant Physiol. *103*, 835–843.

6. Asada, K. (1999). THE WATER-WATER CYCLE IN CHLOROPLASTS: Scavenging of Active Oxygens and Dissipation of Excess Photons. Annu. Rev. Plant Physiol. Plant Mol. Biol. *50*, 601–639.

7. Avenson, T.J., Cruz, J.A., Kanazawa, A., and Kramer, D.M. (2005). Regulating the proton budget of higher plant photosynthesis. Proc Natl Acad Sci USA *102*, 9709–9713.

8. Awai, K., Maréchal, E., Block, M.A., Brun, D., Masuda, T., Shimada, H., Takamiya, K., Ohta, H., and Joyard, J. (2001). Two types of MGDG synthase genes, found widely in both 16:3 and 18:3 plants, differentially mediate galactolipid syntheses in photosynthetic and nonphotosynthetic tissues in Arabidopsis thaliana. Proc Natl Acad Sci USA *98*, 10960–10965.

9. Babiychuk, E., Müller, F., Eubel, H., Braun, H.-P., Frentzen, M., and Kushnir, S. (2003). Arabidopsis phosphatidylglycerophosphate synthase 1 is essential for chloroplast differentiation, but is dispensable for mitochondrial function. Plant J. *33*, 899–909.

10. Baker, N.R., Harbinson, J., and Kramer, D.M. (2007). Determining the limitations and regulation of photosynthetic energy transduction in leaves. Plant Cell Environ. *30*, 1107–1125.

11. Barkan, L., Vijayan, P., Carlsson, A.S., Mekhedov, S., and Browse, J. (2006). A

suppressor of fab1 challenges hypotheses on the role of thylakoid unsaturation in photosynthetic function. Plant Physiol. *141*, 1012–1020.

12. Bates, P.D., Stymne, S., and Ohlrogge, J. (2013). Biochemical pathways in seed oil synthesis. Curr. Opin. Plant Biol. *16*, 358–364.

13. Boudière, L., Michaud, M., Petroutsos, D., Rébeillé, F., Falconet, D., Bastien, O., Roy, S., Finazzi, G., Rolland, N., Jouhet, J., et al. (2014). Glycerolipids in photosynthesis: composition, synthesis and trafficking. Biochim. Biophys. Acta *1837*, 470–480.

14. Boukar, O., Fatokun, C.A., Huynh, B.-L., Roberts, P.A., and Close, T.J. (2016). Genomic tools in cowpea breeding programs: status and perspectives. Front. Plant Sci. *7*, 757.

15. Broman, K.W., Wu, H., Sen, S., and Churchill, G.A. (2003). R/qtl: QTL mapping in experimental crosses. Bioinformatics *19*, 889–890.

16. Brooks, M.D., Jansson, S., and Niyogi, K.K. (2014). PsbS-Dependent Non-Photochemical Quenching. In Non-Photochemical Quenching and Energy Dissipation in Plants, Algae and Cyanobacteria, B. Demmig-Adams, G. Garab, W. Adams III, and Govindjee, eds. (Dordrecht: Springer Netherlands), pp. 297–314.

17. Buchanan, B.B. (1980). Role of light in the regulation of chloroplast enzymes. Annu. Rev. Plant Physiol. *31*, 341–374.

18. Buchanan, B.B., Gruissem, W., and Jones, R.L. (2015). Biochemistry and molecular biology of plants.

19. Carrillo, L.R., Froehlich, J.E., Cruz, J.A., Savage, L.J., and Kramer, D.M. (2016). Multi-level regulation of the chloroplast ATP synthase: the chloroplast NADPH thioredoxin reductase C (NTRC) is required for redox modulation specifically under low irradiance. Plant J. *87*, 654–663.

20. Cejudo, F.J., Ferrández, J., Cano, B., Puerto-Galán, L., and Guinea, M. (2012). The function of the NADPH thioredoxin reductase C-2-Cys peroxiredoxin system in plastid redox regulation and signalling. FEBS Lett. *586*, 2974–2980.

21. Cen, Y.-P., and Sage, R.F. (2005). The regulation of Rubisco activity in response to variation in temperature and atmospheric CO2 partial pressure in sweet potato. Plant Physiol. *139*, 979–990.

22. Clarke, J.E., and Johnson, G.N. (2001). In vivo temperature dependence of cyclic and pseudocyclic electron transport in barley. Planta *212*, 808–816.

23. Collin, V., Issakidis-Bourguet, E., Marchand, C., Hirasawa, M., Lancelin, J.-M., Knaff, D.B., and Miginiac-Maslow, M. (2003). The Arabidopsis plastidial thioredoxins: new functions and new insights into specificity. J. Biol. Chem. *278*, 23747–23752.

24. Cruz, J.A., Savage, L.J., Zegarac, R., Hall, C.C., Satoh-Cruz, M., Davis, G.A., Kovac, W.K., Chen, J., and Kramer, D.M. (2016). Dynamic environmental photosynthetic imaging reveals emergent phenotypes. Cell Syst. *2*, 365–377.

25. Davis, G.A., Kanazawa, A., Schöttler, M.A., Kohzuma, K., Froehlich, J.E., Rutherford, A.W., Satoh-Cruz, M., Minhas, D., Tietz, S., Dhingra, A., et al. (2016). Limitations to photosynthesis by proton motive force-induced photosystem II photodamage. Elife*5*.

26. Demé, B., Cataye, C., Block, M.A., Maréchal, E., and Jouhet, J. (2014). Contribution of galactoglycerolipids to the 3-dimensional architecture of thylakoids. FASEB J. *28*, 3373–3383.

27. Dörmann, P., Hoffmann-Benning, S., Balbo, I., and Benning, C. (1995). Isolation and characterization of an Arabidopsis mutant deficient in the thylakoid lipid digalactosyl diacylglycerol. Plant Cell *7*, 1801–1810.

28. Dorne, A.J., Joyard, J., and Douce, R. (1990). Do thylakoids really contain phosphatidylcholine? Proc Natl Acad Sci USA *87*, 71–74.

29. Fracheboud, Y., Ribaut, J.M., Vargas, M., Messmer, R., and Stamp, P. (2002). Identification of quantitative trait loci for cold-tolerance of photosynthesis in maize (Zea mays L.). J. Exp. Bot. *53*, 1967–1977.

30. Fujii, S., Kobayashi, K., Nakamura, Y., and Wada, H. (2014). Inducible knockdown of MONOGALACTOSYLDIACYLGLYCEROL SYNTHASE1 reveals roles of galactolipids in organelle differentiation in Arabidopsis cotyledons. Plant Physiol. *166*, 1436–1449.

31. Geigenberger, P. (2011). Regulation of starch biosynthesis in response to a fluctuating environment. Plant Physiol. *155*, 1566–1577.

32. Geigenberger, P., Thormählen, I., Daloso, D.M., and Fernie, A.R. (2017). The unprecedented versatility of the plant thioredoxin system. Trends Plant Sci. *22*, 249–262.

33. Guo, J., Zhang, Z., Bi, Y., Yang, W., Xu, Y., and Zhang, L. (2005). Decreased stability of photosystem I in dgd1 mutant of Arabidopsis thaliana. FEBS Lett. *579*, 3619–3624.

34. Gu, L., Hanson, P.J., Post, W.M., Kaiser, D.P., Yang, B., Nemani, R., Pallardy, S.G.,

and Meyers, T. (2008). The 2007 eastern US spring freeze: increased cold damage in a warming world? Bioscience *58*, 253–262.

35. Hagio, M., Sakurai, I., Sato, S., Kato, T., Tabata, S., and Wada, H. (2002). Phosphatidylglycerol is essential for the development of thylakoid membranes in Arabidopsis thaliana. Plant Cell Physiol. *43*, 1456–1464.

36. Härtel, H., Lokstein, H., Dörmann, P., Grimm, B., and Benning, C. (1997). Changes in the composition of the photosynthetic apparatus in the galactolipid-deficient dgd1 mutant of Arabidopsis thaliana. Plant Physiol. *115*, 1175–1184.

37. Hölzl, G., Witt, S., Kelly, A.A., Zähringer, U., Warnecke, D., Dörmann, P., and Heinz, E. (2006). Functional differences between galactolipids and glucolipids revealed in photosynthesis of higher plants. Proc Natl Acad Sci USA *103*, 7512–7517.

38. Hölzl, G., Witt, S., Gaude, N., Melzer, M., Schöttler, M.A., and Dörmann, P. (2009). The role of diglycosyl lipids in photosynthesis and membrane lipid homeostasis in Arabidopsis. Plant Physiol. *150*, 1147–1159.

39. Hugly, S., and Somerville, C. (1992). A role for membrane lipid polyunsaturation in chloroplast biogenesis at low temperature. Plant Physiol. *99*, 197–202.

40. Huner, N.P.A., Öquist, G., and Sarhan, F. (1998). Energy balance and acclimation to light and cold. Trends Plant Sci. *3*, 224–230.

41. Hurlock, A.K., Roston, R.L., Wang, K., and Benning, C. (2014). Lipid trafficking in plant cells. Traffic *15*, 915–932.

42. Hurry, V.M., Strand, A., Tobiaeson, M., Gardestrom, P., and Oquist, G. (1995). Cold hardening of spring and winter wheat and rape results in differential effects on growth, carbon metabolism, and carbohydrate content. Plant Physiol. *109*, 697–706.

43. Ismail, A.M., Hall, A.E., and Close, T.J. (1997). Chilling Tolerance during Emergence of Cowpea Associated with a Dehydrin and Slow Electrolyte Leakage. Crop Sci. *37*, 1270.

44. Ivanov, A.G., Hendrickson, L., Krol, M., Selstam, E., Oquist, G., Hurry, V., and Huner, N.P.A. (2006). Digalactosyl-diacylglycerol deficiency impairs the capacity for photosynthetic intersystem electron transport and state transitions in Arabidopsis thaliana due to photosystem I acceptor-side limitations. Plant Cell Physiol. *47*, 1146–1157.

45. Jarvis, P., Dörmann, P., Peto, C.A., Lutes, J., Benning, C., and Chory, J. (2000). Galactolipid deficiency and abnormal chloroplast development in the Arabidopsis MGD synthase 1 mutant. Proc Natl Acad Sci USA *97*, 8175–8179.

46. Johnson, G.N. (2011). Physiology of PSI cyclic electron transport in higher plants. Biochim. Biophys. Acta *1807*, 384–389.

47. Joliot, P., and Johnson, G.N. (2011). Regulation of cyclic and linear electron flow in higher plants. Proc Natl Acad Sci USA *108*, 13317–13322.

48. Joliot, P., and Joliot, A. (2006). Cyclic electron flow in C3 plants. Biochimica et Biophysica Acta (BBA)-Bioenergetics *1757*, 362–368.

49. Kaiser, E., Morales, A., Harbinson, J., Kromdijk, J., Heuvelink, E., and Marcelis, L.F.M. (2015). Dynamic photosynthesis in different environmental conditions. J. Exp. Bot. *66*, 2415–2426.

50. Kaiser, E., Correa Galvis, V., and Armbruster, U. (2019). Efficient photosynthesis in dynamic light environments: a chloroplast's perspective. Biochem. J. *476*, 2725–2741.

51. Kelly, A.A., and Dörmann, P. (2002). DGD2, an Arabidopsis gene encoding a UDP-galactose-dependent digalactosyldiacylglycerol synthase is expressed during growth under phosphate-limiting …. Journal of Biological Chemistry.

52. Kelly, A.A., Froehlich, J.E., and Dörmann, P. (2003). Disruption of the two digalactosyldiacylglycerol synthase genes DGD1 and DGD2 in Arabidopsis reveals the existence of an additional enzyme of galactolipid synthesis. Plant Cell *15*, 2694–2706.

53. Khorobrykh, S.A., and Ivanov, B.N. (2002). Oxygen reduction in a plastoquinone pool of isolated pea thylakoids. Photosynthesis Research *71*, 209–219.

54. Kiirats, O., Cruz, J.A., Edwards, G.E., and Kramer, D.M. (2009). Feedback limitation of photosynthesis at high CO_2 acts by modulating the activity of the chloroplast ATP synthase. Functional Plant Biol. *36*, 893.

55. Kirchhoff, H. (2014). Structural changes of the thylakoid membrane network induced by high light stress in plant chloroplasts. Phil. Trans. R. Soc. B *369*, 20130225.

56. Kobayashi, K., Kondo, M., Fukuda, H., Nishimura, M., and Ohta, H. (2007). Galactolipid synthesis in chloroplast inner envelope is essential for proper thylakoid biogenesis, photosynthesis, and embryogenesis. Proc Natl Acad Sci USA *104*, 17216–17221.

57. Kobayashi, K., Awai, K., Nakamura, M., Nagatani, A., Masuda, T., and Ohta, H. (2009). Type-B monogalactosyldiacylglycerol synthases are involved in phosphate starvation-induced lipid remodeling, and are crucial for low-phosphate adaptation. Plant J. *57*, 322–331.

58. Kobayashi, K., Narise, T., Sonoike, K., Hashimoto, H., Sato, N., Kondo, M., Nishimura, M., Sato, M., Toyooka, K., Sugimoto, K., et al. (2013). Role of galactolipid biosynthesis in coordinated development of photosynthetic complexes and thylakoid membranes during chloroplast biogenesis in Arabidopsis. Plant J. *73*, 250–261.

59. Kobayashi, K., Fujii, S., Sato, M., Toyooka, K., and Wada, H. (2015). Specific role of phosphatidylglycerol and functional overlaps with other thylakoid lipids in Arabidopsis chloroplast biogenesis. Plant Cell Rep. *34*, 631–642.
60. Kobza, J., and Edwards, G.E. (1987). Influences of leaf temperature on photosynthetic carbon metabolism in wheat. Plant Physiol. *83*, 69–74.

61. Kramer, D.M., Wise, R.R., Frederick, J.R., Alm, D.M., Hesketh, J.D., Ort, D.R., and Crofts, A.R. (1990). Regulation of coupling factor in field-grown sunflower: A Redox model relating coupling factor activity to the activities of other thioredoxin-dependent chloroplast enzymes. Photosyn. Res. *26*, 213–222.

62. Kramer, D.M., Avenson, T.J., and Edwards, G.E. (2004). Dynamic flexibility in the light reactions of photosynthesis governed by both electron and proton transfer reactions. Trends Plant Sci. *9*, 349–357.

63. Kuhlgert, S., Austic, G., Zegarac, R., Osei-Bonsu, I., Hoh, D., Chilvers, M.I., Roth, M.G., Bi, K., TerAvest, D., Weebadde, P., et al. (2016). MultispeQ Beta: a tool for large-scale plant phenotyping connected to the open PhotosynQ network. R. Soc. Open Sci. *3*, 160592.

64. Leegood, R.C., and Furbank, R.T. (1986). Stimulation of photosynthesis by 2% oxygen at low temperatures is restored by phosphate. Planta *168*, 84–93.

65. Lepistö, A., Pakula, E., Toivola, J., Krieger-Liszkay, A., Vignols, F., and Rintamäki, E. (2013). Deletion of chloroplast NADPH-dependent thioredoxin reductase results in inability to regulate starch synthesis and causes stunted growth under short-day photoperiods. J. Exp. Bot. *64*, 3843–3854.

66. Long, S.P., Zhu, X.-G., Naidu, S.L., and Ort, D.R. (2006). Can improvement in photosynthesis increase crop yields? Plant Cell Environ. *29*, 315–330.

67. Loreto, F., and Medrano, H. (2012). Terrestrial Photosynthesis in a Changing Environment (Cambridge University Press).

68. Lyons, J.M. (1973). Chilling Injury in Plants. Annu. Rev. Plant Physiol. *24*, 445–466.

69. Michalska, J., Zauber, H., Buchanan, B.B., Cejudo, F.J., and Geigenberger, P. (2009). NTRC links built-in thioredoxin to light and sucrose in regulating starch synthesis in chloroplasts and amyloplasts. Proc Natl Acad Sci USA *106*, 9908–

9913.

70. Michelet, L., Zaffagnini, M., Morisse, S., Sparla, F., Pérez-Pérez, M.E., Francia, F., Danon, A., Marchand, C.H., Fermani, S., Trost, P., et al. (2013). Redox regulation of the Calvin-Benson cycle: something old, something new. Front. Plant Sci. *4*, 470.

71. Miège, C., Maréchal, E., Shimojima, M., Awai, K., Block, M.A., Ohta, H., Takamiya, K., Douce, R., and Joyard, J. (1999). Biochemical and topological properties of type A MGDG synthase, a spinach chloroplast envelope enzyme catalyzing the synthesis of both prokaryotic and eukaryotic MGDG. Eur. J. Biochem. *265*, 990–1001.

72. Miquel, M., James, D., Dooner, H., and Browse, J. (1993). Arabidopsis requires polyunsaturated lipids for low-temperature survival. Proc Natl Acad Sci USA *90*, 6208–6212.

73. Miura, K., and Furumoto, T. (2013). Cold signaling and cold response in plants. Int. J. Mol. Sci. *14*, 5312–5337.

74. Moellering, E.R., and Benning, C. (2011). Galactoglycerolipid metabolism under stress: a time for remodeling. Trends Plant Sci. *16*, 98–107.

75. Moellering, E.R., Muthan, B., and Benning, C. (2010). Freezing tolerance in plants requires lipid remodeling at the outer chloroplast membrane. Science *330*, 226–228.

76. Moon, B.Y., Higashi, S., Gombos, Z., and Murata, N. (1995). Unsaturation of the membrane lipids of chloroplasts stabilizes the photosynthetic machinery against low-temperature photoinhibition in transgenic tobacco plants. Proc Natl Acad Sci USA *92*, 6219–6223.

77. Mott, K.A., Jensen, R.G., O'leary, J.W., and Berry, J.A. (1984). Photosynthesis and Ribulose 1,5-Bisphosphate Concentrations in Intact Leaves of Xanthium strumarium L. Plant Physiol. *76*, 968–971.

78. Muchero, W., Diop, N.N., Bhat, P.R., Fenton, R.D., Wanamaker, S., Pottorff, M., Hearne, S., Cisse, N., Fatokun, C., Ehlers, J.D., et al. (2009). A consensus genetic map of cowpea [Vigna unguiculata (L) Walp.] and synteny based on EST-derived SNPs. Proc Natl Acad Sci USA *106*, 18159–18164.

79. Murphy, D.J. (1982). The importance of non-planar bilayer regions in photosynthetic membranes and their stabilisation by galactolipids. FEBS Lett. *150*, 19–26.

80. Neuhaus, H.E., and Emes, M.J. (2000). Nonphotosynthetic metabolism in plastids. Annu. Rev. Plant Physiol. Plant Mol. Biol. *51*, 111–140.

81. Neuhaus, H.E., Kruckeberg, A.L., Feil, R., and Stitt, M. %J P. (1989). Reduced-activity mutants of phosphoglucose isomerase in the cytosol and chloroplast of

Clarkia xantiana. *178*, 110–122.

82. Nie, G. (1992). PERTURBATIONS OF PHOTOSYNTHESIS IN MAIZE BY LOW TEMPERATURES.

83. Ojeda, V., Pérez-Ruiz, J.M., and Cejudo, F.J. (2018). 2-Cys Peroxiredoxins Participate in the Oxidation of Chloroplast Enzymes in the Dark. Mol. Plant *11*, 1377–1388.

84. Ortiz, D., Hu, J., and Salas Fernandez, M.G. (2017). Genetic architecture of photosynthesis in Sorghum bicolor under non-stress and cold stress conditions. Journal of Experimental Botany *68*, 4545–4557.

85. ORT, D.R. (2002). Chilling-induced limitations on photosynthesis in warm climate plants: contrasting mechanisms. Environment Control in Biology *40*, 7–18.

86. Paul, M.J., Lawlor, D.W., and Driscoll, S.P. (1990). The Effect of Temperature on Photosynthesis and Carbon Fluxes in Sunflower and Rape. J. Exp. Bot. *41*, 547–555.

87. Pearcy, R.W., Krall, J.P., and Sassenrath-Cole, G.F. (2004). Photosynthesis in fluctuating light environments. In Photosynthesis and the Environment, N.R. Baker, ed. (Dordrecht: Kluwer Academic Publishers), pp. 321–346.

88. Pérez-Ruiz, J.M., Naranjo, B., Ojeda, V., Guinea, M., and Cejudo, F.J. (2017). NTRC-dependent redox balance of 2-Cys peroxiredoxins is needed for optimal function of the photosynthetic apparatus. Proc Natl Acad Sci USA *114*, 12069–12074.

89. Prasad, T.K. (1997). Role of Catalase in Inducing Chilling Tolerance in Pre-Emergent Maize Seedlings. Plant Physiol. *114*, 1369–1376.

90. Pulido, P., Spínola, M.C., Kirchsteiger, K., Guinea, M., Pascual, M.B., Sahrawy, M., Sandalio, L.M., Dietz, K.-J., González, M., and Cejudo, F.J. (2010). Functional analysis of the pathways for 2-Cys peroxiredoxin reduction in Arabidopsis thaliana chloroplasts. J. Exp. Bot. *61*, 4043–4054.

91. Raines, C.A. (2011). Increasing photosynthetic carbon assimilation in C3 plants to improve crop yield: current and future strategies. Plant Physiol. *155*, 36–42.

92. Raison, J.K. (1973). Temperature-induced phase changes in membrane lipids and their influence on metabolic regulation. pp. 485–512.

93. Rakshit, S., Rakshit, A., and Patil, J.V. (2012). Multiparent intercross populations in analysis of quantitative traits. J. Genet. *91*, 111–117.

94. Reifarth, F., Christen, G., Seeliger, A.G., Dörmann, P., Benning, C., and Renger, G. (1997). Modification of the water oxidizing complex in leaves of the dgd1 mutant of Arabidopsis thaliana deficient in the galactolipid digalactosyldiacylglycerol. Biochemistry *36*, 11769–11776.

95. Roston, R.L., Wang, K., Kuhn, L.A., and Benning, C. (2014). Structural determinants allowing transferase activity in SENSITIVE TO FREEZING 2, classified as a family I glycosyl hydrolase. J. Biol. Chem. *289*, 26089–26106.

96. Sassenrath, G.F., Ort, D.R., and Portis Jr, A.R. (1990). Impaired reductive activation of stromal bisphosphatases in tomato leaves following low-temperature exposure at high light. Archives of Biochemistry and Biophysics *282*, 302–308.

97. Schöner, S., and Heinrich Krause, G. (1990). Protective systems against active oxygen species in spinach: response to cold acclimation in excess light. Planta *180*, 383–389.

98. Schürmann, P., and Jacquot, J.P. (2000). Plant thioredoxin systems revisited. Annual Review of Plant Biology *51*, 371–400.

99. Serrato, A.J., Pérez-Ruiz, J.M., Spínola, M.C., and Cejudo, F.J. (2004). A novel NADPH thioredoxin reductase, localized in the chloroplast, which deficiency causes hypersensitivity to abiotic stress in Arabidopsis thaliana. J. Biol. Chem. *279*, 43821–43827.

100. Shamsi, I.H., Shamsi, B.H., and Jiang, L. (2012). Biochemistry of fatty acids. In Technological Innovations in Major World Oil Crops, Volume 2, S.K. Gupta, ed. (New York, NY: Springer New York), pp. 123–150.

101. Sharkey, T.D. (1985). O(2)-insensitive photosynthesis in c(3) plants : its occurrence and a possible explanation. Plant Physiol. *78*, 71–75.

102. Sharkey, T., and Bernacchi, C. (2012). Photosynthetic responses to high temperature. Terrestrial Photosyntesis in a Changing Environment 290–298.

103. Sharkey, T.D., Bernacchi, C.J., Farquhar, G.D., and Singsaas, E.L. (2007). Fitting photosynthetic carbon dioxide response curves for C(3) leaves. Plant Cell Environ. *30*, 1035–1040.

104. Siegenthaler, P.-A., and Murata, N. (2006). Lipids in Photosynthesis: An Overview. In Lipids in Photosynthesis: Structure, Function and Genetics, P.-A. Siegenthaler, and N. Murata, eds. (Springer Science & Business Media), pp. 1–20.

105. Sonoike, K. (1996). Photoinhibition of photosystem I: its physiological significance in the chilling sensitivity of plants. Plant and Cell Physiology *37*, 239–247.

106. Steffen, R., Kelly, A.A., Huyer, J., Dörmann, P., and Renger, G. (2005). Investigations on the reaction pattern of photosystem II in leaves from Arabidopsis thaliana wild type plants and mutants with genetically modified lipid content. Biochemistry *44*, 3134–3142.

107. Stitt, M. (2004). Metabolic regulation of photosynthesis. In Photosynthesis and the Environment, N.R. Baker, ed. (Dordrecht: Kluwer Academic Publishers), pp. 151–190.

108. Strigens, A., Freitag, N.M., Gilbert, X., Grieder, C., Riedelsheimer, C., Schrag, T.A., Messmer, R., and Melchinger, A.E. (2013). Association mapping for chilling tolerance in elite flint and dent maize inbred lines evaluated in growth chamber and field experiments. Plant Cell Environ. *36*, 1871–1887.

109. Takizawa, K., Kanazawa, A., and Kramer, D.M. (2008). Depletion of stromal Pi induces high 'energy-dependent'antenna exciton quenching (qE) by decreasing proton conductivity at CFO-CF1 ATP synthase. Plant, Cell & Environment *31*, 235–243.

110. Tyrka, M., Rapacz, M., Fiust, A., and Wójcik-Jagła, M. (2015). Quantitative trait loci mapping of freezing tolerance and photosynthetic acclimation to cold in winter two- and six-rowed barley. Plant Breeding *134*, 271–282.

111. Vaseghi, M.-J., Chibani, K., Telman, W., Liebthal, M.F., Gerken, M., Schnitzer, H., Mueller, S.M., and Dietz, K.-J. (2018). The chloroplast 2-cysteine peroxiredoxin functions as thioredoxin oxidase in redox regulation of chloroplast metabolism. Elife*7*.

112. Wada, H., and Murata, N. (2004). Membrane lipids in cyanobacteria. In Lipids in Photosynthesis: Structure, Function and Genetics, S. Paul-André, and M. Norio, eds. (Dordrecht: Kluwer Academic Publishers), pp. 65–81.

113. Wei, X., Su, X., Cao, P., Liu, X., Chang, W., Li, M., Zhang, X., and Liu, Z. (2016). Structure of spinach photosystem II-LHCII supercomplex at 3.2 Å resolution. Nature *534*, 69–74.

114. Wolter, F.P., Schmidt, R., and Heinz, E. (1992). Chilling sensitivity of Arabidopsis thaliana with genetically engineered membrane lipids. EMBO J. *11*, 4685–4692.

115. Wu, J., and Browse, J. (1995). Elevated Levels of High-Melting-Point Phosphatidylglycerols Do Not Induce Chilling Sensitivity in an Arabidopsis Mutant. Plant Cell *7*, 17–27.

116. Wu, J., Lightner, J., and Warwick, N. (1997). Low-temperature damage and subsequent recovery of fab1 mutant Arabidopsis exposed to 2 [deg] C. Plant Physiology *113*, 347–356.

117. Wu, W., Ping, W., Wu, H., Li, M., Gu, D., and Xu, Y. (2013). Monogalactosyldiacylglycerol deficiency in tobacco inhibits the cytochrome b6f-mediated intersystem electron transport process and affects the photostability of the photosystem II apparatus. Biochim. Biophys. Acta *1827*, 709–722.

118. Xu, C., Härtel, H., Wada, H., Hagio, M., Yu, B., Eakin, C., and Benning, C. (2002). The pgp1 mutant locus of Arabidopsis encodes a phosphatidylglycerolphosphate synthase with impaired activity. Plant Physiol. *129*, 594–604.

119. Yang, J.T., Preiser, A.L., Li, Z., Weise, S.E., and Sharkey, T.D. (2016). Triose phosphate use limitation of photosynthesis: short-term and long-term effects. Planta *243*, 687–698.

120. Yoshida, K., Matsuoka, Y., Hara, S., Konno, H., and Hisabori, T. (2014). Distinct redox behaviors of chloroplast thiol enzymes and their relationships with photosynthetic electron transport in Arabidopsis thaliana. Plant Cell Physiol. *55*, 1415–1425.

121. Yoshida, K., Hara, A., Sugiura, K., Fukaya, Y., and Hisabori, T. (2018). Thioredoxin-like2/2-Cys peroxiredoxin redox cascade supports oxidative thiol modulation in chloroplasts. Proc Natl Acad Sci USA *115*, E8296–E8304.

122. Yu, B., and Benning, C. (2003). Anionic lipids are required for chloroplast structure and function in Arabidopsis. Plant J. *36*, 762–770.

123. Yu, B., Xu, C., and Benning, C. (2002). Arabidopsis disrupted in SQD2 encoding sulfolipid synthase is impaired in phosphate-limited growth. Proc Natl Acad Sci USA *99*, 5732–5737.

124. Zelitch, I. (1982). The close relationship between net photosynthesis and crop yield. Bioscience *32*, 796–802.

CHAPTER 2

GENETICALLY-CONTROLLED RESPONSES TO LOW TEMPERATURE IDENTIFY ROLES FOR RESPONSES TO THYLAKOID PROTON MOTIVE FORCE, CYCLIC ELECTRON FLOW AND THE RATES OF PHOTODAMAGE AND REPAIR OF PHOTOSYSTEM II.

Work presented is in preparation for publication:

Donghee Hoh, Isaac Osei-Bonsu, Abhijnan Chattopadhyay, Atsuko Kanazawa, Nicholas Fisher, Oliver L Tessmer, Jeffrey Cruz, Philip A. Roberts, Bao-Lam Huynh, Lina Yin, Patrick Horn, David Hall, Christoph Benning and David M. Kramer

2.1 Abstract

The goal of this work is to understand the mechanisms of natural variations in photosynthetic responses to environmental stresses by exploring linkages between genetic polymorphisms and multiple, mechanistically-related phenotypes.

We assessed a population of recombinant inbred lines (RILs) of cowpea (*Vigna unguiculata.* (L.) Walp.) generated from parent lines with significant differences in photosynthetic responses to chilling. The population of RILs displayed significant, partially-transgressive segregation in response to chilling in a range of photosynthetic parameters.

Under chilling (19/13 °C day/night temperatures), we found well-defined, colocalized (overlapping) QTL intervals for a range of parameters reflecting the photosynthetic efficiency, photoprotection, photodamage and capture and feedback regulation by control of the thylakoid proton motive force, including with those for photosystem II (PSII) quantum efficiency (Φ_{II}), nonphotochemical quenching (NPQ) in both the qE and qI forms, the redox state of Q_A (q_L), the redox states of photosystem I (PSI), the activity of the thylakoid ATP synthase (*g*H+,) and the light-driven thylakoid proton motive force (*pmf*). The QTL analysis and follow-up biochemical/biophysical assays show that genetic variations impact low temperature tolerance by modulating: 1) redox states of Q_A; 2) the thylakoid *pmf*, through effects on cyclic electron flow; leading to differences in the rates of photodamage to PSII.

We propose that these processes act by modulating the recombination reactions within PSII that can lead to deleterious singlet O_2 production. We did not observe linkages to PSI redox state, PSI photodamage or ATP synthase activity, likely

indicating that several proposed models are not involved in the genetic control of photosynthesis in our mapping panel. We also observed strong low-temperature-induced nyctinastic leaf movements, but co-association analysis suggested that these variations are not genetically or mechanistically linked to the variations in controlling photosynthetic responses.

The results thus demonstrate the use of genetic diversity to generate and test (support or reject) hypothetical models that can be used to identify the mechanistic bases that underlie the genetic diversity of photosynthetic responses, with potential applications to breeding and engineering of photosynthesis for higher, more climate-resilient productivity.

2.2 Introduction

Photosynthetic performance is strongly impacted by abiotic stress factors, accounting for substantial losses of sustainable plant productivity, and thus critical for maintaining or expanding sustainable agriculture, particularly in a rapidly changing environment. Because photosynthesis directly contributes to yield, understanding how it performs and is regulated under non-ideal conditions may be the key to improving plant productivity (Zelitch 1982; Long, Zhu, Naidu & Ort 2006; Raines 2011). Stress resistance traits are thus the target of intensive efforts at breeding or engineering more robust plant responses. However, the important effects may include complex, rapidly fluctuating combinations of temperature, water availability, light intensity etc. that are not typically seen under controlled laboratory conditions (Tikkanen*et al.* 2012; Cruz *et al.* 2016). Plants have adapted to meet the challenges of specific environments, and it may

be possible to harness this biodiversity to improve crop performance in changing environments (Lawson et al. 2012). However, such traits may not be present in our current crops or well-studied model systems. Thus, discovering the mechanistic bases of useful or adaptive photosynthetic traits will require exploration of wider ranges of genotypes and environmental conditions.

Chilling (or suboptimal) temperatures are often major constraints on photosynthesis, productivity, and geographical distribution of important cultivated crops (Allen & Ort 2001). Counterintuitively, transient chilling (sub-optimal, but non-freezing temperatures) can be a major problem even with global climate change, which induces not only warming but variations in temperatures, leading to unpredictable periods of increased and decreased growth temperatures (Gu *et al.* 2008). Multiple components of photosynthesis can be affected by chilling, including thylakoid electron transport, carbon fixation, stomatal conductance, regulation of gene expression (Allen & Ort 2001). Key steps in the light reactions have also been suggested to be the primary limitations under chilling, e.g. thylakoid electron transport, photodamage and repair of photosystem II (PSII) (Aro, Virgin & Andersson 1993; Moon, Higashi, Gombos& Murata 1995), photosystem I (PSI) (Sonoike 1996), activation of alternative electron sinks (Ivanov *et al.* 2012) and oxidative stress (Sassenrath, Ort & Portis Jr 1990; Hutchison, Groom & Ort 2000). The primary limitations may be specific to differences in species, genotypes, developmental stages or other environmental conditions.

The increasing sophistication of high-throughput photosynthetic phenotyping, combined with powerful genetic approaches and biochemical methods, enables us to test for interactions among natural specific mechanisms that may underlie genetic

variations in tolerance to low temperatures. This can be achieved by identifying statistical associations between measured traits with genetic polymorphisms in a panel or library of genetically diverse lines (Broman 2001). Quantitative Trait Loci (QTL) and genome wide association studies (GWAS) have been extensively used by plant breeders to identify genetic markers for desirable traits that can be used to develop introgression of these multiple traits into elite production lines of crop (Boukar, Fatokun, Huynh, Roberts & Close 2016). For example, bulk or aggregated phenotypes based on the data such as yield or disease resistance were targeted for most QTL analyses (Mucher*et al.* 2013; Huynh *et al.* 2016). It has been much more difficult to identify specific, causative genetic loci associated with QTLs (Roff 2007; Baxter 2020), largely because of the low genomic resolution of the methods (Miles & Wayne 2008).

In this work, we focus on discovering and testing possible mechanistic bases of such variations by assessing cosegregation (or lack thereof) between genetic diversity and multiple traits. To achieve this, we took advantage of recently developed high-throughput phenotyping tools that can measure multiple, mechanistically-related, photosynthetic phenotypes under simulated, field-like environmental conditions (Cruz *et al.* 2016; Kuhlgert*et al.* 2016). We then compared the QTL profiles for the different phenotypes to assess whether the genetic diversity in one process is linked to that of others.

The phenotyping tools used in this work can make time-resolved, semi-simultaneous, measurements of photosynthetic processes in many genotypes. By testing for possible co-associations between genetic components and various phenotypes, it is possible to assess if variations in processes are genetically or

mechanistically linked. Here, we use the term “linked” broadly to mean that processes are either controlled by the same genetic locus or mechanistically connected so that one process impacts the other. In this context, the observation that QTLs for two phenotypes do *not* overlap, would indicate that genetic diversity controlling one process is not measurably controlling the other, at least in the specific population and experimental conditions. In other words, a linkage *could* exist in another population or under different conditions. On the other hand, observing strongly overlapping QTLs can be considered as evidence for genetic or mechanistic linkages, but with the following important caveats: 1) With most diversity panels, there are likely to be many gene polymorphisms under a single QTL, and one cannot exclude the possibility that two processes are influenced by two distinct loci within the statistical resolution of the QTL. 2) Traits may be impacted by a large number of weak linkages, each making only a small impact, and thus may not appear as distinct QTL. Here, we consider only those variations that do show significant associations, implying that a limited number of discrete genetic components measurably affect on a phenotype, and thus one can make (careful) inferences about how they are linked to others. 3) One trait may affect the ability to measure another even though they are not directly functionally linked. For instance, traits that affect the optical properties of a leaf, e.g. leaf thickness, accumulation of anthocyanins etc. may decrease the sensitivity of the measurement of a phenotype so that the phenotype may appear to have a linkage with these traits. This issue above may be particularly important for measurements made using the same basic techniques. For example, a number of our measurements are made using saturation pulse fluorescence kinetics so that artifacts in one measurement may

become evident in the others (see (Baker, Harbinson& Kramer 2007)), giving rise to apparent linkages. However, as discussed in Results, the fact that QTL for these various parameters is conditionally linked, argues against these types of effects in the current data set. 4) It is also possible that the effects of one process may be canceled out by others, masking an effect. This may be expected for homeostatic processes, e.g., where the network of regulatory processes results in compensatory (e.g., feedback and feedforward) regulation. In these cases, effects on some parameters may only be observed when the compensatory homeostatic mechanisms fail. 5) Phenotypes can be linked through indirect and time-dependent intermediates.

Specifically, we explored natural variations in chilling tolerance on photosynthesis in *Vigna unguiculata* (cowpea), a warm-climate species with a high level of genetic diversity and significant variable phenotypic responses to abiotic stress among its cultivars (Huynh *et al.* 2018). We demonstrate strong, genotype-dependent effects of chilling on the primary reactions of photosynthesis that likely involve the network that co-regulates the light and assimilatory reactions of photosynthesis. This network involves the establishment of the thylakoid proton motive force (*pmf*) and subsequent acidification of the thylakoid lumen, which activates the qE response and the “photosynthetic control” of electron flow at the level of the cytochrome b_6f complex (Avenson et al. 2005). The results show qualitatively similar effects, supporting causative linkages.

2.3 Materials and Methods

2.3.1 Plant materials.

Cowpea recombinant inbred lines (RILs) used for QTL mapping were selected by the pre-screening of nine pairs of RIL parental lines (Table S2.1). This population consisted of 90 RILs (F10 generation) originating from a cross between cultivar California Blackeye 27 (CB27) bred by the University of California (UC), Riverside (Ehlers, Hall, Patel, Roberts & Matthews 2000) and breeding line 24-125B-1 developed by Institute de Recherche Agricole pour le Développement (IRAD, Cameroon).

2.3.2 Growth and Experimental conditions.

Cowpea seeds were planted in Suremix (Michigan Grower Products Inc, USA) with half-strength Hoagland's nutrient solution and germinated under a 14hr: 10hr day: night cycle with a daylight intensity of 500 µmol photons m^{-2} s^{-1} and temperatures of 29 °C/19°C (day/night), 60% relative humidity in the growth chamber (BioChambers, Winnipeg, Canada). Seedlings were then transferred to DEPI chambers and allowed to acclimate for one day under growth light and temperature conditions. Imaging of chlorophyll fluorescence parameters was initiated on subsequent days as the light intensity was changed every 30 minutes with a 10/14 hour light/dark pattern based on a sinusoidal curve and a peak intensity of 500 µmol photons m^{-2} s^{-1} (Figure S2.1), imitating a cloudless sunny day. On Day 2, For chilling treatment day/night temperatures were shifted to 19 °C/13°C on the second day of imaging. The temperatures were selected based on average field conditions from 2012 to 2016 in Tulare, Central valley of California where cowpea is normally grown, in April one month

ahead of normal planting. Data is from National Oceanic and Atmospheric Administration, https://www.noaa.gov (Table S2.2).

2.3.3 Photosynthetic phenotyping.

Chlorophyll fluorescence imaging was performed using Dynamic Environmental Phenotype Imager (DEPI) chambers (Cruz et al., 2016), with modifications described in (Tietz, Hall, Cruz & Kramer 2017) . Fluorescence images were captured in fully dark-adapted plants and at different times following illumination to obtain estimates of photosynthetic parameters using the methods described in (Baker & Oxborough 2004; Baker *et al.* 2007; Tietz *et al.* 2017). Values for steady-state F (F_S) and with oxidized Q_A (F_0') or following short (~6s) dark period with far-red illumination to obtain estimates of F_0', or 1 min dark periods to obtain F_M" values to estimate rapidly (q_E) and slowly (q_I and q_Z) relaxing contributions to NPQ. Images of maximum fluorescence yields with Q_A was fully reduced (F_M', F_M") were collected after ~0.3 s of saturating white light (~10,000 µmol m^{-2} s^{-1}), while those of F_0' and F_0" were collected immediately after 6 seconds of far-red illumination (approximately ~4.6 µmol m^{-2} s^{-1})). During the period of sinusoidal illumination, photosynthetic phenotyping was obtained two times per hour. Images of the steady-state (Φ_{II}) PSII quantum yields were derived from images of F_S and F_M' using previously reported methods (Cruz *et al.* 2016). Established methods for non-photochemical quenching use F_M and F_0 images at the beginning of the day. Because of large heliotropic movements of cowpea leaves, alternative equations (Tietz *et al.* 2017) were used for generating images of non-photochemical quenching (NPQt), photoinhibition-related quenching (qIt), energy-dependent quenching (qEt) and Q_A redox state PSII center opened (q_L). All image processing was performed using

software (Visual Phenomics 5, https://caapp-msu.bitbucket.io/projects/visualphenomics5.0/) developed in-house in JAVA (Netbeans, link) and based on the open-source Fiji API (https://imagej.net/Fiji). Fluorescence and absorbance measurements were also performed using the hand-held MultispeQ V2.0, based on that described previously (Kuhlgert*et al.* 2016).

2.3.4 Linkage analysis and QTL mapping.

Single nucleotide polymorphism (SNP) markers of genotype data of CB27 x 24-125B-1 were obtained from (Lonardi et al. 2019), based on EST sequences produced by (Muchero et al. 2009). IciMapping 4.1 (http://www.isbreeding.net) was used for construction of the initial linkage-map (Meng, Li, Zhang & Wang 2015), but this was also followed by Rqtl segregation analysis, as described below. Redundant markers were removed using the IciMapping “BIN’ function before constructing the linkage map. The linkage map was constructed using the Kosambi function using its RECORD ordering algorithm (Van Os, Stam, Visser & Van Eck 2005), then aligned against the cowpea consensus genetic map (Huynh *et al.* 2016). For comparisons, QTL analysis was also performed using Multiple QTL Mapping (MQM) model (genome scan with multiple QTL models), introduced by Ritsert Jansen initially (Jansen 2004), as implemented in the Rqtl package (Broman & Sen 2009). The Rqtlfill.geno function, which is based on a Hidden Markov Model, was used to fill in missing genotypic data. Levels of significance were determined using a permutation analysis implemented with the Rqtlmqmpermutation and mqmscan functions, over all replicates, and with the number of permutations set at 1000 and a nominal significance cutoff of $p < 0.05$.

2.3.5 Lincomycin treatment.

For lincomycin experiment, detached leaves are vacuum infiltrated with 0.2 g/L lincomycin hydrochloride until full inundation of cells by the solution. The control plants were vacuum infiltrated with deionized water (DI) with the same procedure. To avoid dryness of leaves, infiltrated leaves were floated in plates with either lincomycin solution or DI water and the non-leaves area is covered by aquarium black sand to avoid light reflection. Following infiltration, plates containing leaves and solution were kept under low light (50 µmol, m^{-2}, s^{-1}) for 20 min and then dark-adapted 20 min for measuring initial Fv/Fm. After that, Fv/Fm measurements were followed by 1hr of high light (HL) (1000 µmol, m^{-2}, s^{-1}) and 20 min dark adaptation to dissipate qE in the DEPI chamber. For the low temperature treatment (LT), the temperature was decreased from 29°C to 19°C and 10°C every two hours of HL treatment (Figure S2.2).

2.3.6 Quantification of nyctinastic leaf movements (NLM).

Qualitative measurements of nyctinastic leaf movement (NLM) values were obtained by measuring relative changes in the projected leaf tip-to-petiole distances of the time-resolved plant fluorescence images. Fluorescence images were taken during saturation pulses (i.e. which were used to estimate F_M"), which showed the strongest contrast against background interference. Each image was thresholded to separate the leaf area from the background using the triangle thresholding algorithm (Zack, Rogers &Latt 1977) which accounts for vignetting effects of the cameras. The image regions for each plant were determined automatically by the code but verified manually, and the tip-to-petiole distance taken as the long axis of a rectangle fitted to the projected leaf image.

To account for differences in leaf morphology and size, fractional changes peak-to-peak distance normalizing to that of the presumed fully expanded leaf states taken at midday.

2.4 Results and Discussions

2.4.1 Dynamic photosynthetic phenotyping of the RIL population.

Figure 2.1 shows heat maps representing the time- and genotype-dependencies of photosynthetic parameters (Φ_{II}, NPQt, qEt, qIt and qL) obtained from DEPI over the three days of the experiment, for control (Panels A-E) and chilling (F-J) treatments. Each row in Figure 2.1 represents the averaged responses (n≥4) for individual genotypes. The rows were ordered based on the average values of Φ_{II} taken on Day 3 (the second day of chilling). The blue and red rectangles represent the 24-125B-1 and CB27 respectively. Color legends for both conditions are set to the same to compare two conditions. For all parameters, significant changes in the low temperature compared to control conditions are shown in Figure S2.3.

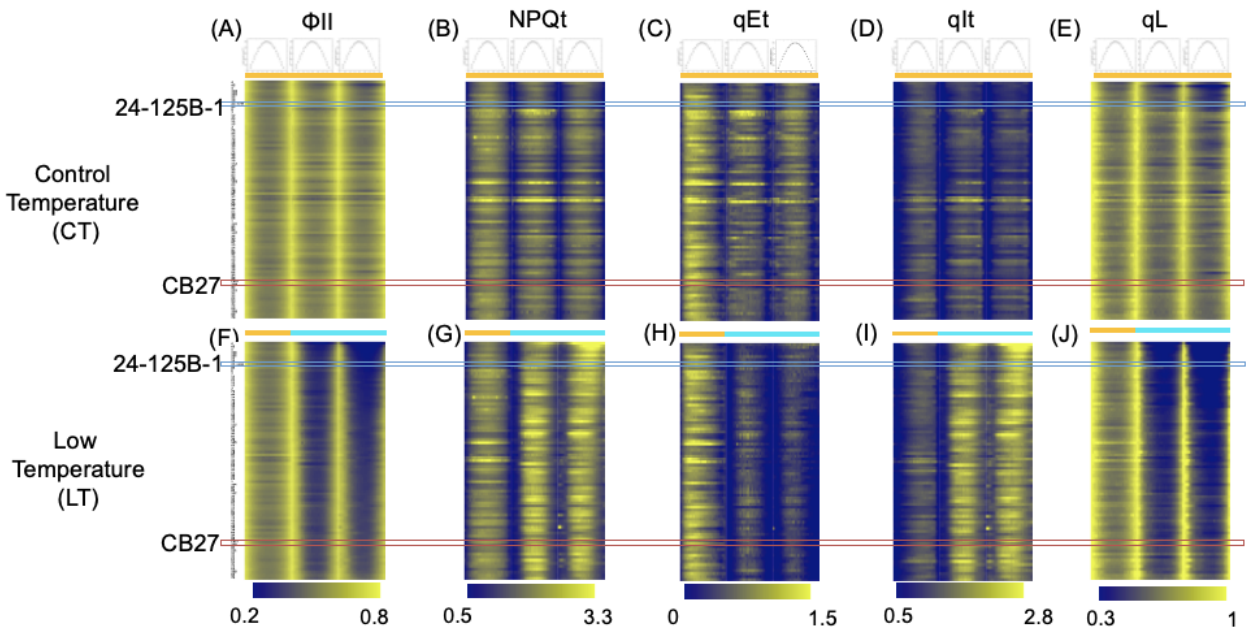

Figure 2.1 High-throughput photosynthetic phenotyping of recombinant lines (RILs) in DEPI chambers under control and low temperatures.
Photosynthetic phenotyping of the CB27 x 24-125B-1 RIL population was performed in a DEPI chamber on five-day-old seedlings over three days. Low (chilling) temperatures were imposed on the second day of imaging under sinusoidal light. Heat maps produced using the OLIVER program (Tessmer et al. 2018) show measured (non-normalized) averaged replicate values over the RIL population (n≥4). Each row represents average values for a different genotype. The blue and red rectangles represent the 24-125B-1 and CB27 respectively. The remaining rows represent individual genotypes over the RIL population. Five photosynthetic parameters were collected by the DEPI chamber during the day, upper panels are control conditions (A - E) and lower panels (F-J) are under chilling conditions. Each row in Figure 1 represents the averaged responses (n≥4) for each genotype. The rows were ordered based on the average values of Φ_{II} taken on Day 3 (the second day of chilling). Color legends for both conditions are set to the same to compare two conditions.

On Day 1, under the control temperature, we observed relatively small variations in Φ_{II} between genotypes and between the first and subsequent days of exposure to the sinusoidal illumination (Figure 2.1, panel A). For each line, Φ_{II} values tended to be high in the morning, decrease towards midday near peak PAR, and essentially fully recover by the end of the day. These patterns indicate that higher PAR levels towards midday partially saturated photosynthesis but did not induce long-lasting

photodamage. Consistent with this interpretation, total NPQt was low in the morning, highest at about midday and fully recovered at the end of illumination. Similar patterns were also seen for the qEt and qIt components of NPQ. Some genotypes showed noticeably larger NPQt values throughout the experiment (e.g. genotypes SRIL-006, SRIL-039, SRIL-105) and these increases could be attributed mainly to increased qEt (compare Figures 2.1B and 2.1C).

Compared to Day 1, measurements under the lower temperatures on Days 2 and 3 showed differences from CT (Figure 2.1 Panels F-J), with lower Φ_{II} values and higher NPQt values, consistent with decreases in productive energy transduction and increases in energy dissipation through NPQ. There were also larger genotype-dependent variations in photosynthetic parameters. In general, we observed a trade-off between fast and slowly relaxing forms of NPQ, with the extent of the rapidly reversible qEt component of NPQ decreased while that of the more slowly reversible components increased. By contrast with CT, Φ_{II} (Figure 2.1F), NPQt (Figure 2.1G) and qIt (Figure 2.1I) values failed to recover at the end of illumination, suggesting that low temperature-induced substantial photoinhibition, photodamage or other long-lasting quenching processes. Another striking feature was the strong decrease in qL during the low temperature treatments, reflecting a more reduced Q_A redox state, after chilling stress (Figure 2.1J), most likely reflecting temperature-dependent decreases in the rates of oxidation of Q_A^- that are not compensated by increases in NPQ.

Figure S2.4 shows histograms of the photosynthetic parameters taken at the middle of the third day of the experiment, at highest light intensity, 500 μmol m^{-2} s^{-1}, under control and low temperature conditions. Going from control to low temperature on

Day 2, Φ_{II}, qL and qEt decreased, while NPQt and qIt increased. Overall, the distributions of values for each parameter across genotypes were substantially larger under the low temperature compared to the control, suggesting the appearance of larger variations in low temperature response traits. The distributions of values substantially exceeded those between the two parental lines, suggesting partial transgressive segregation of traits.

2.4.2 Quantitative Trait Loci (QTL) for photosynthetic parameters show shifting control of photosynthetic processes with stress.

The figure 2.2 shows logarithm of the odds (LOD) score plots of photosynthetic data for a selected time point at 1.5 hr prior to the end of Day 3 (206 μmol m^{-2} s^{-1}), i.e. quantitative trait loci (QTL) for the data in Figure 2.1. We observed several distinct intervals each photosynthetic phenotypes and co-association of intervals on Chrs 4 and 9 (as discussed below). Time course of LOD score plots are in Figure 2.3 and Figure S2.5.

To refer to specific intervals related to different conditions and phenotypes, we established a standard nomenclature to allow comparisons of QTLs that appeared for different parameters, conditions and times that follow the format described in the following:

Chromosome number - Index - Phenotype - Temperature

where control and low temperature are abbreviated as CT and LT. The indexes are numbered with Arabic numerals in the order of genomic loci of identified QTLs in each chromosome for the QTLs for that phenotype. Table 2.1 summarizes the name, genomic locations, flanking markers and conditions for each QTL.

It is important to note that, while we assigned names for apparently overlapping regions of significant associations, multiple causative polymorphisms may underlie these regions, as discussed below). It is also noteworthy that the parameters measured by DEPI were all based on analysis of chlorophyll fluorescence and thus systematic artifacts in measurements could affect all parameters. However, the facts that the individual parameters show distinct patterns over time, and that similar patterns appeared in completely independent parameters, obtained with the MultispeQ instrument (below) further substantiates our interpretation that they reflect different (but interacting) processes.

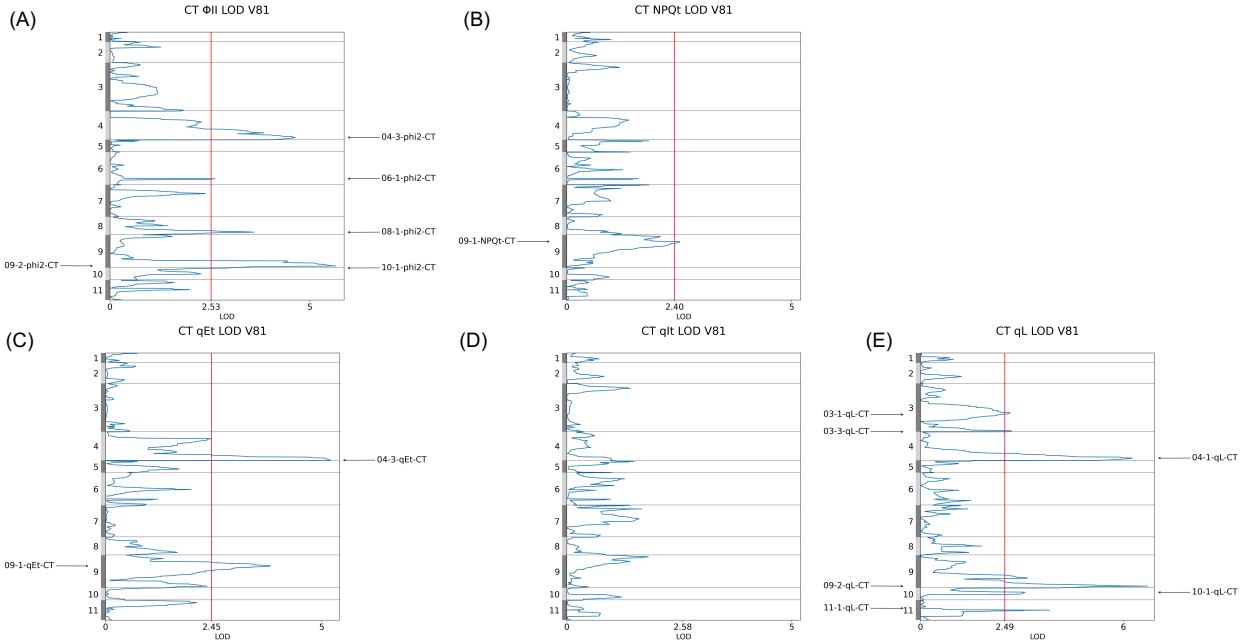

Figure 2.2 QTL analysis of photosynthetic parameters from DEPI in the low temperature condition.
Logarithm of the odds (LOD) score plots of photosynthetic data (A, Φ_{II}; B, NPQt; C, qEt; D, qIt; E, qL) from DEPI in the LT condition measured at 1.5 hr prior to the end of Day 3 (206 µmol m^{-2} s^{-1}). The genetic position is indicated by the y-axis. LOD scores above statistical thresholds, determined by permutation analysis as described in Materials and Methods, are indicated by the red lines. The index is numbered with Arabic numerals in the order of genomic loci in each Chr for the QTLs for that phenotype.

Figure 2.3 shows a time course for statistical associations between genetic markers and photosynthetic parameters. The results are plotted as heat maps with color indicating the log of odds (LOD) scores for the association of phenotypic differences with genomic markers. Distinct patterns of QTL were observed for each control day and chilling treatment days, as well as over the time course of each day.

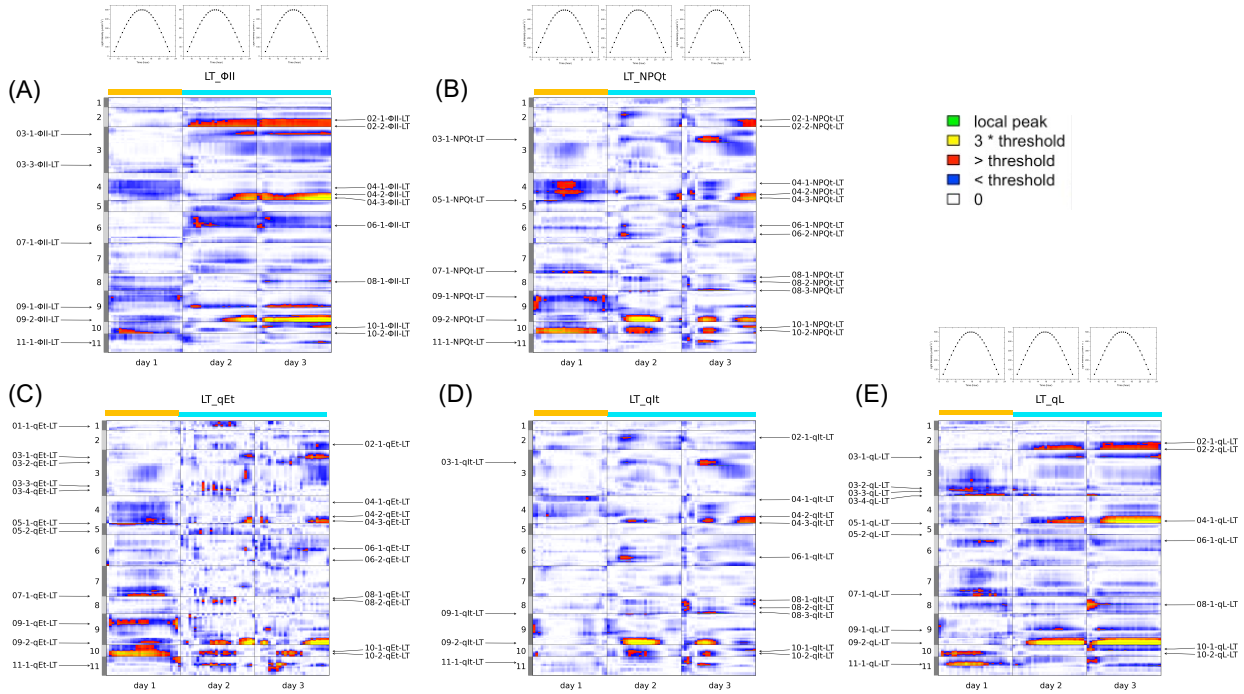

Figure 2.3 Time-resolved QTL associations for five photosynthetic parameters (A, Φ_{II}; B, NPQt; C, qEt; D, qIt; E, qL) from DEPI chamber experiments for the CB27 x 24-125B-1 RIL population.
The logarithm of the odds (LOD)scores through the time represented as heat maps. The time is indicated on the x-axis and the genetic position is indicated on the y-axis. Day 1 was taken under the control temperature (29°C/19°C, day/night temperatures, orange bar), and the following days were conducted under chilling conditions (19°C/13C°day/night temperature, blue bars). The light intensities (photosynthetically active radiation, PAR) patterns and temperatures are shown above each column of panels. The heat map colors indicate the LOD score as indicated in the legend to the upper right of the panels. LOD scores above statistical thresholds, determined by permutation analysis as described in Materials and Methods, are indicated by red coloration. The apparent local peaks for QTL intervals are indicated by green lines. Each apparent QTL region is labeled according to the naming scheme described in the main text, as chromosome- index- phenotypes- temperature condition (low temperature, LT). The index is numbered with Arabic numerals in the order of genomic loci in each Chr for the QTLs for that phenotype.

On Day 1, two significant QTL intervals were observed for Φ_{II} and qIt (Chr 10), but more intervals were observed for NPQt, qEt and qL (Chrs 3, 4, 5, 6, 7, 9, 10 and 11). As discussed below, some of the intervals overlapped those for different parameters and/or different time points, while others did not. The LOD scores for these intervals changed throughout the day with different patterns. For example, a QTL region for Φ_{II} on Chr 10 (10-2-Φ_{II}-CT/LT) appeared stronger in the morning, but decreased at later times, whereas a interval for qIt on 10 (10-2-qIt-CT/LT) appeared transiently at about the second time point of the day. Other QTLs appeared more constantly over the day, e.g. the intervals for NPQt and qEt on Chrs 7 and 10.

On Day 2, the first day of chilling, a distinct set of QTLs and temporal patterns appeared. While a subset of QTL intervals were carried over from Day 1 (Chr 3 for qL and Chr 10 for NPQt, qEt and qIt), some intervals disappeared, e.g. Φ_{II} and qL (e.g. 10-2-Φ_{II}-LT and 10-1-qL-LT on Chr 10), while new intervals appeared, e.g. for Φ_{II} and qL on Chr 2 (02-1,2-Φ_{II}-LT and 02-1,2-qL-LT). These changes in QTL patterns were not seen in the control experiments (Figure S2.5), where the temperature of the chamber was not decreased, indicating that they represent temperature-specific genetic effects. Some of the new intervals appeared at very early time points compared to other parameters (e.g. qEt-04-3-LT and qEt-09-2-LT), suggesting that they represent initial effects of low temperature, while others emerged at later times, suggesting they reflect the accumulation of effects under low temperature.

Most of those QTLs found on Day 2 (Φ_{II}, NPQt and qEt on Chrs 2, 4, 6 and 9), were also observed on Day 3, at least at some time points. However, some intervals disappeared (e.g. qEt on Chrs 1, 3, 5 and 8), while new intervals (e.g. NPQt on Chr 11)

appeared.

The data in Figures 2.1 and Figure S2.4 show that distinct sets of polymorphisms represent potential photosynthetic control mechanisms under different conditions. This type of behavior has been previously observed (e.g., Flood et al. 2011; Prinzenberg et al. 2020), and can be attributed to the imposition of different, genetically-controlled limitations or regulatory mechanisms under different conditions. The patterns of QTLs change over the course of the experiment, indicating that, under different conditions, distinct sets of genetic components contribute to changes in the control and regulation of photosynthesis. In one example, under CT, fewer intervals were observed under low PAR, where photosynthesis is likely to be light-limited, and a larger, distinct set of intervals appeared under higher light (e.g.09-2-Φ_{II}-CT, 09-2-qEt-CT and 09-1-qIt-CT), where we expect more processes to limit photosynthesis.

Going from the CT to LT on Day 2, we observed a loss of some QTL intervals, e.g. Φ_{II} and qL (e.g. 10-1-Φ_{II}-LT and 10-1-qL-LT on Chr 10), and the appearance of a larger number of distinct QTL across the various parameters (Figure 2.2, 02-1/2-Φ_{II}-LT and 02-1/2-qL-LT). This result is consistent with the observed higher variability of parameters across the population for the various parameters (Figure S2.4, suggesting additional impact of genetic components under the non-ideal conditions. Some of the new QTL intervals appeared at very early time points compared to other parameters (e.g. 04-3-qEt-LT and 09-2-qEt-LT), suggesting that they represent initial effects of low temperature, while others emerged at later times, suggesting they reflect the accumulation of effects under low temperature. Overall, these behaviors point to a stress-related shift from one set of processes that is relatively insensitive to the genetic

diversity in the panel, to another set that is more strongly impacted by genetic differences.

2.4.3 Co-association of genomic associations reveal potential genetic and mechanistic control networks.

As can be seen by comparing the LOD plots in Figure 2.2 and heat maps in Figure 2.3, the photosynthetic parameters showed apparent overlaps (co-segregation) with several photosynthetic parameters, consistent with the known interactions among the processes that underlie the measurements. For instance, increasing NPQ often results in a decrease in Φ_{II}, so one may expect apparent linkages. However, as will be seen below, the cases where linkages are not observed, or where the effect directions are not as expected, can be quite informative about possible mechanisms. Note that LOD scores reflect the statistical association rather than effect size, so noisy data can also impact the appearance of a QTL. However, we confirm, below, that the effect sizes show similar behaviors.

Figure 2.4 summarizes the appearance of overlapping QTLs for the strongest QTL intervals for photosynthetic parameters on Chrs 4, 9 and 8. Different combinations of overlapping QTLs for the various photosynthetic processes appeared at different time points under both control and chilling stress (Figure 2.3 and Figure S2.5). The time course of these connections may, to some extent, reflect the sequence of events that leads to the eventual aggregate phenotypes, as discussed in more detail below.

On Day 2, overlapping QTLs appeared on Chr 4 and 9 (04-2/3-Φ_{II}-CT, 04-3-qEt-CT, 04-1-qL-CT, 09-2-Φ_{II}-CT, 09-2-qEt-CT, 09-2-qL-CT, 04-2/3-Φ_{II}-LT, 04-2/3-qEt-LT, 04-1-qL-LT, 09-2-Φ_{II}-LT, 09-2-qEt-LT, 09-2-qL-LT) for Φ_{II}, qEt and qL under both CT

and LT conditions, suggesting that these loci impacted photosynthesis under both conditions (Figure 2.3A-B and D-E). The intervals for qEt and qL appeared earlier than those for the other parameters. This trend was more pronounced at LT compared to CT, where the intervals for qEt and qL appeared substantially earlier at LT, suggesting that genetic variations affected the early onset of the photoprotection with subsequent impact on Q_A redox state.

The most striking differences between CT and LT in the Chr 4 and 9 intervals were the impact on NPQt and qIt. CT induced only a short, transient interval for qIt on Chr 4 in the morning (Figure 2.3A) and none on Chr 9 (Figure 2.3B). By contrast, under LT, qIt-related intervals appeared on both Days 2 and 3 soon after the onset of illumination and persisted for most of Day 2 (Figure 2.3D-E), showing temperature-induced photoinhibition. Similar results were seen for Day 3, with the notable exception that the intervals for NPQt and qIt persisted over longer time periods.

The interval on Chr 8 (08-1-Φ_{II}-LT, 08-2-NPQt-LT, 08-2-qIt-LT and 08-1-qL-LT) showed LT-specific effects, but these were predominantly restricted to the morning and evening of Day 3, when light levels were low, indicating that this interval may be associated with longer-term effects, e.g., accumulated photodamage, repair or acclimation responses.

Overall, these results suggest a model where the photosynthetic responses are qualitatively affected by Chrs 4 and 9 loci under both conditions, but with stronger impacts under LT, giving rise to long-lived forms of NPQ, likely reflecting the accumulation of photodamage to PSII. Further, a locus under the intervals on Chr 8 may modulate the response to LT on photoinhibition over longer time periods.

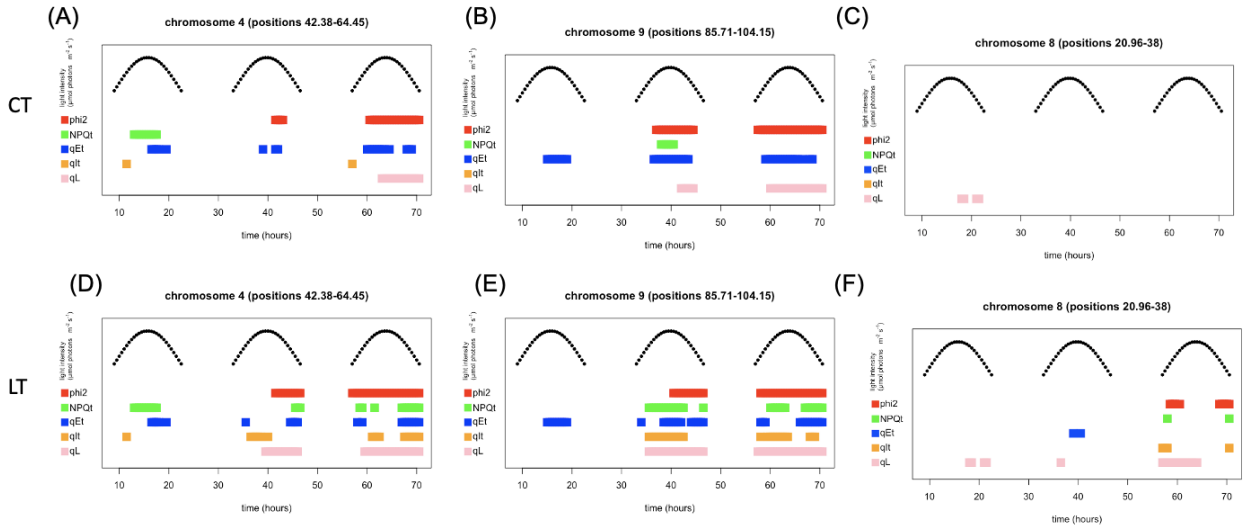

Figure 2.4 Time course for the appearance and disappearance of the QTLs of five photosynthetic parameters in the selected three loci, Chrs 4, 9 and 8.
The appearance and disappearance of the QTLs for three selected loci, Chr 4 42.38-64.45cM (A and D), Chr 9 85.71-104.15 cM (B and E) and chr 8 20.96-36cM (C and F). Conditions were as in Figure 2.1The time course for photosynthetically active radiation (PAR) is shown in the upper part of each panel. The presence of significant QTL intervals at the respective positions for each phenotype are shown as filled rectangles with different colors: Φ_{II}, red; NPQt, green; qEt, blue; qIt, orange; qL.

2.4.4 Time-resolved MultispeQ measurements for two parental lines.

Figure 2.5 shows more detailed photosynthetic measurements made using the MultispeQ instrument taken for the parent lines under the same conditions as the experiment in Figure 2.1 To avoid disturbing the plants, only 5 measurements were made per day, at the times indicated in Figure 2.4. In general, measurements made with both DEPI and MultispeQ showed similar trends. On Day 1, no (or only small) differences were seen between CB27 and 24-125B-1 for all MultispeQ phenotypes, but significant differences emerged under LT treatment on Days 2 and 3.

Compared to CB27, 24-125B-1 showed decreased Φ_{II} (Figure 2.5A), increased NPQt (Figure 2.5B) and decreased qL (Figure2.5C). These effects were accompanied

by significantly higher ECSt, particularly at the beginning of days 2 and 3 (Figure 2.5D), indicating a larger thylakoid *pmf*. However, the thylakoid proton conductivity, *g*H+, was either not significantly different, or differed by only small amounts (Figure 2.5E), implying that the increased *pmf* in the sensitive line could not be explained by slowing of ATP synthase activity. The light-driven protons flux, estimated by the *v*H+ parameter, was increased in the sensitive line, particularly at the beginning of Day 2, suggesting that the increased *pmf* was related to elevated proton fluxes. The ratio of *v*H+/LEF can be used as an indicator of contributions to proton flux from CEF and LEF (Baker *et al.* 2007). In the absence of CEF, we expect a constant *v*H+/LEF because LEF should translocate a constant 3 H^+/e^-. Engagement of CEF should result in increased *v*H+/LEF. As shown in Figure 2.5I, we observed periods of higher *v*H+/LEF, indicating that CEF likely contributed to the observed elevated *pmf* in 24-125B-1 throughout Day 2 and the beginning of Day 3 and Day 4. We observed significantly increased levels of oxidized P_{700}+ in 24-125B-1 on Day 3 (Figure 2.5G), accompanied by the decreased rate constant for P_{700}+ re-reduction (k_{b6f}, Figure 2.5H), consistent with a larger photosynthetic control imposed by the higher *pmf*.

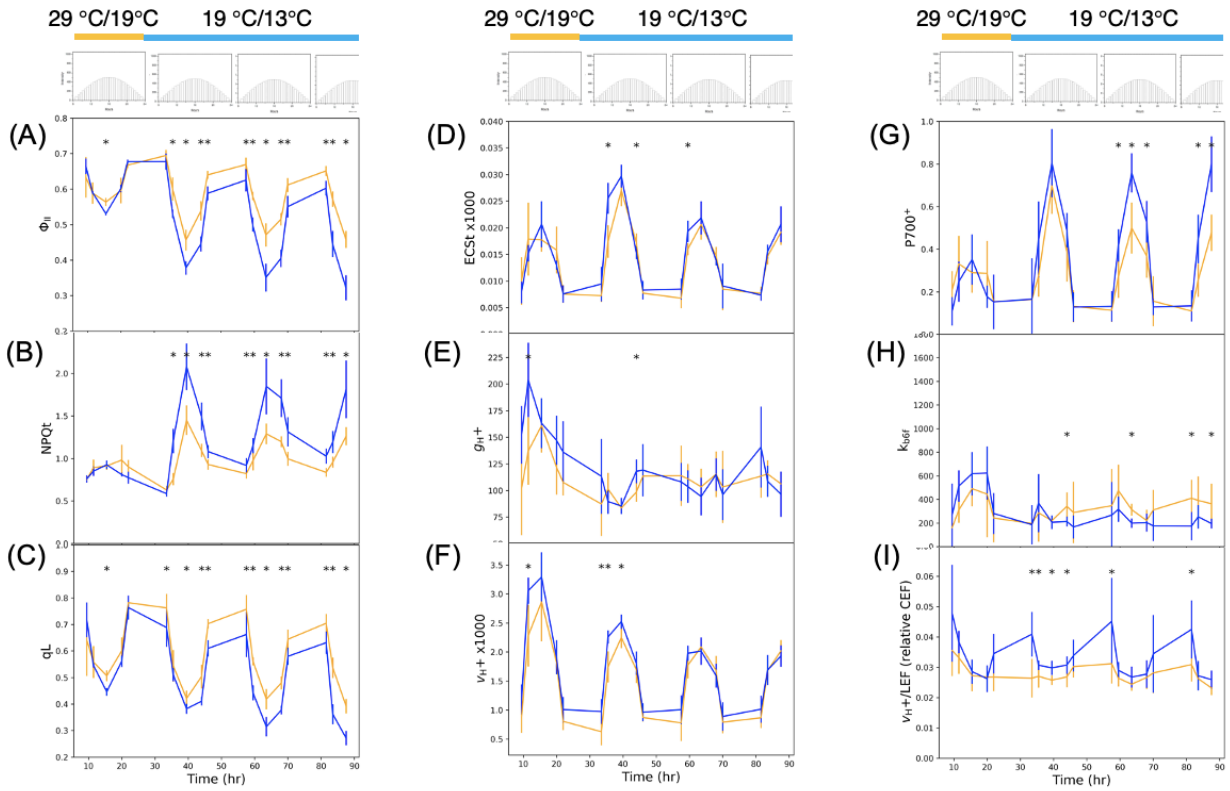

Figure 2.5 Time-resolved MultispeQ measurements of two parental lines at low temperature.
Panel A, Φ_{II}; Panel B, NPQt; Panel C, qL; Panel D, ECSt; panel E, *g*H+; Panel F, *v*H+; Panel G, P700+; Panel H, k_{b6f}; Panel I, relative CEF as estimated by *v*H+ over LEF from MultispeQ. Day 1 was taken under the control temperature (CT, 29°C/19°C, day/night temperatures, orange bar, and the following days were conducted under low temperature (LT, 19°C/13C°day/night temperature, blue bars). The light intensities (photosynthetically active radiation, PAR) patterns and temperatures are shown above each column of panels. The measurements were taken at five light intensities on Day 1 to 3, following a sinusoidal pattern, 103, 301, 500, 301 and 103 µmol m^{-2} s^{-1}(0.5, 2.5, 6.5, 11 and 13 hr after illumination). On Day 4, three measurements are done at 103, 301, 500µmol m^{-2} s^{-1} (0.5, 2.5 and 6.5 hr after illumination). The averaged response of n≥4 biological replicates (n≥4) for each photosynthetic phenotype value of two parental lines are shown as orange for CB27 and blue for 24-125B-1. The significant differences between two parental lines by t-test at each point are shown as asterisks at top of the plot ($p<0.05$).

2.4.5 Detailed phenotyping of the entire RIL population using MultispeQ instruments.

To explore potential underlying genetic connections, we performed measurements across the entire RIL population using MultispeQ instruments. Because

MultispeQ measurements require clamping of individual leaves, measurements were made at a selected time and conditions at control and low temperature conditions at middle of third day of chilling treatment day (highest light intensity), and thus represent both acute and acclimatory responses to the different conditions.

As with the DEPI results (Figure S2.4A-F), LT resulted in decreases (compared to CT) in the average Φ_{II} (Figure S2.6A) and increases in average NPQt (Figure S2.6B); the distributions of both parameters broadened at low temperature, indicating larger diversity in photosynthetic responses under environmental stress, as also seen for the DEPI results (Figure S2.4). The average qL values were increased compared to the DEPI and MultispeQ results on Days 2 and 3 (Figure S2.4C and S2.6C), suggesting that regulation of photosynthesis had partially acclimated.

Figure S2.6G shows that the extent of dark-interval relaxation kinetics (DIRK) absorbance changes at 810 nm, showing that P_{700} became more oxidized when plants were exposed to chilling temperature (Figure S2.6G, $p<0.05$). The rate constant for P_{700}+ re-reduction, as measured by the 810nm decay kinetics (k_{b6f}, Figure S2.6H, $p<0.05$), decreased at low temperature, implying that slowing of electron flow to PSI contributed to the observed net oxidation of P_{700}+. This effect likely reflects the onset of "photosynthetic control" (PCON) due to acidification of the thylakoid lumen and subsequent slowing of PQH_2 oxidation at the cytochrome *b*$_6$*f* complex (Chow & Hope 2004; Takizawa *et al.* 2008).

Figure S2.6D shows the effects of temperature on the distribution of light-induced thylakoid *pmf*, as estimated by the ECSt parameter (Baker *et al.* 2007), normalized to relative chlorophyll content as described in Materials and Methods. Low

temperature-induced significant increases in the average ECSt ($p<0.05$), suggesting an increase in light-driven thylakoid *pmf*.

The proton conductivity of the thylakoid (*g*H+, Figure S2.6E), which predominantly reflects the activity of the thylakoid ATP synthase was significantly decreased at LT compared to CT ($p <0.05$), likely indicating a temperature-dependent decrease in the chloroplast ATP synthase activity. Figure S2.6F shows that the average *v*H+, an estimate of the light-driven proton flux through both LEF and CEF (Takizawa *et al.* 2008), decreased at low compared to control temperature ($p <0.05$), similar to changes in LEF and Φ_{II}. The ratio of *v*H+/LEF, an indicator of the extent of cyclic electron flow (CEF) (Avenson, Cruz, Kanazawa & Kramer 2005a; Baker *et al.* 2007), was higher under LT compared to CT.

Overall, these results indicate substantial alterations in control or regulation of photosynthetic processes on the third day of LT exposure, with (on average) and increase in CEF and decreases in ATP synthase activity, leading to increased *pmf* and PCON, and substantial increases in NPQ and decreases in Φ_{II} and LEF. However, there were strong variations in these responses, likely reflecting genetic differences across the population.

Detailed QTL analyses for MultispeQ parameters are shown in Figures S2.7-S2.8 and Table 2.2. Several QTL intervals were identified in photosynthetic parameters in both CT and LT (Chrs 4,6,8 and 9 etc.); we focus here on intervals on Chrs 4 8 and 9, which showed potential overlaps with those found using the DEPI platform (Figure 2.3). Figure 2.6 shows associations for selected QTL intervals on Chrs 4, 8 and 9 in the form of “Daisy Graphs,” in which specific QTL intervals are indicated in the center circles,

different phenotypes are indicated by surrounding circles, with the thickness of the connecting lines set proportional to the LOD score for association. The solid lines represent significant positive associations between the phenotype and the allele present in the tolerant (CB27, orange) and sensitive (24-125B-1, blue) lines. The overlap in these regions is consistent with co-association of the phenotypes to genetic loci in these regions, though as discussed below, we cannot rule out the participation of multiple loci.

Daisy plots for QTLs showed linkages to QTLs regions on Chrs 4 (marker positions 59.04-64.45 cM), 9 (marker positions 86.93-104.15 cM) under both CT (Panels A and B) and LT (Panels D and E), similar to the results from DEPI. The Chr 4 QTL intervals showed negative associations with the CB27 alleles for one set of parameters (Φ_{II}, k_{b6f}, vH+, gH+, ECSt, and qL) but positive associations for P700+. (Such a positive association means that the presence of the CB27 allele tends to increase the value of that parameter). Only weak associations were observed for relative chlorophyll content (SPAD) and NPQt. Strikingly, the Chr 9 region showed the inverse relationships, i.e., positive associations with the CB27 alleles for one set of parameters (Φ_{II}, k_{b6f}, vH+, gH+, ECSt, and qL) and negative associations for P700+. These results suggest that the loci on Chrs 4 and 9 have opposing effects on photosynthetic responses (see below).

A comparison of CT and LT (Figures 2.4 D and E) shows that the patterns of associations to QTLs on Chrs 4 and 9 were similar, except that significant associations with NPQt only appeared under LT, most obviously to the region on Chr 9. These results are consistent with those from DEPI and suggest that, while the regions on Chrs 4 and 9 had qualitatively similar effects on most photosynthetic parameters, these were

linked to increased photodamage or photoinhibition, specifically under low temperature.

A distinct pattern of associations appeared for the region on Chr 8 (Figure 2.6 Panels E and F, marker positions 22.81- 28.59 cM), which showed no significant associations under control temperature, but significant associations with Φ_{II} and NPQt under low temperature. The lack of connections to the other photosynthetic parameters suggests that Chr 8 controls NPQt through a mechanism that is distinct from that controlled by Chrs 4 and 9 (see also below).

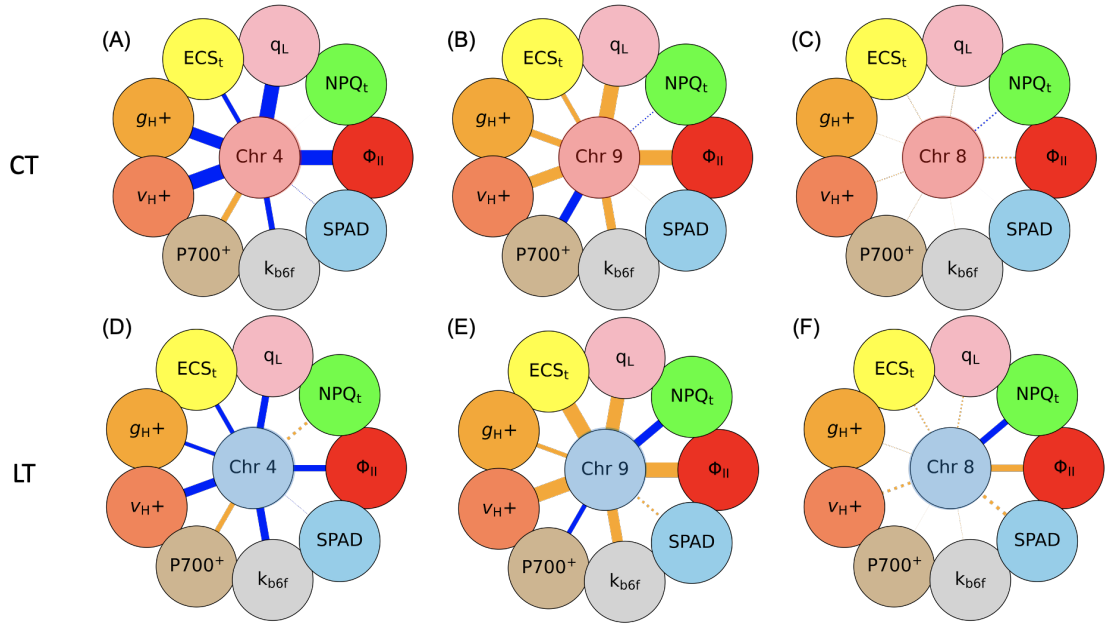

Figure 2.6 The associations for selected QTL intervals of photosynthetic parameters from MultispeQ in CT (A-C) and LT (D-F) at Chr 4, 59.04-64.45 cM (A and D) and Chr 9, 86.93-104.15 cM (B and E), Chr 8, 22.81- 28.59 cM (C and F). LOD score plots from previous figures (Figures S2.7 and S2.8) were replotted as in the form of "Daisy Graphs," in which specific Chr is indicated in the center circles, different phenotypes are indicated by surrounding circles, with the thickness of the connecting lines set proportional to the LOD score for association (Max LOD 10 is set to 10, so above the LOD 10 is shown as same max thickness). (For details of each plot, refer to original figures, Figures S2.7 and S2.8). Solid lines represent significant positive associations between the phenotype and the allele present in the tolerant (CB27, orange) and sensitive (24-125B-1, blue) lines. Below the threshold, each phenotype is shown as dashed lines.

2.4.6 Effect size contributions of specific QTL intervals to photosynthetic phenotypes.

In this section, we explore the effect sizes and directionalities of genetic markers on the observed phenotypes. Individuals of the RIL population are homozygous for each marker in the two parental lines, as indicated by the designations of either AA, having the allele from CB27 (tolerant, maternal line), or BB, having the allele from 24-125B-1 (sensitive, paternal line)

We first estimated genetic contributions from the QTL on Chrs 4 and 9 individually, by dividing the population into groups, having AA or BB markers at the peak positions for the two QTLs. The examples in Figures. 2.7 A-D show the effects of QTL intervals on Chrs 4 and 9 on Φ_{II} (04-2,3-Φ_{II}-CT/LT and 09-2-Φ_{II}-CT/LT) and qIt (04-2,3-qIt-LT and 09-2-qIt-LT) at 1.5 hr prior to the end of day 3. This time point was chosen because it reflects both immediate changes in photosynthesis and the accumulation of photodamage or photoinhibition. However, as implied by the timeline in Figure 2.4, similar results will likely be observed over a range of time points.

At CT, genotypes with the AA allele at 04-2,3-Φ_{II}-CT showed a lower average Φ_{II} compared to those with the BB allele (Figure 2.7A). The opposite effect was seen for the QTL on Chr 9, where the AA allele conferred a higher Φ_{II} compared to BB. At CT, no difference was seen in qIt between the parent lines, indicating that the effects on Φ_{II} and other processes did not result in the accumulation of substantial amounts of photoinhibition (Figure 2.7B).

Across all genotypes, going from CT to LT resulted in decreased in Φ_{II} and increased in qIt. However, qualitatively similar trends were seen for the dependence on

alleles at Chr 4 and 9 for Φ_{II} (04-2,3-Φ_{II}-CT/LT and 09-2-Φ_{II}-LT) and qIt (04-2,3-qIt-LT and 09-2-qIt-LT), but with substantially larger effect sizes in LT.

Larger genotypic effects were observed for qIt. Plants with the AA allele at Chr 4 showed higher average qIt values compared to those with BB, while plants with the AA allele at Chr 9 showed lower average qIt values compared to those with AA (Figure 2.7B). This result is consistent with stronger LT-induced effects that result in the accumulation of photodamage.

To test for additivity or epistasis, we assessed the combined effects of both sets of alleles (Figures. 2.6E and F), dividing the population into the four possible genetic combinations, AAAA, AABB, BBAA and BBBB for alleles from each parent for Chr 4 and Chr, e.g. the AABB genotype has the CB27 allele on the Chr 4 QTL and that for 24-125B-1 in the QTL on Chr 9. Note that AAAA and BBBB showed no significant differences under both conditions and parameters (Figure S2.9), and thus we present averaged AAAA and BBBB for each parameter and condition, only showing three groups in Figure 2.7E-F. Under both temperatures, the AABB genotypes showed the lowest Φ_{II}, while the BBAA genotypes showed the opposite extreme. The AAAA and BBBB genotypes showed only small differences, suggesting that the effects of the two alleles canceled each other out in these genotypes. These results suggest that polymorphisms within the QTL on Chrs 4 and 9 have additive, but opposite effects on Φ_{II}, under both temperatures. These trends were more extreme under LT, suggesting that the lower temperature accentuated the genotypic effects.

Interestingly, qualitatively different effects were observed for qIt between CT and LT. At CT, only small effects were seen between the AABB and BBAA genotypes,

suggesting that the differences in Φ_{II} or other properties did not impose large differences in photodamage or photoinhibition. By contrast, large genetically-controlled effects were seen at LT, with the AABB genotypes showing the largest extents and BBAA showing the smallest. These results support the model where interactions between temperature and genotypes were sufficiently severe that they led to substantial differences in photodamage.

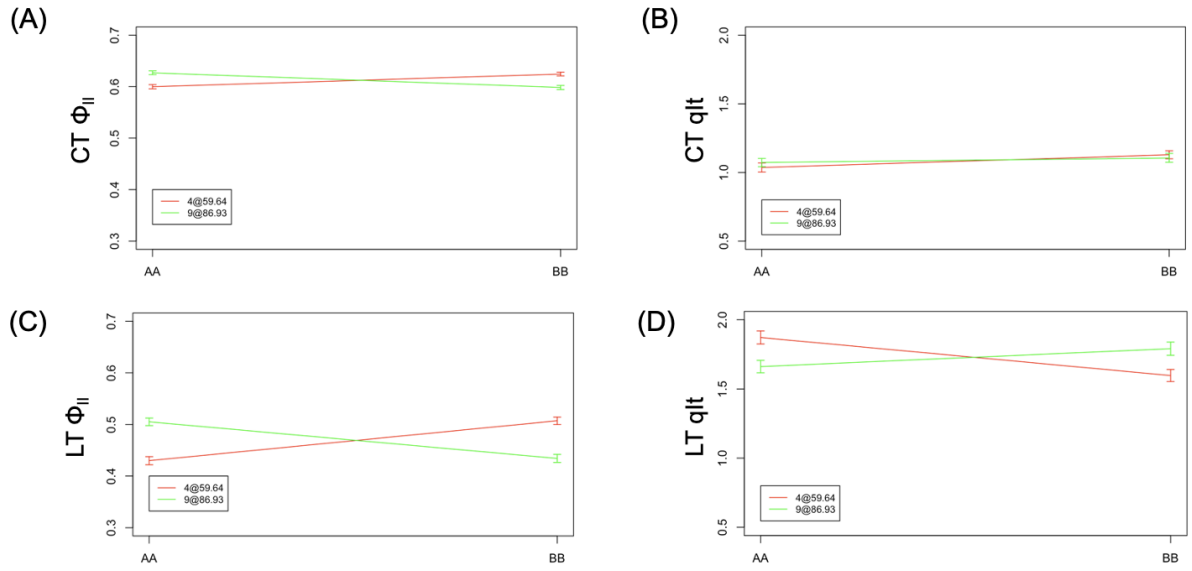

Figure 2.7 Effect plots (A-D) and box plots (E-F) of identified QTLs in Chrs 4 and 9 for Φ_{II} and qIt at 1.5 hr prior to the end of Day 3 (206 µmol, m^{-2}, s^{-1}).
(A-D) Each panel shows the mean of Φ_{II} (A,C) and qIt (B,D) by indicated as y-axis in each condition (CT: A-B and LT: C-D) against allele (either AA or BB) at identified QTLs in chr 4, 59.64 cM (red) and 9, 86.93 cM (green).(E-F) Box plots for Φ_{II} (E) and qIt (F) in both conditions (CT and LT are colored by red and blue respectively) grouped by alleles from identified QTLs in Chrs 4 and 9, AABB, BBAA and averaged AAAA and BBBB. The line connects each mean of the group. Significant differences between conditions for each group ($p<0.05$, t-test) are shown as the asterisk at the bottom of the plots. (E-CT/LT, F-CT/LT) Significant differences of Φ_{II} or qIt between groups ($p<0.05$, t-test) are shown as the asterisk in the bottom of the plots for each condition.

Figure 2.7 (cont'd):

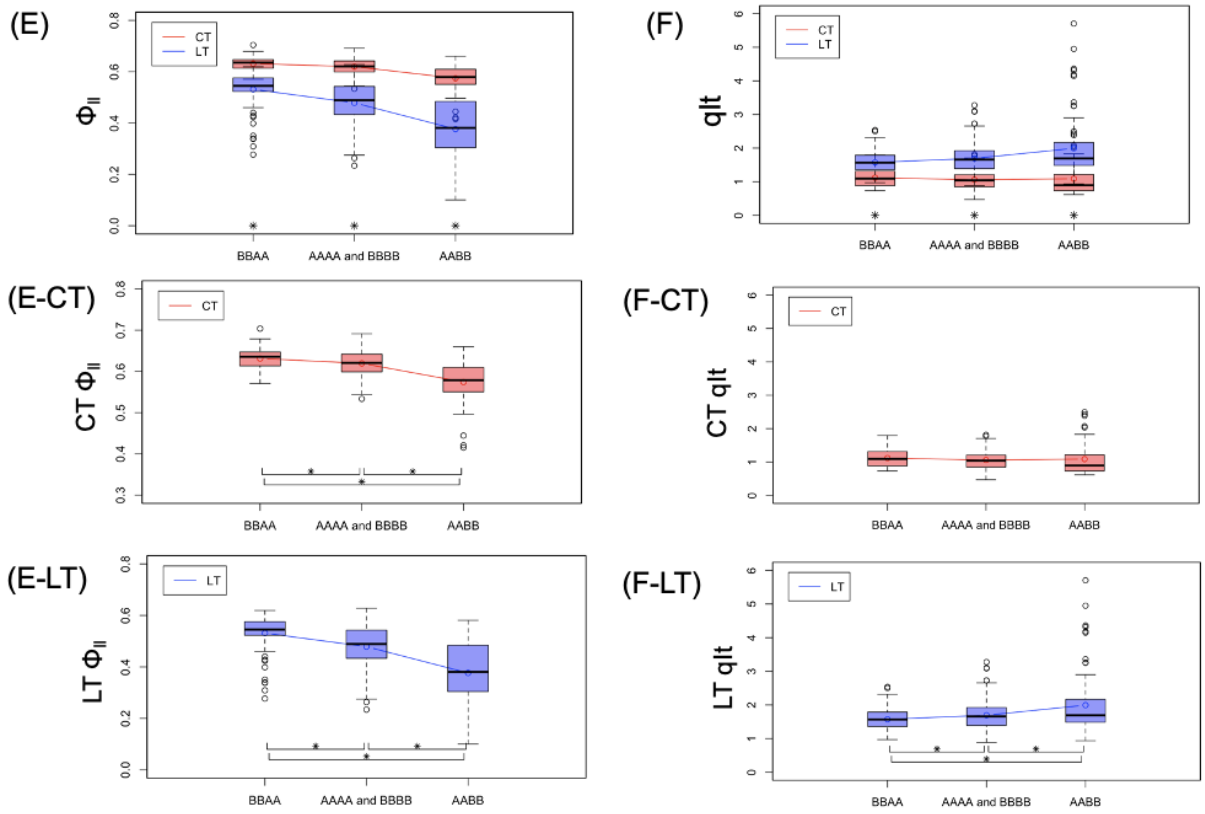

2.4.7 Genetic effects on photoinhibition at low temperature are predominantly controlled by altering rates of photodamage.

The results above suggest that the major QTL polymorphisms impact photosynthesis under both CT and LT, but have cumulative, substantial secondary effects on PSII photoinhibition, as estimated by chlorophyll fluorescence, only at the lower temperatures. Two basic mechanisms have been proposed to control the extent of PSII photoinhibition, altering the rates of PSII photodamage, and altering the rates of PSII repair (Aro*et al.* 1993; Murata, Takahashi, Nishiyama & Allakhverdiev 2007). To distinguish between these mechanisms, we measured (Figure 2.8) the effects of illumination with high light (1000 μmol m^{-2}, s^{-1})on maximal PSII quantum efficiency in the

presence and absence of lincomycin, which blocks PSII repair by inhibiting protein synthesis in the plastid (Tyystjärvi&Aro 1996). Because the effects of the alleles in the QTLs for Chrs 4 and 9 partly compensated for each other, we compared the two parental lines (CB27 and 24-125B-1, Figure 2.7A and B) and two selected progeny lines (Figure 2.8C and D) that contained the AABB and combinations of alleles for the QTL on Chr 4 and 9 and showed the largest differences in Φ_{II} values (Figure 2.7F): RIL-60, with genotype BBAA, which at LT showed the highest Φ_{II} and lowest qIt values at LT, while RIL-4, with genotype AABB, showed the smallest Φ_{II} and largest qIt values.

In the absence of lincomycin, the parent lines show only small differences in loss of PSII efficiency during exposure to high light (Figure 2.8A). However, when infiltrated with lincomycin, the sensitive (24-125B-1) showed stronger losses of PSII efficiency that proportionally increased at lower temperatures (Figure 2.8B). These results imply that PSII was photodamaged more rapidly in the sensitive line, but that repair was sufficient to maintain similar steady-state levels of PSII activity in the two lines. Stronger effects were observed between RIL-4 and RIL-60, which showed progressively larger increases in photoinhibition, even in the absence of lincomycin. These effects were larger in the presence of lincomycin, suggesting that a substantial fraction of the increased photoinhibition was caused by increased rates of photodamage, with smaller contributions from repair.

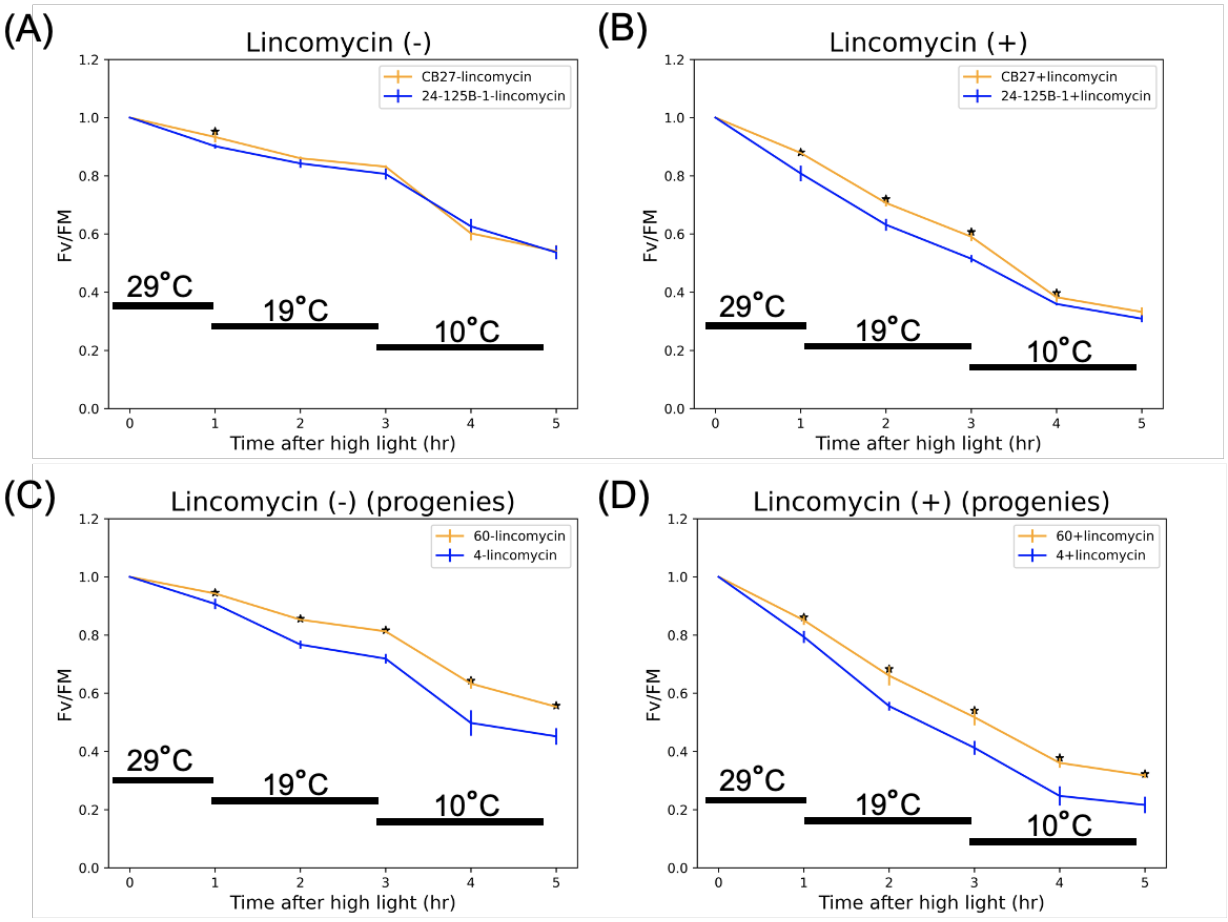

Figure 2.8 PSII photodamage and repair during exposure to high light at a range of temperatures.

Relative changes in the quantum efficiency of photosystem II (PSII) estimated by the saturation flash-induced increases in chlorophyll fluorescence, measured in darkness as described in Materials and Methods. Two pairs of genotypes were compared: Panels A and B show comparisons between the two parental lines and Panels C and D compare two selected progeny lines that contained combinations of alleles for the QTL on Chr 4 and 9 that consistently showed the largest (RIL-60, with genotype BBAA) and lowest (RIL-4, with genotype BBAA) effects on Φ_{II} in the experiments described in Figure 2.5. Intact, detached unifoliate leaves, comparable to those imaged during the experiment described in Figure 2.1, were vacuum infiltrated with either 0.2 g/L lincomycin (B and D) to prevent PSII repair, or deionized water as a control (A and C) and floated on these solutions during exposure to high light to prevent drying. Measurements were conducted using the DEPI chamber described in Figure 2.1, but leaves were exposed to constant, high light (1000 µmol, m^{-2}, s^{-1}) for one hour under a sequence of decreasing temperatures, from control or growth temperature (CT, 29°C), low temperature (LT, 19°C, as used in the DEPI experiments shown in Figure 2.1) and very low temperature (10°C). Values of F_v/F_M'' were measured periodically during the experiment, after a 20 minutes dark period to allow for relaxation of qE, and normalized to the maximum PSII efficiency measured in dark-adapted samples (F_v/F_M). The averaged replicates (n≥3) ± S.D are shown.

2.4.8 The photosynthetic proton circuit and Q_A redox state modulate the genetic effects on temperature stress.

To explore possible mechanisms for the increased rates of photodamage in the sensitive lines, we assessed the genotype dependencies of more detailed photosynthetic parameters taken with MultispeQ across the entire RIL population, as in Figure 2.4. Figure 2.9A shows average values of qL against Φ_{II} at the peak light intensity at CT and LT (Day 3), grouped by their genotypes for QTL on Chr 4 and 9, i.e., those with AAAA, AABB, BBAA and BBBB, as in Figure 2.7.

For CT, there was a continuous, nearly linear relationship between qL on Φ_{II}. However, genotypes having the BBAA and AABB genotypes showed the highest and lowest values for both parameters ($p<0.05$ by t- test), while those with AAAA and BBBB showed intermediate values (NS) (Figure S2.10).

A qualitatively similar trend was observed at LT, but with markedly stronger decreases in the AABB compared to the BBAA genotypes, with qL reaching substantially lower values. These results are consistent with models where increased PSII excitation pressure (Huner, Öquist&Sarhan 1998), caused by the accumulation of reduced Q_A, caused increased rates of PSII photodamage at LT, with this effect being stronger in the genotypes containing the AABB alleles.

Figure 2.9B shows the dependence of NPQt on ECSt, measured using the MultispeQ as in Figure S2.6. It was not possible to distinguish between qE and qI using the rapid MultispeQ protocol, but the observed positive dependence of NPQt on *pmf* is consistent with qE being the major form of NPQt in CT. The genotypic subgroups showed different distributions along with this overall trend, with the tolerant RILs (BBAA)

tending to have the highest values for both NPQt and ECSt, while the sensitive RILs (AABB) showed the opposite, i.e. tending towards the lowest values for both NPQt and ECSt, and the intermediate RILs (AAAA and BBBB) largely showed intermediate values for both parameters. These distributions suggest that, at CT, the QTLs of Chr 4 and 9 contribute to the qE response through effects on the extents of thylakoid *pmf*, with the AABB genotypes tending to have lower ECSt and correspondingly lower NPQt.

A strikingly different behavior was seen at LT, where a negative correlation was observed between NPQt and ECSt, i.e., higher NPQt was associated with lower, rather than higher, *pmf*. This result is the opposite of what one would expect if the major form of NPQt contributed by qEt, but instead supports a model where photoinhibition (qIt) is the dominant form of NPQt. Under these conditions, the AABB genotypes showed the lowest ECSt and the largest NPQt, with many genotypes reaching quite large NPQt extents. This result supports the conclusions drawn from the DEPI results (Figure 2.1 and Figure S2.6) which show a shifting of contributions to NPQt from qEt to qIt at LT. These results are consistent with a breakdown in the relationship between *pmf* formation and activation of qEt at LT that is modulated by the alleles in QTL on Chr 4 and 9.

Figure 2.9C compares ECSt with the thylakoid proton conductivity, g_{H^+}, which is largely controlled by the activity of the ATP synthase (Kanazawa & Kramer 2002). Overall average g_{H^+} values were lower at LT compared to CT but remained similar across the genotypic groups at each temperature. The apparent lack of genetic contributions to g_{H^+} appears to argue against a role for modulating ATP synthase activity in LT responses.

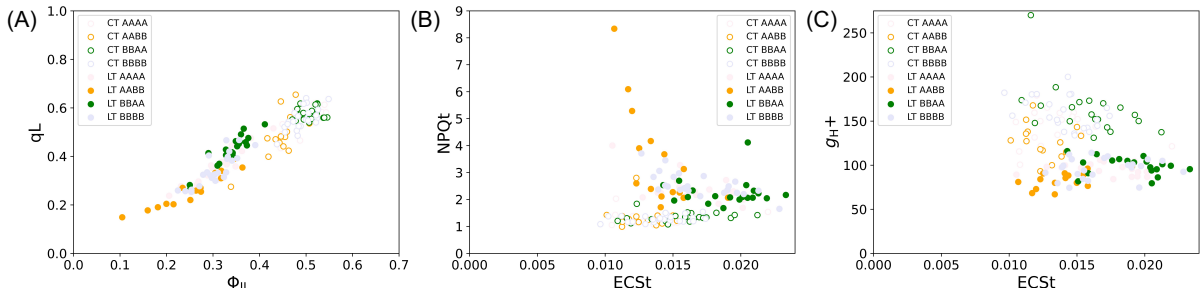

Figure 2.9 Relationships between photosynthetic responses grouped by different combinations of alleles for the identified QTLs in Chrs 4 and 9 for both conditions, CT and LT (CT: opened, LT: closed symbols).
Panel A, qL against Φ_{II} from DEPI data, middle of day 3 (highest light intensity, 500 µmol photons m^{-2} s^{-1}). Panel B, NPQt against ECSt; Panel C, *g*H+ against ECSt from MultispeQ data, middle of day 4 (highest light intensity, 500 µmol photons m^{-2} s^{-1}). The allele groups of AAAA, BBBB are indicated by light pink and light purple, respectively. The allele groups of AABB and BBAA are colored orange and green, respectively. Detailed Statistical analyses testing for differences in phenotypes between the allele groups are shown in Figure S2.1.

2.4.9 Nyctinastic leaf movements (NLM).

During analyses of the DEPI video, we observed large variations in nyctinastic leaf movements (NLM) among RILs population. NLM are motions of leaves. Typically circadian-regulated, induced by changes in the volume of motor cells in the pulvinus, an organ at the base of the petiole (Herbert 1992). NLM appeared specifically under LT conditions on Day 3, suggesting a connection with temperature responses. Indeed, earlier work proposed that low temperature-induced photoinhibition can be partially alleviated by such leaf movements (Huang, Zhang & Cao 2012; Huang, Zhang, Zhang & Hu 2014). Thus, we aimed to determine if variations in NLM could be related to other effects of LT on photosynthesis, and if these effects are related to those controlled by the major QTL intervals on Chrs 4 and 9.

The differences in NLM during LT are readily seen in the example images in Figure 2.10A in which parent line CB27 showed strong paraheliotropism (leaves

pointing up) in the early morning but fully opening within 4 hours of light. By contrast, 24-125B-1 remained nearly fully open (diaheliotropic) under all conditions. As described in Figure S2.12A (see also Materials and Methods), we devised a method for estimating the relative extents of NLM over time. As shown in Figure S2.12B, we observed a wide range of NLM phenotypes in the RIL population, with some genotypes showing extents of motions that exceeded those seen in the two parents.

Figure S2.12C-D shows a time-resolved heat map for NLM LOD scores. The strongest associations appeared on Chrs 8, 10 and 11. The intervals were strongest within about 2 hours after start of illumination in the morning, when leaves were most rapidly transitioning from paraheliotropic to diaheliotropic positions. Additional leaf movement-related QTL intervals were seen (e.g., on Chrs 7 and 9 in the afternoon of Day 3), but appeared to be associated with nutation motions, related to differences in growth of the stems, and thus were not explored in detail. It is interesting to note, however, that these intervals did not overlap with those attributable to NLM, suggesting that different genetic components control these motions.

In principle, NLM can have both immediate effects, e.g. by affecting the instantaneous light absorption, and (potentially) longer-term effects, e.g. on the accumulation of photoinhibition. We thus compared LOD scores for associations across different time points.

Figure 2.9B compares LOD scores for NLM, taken at 2 hours of illumination on Day 3 (at 301 μmol, m^{-2}, s^{-1}), where the associations were the strongest, with Φ_{II}, NPQt and qIt taken at 11.5 hours of illumination, when their associations were strongest

(Figure 2.2) but those for NLM associations had disappeared (Figure S2.12D). No significant overlap in QTLs was observed.

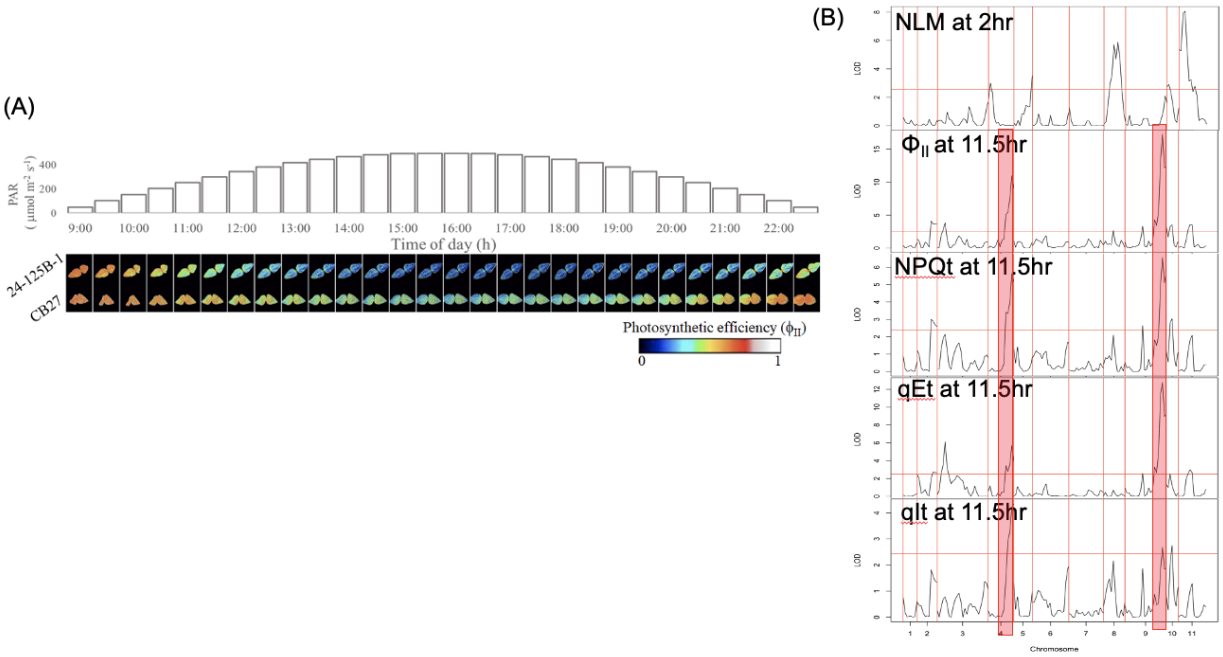

Figure 2.10 (A) Filmstrip view of sequential DEPI images showing changes in nyctinastic leaf movement (NLM) with false-coloring reflecting of ϕ_{II} values over the course of the day for the two parents during Day 2 of LT stress. The light intensity in the DEPI chamber was increased by ~ 50 µmol m^{-2} s^{-1} every 30 min and images were captured at the same interval at the end of every light intensity change over a 14-hour day. The top panel indicates the light intensity for each corresponding image. For the full dataset, see videos in SI Video 1-4. **(B) Logarithm of the odds (LOD) scores for QTL associations for nyctinastic leaf movements (NLM), ϕ_{II}, NPQt and qIt**. The timepoints for NLM at 2 hr after illumination (301µmol, m^{-2}, s^{-1}) and Φ_{II}, NPQt and qIt at end of Day 3 at 11.5 hr after illumination (301 µmol, m^{-2}, s^{-1}) on Day 3 LT conditions. The red dotted horizontal line represents the LOD threshold determined by permutation test at $p<0.05$.

However, some overlap was observed between photosynthetic and NLM intervals at the end of Day 3 at 14 hr after illumination (51 µmol, m^{-2}, s^{-1}) (Figure S2.12E) Chr 8 and Φ_{II}, NPQt and qIt, indicating possible linkages between NLM and photoinhibition. However, no overlaps were observed between the QTL intervals for NLM and those for the photosynthetic phenotypes on Chrs 4 and 9, where the genetic

loci we found genetically controlling photoinhibition under LT. This result suggests that effects of variations in NLM on photosynthetic properties were likely to be independent of those controlled by Chrs 4 and 9.

Figure S2.12F-M quantifies the effect on NLM at times between 0.4 and 2 hours after illumination of alleles (either AA or BB) at identified QTLs in Chr 8, 28.59 cM (red) (A and B). The allele of AA group imposed lower NLM, indicating more paraheliotropic positions, while the BB group imposed more diaheliotropic positions. We additionally compared the allele group of Chr 4 (F-I, green) and Chr 9 (J-M, green) to confirm QTL results, that the alleles under the QTL on Chrs 4 and 9 did not impose significant differences in NLM.

2.4.10 Mechanistic interpretations of the QTL associations.

A range of different processes could result in decreased photosynthetic capacity and photodamage observed at LT. The questions we address in the current work are: which of these processes is modulated by the genetic diversity in the RIL population? How are these effects linked mechanistically? Which of these may contribute to the relative sensitivities of the plant to chilling stress?

The light reactions are known to be controlled by a range of processes that can be (roughly) categorized in the following (see reviews in Avenson*et al.* 2005b; Cruz *et al.* 2005): 1) Limitations in forward reactions, e.g. slowing of electron or proton transfer, leading to buildup of intermediates. In our work, we probed several indicators of these processes, including the redox state of Q_A through the qL parameter, the redox state of P700 and PSI acceptor side electron carriers, the buildup of the thylakoid *pmf*, and the control of electron flow by the cytochrome b_6f complex (PCON). 2) Dissipation of

captured energy. In vascular plants, this occurs most notably through NPQ, either by rapidly inducible and reversible qE or slower processes, including photoinhibition of PSII (qI) and the accumulation of zeaxanthin (qZ). Both categories of processes are influenced by both the capture and utilization of light energy, the energetic matching of these controls the buildup of energetic intermediates of the light reactions. Efficient and safe matching required the chloroplast to balance not only the amount of energy input and used, but the fractionation of this stored energy into NADPH and ATP.

Using the rapid, high throughput methods employed here, we were able to test for the involvement of the following important processes (See Figure 2.11):

A. PSI acceptor-side limitations can occur when electrons accumulate on PSI electron acceptors (NADPH, ferredoxin, F_A, F_B) preventing further LEF.
B. PSII acceptor limitations occur when electrons accumulate on Q_A (decreased qL), blocking PSII photochemistry.
C. Energy-dependent NPQ (q_E) and photosynthetic control activated by acidification of the thylakoid lumen. Metabolic or physiological limitations can result in decreased ATP synthase activity, causing a build-up of pmf. The pH component (ΔpH) of pmf acidifies the lumen, controlling electron transfer through the cytochrome b_6f complex, and induces violaxanthin de-epoxidase, leading to the conversion of violaxanthin (V) to antheraxanthin and Zeaxanthin (Z) and the protonation of PsbS, resulting in quenching of excitation energy through the q_E mechanism.
D. Photoinhibition. In the light, PSII centers can be damaged, directly decreasing the number of active PSII centers, while initiating long-lived photoinhibition-

related NPQ (q_I). Subsequent repair processes restore active PSII centers. The temperature could be affected by the rate of photodamage and repair.

E. Photosynthetic control (PCON) is the control of electron flow related to the acidification of the thylakoid lumen and subsequent slowing of PQH_2 oxidation at the cytochrome b_6f complex (Chow & Hope 2004; Takizawa *et al.* 2008).

F. Cyclic electron flow (CEF) involves transfer of electrons from the acceptor side of PSI back to the plastoquinone pool, generating ATP without net reduction of NADPH (). CEF can thus augment the production of ATP to balance the ratio of ATP/NADPH to meet downstream metabolic needs (Kramer, Avenson& Edwards 2004). The plastoquinone reductases are regulated by ATP levels, allowing for very rapid balancing of ATP/NADPH production (Fisher, Bricker & Kramer 2019). CEF can also result in acidification of the thylakoid, and thus contribute to PCON and the induction of qE.

G. Regulation of the chloroplast ATP synthase. The ATP synthase controls the rate of proton efflux from the lumen. The activity of the ATP synthase is regulated or controlled by a number of factors, including the redox state of the thiol groups on the gamma subunit and the availability of substrates ADP and Pi, which are, in turn, impacted metabolic or physiological state of the chloroplast, resulting in differential accumulation of *pmf* and acidification of the lumen, affecting PCON and qE.

H. Nyctinastic leaf movements (NLM) can adjust the amount of light absorbed by a leaf by changing leaf angle with respect to that of solar influx (Herbert 1992).

The analysis of the RIL library under CT and LT conditions revealed genetically controlled variations in many of these processes. Two notable exceptions were ATP synthase activity (*g*H+, Figure 2.4E, 2.8C) and PSI overreduction (Y_{NA}). We did observe a general reduction on *g*H+ going from CT to LT (Figure S2.6E), as one would expect if the capacities for electron and proton flow and assimilation (Kanazawa & Kramer 2002), sink strength (Takizawa *et al.* 2008) or onset of limitations at triose-phosphate utilization (Yang, Preiser, Li, Weise & Sharkey 2016) were decreased at the lower temperature (Allen & Ort 2001; ORT 2002). However, the effect was not significantly different in the two parent lines, nor we did not observe strong linkages to genetic markers, suggesting that modulation of ATP synthase activity did not contribute to the differences in chilling sensitivities, under the RIL population and under our conditions. These results suggest that, in our RIL population, photosynthesis is tuned to prevent these limitations. It is possible, though, that a different population could exhibit such variations and these may affect chilling tolerance.

The lack of effects on Y_{NA} are interesting in light of the proposal that PSI photodamage, related to over-reduction, is a major factor in chilling-induced photodamage damage in some species, notably *Cucumis sativus* (Sonoike 1996), and in mutants that lack the ability to activate PCON (Tikkanen*et al.* 2012; Takagi, Takumi, Hashiguchi, Sejima& Miyake 2016; Kanazawa *et al.* 2017). Despite being quite chilling sensitive, we did not see any evidence for PSI over-reduction in cowpea. Instead, we observed strong PCON (Figure S2.6H) which resulted in net oxidation of P700 (Figure S2.6G), preventing the accumulation of electrons on PSI electron acceptors. Consistent with this result, we found no significant differences in the loss of active PSI at LT, as

measured by the extent of maximal light-induced absorbance changes at 810 nm, between the two parent lines after either LT or CT exposure ($p>0.7$).

We also observed strong induction of NLM specifically under LT (Figure S2.12 C-D). It has been proposed that these may protect against chilling damage to photosynthesis in some species (Huang *et al.* 2012, 2014). However, we did not observe obvious linkages to processes we measured, including long-term changes in NPQt (Figure 2.10B), arguing against strong impact, at least under our conditions.

The apparent co-linkages of photosynthetic parameters to QTLs on Chrs 4 and 9, and the order of their appearance, suggests a model where the control of the light reactions by these loci is associated with increased thylakoid *pmf* (Figure 2.5D and Figure S2.6D), attributable to the activation of CEF (Figure 2.4I and Figure S2.6J), which results in increased qE and more oxidized Q_A and P_{700}+. While these effects are seen under both experimental temperatures, they appear to have secondary effects at LT, resulting in strong differences in photoinhibition (Figures 2.1, 2.4, 2.8 and Figure S2.3, S2.4), mainly caused by increased rates of photodamage (Figure 2.8). This results in a strong shift in the sensitive lines, from qE to qI as the major form of NPQ (Figure 2.1 and Figure S2.3, S2.4). This increased photodamage rate is associated with a net reduction of Q_A (Figures 2.1E, 2.5C, 2.9A and Figures S2.3E, S2.4E) and elevated *pmf* (Figure 2.5D and Figure S2.6D), both of which will increase the rates of recombination reactions within PSII, resulting in the production of toxic singlet O_2 (Ivanov *et al.* 2012;Telfer 2014; Davis *et al.* 2016), and we thus propose this effect as the major contributor to the observed differences in chilling sensitivity of the light reactions. Such a mechanism is also consistent with the order of appearance of the

linkages we observed in the time-resolved DEPI experiments, where qEt, qL and qIt preceded effects on Φ_{II} and NPQt (Figures 2.3 and 2.4).

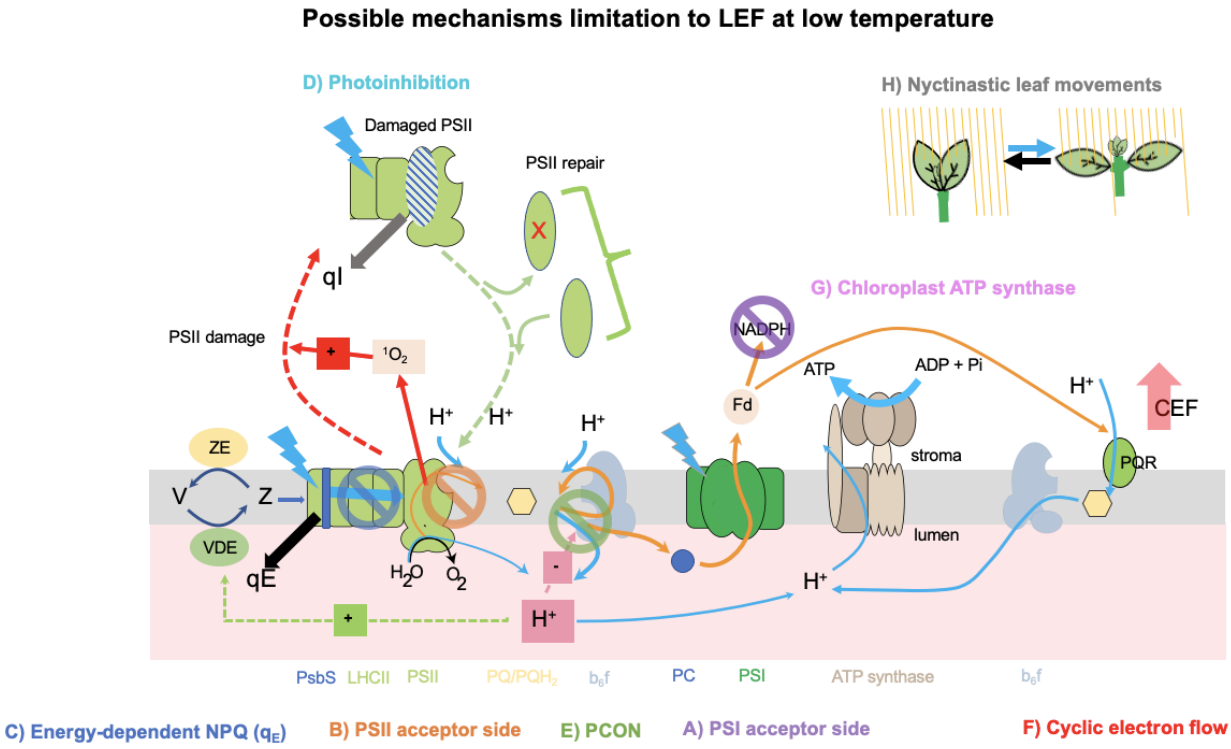

Figure 2.11 Possible mechanisms limitation to linear electron flow (LEF) at low temperature.
Schematics for the regulation of light energy capture and storage by plant photosynthesis. A) PSI acceptor-side limitations (purple), B) PSII acceptor limitations (orange), C) Energy-dependent NPQ (q_E) (blue), D) Photoinhibition (light blue), E) Photosynthetic control (PCON) (green), F) Cyclic electron flow (CEF) (red), G) Regulation of the chloroplast ATP synthase (pink), H) Nyctinastic leaf movements (grey).

2.5 Conclusions

In this work, we explored stress-induced responses of a range of related, rapidly measurable photosynthetic processes in a RIL population of cowpea lines. These responses reflect the genetically-controlled variations in control or regulation of photosynthesis. This approach is distinct from classically genetics, where mutations

typically inactivate, typically, one or a few distinct enzymes in each genotype, leading to discrete loss of function phenotypes. Here, we may see combinations of effects that impact networks of processes are more likely to be adaptive.

Considering that the QTL regions in our study encompass hundreds of genes, we do not extensively explore the identities of specific, causative candidate polymorphisms. In some cases, it is possible to identify the causative genetic components that underlie QTL or GWAS effects (e.g. Caicedo, Stinchcombe, Olsen, Schmitt & Purugganan 2004; Roux, Camilleri, Giancola, Brunel &Reboud 2005), but these cases are relatively few considering the number of published studies on genetic variation and quantitative trait locus (QTL) mapping (Roff, 2007;Baxter, 2020), partly because of the low resolution of the genetic maps of most diversity panels (Miles & Wayne 2008; Baxter (2020). Nevertheless, even at lower resolution, such genomic associations can be used to guide plant breeding efforts. In addition, the colocalization (or lack thereof) can be used to formulate and test scientific hypotheses, as we have demonstrated here, and thus give new insights into the processes that evolution has modulate physiological responses.

This approach makes comparisons across genotype, emphasizing genetically controlled differences, rather than the biophysical mechanisms per se. In other words, we observe how the genetic variations existing in a population “tweak” the mechanisms of photosynthesis. Key to this approach is the fact that each genotype in the population may have many combinations of smaller, quantitative, effects that add up or interact to achieve altered responses. The statistical analyses of associations between the genetic components and measured parameters can give insights into the processes that control

particular phenotypes. By comparing these associations across phenotypes, we can get further insights into how genetic variations affect the connections among related processes, i.e., which processes are potentially mechanistically or genetically linked to others.

Analysis of our cowpea RIL using high time-resolved, high-throughput methods, points to a model where important genetic control at the levels of the redox states of Q_A and *pmf*, which governs the recombination reactions within PSII that can lead to singlet O_2 production. We predict that applying these methods to diversity panels from diverse species will reveal additional mechanisms of adaptation and will guide the breeding and engineering of photosynthesis for higher, more climate resilient productivity.

APPENDIX

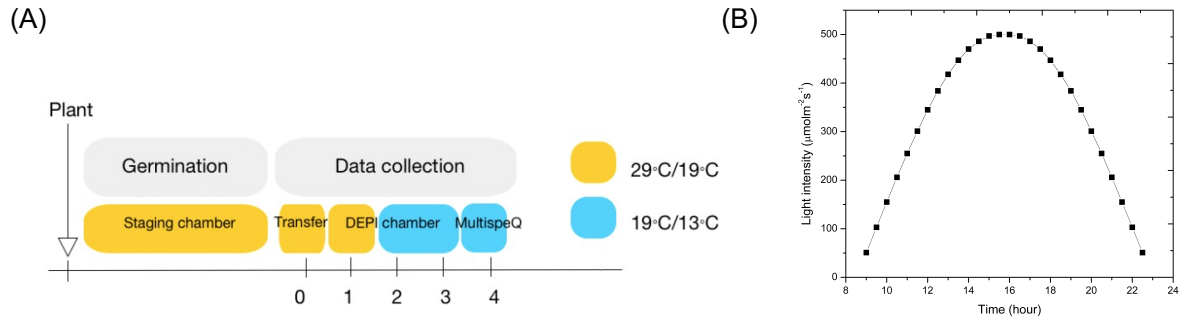

Figure S2.1 Experimental design for growth and photosynthetic assays leading to quantitative trait loci (QTL) mapping results.
Panel A: Timeline for growth and assays. Four days after seed germination, cowpea plants were moved from staging to DEPI chambers. Following one day of acclimation, DEPI measurements were started. On Day 1, assays were performed under standard (control) temperature. The low temperature regime was initiated on the morning of Day 2 and continued throughout Day 4, for a total of three days. Panel B: Sinusoidal pattern of photosynthetically active radiation (PAR) used for days 1-4, simulating outdoor conditions for a cloudless day.

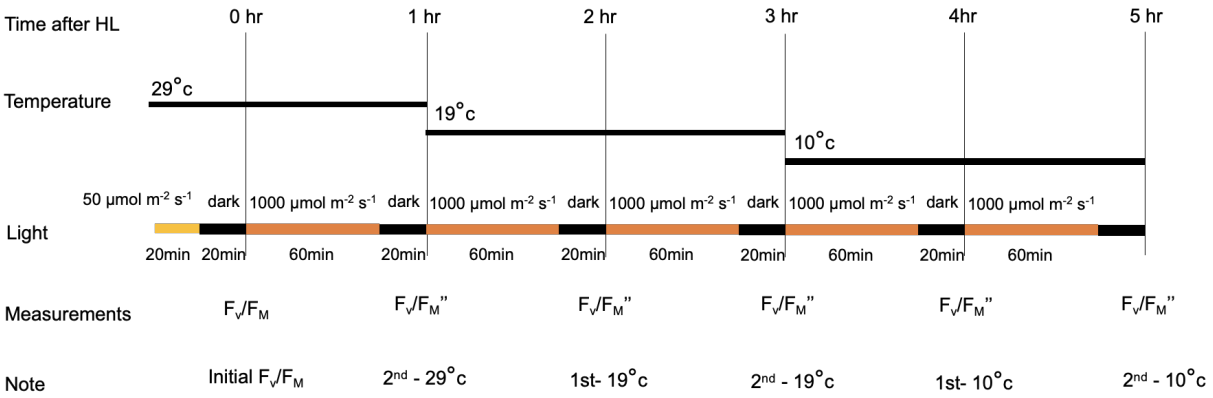

Figure S2.2 Experimental design for lincomycin treatment.
Following infiltration, leaves were kept under low light (50 μmol, m^{-2}, s^{-1}) for 20 min and then dark-adapted 20 min for measuring initial F_v/F_M. After that, F_v/F_M'' measurements were followed by 1hr of high light (HL) (1000 μmol, m^{-2}, s^{-1}) and 20 min dark adaptation to dissipate qE. For the low temperature treatment (LT), the temperature was decreased to 19°C and 10°C every two hours of HL treatment.

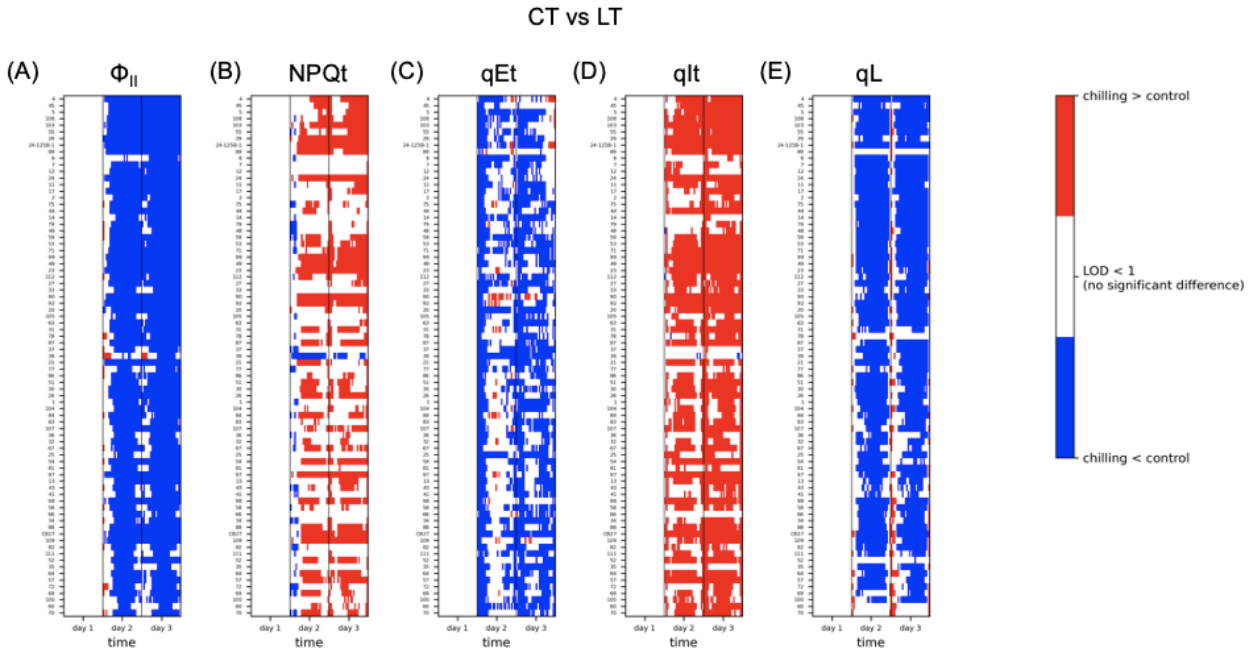

Figure S2.3 Significant changes and directionality of five photosynthetic parameters (A, Φ_{II}; B, NPQt; C, qEt; D, qIt; E, qL) from DEPI in the low temperature (LT) compared to control conditions (CT).
Results from Figure 2.1 were tested for significant changes using the Kolmogorov-Smirnov (KS) statistical test (n≥4). The coloration indicates that the average values for the parameters under chilling were both significant and greater than (red) or lower than (blue) under control temperature, as indicated in the color bar to the right of the panels. Each row represents the significant changes and directionality for a different genotype. The rows were ordered based on the average values of Φ_{II} taken on Day 3 (the second day of chilling), which is the same order as in Figure 2.1.

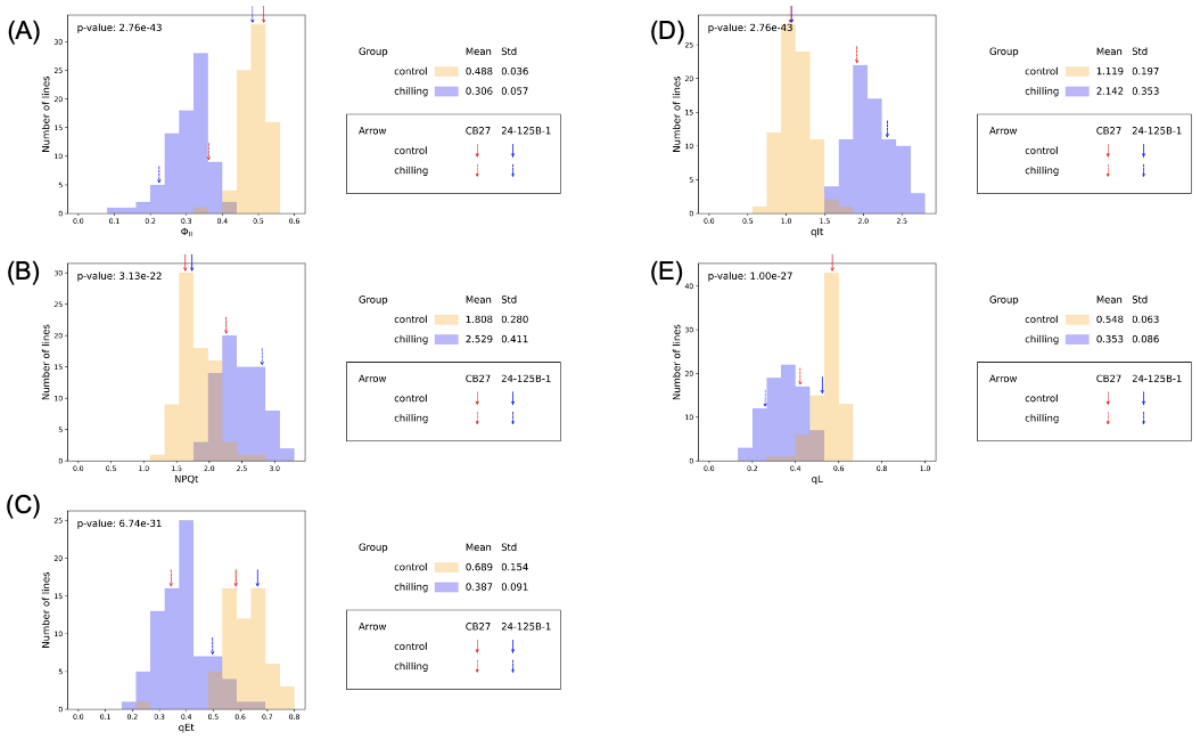

Figure S2.4 Histograms of photosynthetic parameters (A, Φ_{II}; B, NPQt; C, qEt; D, qIt; E, qL) from DEPI across RIL lines taken at the middle of the third day (highest light intensity).

The averaged replicates (n≥4) for each phenotype value of RILs including two parental lines are shown as density plots. As shown by the figure legends, orange and blue boxes represent control and chilling conditions, respectively with mean and standard deviations for each group. P-values by Kolmogorov-Smirnov (KS) for differences between value under control and low temperature are shown in the left top corner of the histogram. The arrows indicate the average values for the two parental lines under two conditions for CB27 (red) and 24-125B-1 (blue), under control (solid arrows) and low temperature (dashed arrows).

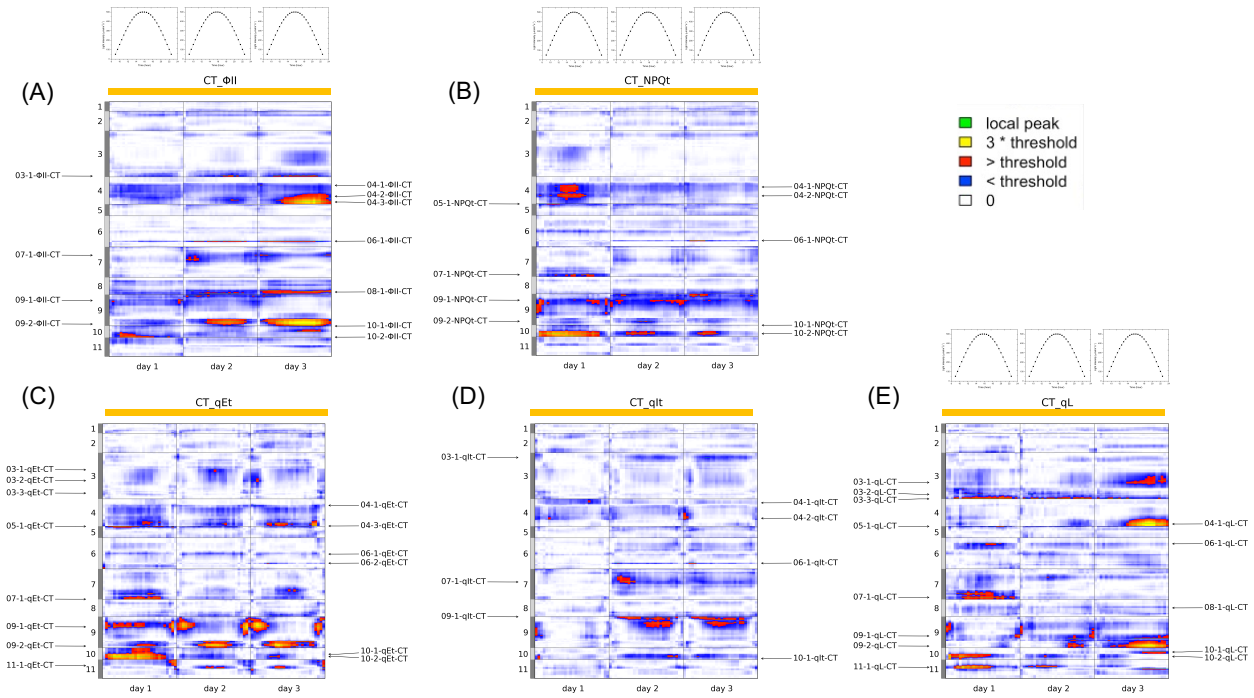

Figure S2.5 Time-resolved QTL analysis of five photosynthetic parameters under the Control temperature (CT).
Panel A, Φ_{II}; Panel B, NPQt; Panel C, qEt; Panel D, qIt, and Panel E, qL from DEPI chamber for the CB27 x 24-125B-1**.** The logarithm of the odds (LOD) scores through time are represented as heat maps. The time is indicated in the X-axis and the genetic position is indicated on the y-axis. The temperature was kept at control temperatures of 29 °C/19°C (day/night) for three days. The light intensities, sinusoidal pattern, and temperature are shown on the top of each parameter. The LOD scores, significance, QTL peak positions are indicated by the heat map coloration and labeled as described in Figure 2.2

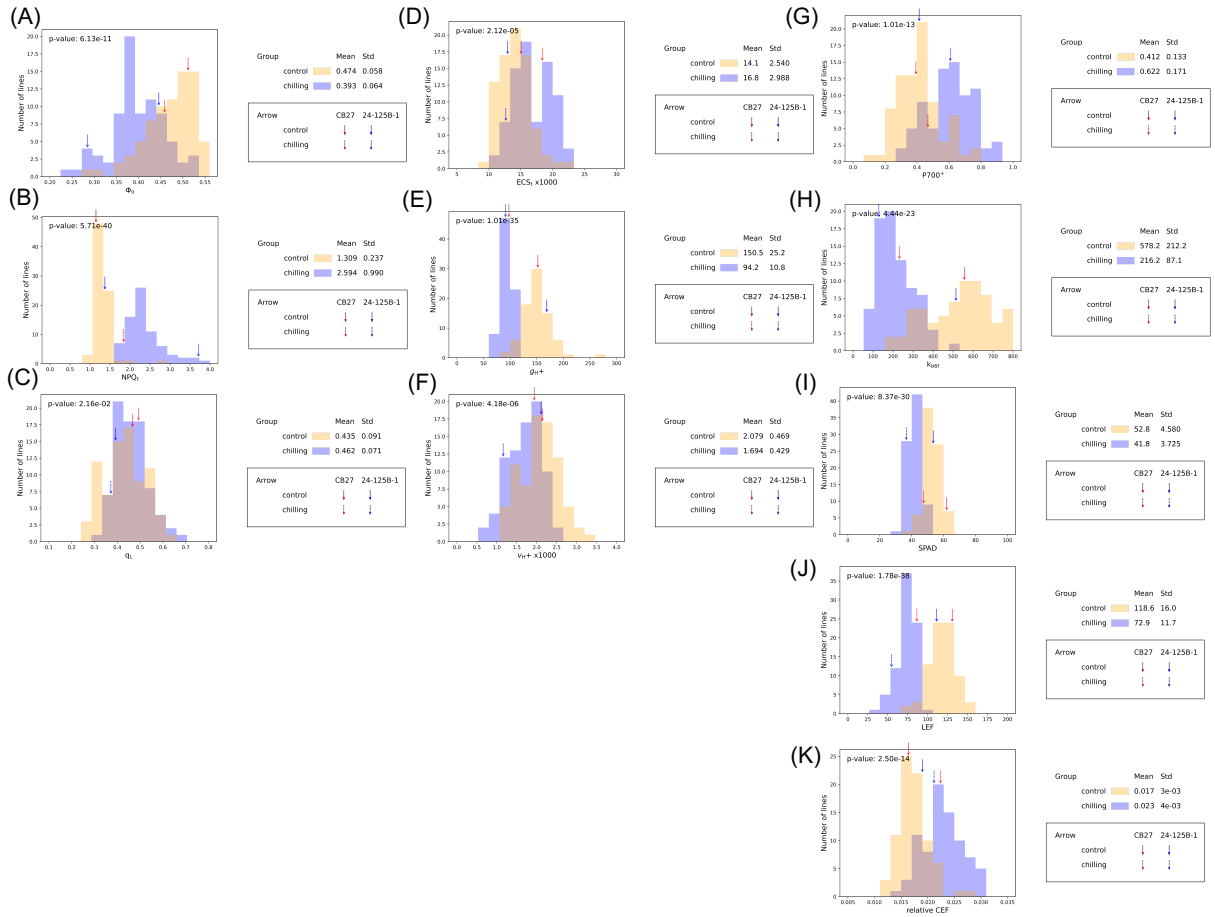

Figure S2.6 Histograms of photosynthetic parameters from MultispeQ in both conditions.

Panel A, Φ_{II}; Panel B, NPQt; Panel C, qL; Panel D, ECSt; panel E, *g*H+; Panel F, *v*H+; Panel G, P700+; Panel H, k_{b6f}; Panel I, LEF; Panel J, relative CEF as estimated by *v*H+ over LEF from MultispeQ across the RIL lines at the middle of the day (highest light intensity) of the fourth day of the experiment. The averaged replicates (n≥4) for each phenotype value of RILs including two parental lines are shown as histogram. As shown by the color to the right of the figure, orange and blue boxes represent control and chilling conditions, respectively with mean and standard deviation in each group. The arrows indicate two parental lines under two conditions (CB27, red; 24-125B-1, blue and control, solid and chilling condition, dashed line). p-values for differences between control and low temperature are shown in the left or right top corner of histogram.

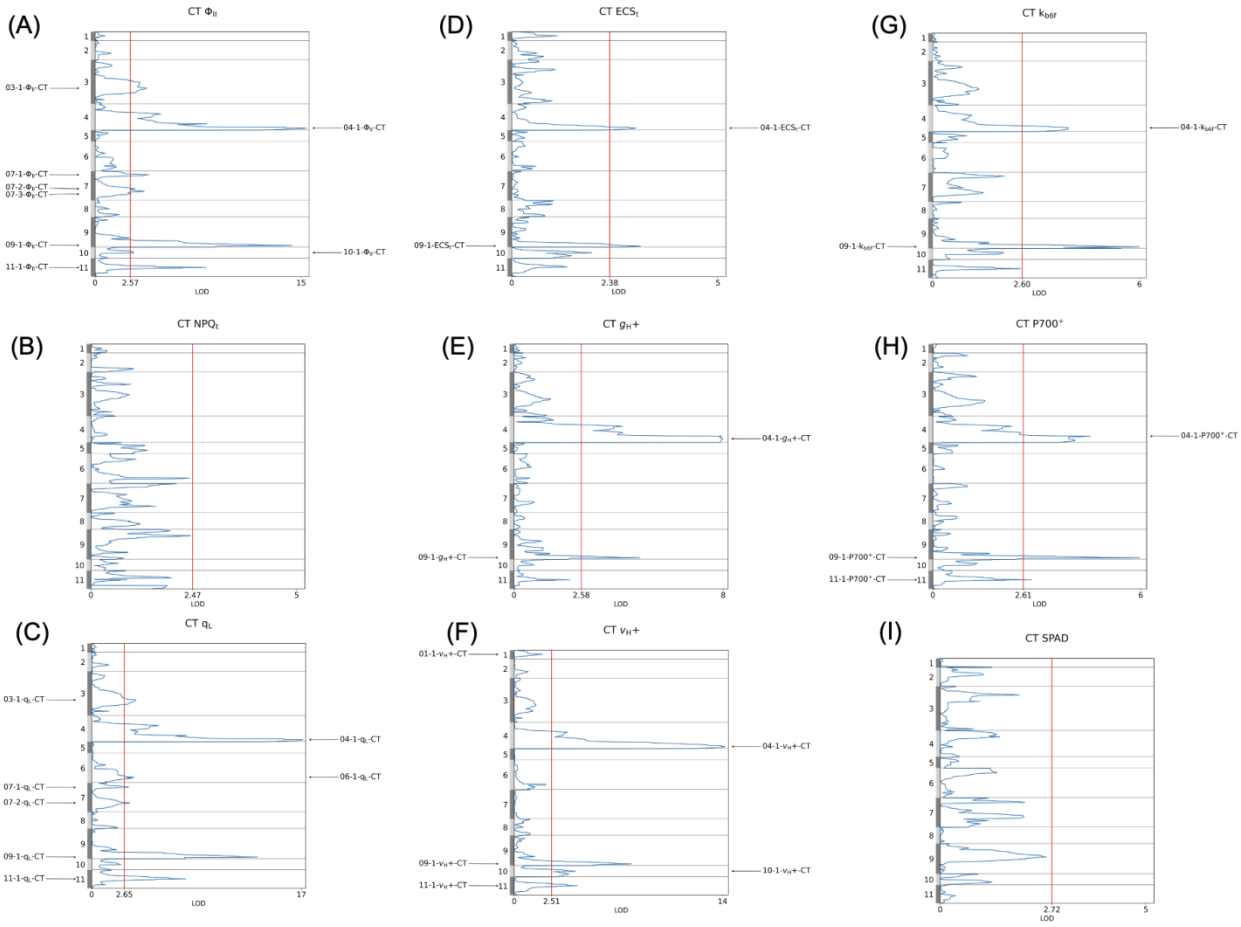

Figure S2.7 QTL analysis of photosynthetic parameters from MultispeQ in the control condition.

The logarithm of the odds (LOD) score plots of photosynthetic data (A Φ_{II}; B, NPQt; C, qL; D, ECSt (*pmf)*; E; *g*H+, F; *v*H+, G: P700+; H; k_{b6f}, I; SPAD) from MultispeQ in the control condition measured in the middle of the fourth day of experiment. The genetic position is indicated by the y-axis. LOD scores above statistical thresholds, determined by permutation analysis as described in Materials and Methods, are indicated by the red lines. The index is numbered with Arabic numerals in the order of genomic loci in each Chr for the QTLs for that phenotype.

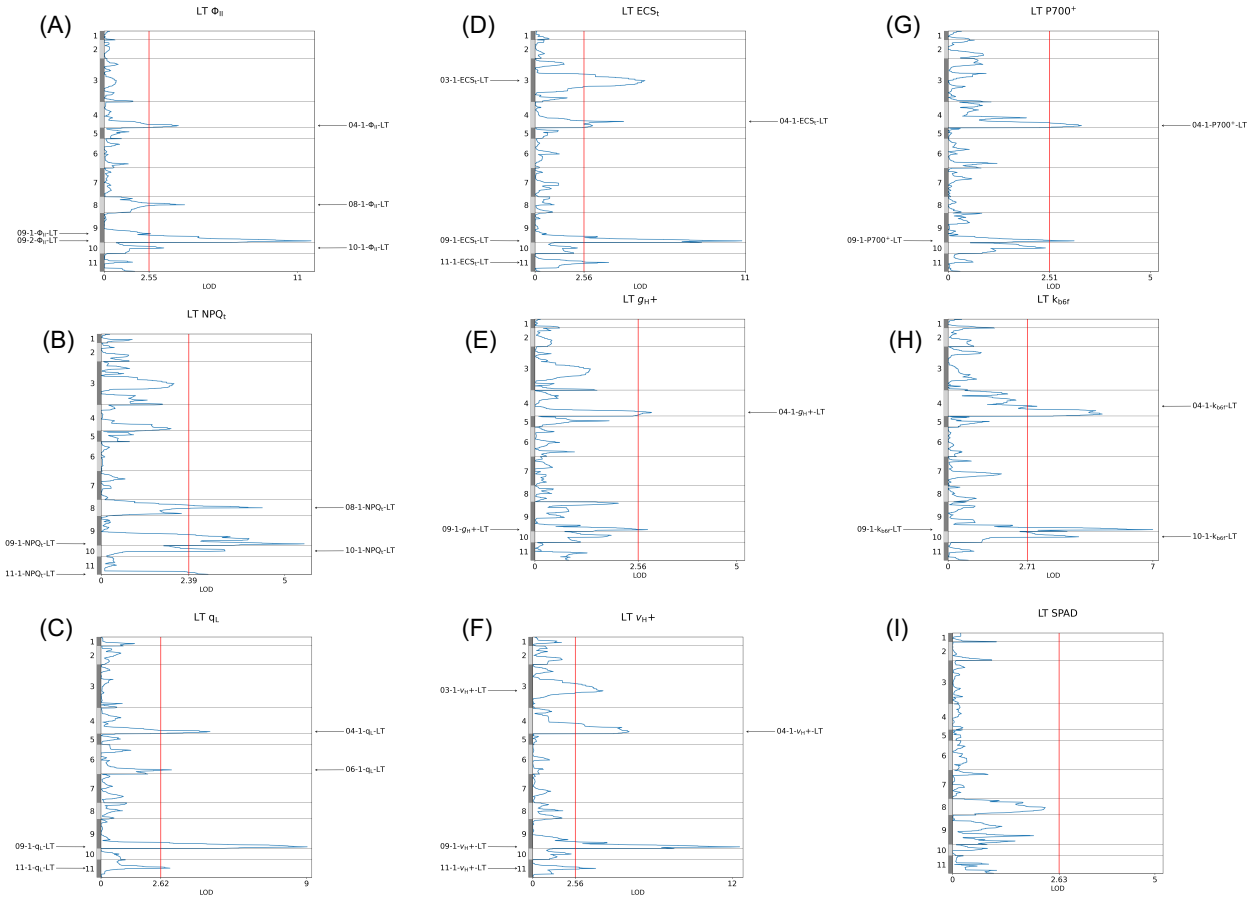

Figure S2.8 QTL analysis of photosynthetic parameters from MultispeQ in the low temperature condition.

The logarithm of the odds (LOD) score plots of photosynthetic data (A Φ_{II}; B, NPQt; C, qL; D, ECSt (*pmf*); E; *g*H+, F; *v*H+, G: P700+; H; k_{b6f}, I; SPAD) from MultispeQ in the low temperature condition measured in the middle of the fourth day of experiment. The genetic position is indicated by the y-axis. LOD scores above statistical thresholds, determined by permutation analysis as described in Materials and Methods, are indicated by the red lines. The index is numbered with Arabic numerals in the order of genomic loci in each Chr for the QTLs for that phenotype.

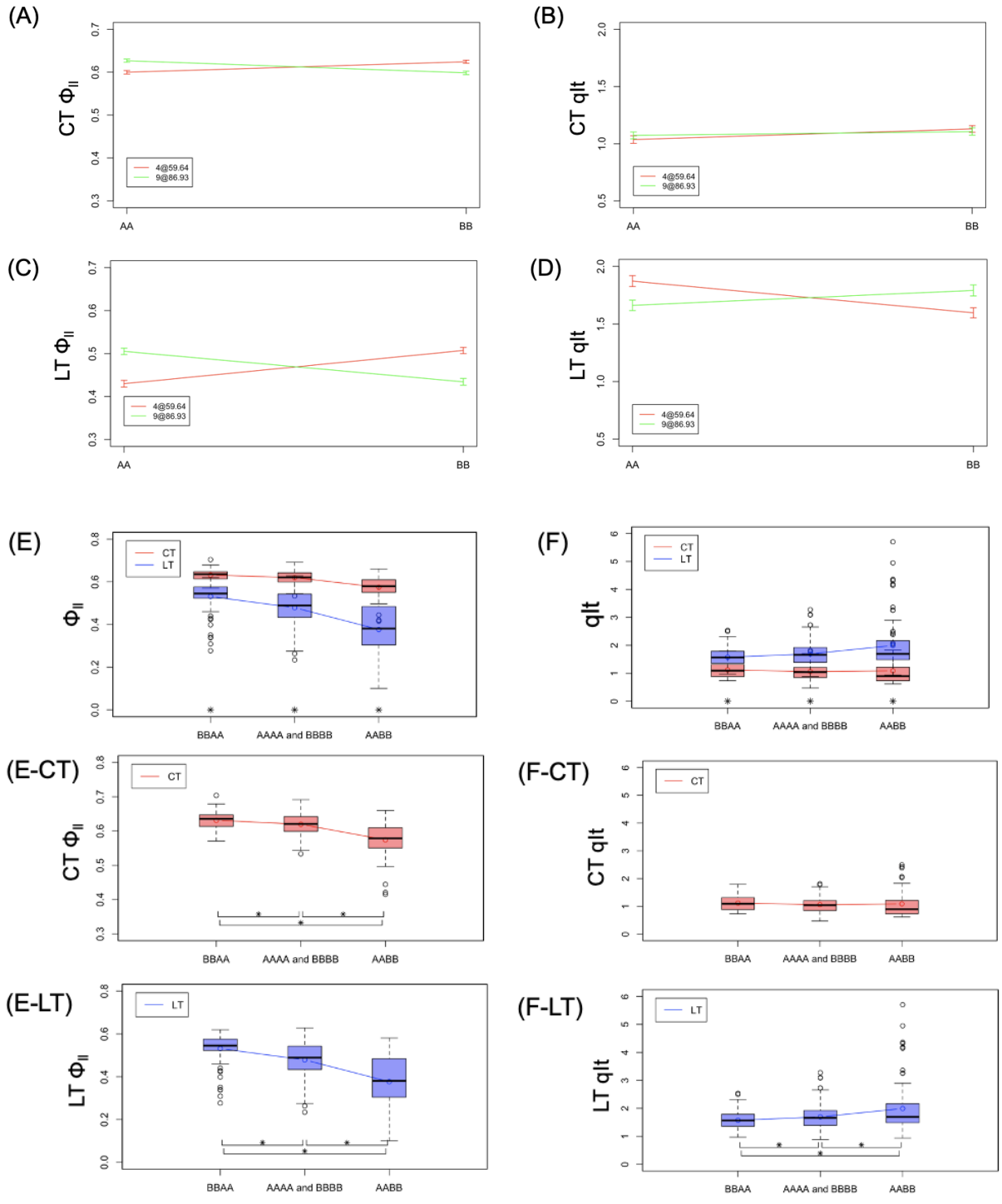

Figure S2.9 Effect plots (A-D) and box plots (E-F) of identified QTLs in Chrs 4 and 9 for Φ_{II} and qIt at 1.5 hr prior to the end of Day 3 (206 µmol, m^{-2}, s^{-1}).
(A-D) Each panel shows the mean of Φ_{II} (A,C) and qIt (B,D) by indicated as y-axis in each condition (CT: A-B and LT: C-D) against allele (either AA or BB) at identified QTLs in chr 4, 59.64 cM (red) and 9, 86.93 cM (green).(E-F) Box plots for Φ_{II} (E) and

Figure S2.9 (cont'd): qIt (F) in both conditions (CT and LT are colored by red and blue respectively) grouped by alleles from identified QTLs in Chrs 4 and 9, AABB, BBAA and averaged AAAA and BBBB. The line connects each mean of the group. Significant differences between conditions for each group ($p<0.05$, t-test) are shown as the asterisk at the bottom of the plots. (E-CT/LT, F-CT/LT) Significant differences of Φ_{II} or qIt between groups ($p<0.05$, t-test) are shown as the asterisk in the bottom of the plots for each condition.

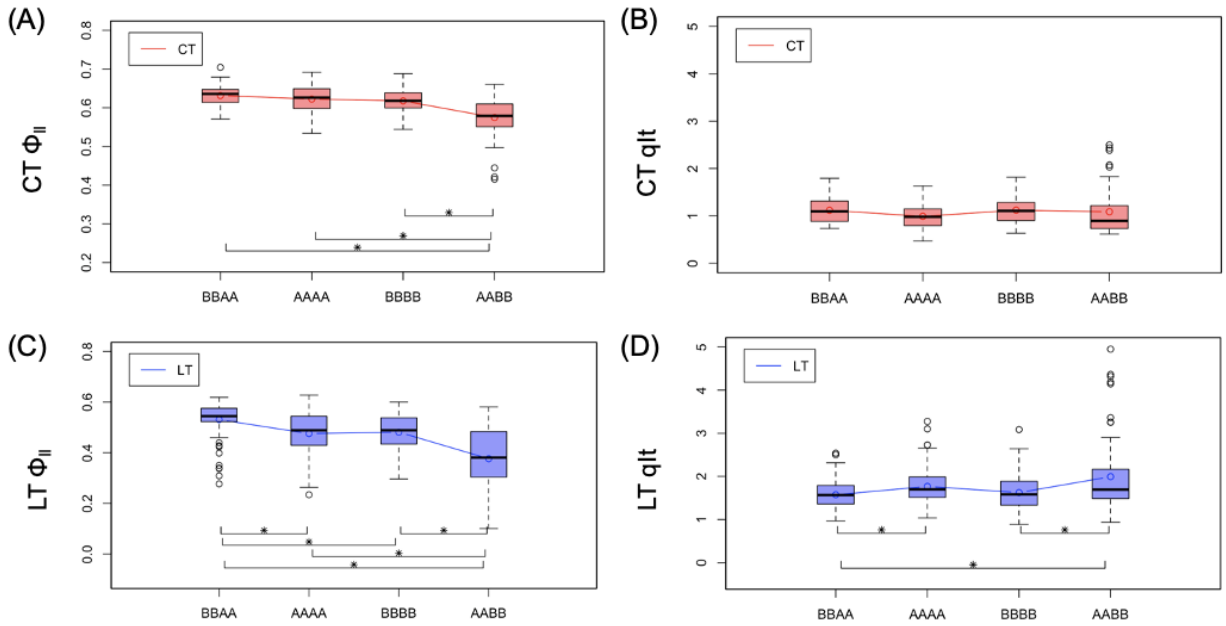

Figure S2.10 Box plots of identified QTLs in Chrs 4 and 9 for Φ_{II} and qIt at 1.5 hr prior to the end of Day 3 (206 µmol, m^{-2}, s^{-1}).
Each panel shows the mean of Φ_{II} (A and C) and qIt (B and D) by indicated as y-axis in each condition (CT: A and B and LT: C and D) against four allele groups, AABB, BBAA, AAAA and BBBB at identified QTLs in chr 4, 59.64 cM and 9, 86.93 cM. The line connects each mean of the group. Significant differences of Φ_{II} or qIt between groups ($p<0.05$, t-test) is shown as the asterisk in the bottom of the plots for each condition.

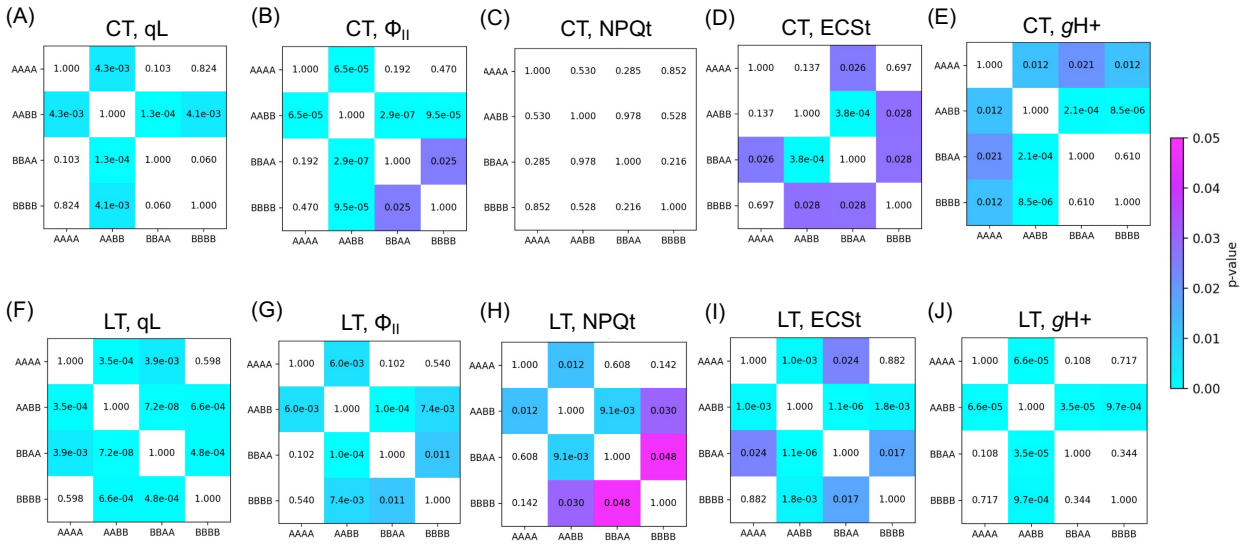

Figure S2.11 Significance matrixes (p-values in each box) of five photosynthetic parameters.

Panel A and F, qL; Panel B and G, Φ_{II}; Panel C and H, NPQt; Panel D and I, ECSt; Panel E and J, *g*H+ for four allele groups shown in Figure 2.8 under CT (A-E) and LT (F-J). Results from Figure 2.9 were tested for significant differences between groups using t-test. The coloration indicates below the thresholds ($p < 0.05$, color codes in the right side of panels).

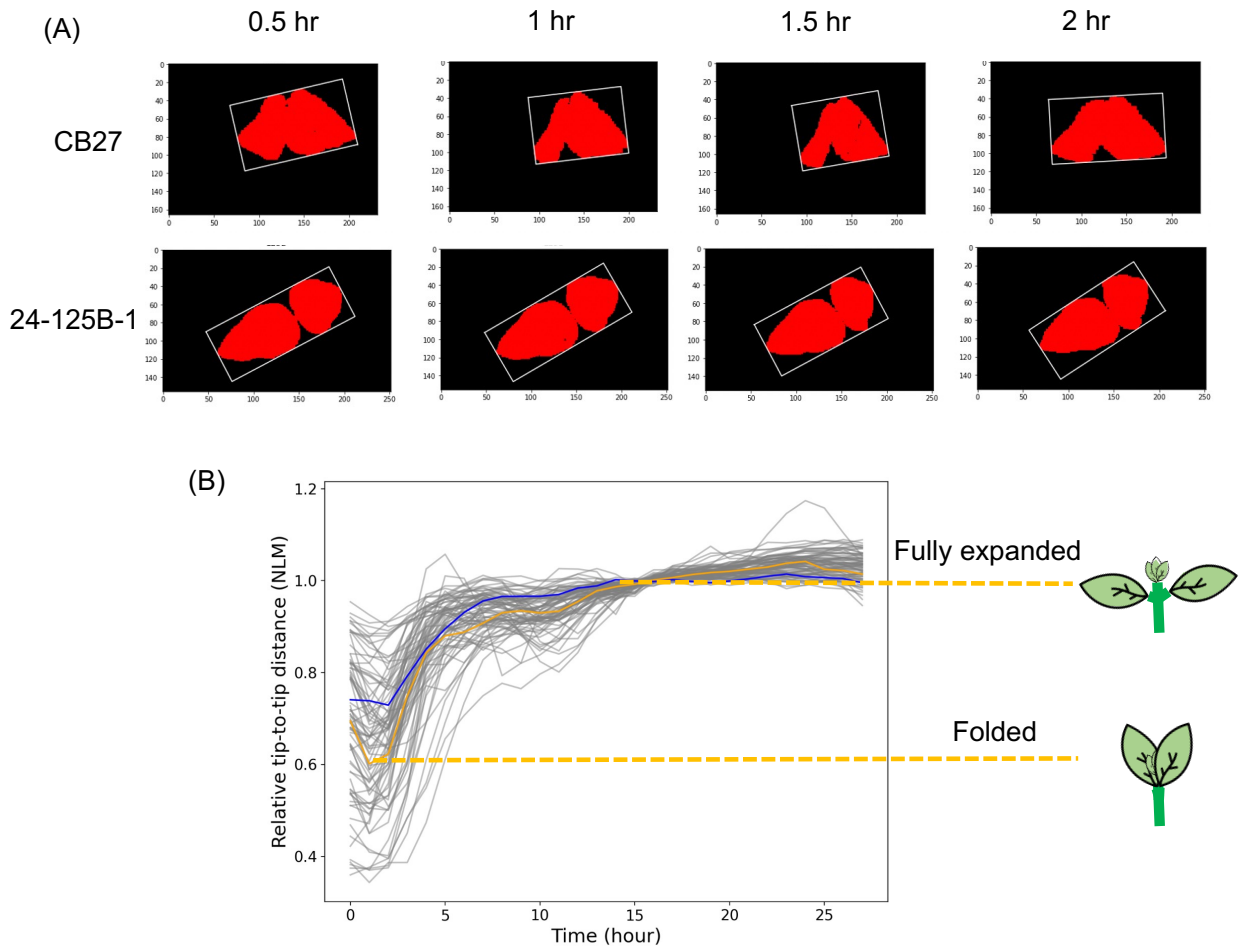

Figure S2.12 Supplemental data for NLM.
A) Relative estimates of nyctinastic leaf movement (NLM). Representative fluorescence images for lines CB27 (top row) and 24-125B-1 (bottom row). The boxes represent the best fit rectangles to the unifoliate leaf pairs, the long axis of which represents the tip-to-tip length projection. These lengths, normalized to that in the fully unfolded states at midday, were used as a measure of the apparent changes in leaf movement. (**B) Average traces of kinetics of tip-to-tip lengths as a function of time after the initiation of illumination.** The orange and blue curves represent the average traces for CB27 and 24-125B-1 respectively. The dashed orange lines represent the folded state of the leaves at the time points indicated. **(C-D) Time-resolved QTL analysis of NLM (or relative tip-to-tip distance) under the both conditions, CT (C) and LT (D) from DEPI chamber experiments for the CB27 x 24-125B-1 RIL population).** The logarithm of the odds scores (LOD) through the time are represented as heat maps. The time is indicated in the X-axis and the genetic position is indicated on the y-axis. The LOD scores, significance, QTL peak positions are indicated by the heat map coloration and labeled as described in Figure 2.2. **(E) Logarithm of the odds (LOD) scores for QTL associations for nyctinastic leaf movements (NLM), ϕ_{II}, NPQt and qIt**. The timepoints for NLM at 2 hr after illumination (301µmol, m^{-2}, s^{-1}) and Φ_{II}, NPQt and qIt at end of Day 3 at 14 hr after illumination (51 µmol, m^{-2}, s^{-1}) on Day 3 LT conditions. The red dotted horizontal line represents the LOD threshold determined

Figure S2.12 (cont'd):
by permutation test at p<0.05. **(F-M) Effect plots for NLM at initial four time points (0.5 hr - 2 hr) on Day 3 LT conditions, mean of allele group from identified Chr 8 compared to Chr 4,59.64 cM (F-I) and 9,86.93 cM (J-M).** (F-I) Each panel shows mean of NLM by indicated as y-axis under LT against allele (either AA or BB) at identified QTLs in Chr 8, 28.59 cM (red) and previously identified main genetic loci for photoinhibition, Chr 4 59.64 cM (green) and (J-M) Chr 9, 86.93 cM (green) compared respectively. NLM shows differences in two alleles from identified QTL in Chr 8, showing more closed in AA group (lower NLM value) and more opened in BB group (higher NLM value). Alleles from Chrs 4 and 9 showed independence from NLM.

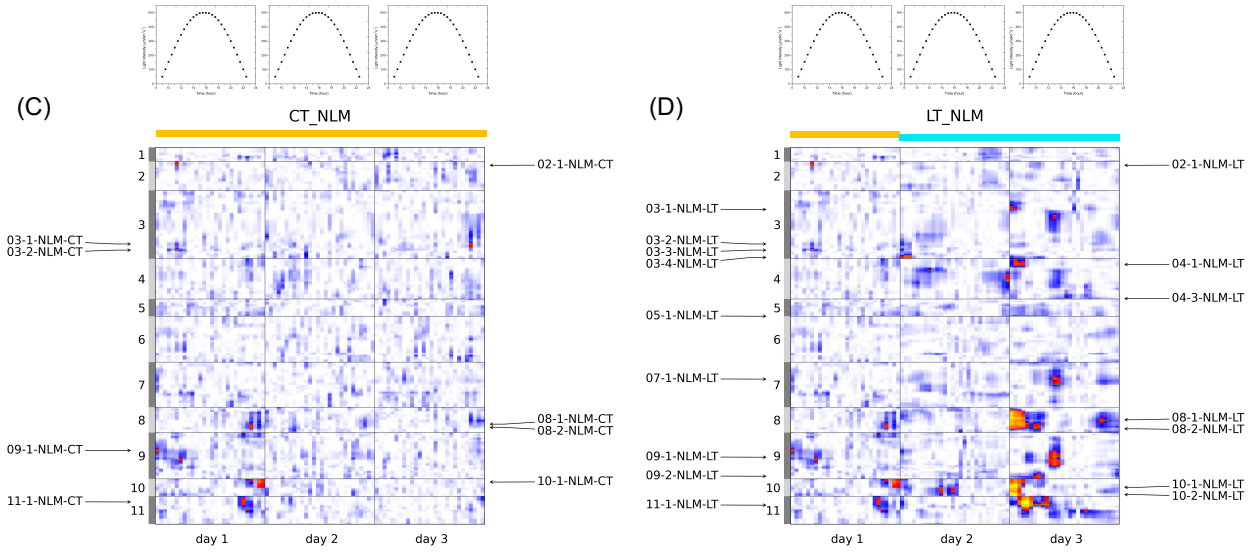

Figure S2.12 (cont'd):

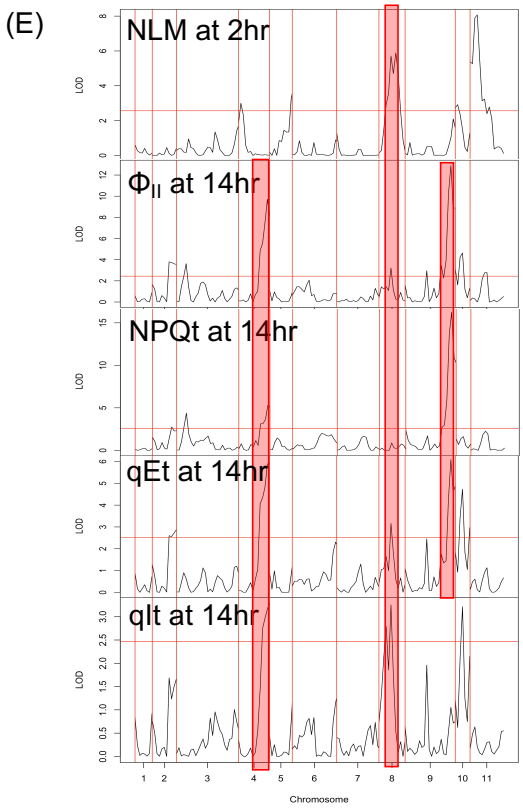

Chr 8 vs Chr 4

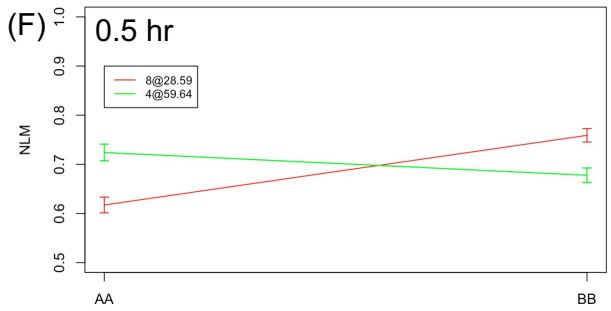

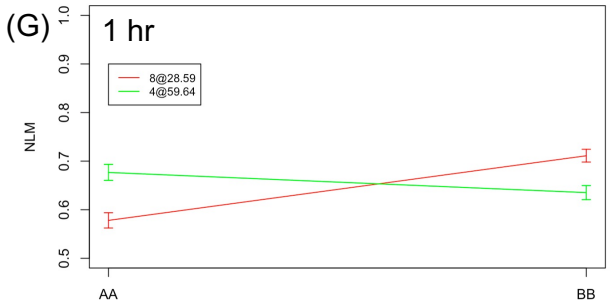

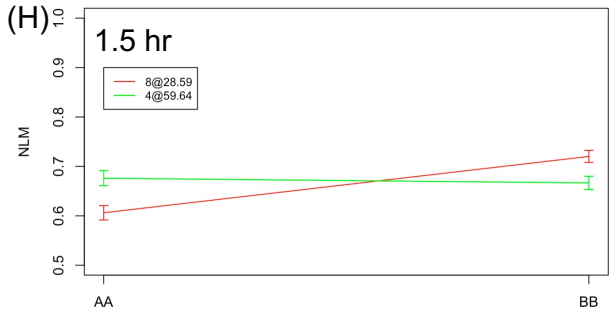

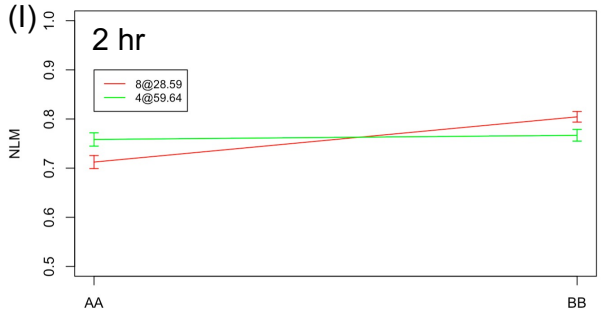

Figure S2.12 (cont'd):

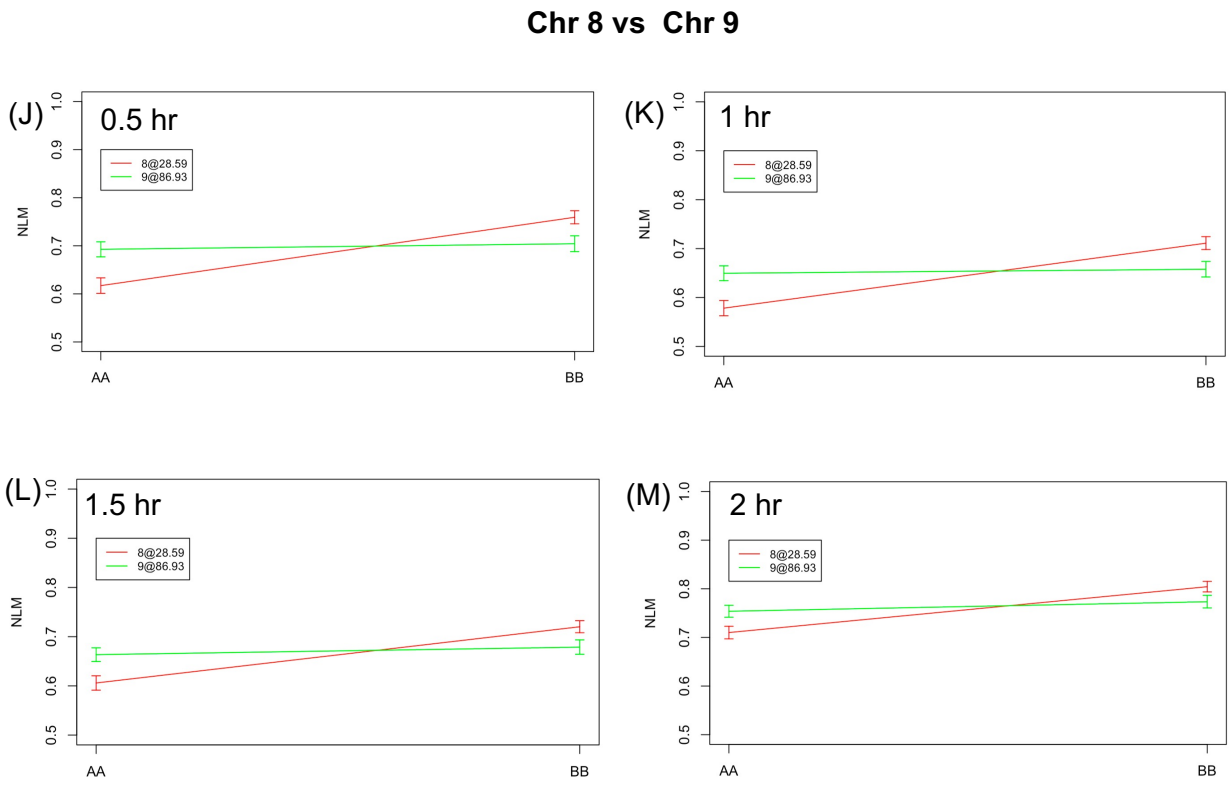

Table 2.1 List of QTL intervals identified in photosynthetic parameters and NLM from DEPI.

To refer to specific intervals related to different conditions and phenotypes, a standard nomenclature was established to allow comparisons of QTLs that appeared for different parameters, conditions and times that follow the format described in the following: Chromosome number - Index - Phenotype - Temperature, where control and low temperature are abbreviated as CT and LT. The indexes are numbered with Arabic numerals in the order of genomic loci of identified QTLs in each chromosome for the QTLs for that phenotype.

Condition & parameter	QTL	Position cM (Max)	Timepoints	Max LOD Score	Max LOD time	Flanking markers (bin ID)
CT_NLM	02-1-NLM-CT	0-5.44(5)	6	3.185	6	2_00017 (150) - 2_55217 (0)
CT_NLM	03-1-NLM-CT	79.25-85.29(80)	29,81	2.917	81	2_17678 (599) - 2_05841 (421)
CT_NLM	03-2-NLM-CT	93.94-96.36(95)	6	3.219	6	2_15499 (0) - 1_0464 (61)
CT_NLM	08-1-NLM-CT	34.73-35.34(35)	27	2.529	27	2_14158 (0) - 2_22265 (631)
CT_NLM	08-2-NLM-CT	34.73-45(40)	25	3.258	25	2_24467 (644) - 2_22265 (631)
CT_NLM	09-1-NLM-CT	32.89-37.75(35)	1,7,23	3.763	23	2_03318 (345) - 2_23951 (640)
CT_NLM	10-1-NLM-CT	0-15.24(5)	24,25,27,28	4.480	28	2_00769 (0) - 2_27368 (661)
CT_NLM	11-1-NLM-CT	4.26-15.65(10)	23-25	3.228	25	2_51243 (0) - 2_01407 (248)
CT_NPQt	04-1-NPQt-CT	21.14-31.48(25)	8,10-16	3.308	16	2_15552 (580) - 1_1180 (132)
CT_NPQt	04-2-NPQt-CT	21.74-55.91(40)	2,6,9-19	3.643	19	2_15552 (580) - 2_19932 (616)
CT_NPQt	05-1-NPQt-CT	0-5(0)	2,5-9	3.245	9	2_27768 (663) - 2_00867 (216)
CT_NPQt	06-1-NPQt-CT	65-65(65)	59-65	3.866	65	2_07111 (453) - 2_28687 (0)
CT_NPQt	07-1-NPQt-CT	85-87.65(85)	5,8,12,14-16,18-22	3.126	22	2_10213 (515) - 1_0445 (57)
CT_NPQt	09-1-NPQt-CT	18.84-51.87(25)	1-3,5,15,20-24,27-29,31-35,44-66,69,70,80-82	4.345	82	2_03318 (345) - 2_06862 (448)
CT_NPQt	09-2-NPQt-CT	90-90(90)	39-44	2.836	44	2_00155 (163) - 2_22085 (0)
CT_NPQt	10-1-NPQt-CT	0-0(0)	13-15	2.828	15	2_00769 (0) - 2_23503 (637)
CT_NPQt	10-2-NPQt-CT	20-30.7(25)	2-24,34-45,62-69	6.715	69	2_01336 (240) - 2_13304 (0)
CT_phi2	03-1-phi2-CT	122.47-128.61(125)	43-49,63-65,67-79	3.364	79	2_07401 (459) - 2_00276 (174)
CT_phi2	04-1-phi2-CT	19.29-21.14(20)	5,58	2.621	58	2_29604 (670) - 2_31549 (675)
CT_phi2	04-2-phi2-CT	39.38-45(40)	83	2.811	83	2_02276 (298) - 2_04962 (402)
CT_phi2	04-3-phi2-CT	37.54-64.45(60)	46-49,64-84	7.349	84	2_28660 (0) - 2_04962 (402)
CT_phi2	06-1-phi2-CT	65-70(65)	32-36,38-52,58-78,80,81	4.161	81	2_07111 (453) - 2_28687 (0)
CT_phi2	07-1-phi2-CT	23.82-25.61(25)	28,30-34,56,58-62,82-84	3.132	84	2_04614 (389) - 2_23639 (639)
CT_phi2	08-1-phi2-CT	39.6-50.02(45)	30-32,35-49,51,58-84	4.060	84	2_35933 (0) - 1_0119 (21)
CT_phi2	09-1-phi2-CT	18.24-28.68(20)	2,27,28,30-36,38,55,57,59-63	3.505	63	2_03318 (345) - 2_23951 (640)
CT_phi2	09-2-phi2-CT	70.68-104.15(95)	37-52,58-84	9.238	84	1_0566 (73) - 2_10754 (0)
CT_phi2	10-1-phi2-CT	0-0(0)	45,49-51,67,69-81	3.423	81	2_00769 (0) - 1_0960 (113)
CT_phi2	10-2-phi2-CT	24.06-30.7(30.7)	4-17,22,23	4.198	23	2_03594 (353) - 2_02764 (321)
CT_qEt	03-1-qEt-CT	50-50(50)	41,43	2.604	43	2_18360 (606) - 2_52429 (704)
CT_qEt	03-2-qEt-CT	60-60(60)	57,59	3.472	59	1_0139 (23) - 2_29505 (0)
CT_qEt	03-3-qEt-CT	95-95(95)	83	2.601	83	2_05841 (421) - 1_0464 (61)
CT_qEt	04-1-qEt-CT	15-15(15)	22,58	2.646	58	2_29604 (670) - 2_15552 (580)
CT_qEt	04-3-qEt-CT	52.26-64.45(64.45)	16,18,22,41,46,47,63-70,72,79-81	5.212	81	2_00148 (161) - 2_04962 (402)
CT_qEt	05-1-qEt-CT	0-5(0)	5-12,18,20,22,23,27	3.928	27	2_00867 (216) - 2_00867 (216)
CT_qEt	06-1-qEt-CT	35-35(35)	53	2.418	53	1_0706 (93) - 2_02761 (320)
CT_qEt	06-2-qEt-CT	65-65(65)	63	2.772	63	2_07111 (453) - 2_28687 (0)
CT_qEt	07-1-qEt-CT	83.97-87.65(87.65)	8-22,71,73,74	3.644	74	2_00368 (180) - 1_0445 (57)
CT_qEt	09-1-qEt-CT	30-30(30)	2-16,21,22,24-27,29-35,53-63,81-84	7.669	84	2_02910 (326) - 2_22930 (634)
CT_qEt	09-2-qEt-CT	72.51-104.15(95)	13-20,36-50,61-80	7.754	80	2_26780 (0) - 1_1393 (142)
CT_qEt	10-1-qEt-CT	20-30.7(20)	2,3,13-16	4.340	16	2_01336 (240) - 2_02764 (321)
CT_qEt	10-2-qEt-CT	20-30.7(25)	4-20,22,23,64-67	6.329	67	2_01336 (240) - 2_02764 (321)
CT_qEt	11-1-qEt-CT	0-18.73(15)	26-28,40-42,44-46,56,57,66-69,82,84	4.401	84	2_01374 (245) - 2_40688 (0)
CT_qIt	03-1-qIt-CT	10-10(10)	65,66	2.651	66	2_22512 (632) - 2_01216 (235)
CT_qIt	04-1-qIt-CT	1.85-5(5)	21,22	2.832	22	2_03034 (337) - 2_14079 (563)
CT_qIt	04-2-qIt-CT	28.41-45(40)	6,57,58	3.865	58	2_54080 (0) - 2_02591 (312)
CT_qIt	06-1-qIt-CT	60-70(65)	31,32,59-61	3.696	61	2_07111 (453) - 2_28687 (0)
CT_qIt	07-1-qIt-CT	26.21-40(35)	32-38	3.542	38	2_00708 (202) - 2_12852 (548)
CT_qIt	09-1-qIt-CT	0-9.68(0)	1,3,32-40,42-52,54,60-76,78-80	3.826	80	2_03318 (345) - 2_06862 (448)
CT_qIt	10-1-qIt-CT	24.06-30.7(30)	2,50-54,62	3.314	62	2_01336 (240) - 2_03621 (355)
CT_qL	03-1-qL-CT	54.69-70(65)	6,12,13,19,69-79,81-83	3.244	83	2_00856 (213) - 2_05364 (0)
CT_qL	03-2-qL-CT	82.91-110.78(105)	5-15,19,32,33	3.935	33	1_0464 (61) - 2_00276 (174)
CT_qL	03-3-qL-CT	120-128.61(128.61)	7-27,30,31,33-37,39-47,49-55,58,61-66,68,69,81	4.398	81	2_28969 (667) - 2_00276 (174)
CT_qL	04-1-qL-CT	41.18-64.45(60)	69-84	9.745	84	2_19932 (616) - 2_04962 (402)
CT_qL	05-1-qL-CT	0-1.24(0)	20,22,44,45	3.557	45	2_27768 (663) - 2_15996 (585)
CT_qL	06-1-qL-CT	9.05-11.46(10)	14-22	3.480	22	2_00562 (194) - 2_15517 (579)
CT_qL	07-1-qL-CT	82.17-87.65(85)	9-12,14-22,39,41	4.252	41	2_05041 (406) - 1_0445 (57)
CT_qL	08-1-qL-CT	24.03-25(25)	19,20,25,26	3.128	26	2_01018 (224) - 2_18484 (0)
CT_qL	09-1-qL-CT	55-55(55)	1,29,55,56	3.583	56	2_31633 (676) - 2_04495 (386)
CT_qL	09-2-qL-CT	70.08-104.15(95)	47-52,62-84	9.355	84	2_00704 (201) - 1_1393 (142)
CT_qL	10-1-qL-CT	9.76-15(10)	75-83	3.210	83	2_10282 (517) - 2_27368 (661)
CT_qL	10-2-qL-CT	20-30.7(25)	2-17,38,41	5.823	41	2_01336 (240) - 2_03621 (355)
CT_qL	11-1-qL-CT	12.04-30(20)	4-21,24,31-33,35-42,74-84	7.870	84	2_05408 (413) - 2_43772 (0)

Table 2.1 (cont'd):

LT_NLM	02-1-NLM-LT	0-5.44(5)	6	3.185	6	2_00017 (150) - 2_55217 (0)
LT_NLM	03-1-NLM-LT	25-35.59(35)	57,58,68	3.169	68	2_04902 (0) - 2_00276 (174)
LT_NLM	03-2-NLM-LT	80-80(80)	29	2.822	29	2_03696 (363) - 2_32628 (678)
LT_NLM	03-3-NLM-LT	93.94-96.36(95)	6	3.219	6	2_15499 (0) - 1_0464 (61)
LT_NLM	03-4-NLM-LT	118.75-128.61(125)	29-31	4.473	31	2_07401 (459) - 2_11085 (531)
LT_NLM	04-1-NLM-LT	0-6.75(5)	36,56,58-60	3.806	60	2_30806 (0) - 2_12502 (543)
LT_NLM	04-3-NLM-LT	63.24-64.45(64.45)	71	2.938	71	2_00148 (161) - 2_04962 (402)
LT_NLM	05-1-NLM-LT	45-47.05(47.05)	59,60	3.461	60	2_37534 (0) - 2_37534 (0)
LT_NLM	07-1-NLM-LT	27.4-40(30)	68,69	3.202	69	2_14066 (562) - 2_49566 (0)
LT_NLM	08-1-NLM-LT	3.62-47.61(25)	27,57-61,64,80,81	7.751	81	2_08836 (0) - 2_01656 (263)
LT_NLM	08-2-NLM-LT	34.73-47.61(45)	25,62-64	3.442	64	2_25875 (652) - 2_06817 (0)
LT_NLM	09-1-NLM-LT	35.93-66.41(45)	1,7,23,67-69	4.155	69	2_09913 (510) - 2_01767 (269)
LT_NLM	09-2-NLM-LT	91.31-104.15(95)	63,64	3.703	64	2_20425 (619) - 2_23951 (640)
LT_NLM	10-1-NLM-LT	0-30.7(15)	24,25,27-30,39,58-60	8.643	60	2_00769 (0) - 2_03668 (360)
LT_NLM	10-2-NLM-LT	0-30.7(30)	42,57	8.842	57	2_13304 (0) - 2_02764 (321)
LT_NLM	11-1-NLM-LT	0-36.51(15)	23-25,59-67,76	8.583	76	2_05408 (413) - 2_02538 (308)
LT_NPQt	02-1-NPQt-LT	34.08-50.37(35)	34-36,78-83	3.302	83	2_04228 (382) - 1_0016 (3)
LT_NPQt	02-2-NPQt-LT	46.16-50.37(50.37)	56,84	3.037	84	1_0270 (33) - 1_0016 (3)
LT_NPQt	03-1-NPQt-LT	29.51-41(35)	34,36,63-74	5.070	74	2_52693 (0) - 2_03074 (339)
LT_NPQt	04-1-NPQt-LT	21.14-31.48(25)	8,10-16,66	3.308	66	2_01982 (0) - 2_02474 (305)
LT_NPQt	04-2-NPQt-LT	44.88-64.45(50)	2,6,9-19,32,54-56,60,61	4.140	61	2_02409 (302) - 2_19932 (616)
LT_NPQt	04-3-NPQt-LT	44.88-64.45(60)	55,66,77-84	6.220	84	2_34117 (0) - 2_04962 (402)
LT_NPQt	05-1-NPQt-LT	0-5(0)	2,5-9	3.245	9	2_27768 (663) - 2_00867 (216)
LT_NPQt	06-1-NPQt-LT	30-30(30)	34,35,57	3.399	57	2_18129 (605) - 2_07111 (453)
LT_NPQt	06-2-NPQt-LT	50-50(50)	34-37,62	3.917	62	1_1007 (116) - 2_00431 (185)
LT_NPQt	07-1-NPQt-LT	85-87.65(85)	5,8,12,14-16,18-22	3.126	22	2_10213 (515) - 1_0445 (57)
LT_NPQt	08-1-NPQt-LT	15-15(15)	37	2.618	37	2_14158 (0) - 2_49638 (0)
LT_NPQt	08-2-NPQt-LT	23.42-25(25)	41,57-59,84	3.315	84	2_01018 (224) - 2_40055 (0)
LT_NPQt	08-3-NPQt-LT	51.88-54.29(54.29)	63-74	3.485	74	2_16563 (588) - 2_11907 (540)
LT_NPQt	09-1-NPQt-LT	18.84-51.87(25)	1-3,5,15,20-24,27,28,30,35-37,39,41,42,44,78,79,81-83	4.345	83	1_0410 (53) - 2_08769 (483)
LT_NPQt	09-2-NPQt-LT	74.98-104.15(95)	34-48,56,63-69,77-84	9.331	84	2_00704 (201) - 2_10754 (0)
LT_NPQt	10-1-NPQt-LT	9.76-15.83(15)	13-15,36-45,80-84	4.732	84	2_08475 (477) - 2_27368 (661)
LT_NPQt	10-2-NPQt-LT	20-30.7(25)	2-24,65-69,84	6.715	84	2_10944 (528) - 2_02764 (321)
LT_NPQt	11-1-NPQt-LT	18.12-30(25)	58,59,63-68	4.632	68	2_00471 (188) - 2_05408 (413)
LT_phi2	02-1-phi2-LT	33.49-50.37(35)	45,57-59,65,76-84	4.227	84	1_0270 (33) - 1_0016 (3)
LT_phi2	02-2-phi2-LT	34.69-50.37(50.37)	31-56,58,60-64,66-75	4.654	75	1_0270 (33) - 1_0016 (3)
LT_phi2	03-1-phi2-LT	16.64-22.08(20)	48-55,61-84	4.001	84	2_06509 (435) - 2_08749 (482)
LT_phi2	03-3-phi2-LT	85-85(85)	32	2.797	32	2_39493 (689) - 2_05841 (421)
LT_phi2	04-1-phi2-LT	30-30(30)	5	2.503	5	2_15552 (580) - 2_01894 (275)
LT_phi2	04-2-phi2-LT	44.88-54.71(50)	57,58	4.002	58	2_01952 (278) - 1_0606 (79)
LT_phi2	04-3-phi2-LT	42.38-64.45(60)	46-56,59-84	9.847	84	2_00148 (161) - 2_10838 (526)
LT_phi2	06-1-phi2-LT	23.52-33.79(30)	33-42,45,57-62	4.324	62	2_00478 (190) - 2_25422 (0)
LT_phi2	07-1-phi2-LT	0-0(0)	28	2.804	28	2_05041 (406) - 2_15610 (581)
LT_phi2	08-1-phi2-LT	24.03-25(25)	60-62,64,81-84	3.131	84	2_01018 (224) - 2_49638 (0)
LT_phi2	09-1-phi2-LT	42.16-46.42(45)	2,27,28,32-35,38,42,44,46,49-54,60-84	4.675	84	1_0410 (53) - 2_08769 (483)
LT_phi2	09-2-phi2-LT	85.71-104.15(95)	44-56,59-84	9.775	84	2_05643 (416) - 2_22085 (0)
LT_phi2	10-1-phi2-LT	6.7-15.83(15)	56,59-66,71-84	4.633	84	2_00495 (192) - 2_27368 (661)
LT_phi2	10-2-phi2-LT	24.06-30.7(30.7)	4-17,22,23	4.198	23	2_03594 (353) - 2_02764 (321)
LT_phi2	11-1-phi2-LT	23.92-36.51(30)	59,77-84	3.769	84	2_26255 (656) - 2_06463 (0)
LT_qEt	01-1-qEt-LT	15-15(15)	41-44,62,63	3.520	63	1_0052 (13) - 2_26118 (654)
LT_qEt	02-1-qEt-LT	40-40(40)	42,78,80-82	3.041	82	1_0270 (33) - 1_0016 (3)
LT_qEt	03-1-qEt-LT	12.95-26.38(20)	52-56,73,74,76-84	6.980	84	2_06509 (435) - 2_08749 (482)
LT_qEt	03-2-qEt-LT	30.73-40.4(35)	53,67,70	4.208	70	2_52693 (0) - 2_53153 (0)
LT_qEt	03-3-qEt-LT	80-80(80)	37,82,83	3.097	83	2_04902 (0) - 2_00276 (174)
LT_qEt	03-4-qEt-LT	95-95(95)	37,42,44,46,47	3.529	47	2_00136 (159) - 2_20215 (0)
LT_qEt	04-1-qEt-LT	15-15(15)	22	2.646	22	2_14079 (563) - 2_04962 (402)
LT_qEt	04-2-qEt-LT	44.88-64.45(45)	83	2.984	83	2_00148 (161) - 2_10838 (526)
LT_qEt	04-3-qEt-LT	46.73-64.45(60)	16,18,22,32,34,51-55,59-62,77,78,80-84	6.875	84	2_00148 (161) - 2_04962 (402)
LT_qEt	05-1-qEt-LT	0-5(0)	5-12,18,20,22,23,27	3.928	27	2_00867 (216) - 2_00867 (216)
LT_qEt	05-2-qEt-LT	35-35(35)	33,34,36,40,48,51,70	3.485	70	2_10000 (0) - 2_37534 (0)
LT_qEt	06-1-qEt-LT	28.96-32.57(30)	35,53,57,76	3.271	76	2_14092 (564) - 2_02029 (285)
LT_qEt	06-2-qEt-LT	60-70(65)	55,56	3.793	56	2_07111 (453) - 1_0369 (45)
LT_qEt	07-1-qEt-LT	83.97-87.65(87.65)	8-22,52,53	3.644	53	2_05041 (406) - 1_0445 (57)
LT_qEt	08-1-qEt-LT	5-5(5)	49	3.676	49	2_29455 (0) - 2_16123 (586)
LT_qEt	08-2-qEt-LT	15-15(15)	37,41,42,44,49	3.937	49	2_14158 (0) - 2_13241 (552)
LT_qEt	09-1-qEt-LT	14.52-50.08(30)	2-16,21,22,24-27,32,34,61,62,81	6.700	81	2_31633 (676) - 2_08769 (483)
LT_qEt	09-2-qEt-LT	74.98-104.15(95)	13-20,37,39-47,51-56,59-61,75-84	9.717	84	2_11917 (0) - 2_22085 (0)
LT_qEt	10-1-qEt-LT	20-30.7(20)	2,3,13-16,36,38	4.340	38	2_01336 (240) - 1_1520 (149)
LT_qEt	10-2-qEt-LT	20-30.7(25)	4-20,22,23,37,42,45,47,49,65,67-72,74	6.329	74	2_17839 (602) - 2_13304 (0)
LT_qEt	11-1-qEt-LT	18.12-30(25)	26-28,36,37,40-42,44,45,47,54,55,62,63,65-68,78,80,82,83	5.646	83	2_44401 (0) - 2_06463 (0)

Table 2.1 (cont'd)

LT_qIt	02-1-qIt-LT	24.47-27.48(25)	34-37,57	2.875	57	2_20629 (0) - 1_0270 (33)
LT_qIt	03-1-qIt-LT	30-45(35)	35,36,63-74	4.170	74	2_53153 (0) - 1_0145 (24)
LT_qIt	04-1-qIt-LT	1.85-5(5)	21,22	2.832	22	2_03034 (337) - 2_14079 (563)
LT_qIt	04-2-qIt-LT	39.98-45(45)	6	2.518	6	2_02276 (298) - 2_01952 (278)
LT_qIt	04-3-qIt-LT	50-64.45(64.45)	36-40,43,65-68,78-84	4.354	84	2_01952 (278) - 2_04962 (402)
LT_qIt	06-1-qIt-LT	48.76-52.48(50)	34-38	3.547	38	2_02891 (324) - 2_19095 (0)
LT_qIt	08-1-qIt-LT	12.93-15.41(15)	84	2.741	84	2_46774 (0) - 2_46251 (0)
LT_qIt	08-2-qIt-LT	20.96-40.21(35)	57-59,84	3.543	84	2_01018 (224) - 2_49638 (0)
LT_qIt	08-3-qIt-LT	49.41-54.29(50)	63,65-69	3.039	69	2_03440 (347) - 2_11907 (540)
LT_qIt	09-1-qIt-LT	0-1.79(0)	1,3,29,34,36-38,41,43-45	3.960	45	2_03318 (345) - 2_01512 (253)
LT_qIt	09-2-qIt-LT	78.71-104.15(95)	34-48,59,62-70,79-81	9.965	81	2_54820 (0) - 2_23951 (640)
LT_qIt	10-1-qIt-LT	14.03-30.7(20)	36-44,81-84	3.492	84	2_08475 (477) - 2_27368 (661)
LT_qIt	10-2-qIt-LT	21.04-30.7(25)	2,41,65-67	3.670	67	2_17839 (602) - 2_02764 (321)
LT_qIt	11-1-qIt-LT	0-20(15)	57-60,63-67	4.585	67	2_01687 (264) - 2_05408 (413)
LT_qL	02-1-qL-LT	34.69-50.37(35)	64,65,71,74,76,78,79,84	2.930	84	2_04228 (382) - 1_0016 (3)
LT_qL	02-2-qL-LT	42.53-50.37(50.37)	37-55,62-83	4.633	83	1_0270 (33) - 1_0016 (3)
LT_qL	03-1-qL-LT	12.95-24.53(20)	49-55,62-66,76,77,79-84	5.441	84	1_0459 (60) - 2_04251 (0)
LT_qL	03-3-qL-LT	64.79-67.8(65)	6,12,13,19,14	3.124	19	2_20457 (0) - 2_00276 (174)
LT_qL	03-4-qL-LT	82.91-110.78(105)	5-15,19,29,30	3.935	30	2_52628 (0) - 2_20215 (0)
LT_qL	03-5-qL-LT	120-128.61(128.61)	7-27,32-34,36,37,57-61	4.398	61	2_28969 (667) - 2_00276 (174)
LT_qL	04-1-qL-LT	44.88-64.45(60)	42-55,62-84	9.950	84	2_00148 (161) - 2_10537 (520)
LT_qL	05-1-qL-LT	0-1.24(0)	20,22	3.557	22	2_27768 (663) - 2_15996 (585)
LT_qL	05-2-qL-LT	45-47.05(47.05)	58-60	3.827	60	2_37534 (0) - 2_37534 (0)
LT_qL	06-1-qL-LT	9.05-11.46(10)	14-22,39	3.480	39	2_00562 (194) - 2_06302 (430)
LT_qL	07-1-qL-LT	82.17-87.65(85)	9-12,14-22	4.252	22	2_15784 (583) - 1_0445 (57)
LT_qL	08-1-qL-LT	14.8-37.16(25)	19,20,25,26,36,57-66,68,69,71	6.727	71	2_01018 (224) - 2_49638 (0)
LT_qL	09-1-qL-LT	42.75-46.42(45)	1,39,41,42,44-47,60-64,66	3.627	66	2_02459 (304) - 2_08769 (483)
LT_qL	09-2-qL-LT	85-104.15(95)	34-56,58-84	9.866	84	2_20425 (619) - 2_22085 (0)
LT_qL	10-1-qL-LT	0-15.83(10)	57-59,64-66,68,71,77-79,81-83	5.301	83	2_00769 (0) - 2_01356 (243)
LT_qL	10-2-qL-LT	20-30.7(25)	2-17	5.823	14	2_01336 (240) - 2_03621 (355)
LT_qL	11-1-qL-LT	12.04-30(20)	4-21,24,30,31,57-60,69,75,80-84	7.870	84	2_26255 (656) - 2_06463 (0)

Table 2.2 List of QTL intervals identified in photosynthetic parameters from MultispeQ.

To refer to specific intervals related to different conditions and phenotypes, a standard nomenclature was established to allow comparisons of QTLs that appeared for different parameters, conditions and times that follow the format described in the following: Chromosome number - Index - Phenotype - Temperature, where control and low temperature are abbreviated as CT and LT. The indexes are numbered with Arabic numerals in the order of genomic loci of identified QTLs in each chromosome for the QTLs for that phenotype.

Condition & parameter	QTL	position(max)	Max LOD Score	Flanking markers (bin ID)
CT_ECSt	04-1-ECSt-CT	59.04-63.24(60)	3.0123	2_19932 (616) - 2_04962 (402)
CT_ECSt	09-1-ECSt-CT	92.51-104.15(100)	3.1233	2_54820 (0) - 2_23951 (640)
CT_gH+	04-1-gH+-CT	21.74-64.45(55)	7.9810	2_02591 (312) - 2_04962 (402)
CT_gH+	09-1-gH+-CT	91.31-98.07(95)	4.8152	2_05643 (416) - 2_22085 (0)
CT_kb6f	04-1-kb6f-CT	50-64.45(55)	3.9373	2_28660 (0) - 2_04962 (402)
CT_kb6f	09-1-kb6f-CT	90-104.15(95)	5.9968	2_05643 (416) - 2_22085 (0)
CT_LEF	04-1-LEF-CT	23.56-27.19(25)	3.1053	2_01982 (0) - 2_03603 (354)
CT_LEF	04-2-LEF-CT	39.38-64.45(60)	11.9082	2_00148 (161) - 2_04962 (402)
CT_LEF	07-1-LEF-CT	34.59-38.79(35)	2.8014	2_46826 (0) - 2_01440 (251)
CT_LEF	07-2-LEF-CT	46.89-55(50)	3.7210	2_03655 (359) - 2_26701 (0)
CT_LEF	09-1-LEF-CT	85.71-104.15(95)	6.9620	2_05643 (416) - 2_22085 (0)
CT_LEF	10-1-LEF-CT	10-15.83(15)	3.3780	2_00495 (192) - 2_27368 (661)
CT_LEF	10-2-LEF-CT	28.88-30.7(30.7)	2.8321	2_08301 (469) - 2_02764 (321)
CT_LEF	11-1-LEF-CT	30-36.51(35)	3.3516	2_05408 (413) - 2_06463 (0)
CT_P700+	04-1-P700+-CT	40.57-64.45(45)	4.4239	2_01894 (275) - 2_04962 (402)
CT_P700+	09-1-P700+-CT	90-100(95)	5.9710	2_11917 (0) - 2_22085 (0)
CT_P700+	11-1-P700+-CT	35-35(35)	2.8495	2_05408 (413) - 2_06463 (0)
CT_Phi2	03-1-Phi2-CT	54.09-75.65(65)	3.7675	2_52429 (704) - 2_01134 (231)
CT_Phi2	04-1-Phi2-CT	21.14-64.45(60)	15.3810	2_01351 (242) - 2_41020 (0)
CT_Phi2	07-1-Phi2-CT	7.3-15(10)	3.9174	1_0021 (6) - 1_0164 (27)
CT_Phi2	07-2-Phi2-CT	49.3-63.83(50)	2.9135	2_03655 (359) - 2_06408 (432)
CT_Phi2	07-3-Phi2-CT	69.31-70(70)	2.6224	2_03655 (359) - 2_02124 (292)
CT_Phi2	09-1-Phi2-CT	70-104.15(95)	14.3357	2_22085 (0) - 2_22085 (0)
CT_Phi2	10-1-Phi2-CT	10-15.24(15)	2.8313	2_10282 (517) - 2_27368 (661)
CT_Phi2	11-1-Phi2-CT	23.29-39.54(35)	8.0677	2_05408 (413) - 2_06463 (0)
CT_qL	03-1-qL-CT	60.18-75.04(65)	3.5842	1_1162 (130) - 2_17678 (599)
CT_qL	04-1-qL-CT	21.14-64.45(60)	17.1441	2_01351 (242) - 2_10537 (520)
CT_qL	06-1-qL-CT	53.1-80(60)	3.3071	2_28423 (0) - 2_05713 (417)
CT_qL	07-1-qL-CT	11.72-15(15)	3.0113	2_11430 (0) - 2_01552 (255)
CT_qL	07-2-qL-CT	59.64-62.03(60)	3.0969	1_0985 (115) - 2_19635 (0)
CT_qL	09-1-qL-CT	72.51-104.15(95)	13.4421	2_11917 (0) - 2_22085 (0)
CT_qL	11-1-qL-CT	18.12-38.94(30)	7.6393	2_05408 (413) - 2_05408 (413)
CT_vH+	01-1-vH+-CT	10-10(10)	2.6992	2_03707 (364) - 2_03947 (374)
CT_vH+	04-1-vH+-CT	22.35-64.45(60)	14.1826	2_00148 (161) - 2_10838 (526)
CT_vH+	09-1-vH+-CT	85-104.15(95)	7.8861	2_11917 (0) - 2_22085 (0)
CT_vH+	10-1-vH+-CT	9.76-30.7(15)	4.1291	2_08475 (477) - 2_27368 (661)
CT_vH+	11-1-vH+-CT	19.34-36.51(30)	4.2447	2_44401 (0) - 2_06463 (0)

Table 2.2 (cont'd):

LT_ECSt	03-1-ECSt-LT	49.89-65.4(55)	5.7556	2_43060 (0) - 1_1162 (130)
LT_ECSt	04-1-ECSt-LT	41.18-63.24(45)	5.0845	2_02591 (312) - 2_00557 (193)
LT_ECSt	09-1-ECSt-LT	74.98-104.15(95)	10.8291	2_22085 (0) - 2_22085 (0)
LT_ECSt	11-1-ECSt-LT	24.52-36.51(35)	3.8566	2_05408 (413) - 2_06463 (0)
LT_gH+	04-1-gH+-LT	52.87-60.83(55)	2.8933	2_28660 (0) - 2_04962 (402)
LT_gH+	09-1-gH+-LT	93.76-95.59(95)	2.7938	2_54820 (0) - 2_10754 (0)
LT_kb6f	04-1-kb6f-LT	34.47-64.45(35)	3.0402	2_47522 (0) - 2_04962 (402)
LT_kb6f	09-1-kb6f-LT	86.93-104.15(95)	6.9986	2_05643 (416) - 2_22085 (0)
LT_kb6f	10-1-kb6f-LT	3.68-15.83(15)	4.4668	2_00495 (192) - 2_27368 (661)
LT_LEF	04-1-LEF-LT	60-64.45(64.45)	2.7188	2_00148 (161) - 2_04962 (402)
LT_LEF	08-1-LEF-LT	25-25(25)	2.7418	2_01018 (224) - 2_40055 (0)
LT_LEF	09-1-LEF-LT	74.98-75.58(75)	2.8359	2_30840 (0) - 2_23951 (640)
LT_LEF	09-2-LEF-LT	85-104.15(95)	8.2250	2_05643 (416) - 2_22085 (0)
LT_NPQt	08-1-NPQt-LT	20.35-28.59(25)	4.3497	2_01018 (224) - 2_49638 (0)
LT_NPQt	09-1-NPQt-LT	56.08-104.15(95)	5.5294	2_05643 (416) - 2_10754 (0)
LT_NPQt	10-1-NPQt-LT	6.7-15.83(15)	3.3773	2_01589 (257) - 2_27368 (661)
LT_NPQt	11-1-NPQt-LT	63.86-69.43(69.43)	2.7480	1_0377 (47) - 2_11549 (0)
LT_P700+	04-1-P700+-LT	52.26-63.24(60)	3.2979	2_28660 (0) - 2_14029 (0)
LT_P700+	09-1-P700+-LT	93.15-95.59(95)	3.1144	2_29667 (0) - 2_10754 (0)
LT_Phi2	04-1-Phi2-LT	55.91-63.24(60)	4.2266	2_00148 (161) - 2_10838 (526)
LT_Phi2	08-1-Phi2-LT	22.81-29.25(25)	4.5566	2_09438 (502) - 2_49638 (0)
LT_Phi2	09-1-Phi2-LT	59.73-60(60)	2.6431	2_01496 (252) - 2_23951 (640)
LT_Phi2	09-2-Phi2-LT	67.61-104.15(95)	11.7674	2_22085 (0) - 2_22085 (0)
LT_Phi2	10-1-Phi2-LT	10-15.83(15)	3.3966	2_00495 (192) - 2_27368 (661)
LT_qL	04-1-qL-LT	55.91-63.24(60)	4.7756	2_00148 (161) - 2_10537 (520)
LT_qL	06-1-qL-LT	78.86-81.33(80)	3.0791	2_28687 (0) - 2_05713 (417)
LT_qL	09-1-qL-LT	74.98-104.15(95)	9.0305	2_00704 (201) - 2_22085 (0)
LT_qL	11-1-qL-LT	23.29-25(25)	3.0237	2_44401 (0) - 2_05408 (413)
LT_vH+	03-1-vH+-LT	52.89-65.4(60)	4.2323	2_52429 (704) - 2_29505 (0)
LT_vH+	04-1-vH+-LT	34.47-64.45(60)	5.7996	2_02591 (312) - 2_04962 (402)
LT_vH+	09-1-vH+-LT	70-104.15(95)	12.4418	2_22085 (0) - 2_22085 (0)
LT_vH+	11-1-vH+-LT	23.29-36.51(30)	3.7875	2_26255 (656) - 2_06463 (0)

Table S2.1 List of Recombinant inbred line (RIL) parental crossings used for screening.

	Mapping Population
1	524B x IT84S-2049
2	CB27 x 24-125B-1
3	CB27 x IT82E-18
4	CB27 x IT97K-556-6
5	CB27 x UCR 779
6	CB46 x IT93K-503-1
7	Dan Ila x Tvu-7778
8	Sanzi x Vita 7
9	Yacine x 58-77

Table S2.2 Average temperatures experienced in cowpea fields.
Values are average field conditions from 2012 to 2016 in Tulare, Central valley of California where cowpea is normally grown in April one month ahead of normal planting, taken from the data available from the National Oceanic and Atmospheric Administration, https://www.noaa.gov. Temperatures in the highlighted cells were replicated in the DEPI chambers for the cowpea experiments described in the main text.

	2016		2015		2014		2013		2013		2012		2012 - 2016	
	Average	Minimum	Average	Minimum	Average	Minimum	Average	Minimum	Average	Minimum	Average	Minimum	Average	Minimum
Max	25°C	19°C	25°C	13°C	25°C	13°C	27°C	21°C	24°C	13°C	24°C	13°C	25.6°C	16.6°C
Mean	19°C	14°C	18°C	11°C	18°C	11°C	20°C	14°C	17°C	11°C	17°C	11°C	18.6°C	12.4°C
Min	12°C	8°C	11°C	6°C	11°C	6°C	12°C	6°C	11°C	3°C	11°C	3°C	11.6°C	5.8°C

BIBLIOGRAPHY

BIBLIOGRAPHY

1. Allen D.J. & Ort D.R. (2001) Impacts of chilling temperatures on photosynthesis in warm-climate plants. *Trends in Plant Science* **6**, 36–42.

2. Aro E.-M., Virgin I. & Andersson B. (1993) Photoinhibition of photosystem II. Inactivation, protein damage and turnover. *Biochimica et Biophysica Acta (BBA)-Bioenergetics* **1143**, 113–134.

3. Avenson T.J., Cruz J.A., Kanazawa A. & Kramer D.M. (2005a) Regulating the proton budget of higher plant photosynthesis. *Proceedings of the National Academy of Sciences of the United States of America* **102**, 9709–9713.

4. Avenson T.J., Kanazawa A., Cruz J.A., Takizawa K., Ettinger W.E. & Kramer D.M. (2005b) Integrating the proton circuit into photosynthesis: progress and challenges. *Plant, Cell & Environment* **28**, 97–109.

5. Baker N.R., Harbinson J. & Kramer D.M. (2007) Determining the limitations and regulation of photosynthetic energy transduction in leaves. *Plant, Cell & Environment* **30**, 1107–1125.

6. Baker N.R. & Oxborough K. (2004) Chlorophyll fluorescence as a probe of photosynthetic productivity. In *Chlorophyll a Fluorescence*. pp. 65–82. Springer.

7. Baxter I. (2020) We aren't good at picking candidate genes, and it's slowing us down. *Current Opinion in Plant Biology* **54**, 57–60.

8. Boukar O., Fatokun C.A., Huynh B.-L., Roberts P.A. & Close T.J. (2016) Genomic tools in cowpea breeding programs: status and perspectives. *Frontiers in plant science* **7**, 757.

9. Broman K.W. & Sen S. (2009) *A Guide to QTL Mapping with R/qtl*. Springer New York, New York, NY.

10. Broman K.W. (2001) Review of statistical methods for QTL mapping in experimental crosses. *Lab animal* **30**, 44–52.

11. Caicedo A.L., Stinchcombe J.R., Olsen K.M., Schmitt J. & Purugganan M.D. (2004) Epistatic interaction between Arabidopsis FRI and FLC flowering time genes generates a latitudinal cline in a life history trait. *Proceedings of the National Academy of Sciences of the United States of America* **101**, 15670–15675.

12. Chow W.S. & Hope A.B. (2004) Kinetics of reactions around the cytochrome bf complex studied in intact leaf disks. *Photosynthesis Research* **81**, 153–163.

13. Cruz J.A., Avenson T.J., Kanazawa A., Takizawa K., Edwards G.E. & Kramer D.M. (2005) Plasticity in light reactions of photosynthesis for energy production and photoprotection. *Journal of Experimental Botany* **56**, 395–406.

14. Cruz J.A., Savage L.J., Zegarac R., Hall C.C., Satoh-Cruz M., Davis G.A., … Kramer D.M. (2016) Dynamic environmental photosynthetic imaging reveals emergent phenotypes. *Cell Systems* **2**, 365–377.

15. Davis G.A., Kanazawa A., Schöttler M.A., Kohzuma K., Froehlich J.E., Rutherford A.W., … Kramer D.M. (2016) Limitations to photosynthesis by proton motive force-induced photosystem II photodamage. *eLife* **5**.

16. Ehlers J.D., Hall A.E., Patel P.N., Roberts P.A. & Matthews W.C. (2000) Registration ofCalifornia Blackeye 27'Cowpea. *Crop Science* **40**, 854–854.

17. Fisher N., Bricker T.M. & Kramer D.M. (2019) Regulation of photosynthetic cyclic electron flow pathways by adenylate status in higher plant chloroplasts. *Biochimica et biophysica acta. Bioenergetics* **1860**, 148081.

18. Gu L., Hanson P.J., Post W.M., Kaiser D.P., Yang B., Nemani R., … Meyers T. (2008) The 2007 eastern US spring freeze: increased cold damage in a warming world? *Bioscience* **58**, 253–262.

19. Herbert T.J. (1992) Geometry of heliotropic and nyctinastic leaf movements. *American Journal of Botany* **79**, 547–550.

20. Huang W., Zhang J.-L., Zhang S.-B. & Hu H. (2014) Evidence for the regulation of leaf movement by photosystem II activity. *Environmental and experimental botany* **107**, 167–172.

21. Huang W., Zhang S.-B. & Cao K.-F. (2012) Evidence for leaf fold to remedy the deficiency of physiological photoprotection for photosystem II. *Photosynthesis Research* **110**, 185–191.

22. Huner N.P.A., Öquist G. & Sarhan F. (1998) Energy balance and acclimation to light and cold. *Trends in Plant Science* **3**, 224–230.

23. Hutchison R.S., Groom Q. & Ort D.R. (2000) Differential effects of chilling-induced photooxidation on the redox regulation of photosynthetic enzymes. *Biochemistry* **39**, 6679–6688.

24. Huynh B.-L., Ehlers J.D., Huang B.E., Muñoz-Amatriaín M., Lonardi S., Santos J.R.P., … Roberts P.A. (2018) A multi-parent advanced generation inter-cross

(MAGIC) population for genetic analysis and improvement of cowpea (Vigna unguiculata L. Walp.). *The Plant Journal: for Cell and Molecular Biology* **93**, 1129–1142.

25. Huynh B.-L., Matthews W.C., Ehlers J.D., Lucas M.R., Santos J.R.P., Ndeve A., … Roberts P.A. (2016) A major QTL corresponding to the Rk locus for resistance to root-knot nematodes in cowpea (Vigna unguiculata L. Walp.). *TAG. Theoretical and Applied Genetics. Theoretische und Angewandte Genetik* **129**, 87–95.

26. Ivanov A.G., Rosso D., Savitch L.V., Stachula P., Rosembert M., Oquist G., … Hüner N.P.A. (2012) Implications of alternative electron sinks in increased resistance of PSII and PSI photochemistry to high light stress in cold-acclimated Arabidopsis thaliana. *Photosynthesis research* **113**, 191–206.

27. Jansen R.C. (2004) Quantitative trait loci in inbred lines. In *Handbook of statistical genetics*. (eds D.J. Balding, M. Bishop & C. Cannings), John Wiley & Sons, Ltd, Chichester.

28. Kanazawa A. & Kramer D.M. (2002) In vivo modulation of nonphotochemical exciton quenching (NPQ) by regulation of the chloroplast ATP synthase. *Proceedings of the National Academy of Sciences of the United States of America* **99**, 12789–12794.

29. Kanazawa A., Ostendorf E., Kohzuma K., Hoh D., Strand D.D., Sato-Cruz M., … Kramer D.M. (2017) Chloroplast ATP synthase modulation of the thylakoid proton motive force: implications for photosystem I and photosystem II photoprotection. *Frontiers in plant science* **8**, 719.

30. Kramer D.M., Avenson T.J. & Edwards G.E. (2004) Dynamic flexibility in the light reactions of photosynthesis governed by both electron and proton transfer reactions. *Trends in Plant Science* **9**, 349–357.

31. Kuhlgert S., Austic G., Zegarac R., Osei-Bonsu I., Hoh D., Chilvers M.I., … Kramer D.M. (2016) MultispeQ Beta: a tool for large-scale plant phenotyping connected to the open PhotosynQ network. *Royal Society Open Science* **3**, 160592.

32. Long S.P., Zhu X.-G., Naidu S.L. & Ort D.R. (2006) Can improvement in photosynthesis increase crop yields? *Plant, Cell & Environment* **29**, 315–330.

33. Lucas M.R., Diop N.-N., Wanamaker S., Ehlers J.D., Roberts P.A. & Close T.J. (2011) Cowpea–Soybean Synteny Clarified through an Improved Genetic Map. *The Plant Genome Journal* **4**, 218.

34. Meng L., Li H., Zhang L. & Wang J. (2015) QTL IciMapping: Integrated software

for genetic linkage map construction and quantitative trait locus mapping in biparental populations. *The Crop journal* **3**, 269–283.

35. Miles C.M. & Wayne M. (2008) Quantitative trait locus (QTL) analysis. *Nature Education 1 (1)* **208**.

36. Moon B.Y., Higashi S., Gombos Z. & Murata N. (1995) Unsaturation of the membrane lipids of chloroplasts stabilizes the photosynthetic machinery against low-temperature photoinhibition in transgenic tobacco plants. *Proceedings of the National Academy of Sciences of the United States of America* **92**, 6219–6223.

37. Muchero W., Diop N.N., Bhat P.R., Fenton R.D., Wanamaker S., Pottorff M., … Close T.J. (2009) A consensus genetic map of cowpea [Vigna unguiculata (L) Walp.] and synteny based on EST-derived SNPs. *Proceedings of the National Academy of Sciences of the United States of America* **106**, 18159–18164.

38. Muchero W., Roberts P.A., Diop N.N., Drabo I., Cisse N., Close T.J., … Ehlers J.D. (2013) Genetic architecture of delayed senescence, biomass, and grain yield under drought stress in cowpea. *Plos One* **8**, e70041.

39. Murata N., Takahashi S., Nishiyama Y. & Allakhverdiev S.I. (2007) Photoinhibition of photosystem II under environmental stress. *Biochimica et Biophysica Acta* **1767**, 414–421.

40. ORT D.R. (2002) Chilling-induced limitations on photosynthesis in warm climate plants: contrasting mechanisms. *Environment Control in Biology* **40**, 7–18.

41. Raines C.A. (2011) Increasing photosynthetic carbon assimilation in C3 plants to improve crop yield: current and future strategies. *Plant Physiology* **155**, 36–42.

42. Roff D.A. (2007) A centennial celebration for quantitative genetics. *Evolution* **61**, 1017–1032.

43. Roux F., Camilleri C., Giancola S., Brunel D. & Reboud X. (2005) Epistatic interactions among herbicide resistances in Arabidopsis thaliana: the fitness cost of multiresistance. *Genetics* **171**, 1277–1288.

44. Sassenrath G.F., Ort D.R. & Portis Jr A.R. (1990) Impaired reductive activation of stromal bisphosphatases in tomato leaves following low-temperature exposure at high light. *Archives of Biochemistry and Biophysics* **282**, 302–308.

45. Savitch L.V., Ivanov A.G., Gudynaite-Savitch L., Huner N.P.A. & Simmonds J. (2011) Cold stress effects on PSI photochemistry in Zea mays: differential increase of FQR-dependent cyclic electron flow and functional implications. *Plant & Cell Physiology* **52**, 1042–1054.

46. Sonoike K. (1996) Photoinhibition of photosystem I: its physiological significance in the chilling sensitivity of plants. *Plant and Cell Physiology* **37**, 239–247.

47. Takagi D., Takumi S., Hashiguchi M., Sejima T. & Miyake C. (2016) Superoxide and Singlet Oxygen Produced within the Thylakoid Membranes Both Cause Photosystem I Photoinhibition. *Plant Physiology* **171**, 1626–1634.

48. Takizawa K., Kanazawa A., Kramer D.M., Takizawa K., Cruz J.A., Kanazawa A., … Kramer D.M. (2008) Depletion of stromal P(i) induces high "energy-dependent" antenna exciton quenching (q(E)) by decreasing proton conductivity at CF(O)-CF(1) ATP synthase. *Plant Cell Environ* **31**, 235–43.

49. Telfer A. (2014) Singlet oxygen production by PSII under light stress: mechanism, detection and the protective role of β-carotene. *Plant & Cell Physiology* **55**, 1216–1223.

50. Tietz S., Hall C.C., Cruz J.A. & Kramer D.M. (2017) NPQ(T) : a chlorophyll fluorescence parameter for rapid estimation and imaging of non-photochemical quenching of excitons in photosystem-II-associated antenna complexes. *Plant, Cell & Environment* **40**, 1243–1255.

51. Tikkanen M., Grieco M., Nurmi M., Rantala M., Suorsa M. & Aro E.-M. (2012) Regulation of the photosynthetic apparatus under fluctuating growth light. *Philosophical Transactions of the Royal Society of London. Series B, Biological Sciences* **367**, 3486–3493.

52. Tyystjärvi E. & Aro E.M. (1996) The rate constant of photoinhibition, measured in lincomycin-treated leaves, is directly proportional to light intensity. *Proceedings of the National Academy of Sciences of the United States of America* **93**, 2213–2218.

53. Van Os H., Stam P., Visser R.G.F. & Van Eck H.J. (2005) RECORD: a novel method for ordering loci on a genetic linkage map. *TAG. Theoretical and Applied Genetics. Theoretische und Angewandte Genetik* **112**, 30–40.

54. Yang J.T., Preiser A.L., Li Z., Weise S.E. & Sharkey T.D. (2016) Triose phosphate use limitation of photosynthesis: short-term and long-term effects. *Planta* **243**, 687–698.

55. Zack G.W., Rogers W.E. & Latt S.A. (1977) Automatic measurement of sister chromatid exchange frequency. *The Journal of Histochemistry and Cytochemistry* **25**, 741–753.

56. Zelitch I. (1982) The close relationship between net photosynthesis and crop yield. *Bioscience* **32**, 796–802.

CHAPTER 3

GENETICALLY-CONTROLLED VARIATIONS IN PHOTOSYNTHESIS INDICATE NEW ROLES FOR FATTY ACID IN RESPONSE

Work presented is in preparation for publication:

Donghee Hoh, Isaac Osei-Bonsu, Abhijnan Chattopadhyay, Atsuko Kanazawa, Nicholas Fisher, Oliver L Tessmer, Jeffrey Cruz, Philip A. Roberts, Bao-Lam Huynh, Lina Yin, Patrick Horn, David Hall, Christoph Benning and David M. Kramer

3.1 Abstract

Our recent work (Hoh et al., 2021) showed that genetic diversity in chilling stress responses in a recombinant inbred line (RIL) population of cowpea (*Vigna unguiculata. Walp*), a crop species sensitive to both heat and chilling stress, modulated a network of feedback regulatory processes of the light reactions, involving the thylakoid proton motive force (*pmf*), cyclic electron flow (CEF), the redox state of Q_A in photosystem II (PSII), which control the rate of PSII photodamage. Here we extend these studies by testing for linkages between photosynthetic processes and thylakoid lipid membrane components, including lipid class and fatty acid (FA) compositions, which have been proposed to be involved in photosynthetic responses to environmental stress.

Under low temperature (LT) conditions (19°C/13°C, day/night), quantitative trait loci (QTL) intervals were observed for variations incompositions of specific lipid categories, the ratio of digalactosyldiacylglycerol (DGDG) to monogalactosyldiacylglycerol (MGDG), and (most strikingly) the composition of the thylakoid-specific FA, phosphatidylglycerol (PG) 16:1 $^{\Delta 3trans}$ or PG 16:1t. The PG 16:1t composition, and to a lesser extent the DGDG/MGDG ratio showed potential co-associations with the network of photosynthetic parameters observed in our previous work. These co-associations appear to be specific, since QTL for other fatty acids, e.g. PG 16:0 and PG 18:0, previously proposed to be involved in plant chilling sensitivity, did not overlap those for photosynthetic parameters. Support for such a co-association also comes from the nearly linear dependence of PSII quantum efficiency (ΦII) and the compositions of PG 16:1t across the RIL population. These results suggest that the genetically determined variations in chilling responses of photosynthesis involve

common, mechanistic or genetic linkages with PG 16:1t levels. This correlation between lipid composition and photosynthetic responses at low temperature were qualitatively recapitulated in mutants or transgenic *Arabidopsis* lines with altered PG 16:1t composition, suggesting that differential accumulation of this FA leads to changes in photosynthetic responses. Because this fatty acid synthesis requires the activity of peroxiredoxin-Q, which is activated by H_2O_2 and known to be involved in redox signaling, we hypothesize that the accumulation of PG 16:1t occurs as a result of upstream lesions that result in ROS production.

3.2 Introduction

The chloroplast thylakoid membrane, which houses the central complexes catalyzing the light reactions, contains a set of lipids that is distinct from other cellular components, and differences in the thylakoid lipid profile have been linked to specific environmental responses (Cook, Lupette& Benning 2021; Yu, Zhou, Fan, Shanklin & Xu 2021). It has been proposed that changes in thylakoid lipid compositions, and in particular the balance of fatty acid (FA) saturation and unsaturation of membrane lipids, influence viability and photosynthetic capacity in response to chilling temperature (Hugly& Somerville 1992; Miquel, James, Dooner& Browse 1993; Wu, Lightner & Warwick 1997), leading to the hypothesis that a reduced poly-unsaturation level contributes to chilling sensitivity, while the opposite is proposed to limit heat tolerance.

However, this view remains to be thoroughly tested, and while in some cases clear correlations have been reported between the loss of specific classes of lipids and tolerance to low temperatures, this is not always the case. Here, we introduce two main hypotheses: 1) a reduced poly-unsaturation level contributes to chilling sensitivity and 2) an alternative hypothesis is that specific species of PGs, high-melting-point phosphatidylglycerol (HMP-PG) confer chilling sensitivity.

The *Arabidopsis fad6* mutant, which shows lower level of the polyunsaturated acyl group of 16:3 (carbons : double bonds), was indistinguishable in appearance from wild type at 22 °C, but became chlorotic after 3 weeks exposure to low temperature (5°C) (Hugly& Somerville 1992; Miquel *et al.* 1993; Wu *et al.* 1997). In an *Arabidopsis fad2* mutant, which has reduced levels of polyunsaturated phosphatidylcholine (PC) 18:3, no distinctive phenotype was observed at 22°C whereas *fad2* died after 7 weeks

at 6°C (Hugly& Somerville 1992; Miquel *et al.* 1993; Wu *et al.* 1997). Also, while some *Arabidopsis* mutants (e.g., *fad6* and *fad2*) with lower ratios of unsaturated: saturated FAs showed reduced photosynthesis activity at low temperature, there are also clear counterexamples (Barkan, Vijayan, Carlsson, Mekhedov& Browse 2006). For example, a suppressor screen of *fab1* (a mutant line that alters the ratio of 16C : 18C fatty acids through a disruption of plastidic beta-ketoacyl-ACP synthase II) produced a line with increased lipid saturation but improved photosynthetic performance at low temperature (Barkan*et al.* 2006). One suppressor contained an allele of FAD5, which codes for a chloroplast delta 7 desaturase, which uses a 16C FA that is specifically esterified at the *sn*-2 position of MGDG (Kunst, Browse & Somerville 1989), leading to increased lipid saturation.

An alternative hypothesis is that specific species of phosphatidylglycerol (PG), high-melting-point PG (HMP-PG) (e.g., molecules that contain only 16:0, 16:1 $^{\Delta 3trans}$ or PG 16:1t, and 18:0 fatty acids confer chilling sensitivity (Murata, Sato, Takahashi, Hamazaki& Cell Physiology 1982; Murata 1983; Murata &Yamaya 1984; Roughan 1985; Murata & Nishida 1990). Starting from the early 1970s, it has been suggested that the primary event of chilling sensitivity is an thermal transition, liquid-crystalline phase to gel phase, in the cellular membrane and that molecular species of chloroplast HMP-PG contribute to chilling sensitivity. This hypothesis is supported by the liquid-crystalline phase to gel phase transitions observed only in chilling-sensitive but not in chilling-resistant plants ((Murata *et al.* 1982; Murata 1983; Murata &Yamaya 1984; Roughan 1985; Murata & Nishida 1990). Other studies supporting this hypothesis show the correlation between chilling sensitivity and the percentage of HMP-PG molecular

species by surveying 74 plant species (Murata *et al.* 1982; Murata 1983; Murata &Yamaya 1984; Roughan 1985; Murata & Nishida 1990). As a follow up to studies in the 1980s, changes in level of HMP-PGs in mutant studies were tried in the 1990s (Wolter *et al.* 1992; Wu & Browse 1995). As an example, Wolter et al., showed that when more than 50% of the PG molecules were HMP-PG, that led to chilling sensitivity (Wolter *et al.* 1992). However, contrary result have also been presented, demonstrating that an increased portion of HMP-PG, *fab1* which has higher PG 16:0 composition, were unable to confer chilling sensitivity, concluding that the high-melting-point molecular species of PG cannot be a primary determinant of chilling sensitivity in this transgenic plant (Wu & Browse 1995).

Such results suggest that the impact of lipid changes may be governed by specific interactions with protein complexes, rather than bulk physico-chemical properties (Barkan*et al.* 2006), and the mechanisms for contributions of specific lipids or FAs remain unclear (Siegenthaler& Murata 2006). Indeed, the thylakoid membrane is composed of a complex mixture of lipids, protein complexes (Pribil, Labs & Leister 2014) and lipid-soluble components such as quinones (Anderson 1986) that can interact in complex ways. Thus, it may not be possible to draw straightforward conclusions about the roles of lipids based simply on their bulk physico-chemical properties in isolation. Indeed, there is evidence for specific interactions between certain lipid components and specific photosynthetic complexes (Dörmann, Hoffmann-Benning, Balbo & Benning 1995; Reifarth*et al.* 1997; Härtel, Lokstein, Dörmann, Grimm & Benning 1997; Xu *et al.* 2002; Hagio*et al.* 2002; Babiychuk*et al.* 2003; Yu & Benning 2003; Steffen, Kelly, Huyer, Dörmann&Renger 2005; Guo *et al.* 2005; Hölzl*et al.* 2006, 2009; Ivanov *et al.* 2006;

Kobayashi, Kondo, Fukuda, Nishimura &Ohta 2007; Kobayashi *et al.* 2013; Aronsson *et al.* 2008; Wu *et al.* 2013; Fujii, Kobayashi, Nakamura & Wada 2014). It is also clear that the loss of one lipid component may be compensated by the up- or down-regulation of others, though the mechanism by which such compensation occurs is not clear. Moreover, it is also clear that loss-of-function mutations might have a strong impact only under specific sets of conditions not typically imposed in the laboratory.

In recent work (Hoh et al., 2021), we applied detailed, high-throughput phenotyping to a recombinant inbred line (RIL) population of *Vigna unguiculata* (cowpea), exhibiting large variations in chilling sensitivity. We tested a range of possible mechanistic bases for these variations by assessing co-segregation (or lack thereof) between genetic diversity and multiple traits by taking advantage of advanced high-throughput phenotyping tools. We found that genetic loci which affects the primary reactions of photosynthesis that involves redox states of Q_A; establishment of the thylakoid proton motive force (*pmf*) through effects on cyclic electron flow (CEF); and subsequent acidification of the thylakoid lumen leading to differences in the rates of photodamage to PSII.

In this work, we followed up with more specific biochemical techniques to determine if these interaction effects could be associated with change in lipid composition. To accomplish this, we measured variations in lipid compositions across the RIL population, allowing us to test for potential linkages among photosynthetic processes and lipid properties. We found specifically, PG 16:1t, not all species of HMP-PG, is negatively associated with robustness of photosynthesis and we recapitulated this results in a series of mutants of *Arabidopsis* with differences in specific fatty acids

contents. The results show qualitatively similar effects, supporting causative linkages and universal role (unspecific to genotypes) of PG 16:1t conferring chilling sensitivity.

3.3 Material and Methods

3.3.1 Plant materials, growth and experimental conditions.

Cowpea genotypes and growth conditions.

Cowpea genotypes were as described in (Hoh et al, 2021 submitted). Seedlings at the “VC” stage (4 d after seed germination, https://beanipm.pbgworks.org/cowpea) were transferred from the staging chamber to DEPI chamber (Figure S3.1). The light intensity was changed in a sinusoidal pattern at 30 min intervals over the course of a 14 h day with the highest light intensity (500 µmol m^{-2} s^{-1}) occurring midday. The lowest light intensity (50 µmol m^{-2} s^{-1}) was at the beginning and end of the day. For the detailed light intensity changes, see Figure S3.1B. On Day 1, control for the low temperature (LT) experiment plants were assayed under lighting conditions at 29 °C/19 °C (control temperature: CT). After Day 1, plants were subjected to temperatures of 19°C/13 °C for 3 days at low temperature: LT) (Figure S3.1A).

Arabidopsis mutants with altered fatty acid composition.

Wild type *Arabidopsis thaliana* ecotypes Columbia-0 (Col-0) and Columbia-2 (Col-2), as well as fatty acid desaturase 4 (FAD4) (locus AT4G27030) knockout (KO) (Alonso *et al.* 2003; Gao *et al.* 2009) and overexpression (OX) lines (by adding pMDC85-FAD4) were used in this study. FAD4 is a desaturase required for the synthesis of 16:1t at the *sn*-2 position of PG (Gao *et al.* 2009). Overexpression lines in the pMDC binary vector system (Curtis &Grossniklaus 2003) were generated as described previously (Horn, Smith, Clark, Froehlich & Benning 2020) using the

FAD4coding sequence.

Arabidopsis growth conditions.

Arabidopsis seeds are planted in Redi-earth soil (Hummert Cat. # 10-2030-1) and stratified at 5°C for 3 days and grown under 100 µmol photons m^{-2} s^{-1} light cool fluorescent lights 16h: 8h day: night cycle at constant 21°C, 60% relative humidity. The 16-day-old plants were moved to DEPI chambers and exposed to an actinic light intensity regime similar to that of the cowpea experiments, every 30 minutes with a pattern based on sinusoidal curve and a peak intensity of 500 µmol photons m^{-2} s^{-1} except that the light/dark pattern was 16/8 hours and that, on Day 1, the daytime temperature was set to 21°Cand decreased to 6 °C on Day 2 for measurements under chilling stress.

3.3.2 Photosynthetic phenotyping.

Chlorophyll fluorescence imaging was performed using Dynamic Environmental Phenotype Imager (DEPI) chambers (Cruz et al., 2016), with modifications described in (Tietz, Hall, Cruz & Kramer 2017). Detailed experimental procedures were performed as described in Hoh et al. ().

3.3.3 Polar Glycerolipid profiling of cowpea population.

Polar lipid contents were determined for each of the cowpea RIL accessions using the methods described previously (Wang & Benning 2011). Samples were collected following the three-day experiments, so that the results should reflect chilling-induced lipid profiles. Lipid was extracted from fresh leaves with the solvent composed of methanol, chloroform and formic acid (20:10:1, v/v/v) followed by 0.2 M phosphoric

acid (H_3PO_4) and 1 M KCl buffer. Lipid classes were separated by thin layer chromatography (TLC) using a mobile phase of (acetone: toluene: water 91: 30:7.5 mL), followed by brief iodine staining and isolation of silica of bands representing Monogalactosyldiacylglycerol (MGDG), Digalactosyldiacylglycerol (DGDG), Sulfoquinovosyldiacylglycerol (SQDG), Phosphatidylcholine (PC), Phosphatidylglycerol (PG), and a combination of Phosphatidylinositol (PI) and Phosphatidylethanolamine (PE). Third, fatty acyl methyl esters (FAMEs) were produced from the lipids with 1 N hydrochloric acid (HCl) in anhydrous methanol and pentadecanoic acid (15:0) as internal standard by incubating in an 80°C degree water bath for 25 min. Fourth, gas-liquid chromatography together with flame ionization detection (GLC-FID) was used for analysis of FAMEs. FAME contents were normalized using an internal standard. The mole fractions for FAME species were calculated by normalizing to the estimated sum for all lipid species.

3.3.4 Linkage analysis and QTL mapping.

Analyses of QTL associations were performed as described in Hoh et al. 2021 using single nucleotide polymorphism (SNP) markers for genotype data of CB27 x 24-125B-1, which were obtained from (Lonardi*et al.* 2019) based on EST sequences produced by (Mucheroe*t al.* 2009). The construction of the linkage-map was performed as described in Hoh et al. (2021). QTL analysis was conducted using the Multiple QTL Mapping (MQM) model (genome scan with multiple QTL models) in the Rqtl package (Broman & Sen 2009). Levels of significance were determined by the number of permutations set at 1000 and a nominal significance cutoff of $p < 0.05$ over all replicates. More details of the analysis are described in Hoh et al. ()

3.4 Results and Discussion

3.4.1 Temperature effects on lipid profiles for parent lines.

RIL population parent lines, CB27 and 24-125B-1, were chosen based on differential sensitivity to temperature, as described in Hoh et al. (2021). The two lines showed only small differences in photosynthetic phenotypes under control temperature (CT, 29°C/19°C, day/night) but large differences under low temperature (LT, 19°C/13°C). CB27 showed stronger tolerance (relatively high Φ_{II} and low photoinhibition). 24-125B showed strong decreases in Φ_{II} and large increases in photoinhibition.

To determine conditions under which significant differences between genotypes are most likely to be apparent, we performed lipid profiling of two parents of RILs under three different conditions, control (CT), and 2nd day (LT 2d) or third day of (LT 3d) of low temperature (LT) conditions.

Relative abundances of lipid classes

Figure S3.2 compares relative abundances for lipid classes and ratios of DGDG/MGDG. Under CT, CB27 showed significantly higher MGDG, lower DGDG and PEPI ($p<0.05$) compared to 24-125B-1, whereas no significant differences were observed in the other lipid classes (Figure S3.2A). Exposure to low temperature (LT) led to significant changes in MGDG and DGDG in CB27 and SQDG in 24-125B-1 (Figure S3.2). In CB27, MGDG content was decreased while DGDG content was increased. CB27 showed a relatively low DGDG/MGDG ratio under CT but showed significant increases on both the second and third day of LT ($p<0.05$). 24-125B-1 showed a transiently higher DGDG/MGDG ratio compared to CB27 on CT on Day 1 ($p<0.05$), but no significant differences on Days of LT 2 and 3 (n.s.) (Figure S3.3). This pattern of

changes is qualitatively similar to that found by (Moellering, Muthan& Benning 2010), who found increased DGDG and decreased MGDG after freezing treatment -2 °C in *Arabidopsis*.

Relative fatty acid compositions

Figure S3.4 shows the relative composition of fatty acids for each lipid class for two parental lines under CT and after two (LT 2d) or three days (LT 3d) of LT. The fatty acid contents of the lipid classes were similar (see Figure S3.4 and Figure S3.5 for MGDG and DGDG), with the notable exception of PG (Figure S3.4), for which 24-125B-1 showed an increase in PG 16:1t ($p<0.05$) and decrease in PG 18:3 content ($p<0.05$) while CB27 showed decreased PG 16:1t ($p<0.05$) and increased PG 18:3 ($p<0.05$) over the chilling conditions (Figure S3.5C).

HMP-PG

Comparing to CT, LT led to decreased PG polyunsaturated FAs and increased PG saturated FAs in the sensitive line (24-125B-1) but the opposite patterns in the tolerant line (CB27) (Figure S3.4 and S3.5), consistent with the “HMP-PG hypothesis” (see Introduction), which posits that the combination of saturated fatty acid (16:0 and 18:0) or 16:1t contributes chilling sensitivity (Raison 1973; Lyons 1973; Murata & Yamaya 1984; Roughan 1985).

Compared to CT, CB27 showed decreases in HMP-PG ($p<0.05$) on Day 2 and 3, the first and second days of LT (Figure 3.1). By contrast, 24-125B-1 showed a transiently increased HMP-PG on Day 2 (first day of LT) ($p<0.05$), but no significant differences on the third day of LT (Figure 3.1). This result is consistent with a transient involvement of HMP-PG in sensitivity (but see also below).

Figure S3.6 shows more detailed analyses of HMP-PG components, PG 16:0, PG 18:0 and PG 16:1t individually (Figure S3.6). CB27 showed decreases in PG 16:0, PG 18:0 and PG 16:1t after chilling stress ($P<0.05$), whereas 24-125B-1 showed increased PG 16:1t ($P<0.05$) (Figure S3.6). These results suggest that, rather than the sum of HMP-PG content, specific fatty acid content could affect chilling sensitivity. To tease apart the effect of specific fatty acid content, each FA composition and HMP-PG is analyzed for QTL associations separately.

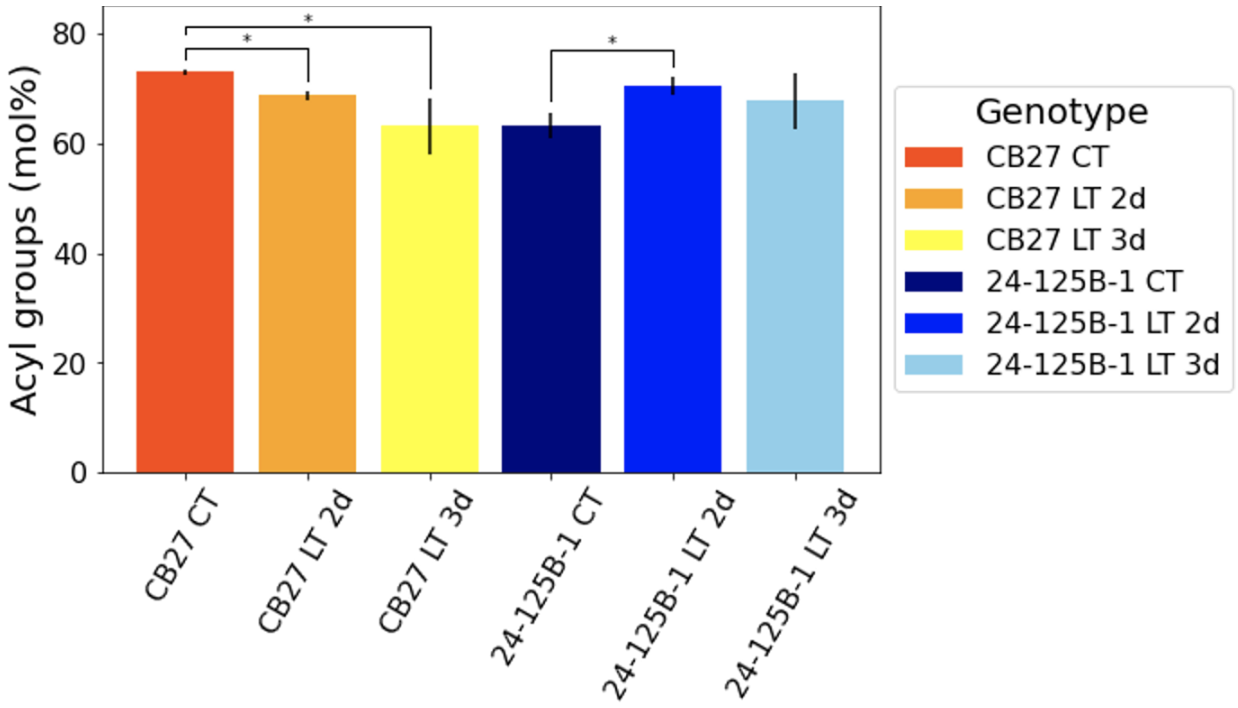

Figure 3.1 HMP-PG for two parental lines (CB27 and 24-125B-1) in three temperature conditions.
CT, control temperature; LT 2d, 2nd Day of low temperature; LT 3d 3rd Day of low temperature. HMP-PG is total composition for molecular species of PG 16:0, 18:0 and PG 16:1t. The averaged replicates ($n\geq3$) for each value are shown as a bar graph with error bar (SD). The asterisks show significant differences between the groups (as shown in brackets) from t-test ($p<0.05$). CB27 showed decreased HMP-PG after chilling treatment ($p<0.05$), but 24-125B-1 showed increased mol % ($p<0.05$ for LT 2d, n.s. for LT 3d).

3.4.2 Effects of chilling temperatures on lipid classes and fatty acid profiles for the diversity panel.

Based on lipid profiling for two parental lines (Figure 3.1 and Figure S3.3 and S3.4) and photosynthetic responses (Hoh et al., 2021), we chose the third day of LT for detailed lipid and fatty acid profiling over the entire RIL population.

Relative abundances of lipid classes

Figure S3.7 A-F show distributions of relative abundance of classes across genotypes. Compared to CB27, the sensitive line, 24-125B-1, showed lower MGDG (34.39 ± 2.11, 31.08 ± 3.38, p=0.057) and DGDG (24.67 ± 2.32, 22.68 ± 3.39, p=0.23), but higher PG (10.58 ±1.42, 11.91 ± 0.96, p=0.058) and SQDG (4.85 ± 0.93, 5.78 ± 0.71, p=0.055). The population consistently showed larger variations in the lipid class compositions. In particular, PC (Figure S3.7E) and PEPI (Figure S3.7F) showed much larger variations in the progeny compared to the parent lines. Figure S3.7G shows distribution of DGDG/MGDG ratio across the population, showing no significant differences in the parent lines (0.72 ± 0.05, 0.73 ± 0.08, $p>0.05$) but showed larger variations in the progeny lines.

Relative fatty acid compositions

Figure S3.8A-T show histograms for fatty acid contents across the RIL population, with values for the parent lines indicated by color-coded arrows. The tolerant parental lines, CB27, showed significantly higher polyunsaturated fatty acid contents than 24-125B-1, for example, MGDG 18:2 (Figure S3.8B), DGDG 18:2 (Figure S3.8E) and PG 18:2 (Figure S3.8G) (all with $p<0.05$). The sensitive line showed slightly higher, but barely significantly, saturated fatty acid contents, MGDG 16:0 (Figure S3.8A),

DGDG 16:0 (Figure S3.8D), SQDG 16:0 (Figure S3.8I), SQDG 18:0 (Figure S3.8J) and PEPI 16:0 (Figure S3.8R) but those are not significantly higher than CB27 (all, $p>0.05$).

Figure 3.2 shows distributions of contents of selected fatty acids across the RIL population (A-D) and the correlation between each fatty acid content and Φ_{II} (taken from Hoh et al., c.f. Figure 1) from the middle of the 3rd day of the experiment. Compared to CB27, the sensitive 24-125B-1 showed PG 16:1t (32.34 ± 2.66, 35.64± 1.96, $p<0.05$, Figure3.2A), PG 18:0 (2.21 ±0.56, 2.92 ± 0.49, $p<0.05$, Figure 3.2B), higher PG 16:0 (30.70 ± 3.85, 32.05 ± 3.51, $p>0.05$, Figure 3.2C), but lower PEPI 18:1 (2.80 ± 0.56, 2.13 ± 0.43, $p>0.05$, Figure 3.2D). Figures 3.2 E-H show dependencies of Φ_{II} on FA contents, with a strong negative correlation with PG 16:1t (Figure 3.2E, $R^2 = 0.741$, $p<0.0001$), weaker but still significant negative correlation with PG 18:0 (Figure 3.2F, $R^2 = 0.126$, $p = 0.001$), and weakly positive correlations with PEPI 18:1 (Figure 3.2G, $R^2 = 0.348$, $p < 0.0001$) and PG 16:0 (Figure 3.2H, $R^2 = 0.063$, $p = 0.025$).

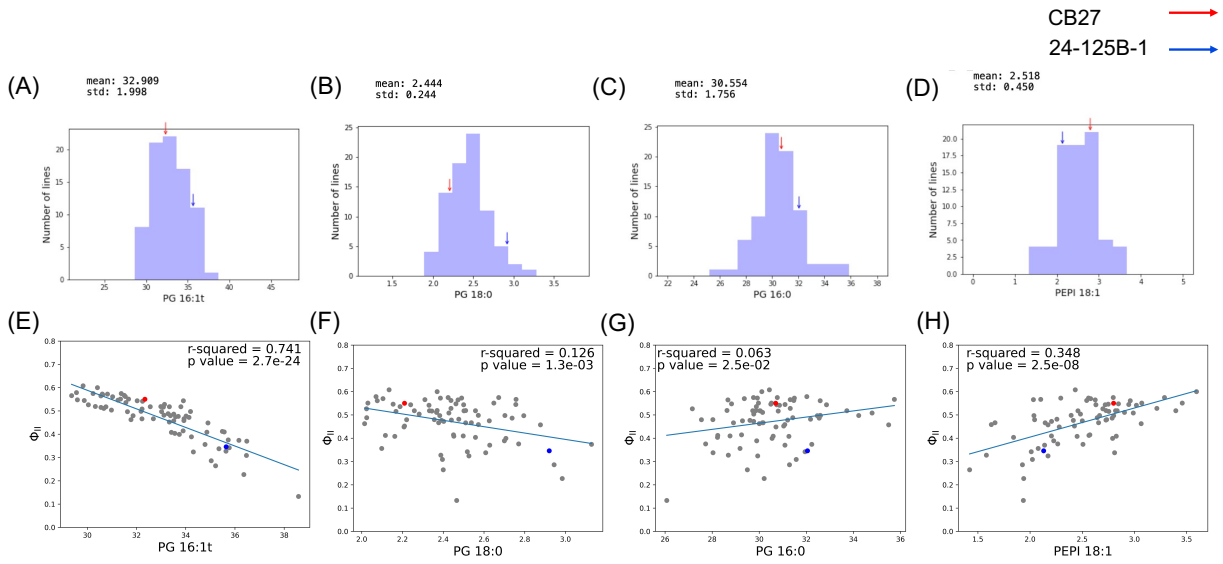

Figure 3.2 Histograms of the contents of selected fatty acids across genotypes (A: PG 16:1t, B:PG 18:0, C: PG 16:0, C: PEPI 18:1) and the correlation of selected fatty acids and PSII quantum efficiency (Φ_{II}) across the RIL lines in chilling condition (E-H).

(A-D) The averaged replicates (n≥3) for each phenotype value of RILs including two parental lines are shown as histograms. The mean and standard deviation of the population are shown above each histogram. The arrows indicate two parental lines (CB27, red; 24-125B-1, blue). (E-H) Correlation plot of selected fatty acids against Φ_{II} data from DEPI data, at 1.5 hr prior to the end of Day 3 (206 µmol, m^{-2}, s^{-1}) for the RILs and parental lines Hoh et al. (2021). The r-squared and p-value of the population are shown in the left upper corners of each plot. The progeny are colored as grey dots and the parental lines CB27 and 24-125B-1 indicated by red and blue respectively.

3.4.3 Association of lipid classes and fatty acid profiles with genetic markers.

Relative abundances of lipid classes

Figure S3.9 and Table 3.1 describe genetic associations (LOD scores) for relative abundances of classes of lipids, inclusive of desaturation states. Certain lipid categories showed significant associations with genetic markers (QTL intervals) at low temperatures, including MGDG (intervals on Chrs 3 and 4), DGDG (Chrs 4, 6, 8, 9, 10, 11), PG (Chr 11) and PEPI (Chr 3) (Figure S3.9A-C and F). By contrast, no significant QTLs were found for PC and SQDG contents (Figure S3.9D-E).

Relative fatty acid compositions

Figure S3.10 describe genetic associations for FAs contents. The total contents of MGDG, DGDG and PG showed significant but weak associations with genetic markers (QTL intervals Figure S3.9A-C), but others from these groups, such as MGDG 16:0, MGDG 18:3, DGDG 18:3, PG 18:3 did not (Figure S3.10A, C, F and H). Whereas general categories of lipids showed only weak associations with genetic markers for PC and SQDG (Figure S3.9D and F), the contents of a limited number of specific fatty acids showed strong associations to several genomic loci (Figure S3.10I-M and O-Q).

Figure 3.3 plots genomic associations for selected fatty acid contents, PG 16:0, PG 18:0, PG 16:1t and PEPI 18:1 with genetic markers across the RIL population. Several distinct patterns of associations were observed. The strongest QTLs were observed for PG 16:1t on Chrs 4 and 9 (Figure 3.3A), with associations for PEPI 18:1 on Chr 7 (Figure 3.3B), PG 18:0 on Chrs 3 and 7 (Figure 3.3C) and PG 16:0 on Chr 7 (Figure 3.3D). PG 16:0 and PG 18:0 showed associations with a QTL region Chr 7 (Figure 3.3 A-D).

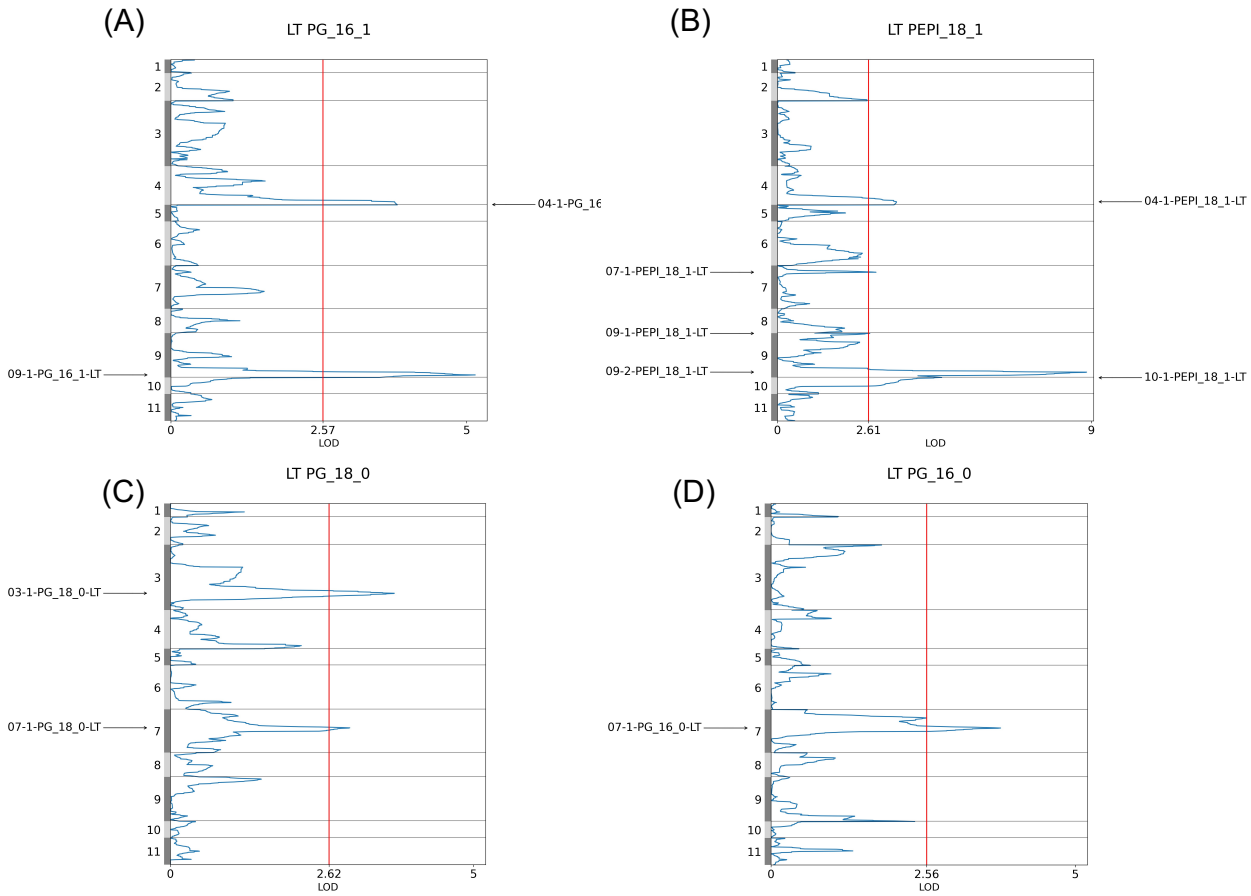

Figure 3.3 QTL analysis of the contents of selected fatty acids in the chilling condition.

Logarithm of the odd (LOD) score plots of the contents of selected fatty acids (A, PG 16:1t; B, PEPI 18:1; C, PG 18:0; D, PG 16:0) in the chilling condition measured on the third day of LT. The genetic position is indicated by the y-axis. Significance threshold of 0.05 for each parameter based on 1000 permutations is indicated by the red vertical line. Each QTL named chromosome- index- phenotypes- temperature condition (low temperature, LT) is shown either on the left or right side of the panel with arrows.

3.4.4 Potential co-linkages among photosynthetic parameters and lipid composition.

Co-localization of QTL regions can suggest potential genetic and mechanistic linkages. We observed such overlaps in for FAs, PG 16:0, PG 18:0, PG16:1t, and PEPI 18:1 and photosynthetic responses and the network of photosynthetic parameters measured in Hoh et al (2021). These observations are summarized in "Daisy Graphs" (Figure 3.4) which describe potential associations to common genetic loci; specific QTL intervals are indicated in the center circles, different phenotypes are indicated by surrounding circles, and the width (thickness) of the connecting lines indicate the LOD score for association. The color of the connecting lines indicates the "directionality" of the association, with between the phenotype and the allele present in the tolerant (CB27, orange) and sensitive (24-125B-1, blue) lines. For example, an orange line indicates a positive association between the presence of the CB27 allele and the measured phenotype.

Here, we focus on results from 1.5 hours prior to the end of Day 3, because this time represents an aggregate of LT effects, but similar conclusions can be drawn from other time points. In our previous work (Hoh et al., 2021), we found significant co-linkages of a range of photosynthetic parameters to specific QTL intervals on Chrs 4 and 9 at these times. In the current work, we also observed strong QTL for lipid contents on Chrs 4 (marker positions 50.04 - 64.45cM), and Chr 9 (marker positions 86.93-104.15cM), which clearly overlap those seen for the photosynthesis parameters, as well as an interval on Chr 7 (marker positions 31-40cM), which did not show apparent overlaps. The observation of overlaps suggests possible co-association of the

phenotypes with genetic loci in these regions, though as discussed below, we cannot rule out the contributions from multiple loci within these intervals.

The presence of the CB27 alleles in the Chr 4 interval was negatively associated with Φ_{II}, qL, ECSt and PEPI 18:1, positively associated with qIt and PG 16:1. PG 16:0 and PG 18:0 showed no significant associations with other parameters in Chr 4 (Figure 3.4A). Strikingly, the Chr 9 region showed the inverse relationships, i.e. positive associations with the CB27 alleles for one set of parameters (Φ_{II}, qL, ECSt, PEPI 18:1) and negative associations for qIt and PG 16:1t. Similar to Chr 4, PG 16:0 and PG 18:0 showed no measurable associations with other parameters in Chr 9 (Figure 4.4B). On Chr 7, only PG 16:0, PG 18:0 and HMP-PG showed negative associations with the CB27 and no other photosynthetic parameters and PG 16:1t and PEPI 18:1 showed association (Figure 3.4C). PG 16:0 and PG 18:0, showed QTL intervals in Chr 7 but these did not overlap those for photosynthetic parameters, arguing against models where variations in HMP-PG confer altered photosynthetic responses to chilling. These results suggest that the loci on Chrs 4 and 9 have opposing effects on photosynthetic responses which are likely to be linked to PG 16:1t and/or PEPI 18:1. Interestingly, RIL with combinations of the two parent genotypes at these locations show more extreme behaviors (see below).

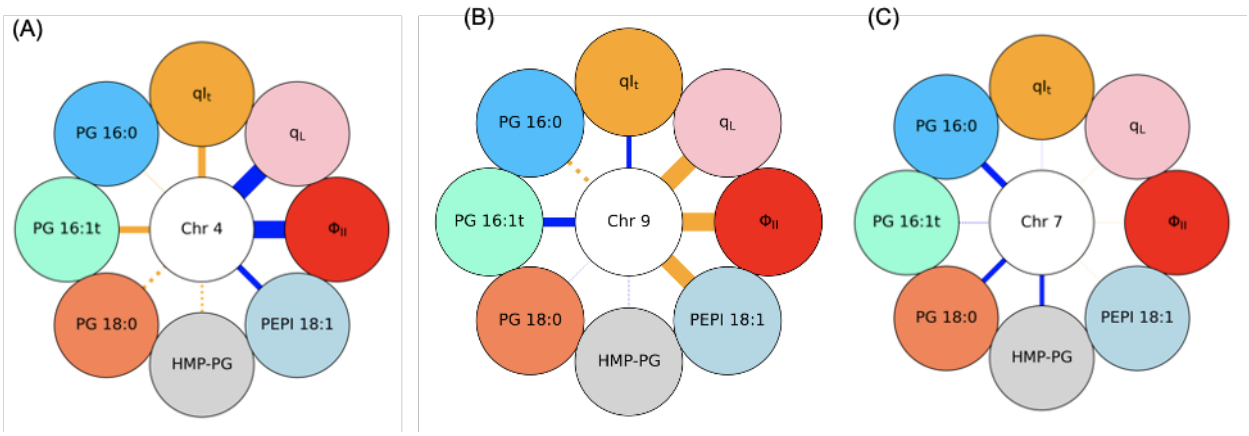

Figure 3.4 The associations for selected QTL intervals of photosynthetic parameters from DEPI and selected fatty acids in LT at Chr 4, 59.04-64.45 cM (A) and Chr 9, 86.93-104.15 cM (B), Chr 7, 31- 40 cM (C).
LOD score plots from the previous paper (*c.f.* Figure 3 in Hoh et al.) were replotted in the form of "Daisy Graphs," in which a specific Chr is indicated in the center circles, different phenotypes are indicated by surrounding circles, with the thickness of the connecting lines set proportional to the LOD score for association. For more clear visualization, the maximum line width was set at LOD = 10, i.e., scores above 10 were set to this thickness. Solid lines represent significant positive associations between the phenotype and the allele present in the tolerant (CB27, orange) and sensitive (24-125B-1, blue) lines. Phenotypes with associations to the QTL intervals are indicated by dashed lines.

3.4.5 Effect size contributions of specific QTL intervals to two fatty acids (FAs).

The QTL intervals in Figures S3.9 and S3.10 reflects statistical associations between phenotypes and genetic markers. They can indicate if something is different in one set of genotypes, but do not tell us by how much or even in what direction. In this section, we quantify the apparent impact of a genotype having a particular set of markers. Here, we explore the quantitative effects on phenotypes associated with genetic markers from two parent lines. Individual genotypes in the RIL population are homozygous for markers that come from either of the two parental lines. When discussing a single locus, we designate these by letters "AA," having the allele from

CB27 (tolerant, maternal line), or “BB,” having the allele from 24-125B-1 (sensitive, paternal line). The effect sizes were obtained by splitting the population into two groups (those with AA and BB) and averaging the measured values.

Figure 3.5 shows the effects on PG 16:1t (Figure 3.5A) and PEPI 18:1 (Figure 3.5B), of markers in the QTL on Chr 4 (59.64 cM) and 9 (86.93 cM). Genotypes with AA at the QTL on Chr 4 showed higher PG 16:1t content compared to those with BB (Figure 3.5A). By contrast, the opposite was observed for the QTL on Chr 9, with the AA allele imposing a decrease in PG 16:1t content compared to those with BB. Similar, additive but opposing effects of the two QTL regions were also observed in the photosynthetic parameters (e.g. c.f. Figure 6 in Hoh et al.), supporting a mechanistic connection between the observed variations in lipids and photosynthetic responses.

To test for additivity or epistasis, we assessed the combined effects of both sets of alleles (Figures 3.5C and 3.5D), dividing the population into the four possible genetic combinations, AAAA, AABB, BBAA and BBBB for alleles from each parent for Chr 4 and Chr, e.g. the AABB genotype has the CB27 allele on the Chr 4 QTL and that for 24-125B-1 in the QTL on Chr 9. Note that AAAA and BBBB showed no significant differences between FA compositions (Figure S3.11), and thus we present averaged AAAA and BBBB for each parameter, only showing three groups in Figure 3.5 C-D. Interestingly, both FAs in AAAA and BBBB genotypes showed similar compositions, whereas AABB genotypes showed the highest compositions for PG 16:1t and lowest for PEPI 18:1 composition and the BBAA showed the opposite. This result parallels those seen for the photosynthetic parameters (c.f. Figure 6 in Hoh et al.) and partly explains the observed transgressive FA and photosynthetic phenotypes across the RIL

population.

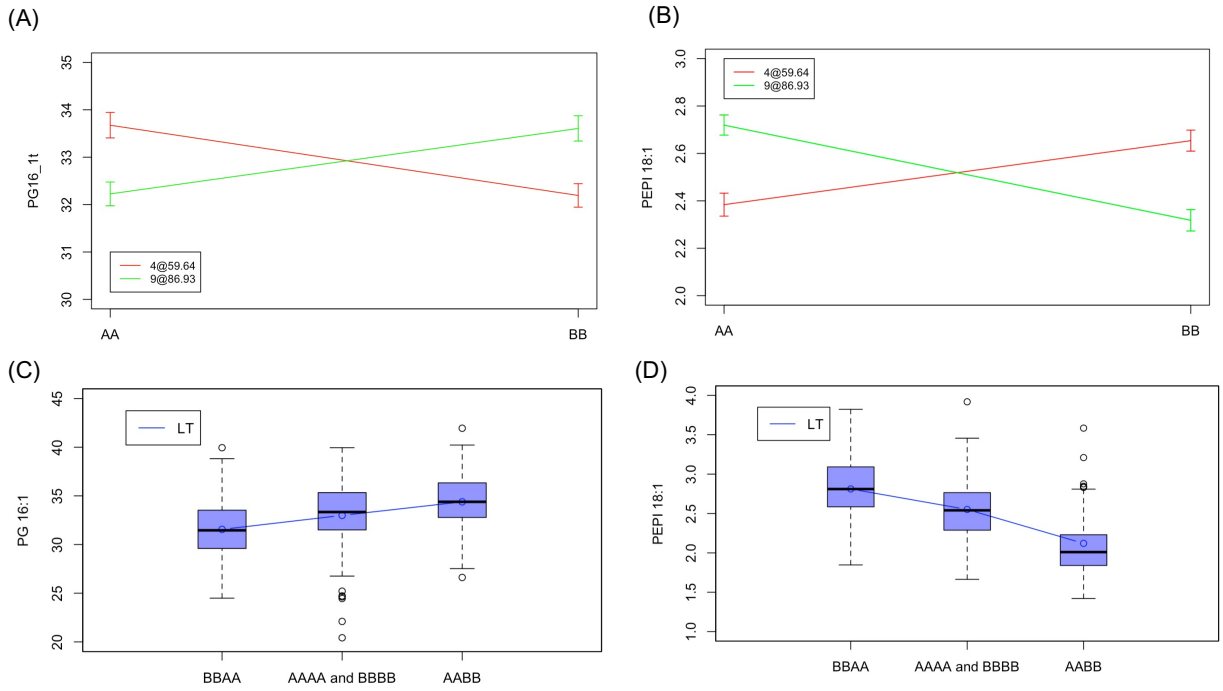

Figure 3.5 Effect plots for identified QTLs in Chrs 4 and 9 for fatty acid compositions.
Panels A and B show mean fatty acid compositions (A, PG 16:1t; B, PEPI 18:1) as dependent on allele for the major QTL intervals on Chr 4, 59.64 cM (red) and Chr 9, 86.93 cM (green). AA and BB represent genotypes with markers for CB27 and 24-125B-1, respectively. Panels C and D show the allelic contributions to fatty acid compositions from combinations from both QTL intervals, where the first two letters represent markers for Chr 4 and the second two letters for Chr 9. See more details in text.

3.4.6 Linkages between Q_A redox state modulating the genetic effects on temperature stress.

To explore possible mechanisms for the FAs and photosynthetic responses, we compared genotype dependencies of more detailed photosynthetic parameters taken from Hoh et al () across the entire RIL population. Figure 3.6A and B shows average values of qL and qIt against Φ_{II} respectively at 1.5 hr prior to the end of Day 3 (206 µmol, m^{-2}, s^{-1}) on Day 3, grouped by their genotypes for QTL on Chr 4 and 9, i.e., those with AAAA, AABB, BBAA and BBBB, as in Figure 3.5.

Genotypes having the BBAA and AABB genotypes showed the highest and lowest qL on Φ_{II} values ($p<0.05$ by t- test), while those with AAAA and BBBB showing intermediate values (NS) (Figure 3.6A and Figure S3.11). The BBAA and AABB genotypes showed the most extreme differences, with the former having lower qIt ($p<0.05$ by t- test) and higher Φ_{II} values ($p<0.05$ by t- test) (Figure S3.11). These results are consistent with a model (Huner, Öquist&Sarhan 1998) where increased PSII excitation pressure or accumulation of reduced Q_A^-, estimated here by the qL parameter, caused increased rates of PSII photodamage at LT, measured by the qIt parameter. These effects were stronger in the genotypes containing the AABB alleles, which also had highest PG 16:1t and lowest PEPI 18:1. The opposite was seen for genotypes containing BBAA.

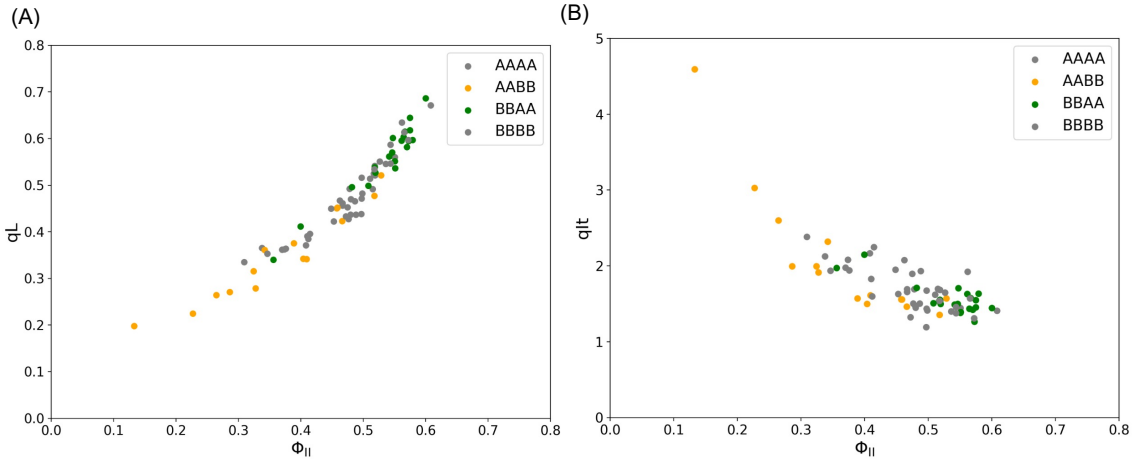

Figure 3.6 Relationships between photosynthetic responses grouped by different combinations of alleles for the identified QTLs in Chrs 4 and 9 (data is from Hoh et al. 2021).
(A) qL and (B) qIt against Φ_{II} from DEPI data, at 1.5 hr prior to the end of Day 3 (206 µmol, m^{-2}, s^{-1}). The allele groups of AAAA, BBBB are indicated by gray dots. The allele groups of AABB and BBAA are colored orange and green, respectively. Detailed statistical analyses testing for differences in phenotypes between the allele groups are given in Figure S3.11

3.4.7 Altering PG 16:1t composition in Arabidopsis recapitulates the low temperature effects seen in cowpea.

The above quantitative genomics results on the cowpea RIL population are consistent with a linkage between PG 16:1t composition, Q_A redox state and photodamage. If these represent true mechanistic linkages, they could operate in two distinct modes: 1) PG 16:1t composition may impact photosynthesis, resulting in modulation of photodamage; or 2) photosynthesis may be impacted by 16:1t composition, e.g. photodamage initiating changes in FA composition. To test these possibilities, we assessed the chilling responses of photosynthesis in Arabidopsis lines with modified PG 16:1t composition, including twoFAD4 knockout (KO) mutants (Alonso *et al.* 2003; Gao *et al.* 2009), a FAD4 overproducing (OX) line, which was generated as described in Materials and Methods, and appropriate wild types (WT), and confirmed earlier work () that the knockout lines lacked 16:1t whereas the overexpression line showed a ~34% increased. Photosynthesis responses were measured using the fluorescence imaging DEPI chamber under the light regime as used in Figure S3.1. Because Arabidopsis is more tolerant of LT, we used 21ºC and 6ºC as the CT and LT conditions.

The photosynthetic responses of *Arabidopsis* WT and mutant lines over a five day experiment are shown in Figure 3.7. Day 1 of the experiment was performed at 21°C, named “Arabidopsis Control Temperature” (ACT) to distinguish it from that used in the cowpea experiments. Days 2-5 were performed at 6°C, i.e., “Arabidopsis Low Temperature” (ALT). As described in Cruz et al. (Cruz *et al.* 2016), values are presented as heat maps, comparing mutants with Col-0 at each time point. For Φ_{II} and qL,

differences were calculated as log fold changes; for NPQt, qE and qI the direct differences were calculated. The lower panel in Figure 3.7 shows Z-scores for these differences, Values beyond the range of -1 to +1 indicate significant differences and are indicated by blue and red coloration.

Under ACT, only small differences were seen in photosynthetic parameters between Col-0 and the mutant lines. Small increases in qE and qL were seen in the *fad4* lines, but these were marginally significant. Larger differences emerged under ALT, consistent with previous work showing that stronger phenotypes tend to emerge under more stressful environmental conditions (Cruz *et al.* 2016).

Under these conditions, *fad4*, which is deficient in PG 16:1t, showed higher Φ_{II} and qL and lower NPQ, qE, qI compared to WT. On the other hand, the FAD4 OX line, which has more PG 16:1t compared to WT, showed the opposite effects, with lower Φ_{II} and qL, higher NPQ, qE, qI. The results are qualitatively similar to those obtained with the chilling sensitive and tolerant genotypes of cowpea, i.e., with the genotypes with higher levels of PG 16:1t tending to be more sensitive to chilling, with lower Φ_{II} and qL, and higher NPQ and qI (Hoh et al., 2021). This result supports a similar impact of 16:1t in both species, and further suggests that the changes in this FA lead to altered photosynthetic responses.

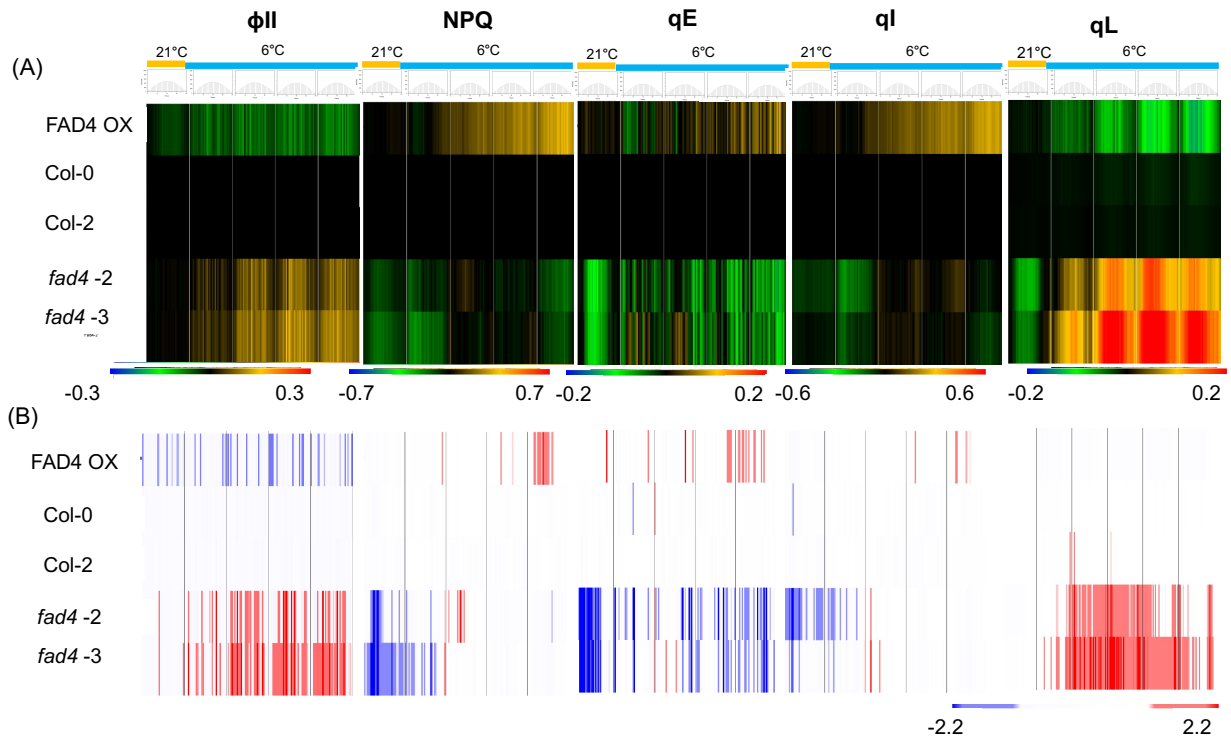

Figure 3.7 Photosynthetic responses of *Arabidopsis fad4* and FAD4 OX mutants varying PG 16:1t composition.
(a) Photosynthesis measurements (Φ_{II}, NPQ, qE, qI and qL) from DEPI chamber under chilling, sinusoidal light conditions. Φ_{II} and qL are presented as log fold changes compared to WT, whereas NPQ, qE, qI are presented as the straight differences with WT (n≥4). FAD4 OX line showed lower Φ_{II} and qL while KO line showed higher Φ_{II} and qL. FAD4 OX line showed higher qE, qI compared to WT whereas KO lines showed lower qE and qI compared to WT. (b) Z-Score of photosynthesis parameters showing statistical significance.

3.4.8 DGDG/MGDG ratio for the chilling photosynthetic tolerance.

After LT treatment, we observed increases in the ratio of DGDG/MGDG ratio in the tolerant line (CB27) after chilling stress (Figure S3.3), but no significant changes in 24-125B-1. When measured over the RIL population, DGDG/MGDG ratio showed a QTL interval on Chr 9, which overlapped that of the photosynthetic parameter under LT (Figure 3.8B), but not with the QTL on Chr 4. These results suggest a partial co-linkage with 16:1t and subsequent photosynthetic responses, as indicated in the Daisy plots in Figure 8. The DGDG/MGDG ratio showed higher average values in the tolerant allele

group for the QTL on Chr 9 (Figure 3.8B), consistent with a role in chilling responses. MGDG is a non-bilayer forming lipid and DGDG/MGDG ratio affects membrane stability, phase transition, ability for proteins to insertion (Williams 2004; Shimojima & Ohta 2011). Lipid remodeling under freezing temperatures is controlled by SENSITIVE TO FREEZING 2 (SFR2), an gene required for freezing tolerance, which acts by transferring galactosyl residues from monogalactolipid to different galactolipid acceptors, forming oligogalactolipids, diacylglycerol and triacylglycerol, leading to the membranes stabilization during freezing conditions (Moellering *et al.* 2010). Though *sfr2* has not yet been linked to lipid remodeling under chilling (non-freezing) stress, such a role would be consistent with our observation of potential linkages between DGDG/MGDG ratio and photosynthetic responses.

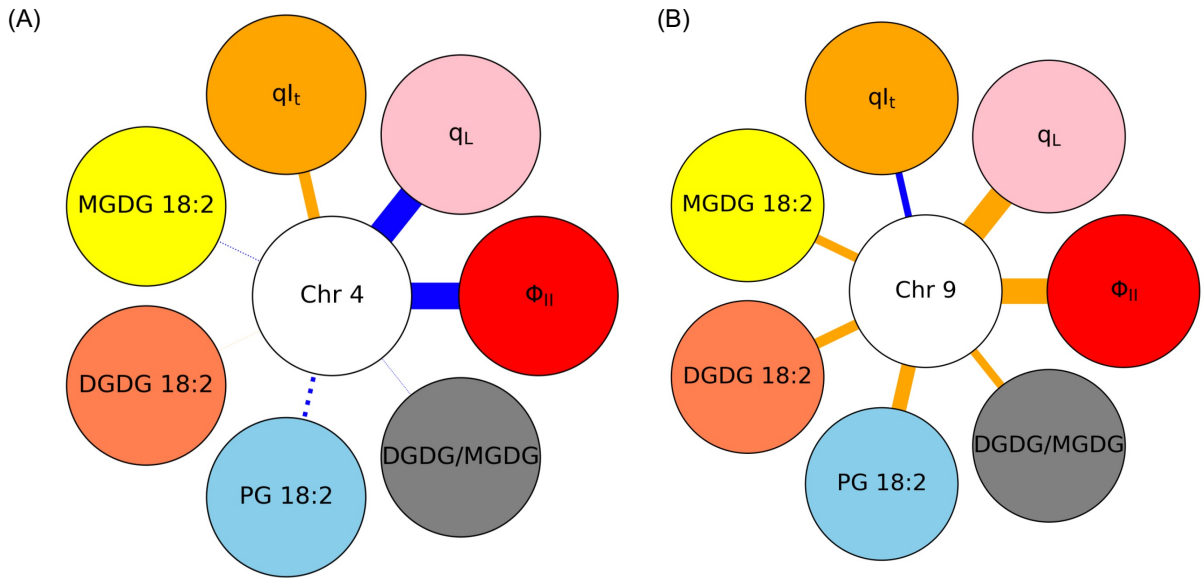

Figure 3.8 The associations for selected QTL intervals of photosynthetic parameters from DEPI and selected fatty acids in LT at Chr 4, 59.04-64.45 cM (A) and Chr 9, 86.93-104.15 cM (B). LOD score plots from the previous paper (*c.f.* Figure 3 in Hoh et al.) were replotted in the form of "Daisy Graphs," in which a specific Chr is indicated in the center circles, different phenotypes are indicated by surrounding circles, with the thickness of the connecting lines set proportional to the LOD score for association. The maximum line width was set at LOD = 10, and scores above 10 were set to this thickness. Solid lines represent significant positive associations between the phenotype and the allele present in the tolerant (CB27, orange) and sensitive (24-125B-1, blue) lines. Below the threshold each phenotype is shown as dashed lines.

3.4.9 Specific FA and lipid species, rather than bulk unsaturation levels, appear to control photosynthetic responses to LT.

The lack of significant QTL intervals for FAs 18:3 of MGDG, DGDG, PG (Figure S3.10C, F and H), suggesting that genetic variations in these components are weak or not linked to specific genetic markers, arguing against roles for 18:3 FA species in controlling the observed genetic variations in photosynthetic responses in our cowpea RIL population.

Significant QTL intervals did appear for PG 16:0, PG 18:0 and HMP-PG on Chr 7 (Figure 3.4C) as well as for the 18:2 FAs, MGDG, DGDG, PG (Figure S3.10B, E and

G) on Chr 9. However, the regions for PG 16:0, PG 18:0 and HMP-PG did not overlap those for photosynthetic parameters, arguing that genetic variations in these components were not linked to photosynthetic responses (Figure 3.4). The QTL interval for MGDG 18:2, DGDG 18:2, and PG 18:2 on Chr 9 overlapped that found for photosynthetic parameters (Figure 3.8B), suggesting a potential linkage, as supported by the positive correlation between these FAs and the presence of alleles from the tolerant line in this interval (Figure 3.8B). A reasonable interpretation of these results is that MGDG 18:2, DGDG 18:2, and PG 18:2, but not PG 16:0, PG 18:0 and HMP-PG or 18:3 FAs, modulate photosynthetic tolerance under chilling in our cowpea RIL population.

3.4.10 PG 16:1t composition is functionally linked to photosynthetic responses under chilling conditions.

By analyzing genetic variations in cowpea RILs, we observed co-segregation patterns among photosynthetic parameters, Φ_{II}, q_L, qIt and PG 16:1t and PEPI 18:1, suggesting those FAs are genetically/ mechanistically co-linked with photosynthetic regulation under chilling stress on Chrs 4 and 9 (Figure 3.4). Higher levels of PG 16:1t and lower levels of PEPI 18:1 are associated with lower photosynthetic efficiency, more reduced QA (decreased qL), and increased photoinhibition (qI) at low temperature (see Figure 3.6). Overall, the results are consistent models where increased PSII excitation pressure or accumulation of reduced Q_A^-, estimated here by the qL parameter, caused increased rates of PSII photodamage at LT, measured by the qIt parameter (Huner *et al.* 1998).

PG 16:1t is of particular interest to photosynthesis because it is localized in

thylakoid membrane (Selstam 2004) and has been proposed to be important for temperature stress responses (Xu & Siegenthaler 1997) and has been linked to redox responses (Horn *et al.* 2020). The fact that *increased* levels of PG 16:1t were associated with *decreased* tolerance to chilling suggests several possible mechanisms. First, PG 16:1t could have induced sensitivity to cold, e.g., by altering the fluidity of membranes associated with photosynthetic processes. Alternatively, PG 16:1t may accumulate as a result of chilling stress, and thus would be associated with sensitive genotypes. FAD4 has been shown to require the activity of PrxQ, which uses H_2O_2 as a substrate to oxidize thiol regulated enzymes (Horn *et al.* 2020). For instance, it is possible that chilling stress results in increased H_2O_2 production, leading to activation of PrxQ and accumulation of PG 16:1t. Experiments on a series of *Arabidopsis* lines that either lack (*fad4*) or contain elevated levels (FAD4 OX) of FAD4 show that increased levels of PG 16:1t result in decreased photosynthetic efficiency, more reduced Q_A and increased photoinhibition (showing lower Φ_{II} and qL, higher NPQ, qE, qI) at low temperature (Figure 3.7). Remarkably, decreasing PG 16:1t in cowpea, and eliminating it in the FAD4 mutant, led to increased photosynthetic efficiency and decreased photoinhibition under LT. These results support the former model, where PG 16:1t controls the photosynthetic responses at LT, rather than resulting from the stress (but see also below).

If PG 16:1t does control LT photosynthetic responses, one may reasonably ask why PG 16:1t would accumulate if it led to decreased performance. One possibility is that PG 16:1t may have a protective (or adaptive) role under different conditions, e.g., at higher temperatures, resulting in the tradeoff of less resilient photosynthesis under LT. In

this context, it is noteworthy that cowpea is mainly a warm climate crop, and may not be selected for optimal responses to chilling. Another possibility is that PG 16:1t is involved in a signaling pathway that both responds to stress and downregulates photosynthetic responses, as suggested by the involvement of PrxQ and H_2O_2 in its activity (Horn *et al.* 2020). In this scenario, the increased PG 16:1t levels in the cowpea lines could reflect increased ROS production under LT stress, while manipulating FAD4 in Arabidopsis could reflect a bypassing of the normal regulatory processes, leading to altered effects on photosynthesis.

3.5 Conclusions: Exploring natural variations to identify linkages and their mechanistic bases and implications for improving crop responses to climate change

The results highlight some advantages of using natural genetic variations to identify underlying mechanisms. Because classical genetics approaches introduce (typically deleterious) mutations that are not commonly found in natural populations, it can miss variations that have evolved to adapt to specific environments, and thus may be important for improving crop responses to changing environmental conditions.

The current work identified several QTL intervals for photosynthetic responses to chilling. In principle, these loci can be immediately used in breeding efforts to address a key limitation to cowpea cultivation. One interesting observation is that the parent lines contain two major QTL, on Chrs 4 and 9, that appear to operate with opposing effects on both FA composition (Figures 3.4 and 3.5) and photosynthetic responses to chilling (Hoh et al., 2021). Thus, the RIL population, containing allelic combinations of these two loci, show more extreme (transgressive) responses than the parents, and may reflect

tradeoffs that impact performance under a range of environmental conditions.

The observed linkages with photosynthetic parameters and lipid composition support the importance of lipid composition in chloroplast responses to adverse environmental conditions and identify potential mechanistic bases for these variations. Of particular interest is the identification of strong linkages to specific chloroplast FAs, rather than bulk properties, e.g., unsaturation levels, pointing to potential roles for these components in maintaining the photosynthetic apparatus or signaling. These linkages were substantiated by experiments using genetically modified Arabidopsis, leading to a model where PG 16:1t controls photosynthetic responses under LT, possibly as a component of a signaling pathway.

Care must be taken, though, in interpreting such linkages. As discussed in Hoh et al. (2021), there are several caveats on inferring causation from co-linkages, including the possibilities of multiple traits under QTL intervals (see also above). Some variations can be controlled by numerous, small-effect, polymorphisms, and thus not be revealed by statistical analyses. On the other hand, these variations are unlikely to be manipulable by breeding, and thus we focused on those that are highly correlated with variations in markers. One must also be circumspect in extrapolating from these to different species, which can be adapted to different environments. For instance, the species that are more adapted to chilling temperatures exhibit different additional variations that modulate these responses. Indeed, as discussed above, the apparent negative effects of elevated PG 16:1t on photosynthesis at LT in cowpea may reflect adaptations of this species to warm climates.

APPENDIX

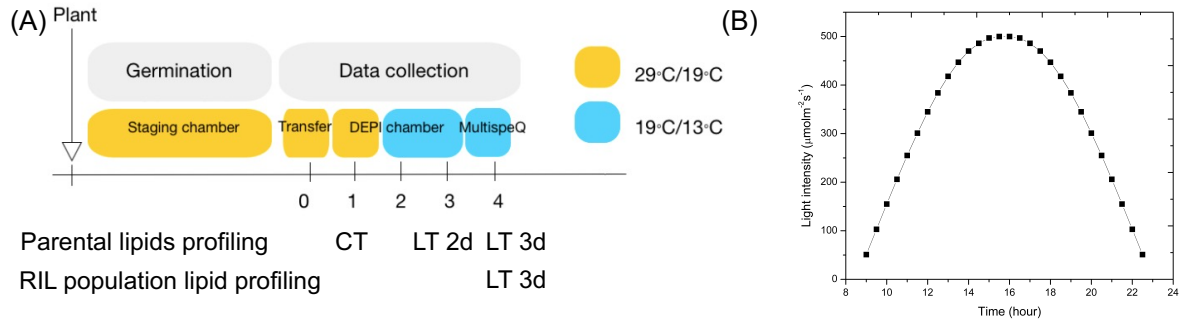

Figure S3.1 Experimental design for growth, lipid profiling and photosynthetic assays leading to quantitative trait loci (QTL) mapping results.
Panel A: Timeline for growth and assays. Four days after seed germination, cowpea plants were moved from staging to DEPI chambers. Following one day of acclimation, DEPI measurements were started. On Day 1, assays were performed under standard (control) temperature. The low temperature regime was initiated on the morning of Day 2 and continued throughout Day 4, for a total of three days. For detailed photosynthetic QTL data found in (Hoh et al., 2021). The lipid profiling of two parents of RILs were performed under three different conditions, control (CT), and 2nd day (LT 2d) or third day of (LT 3d) of low temperature (LT) conditions (indicated as black arrows) to determine conditions under which significant differences between genotypes are most likely to be apparent. The lipid profiling for the RIL population was conducted on LT 3d. Panel B: Sinusoidal pattern of photosynthetically active radiation (PAR) used for days 1-4, simulating outdoor conditions for a cloudless day.

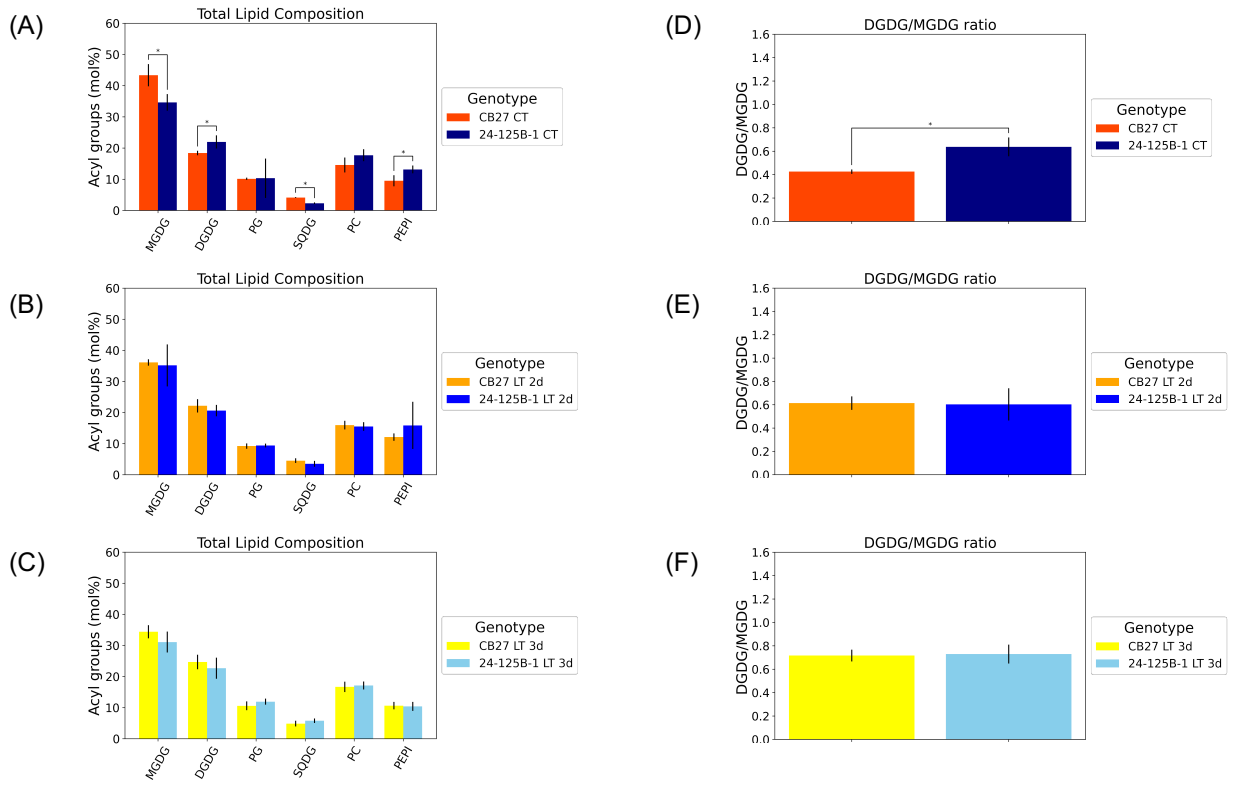

Figure S3.2 The relative abundance of lipid classes of two parental lines (A-C) and ratio of DGDG/MGDG (D-F) for each condition.
CT: control temperature (A and D), LT 2d: 2nd Day of low temperature (B and E), LT 3d: 3rd Day of low temperature (C and F). The averaged replicates (n≥3) for each value as a bar graph with error bar (SD). The asterisks show significant differences between the genotype groups (as shown in brackets) by t-test ($p<0.05$). (A-C) The relative abundance of lipid classes (MGDG, DGDG, PG, SQDQ, PC and PEPI). (D-F) DGDG/MGDG ratio, CB27 showed a lower ratio in CT.

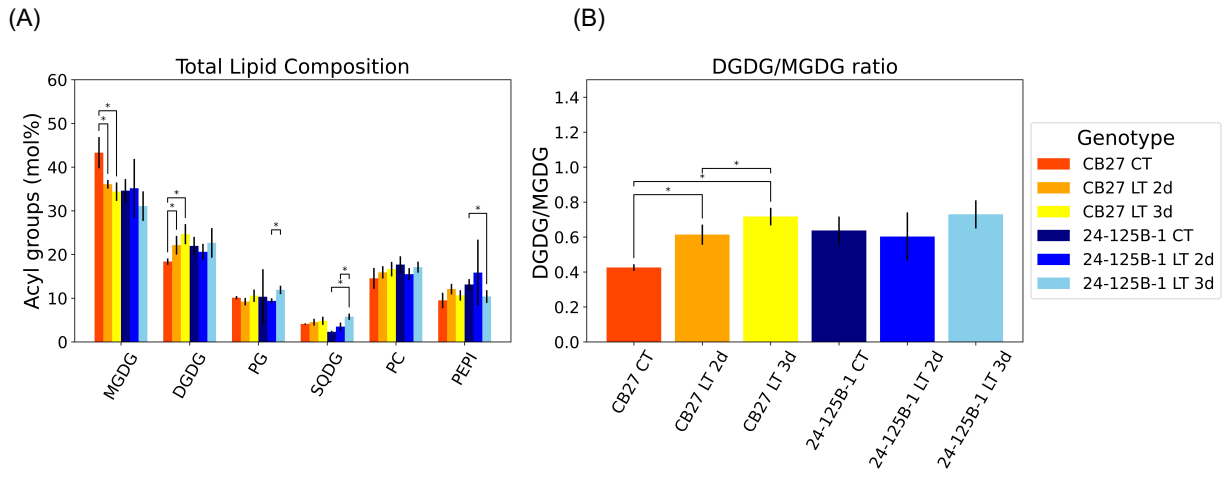

Figure S3.3 The relative abundance of lipid classes (A) and DGDG/MGDG ratio (B) for two parental lines in three temperature conditions.
CT: control temperature (A and D), LT 2d: 2nd Day of low temperature (B and E), LT 3d: 3rd Day of low temperature (C and F).The averaged values for biological replicates (n≥3) for each value as a bar graph with error bar (SD). The asterisks showed significant differences between the conditions in one genotype (as shown in brackets) by t-test ($p<0.05$).

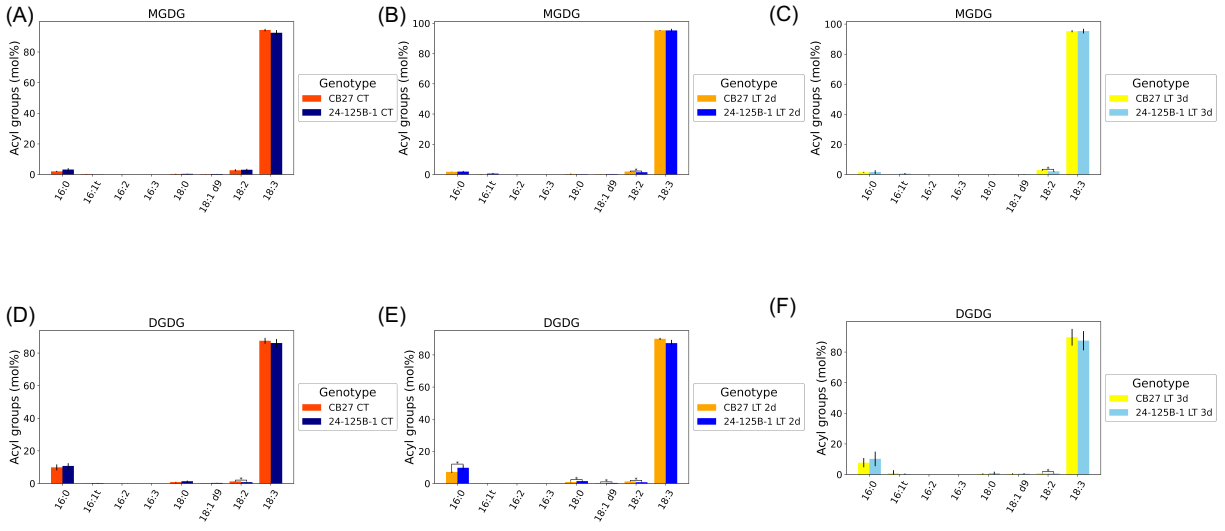

Figure S3.4 The fatty acid contents of each lipid class for two parental lines in each condition.
Panels A-C, MGDG; Panels D-F, DGDG; Panels G-I, PG; Panels J-L, SQDG; Panels M-O, PC and Panels P-R, PEPI. Left Panels, CT; Middle Panels, LT 2d; Right Panels, LT 3d. The average values for biological replicates (n≥3) for each value as a bar graph with error bar (SD). The asterisks showed significant differences between the genotype groups (as shown in brackets) by t-test ($p<0.05$).

Figure S3.4 (cont'd):

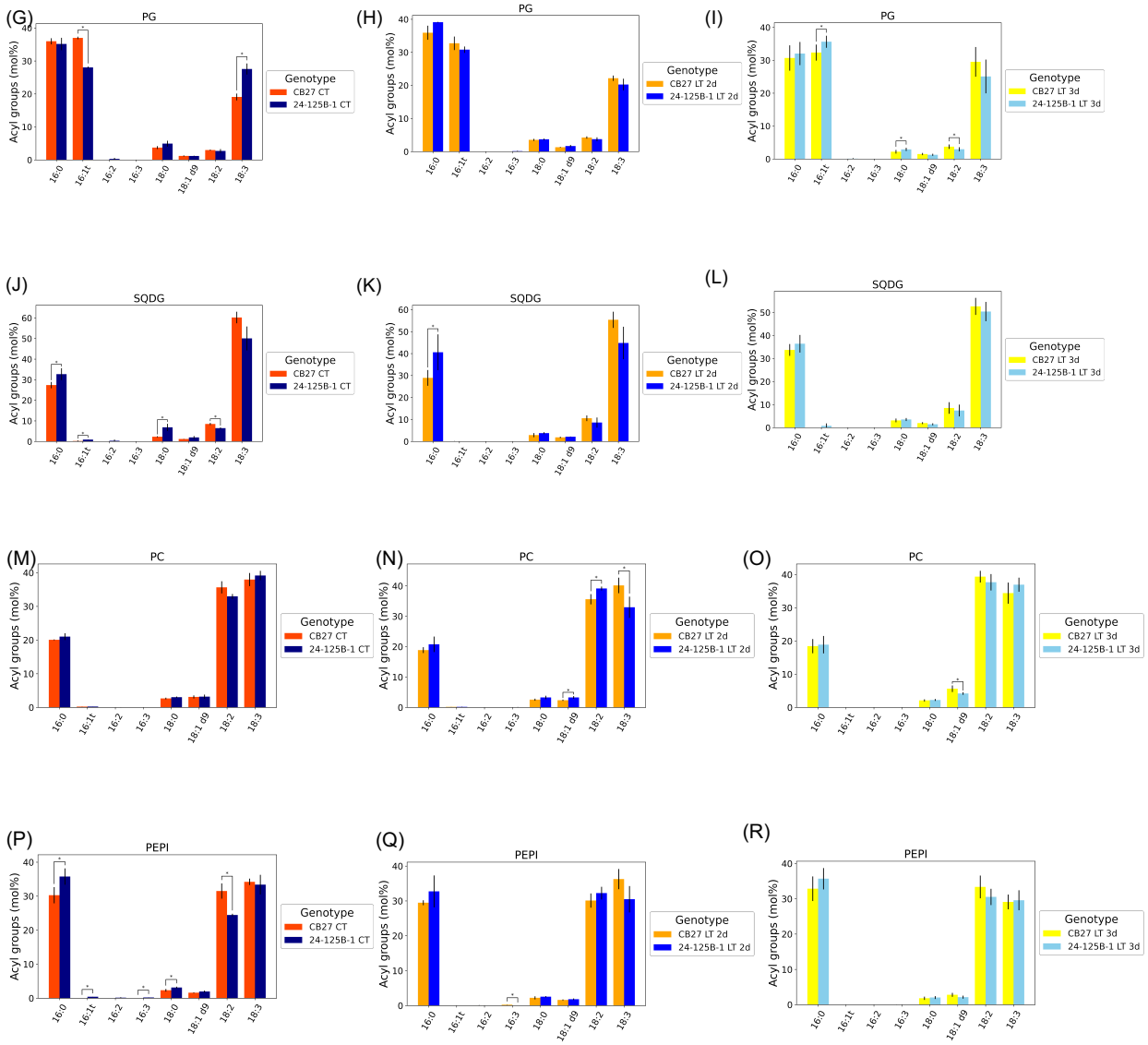

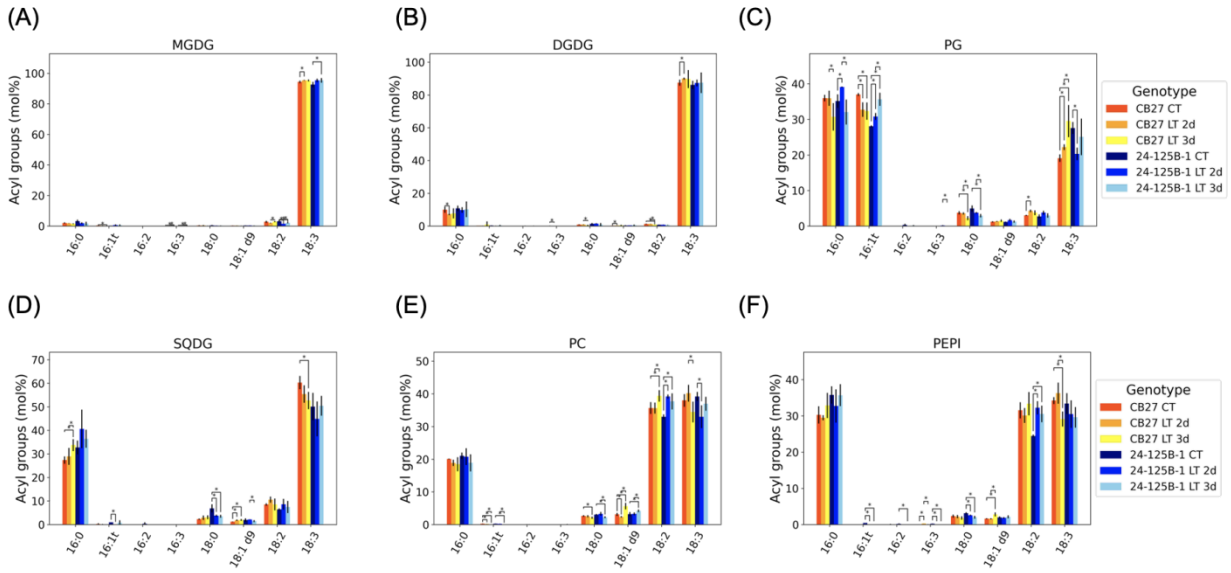

Figure S3.5 The fatty acid contents of each lipid class for two parental lines in three temperature conditions.
CT, control temperature; LT 2d, 2nd Day of low temperature; LT 3d, 3rd Day of low temperature. The average values for biological replicates (n≥3) as bar graphs; error bars represent standard deviations (SD). The asterisks showed significant differences between the conditions in one genotype (as shown in brackets) by t-test ($p<0.05$).

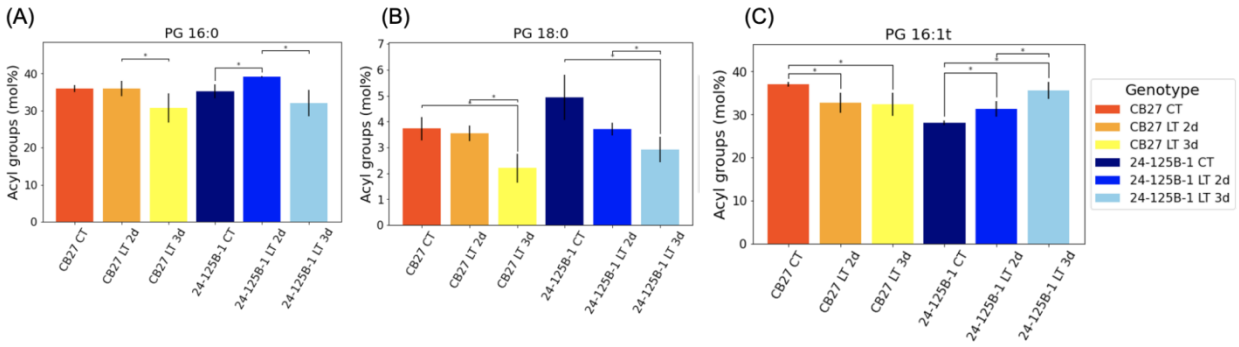

Figure S3.6 The individual fatty acid composition of HMP-PG for two parental lines in three temperature conditions.
CT, control temperature; LT 2d, 2nd Day of low temperature; LT 3d 3rd Day of low temperature. Panel A, PG 16:0; Panel B, PG 18:0; Panel C, PG 16:1t. The averaged values of biological replicates (n≥3) as a bar graph; error bars represent the standard deviation (SD). The asterisks showed significant differences between the conditions in one genotype (as shown in brackets) by t-test ($p<0.05$).

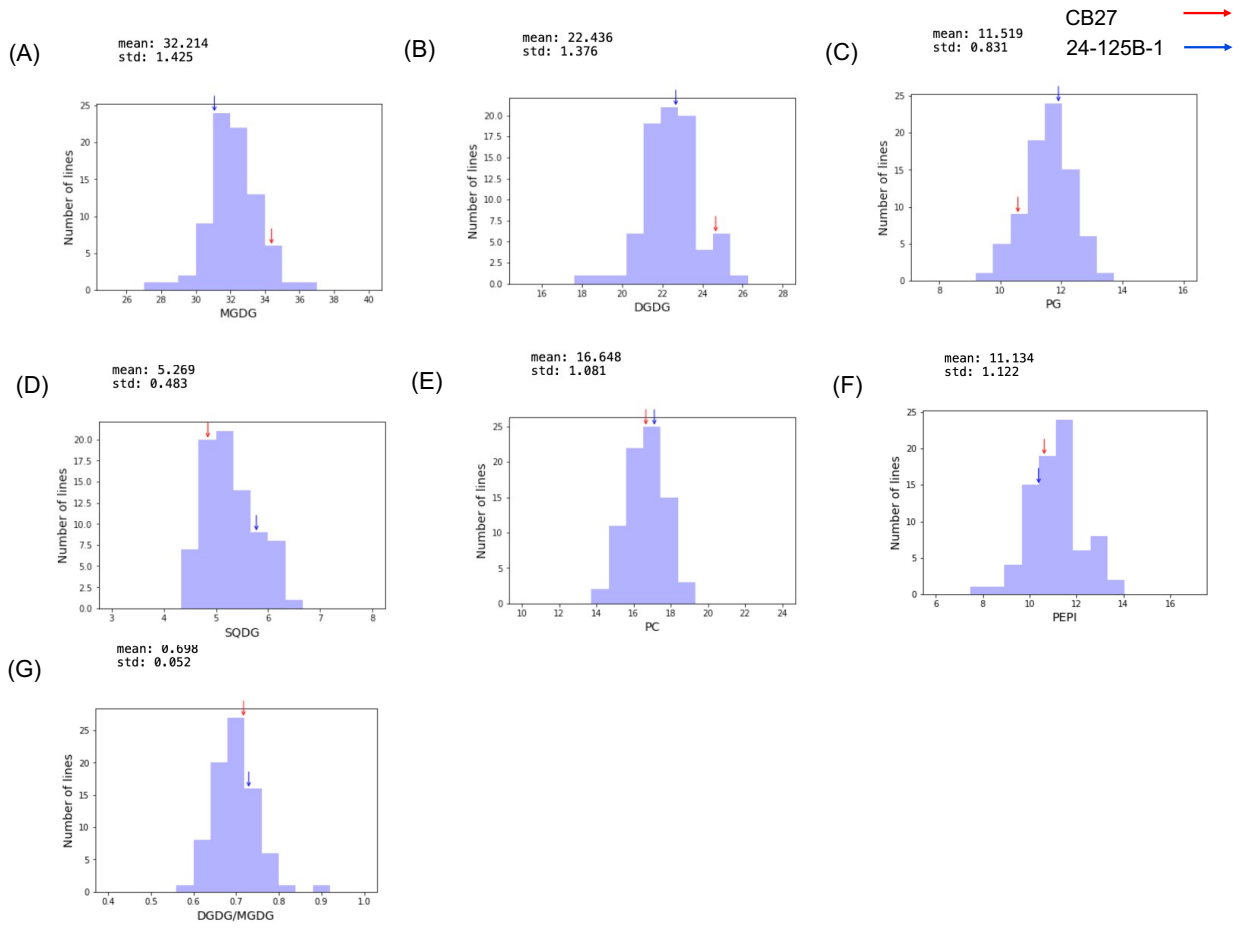

Figure S3.7 Histograms of the relative abundance of lipid classes across genotypes across the RIL lines on the third day of experiment in chilling condition.

Panel A, MGDG; Panel B, DGDG; Panel C, PG; Panel D, SQDG; Panel E, PC; Panel F, PEPI; Panel G, DGDG/MGDG ratio. The averaged replicates (n≥3) for each phenotype value of RILs including two parental lines are shown as histograms. The mean and standard deviation of the population are shown above each histogram. The arrows indicate two parental lines (CB27, red; 24-125B-1, blue).

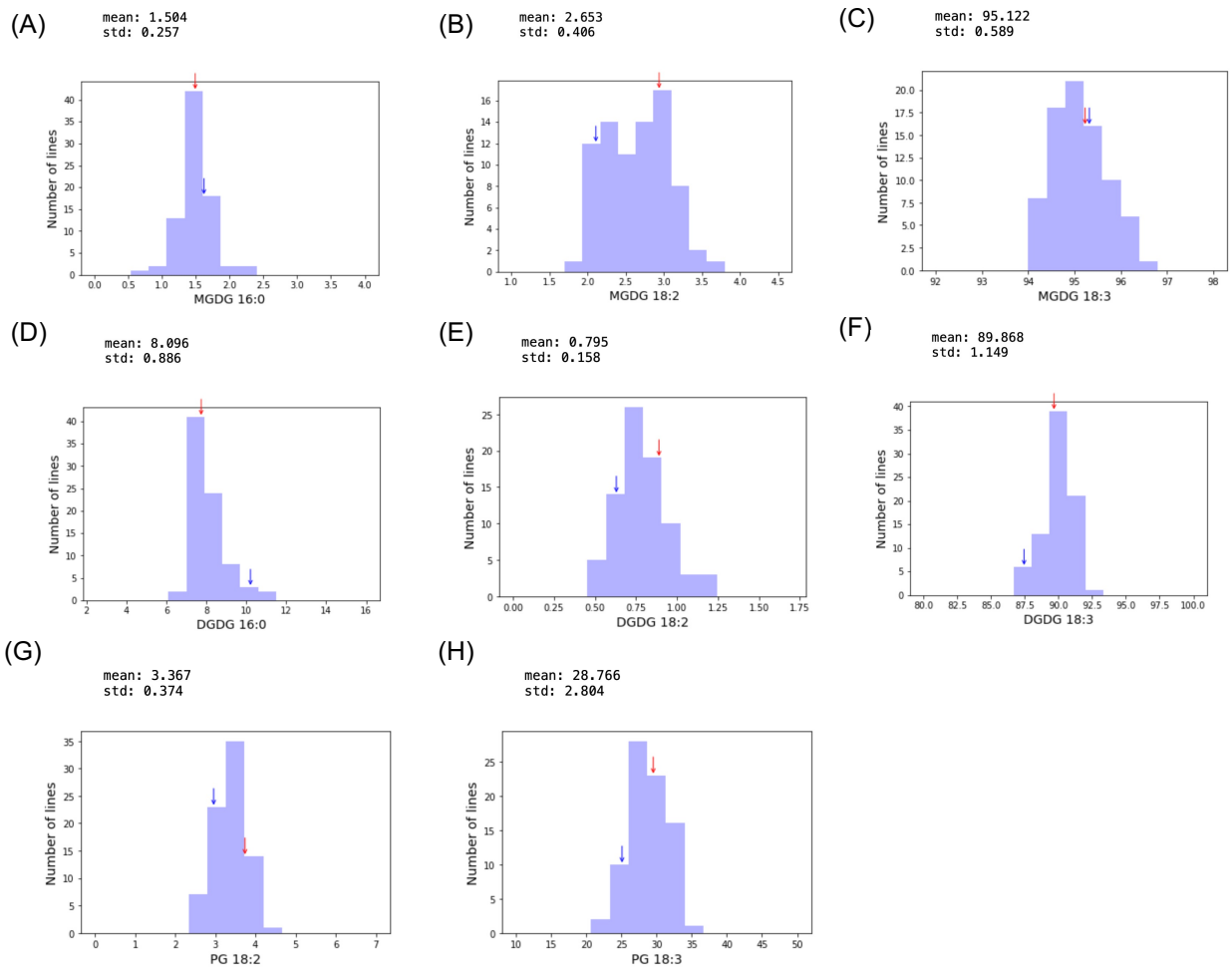

Figure S3.8 Histograms of the contents of fatty acids in the chilling condition. Averages of biological replicates (n≥3) for each phenotype value of RILs including two parental lines are shown as histograms. The mean and standard deviation of the population are shown above each histogram. The arrows indicate two parental lines (CB27, red; 24-125B-1, blue). Panel A, MGDG 16:0; Panel B, MGDG 18:2; Panel C, MGDG 18:3;PanelD, DGDG 16:0;PanelE, DGDG 18:2; Panel F, DGDG 18:3;PanelG, PG 18:2; Panel H, PG 18:3; Panel I, SQDG 16:0; Panel J, SQDG 18:0; Panel K, SQDG 18:1; Panel L, SQDG 18:2; Panel M, SQDG 18:3; Panel N, PC 16:0; Panel O, PC 18:1; Panel P, PC 18:2; Panel Q, PC 18:3; Panel R, PEPI 16:0; Panel S, PEPI 18:2; Panel T, PEPI 18:3 in the chilling condition measured in the third day of LT.

Figure S3.8 (cont'd):

(I) mean: 34.145
std: 1.917

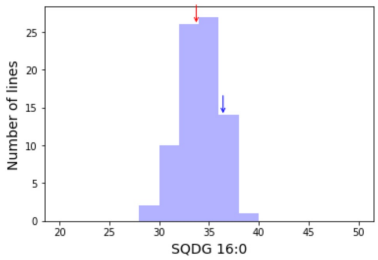

(J) mean: 3.148
std: 0.407

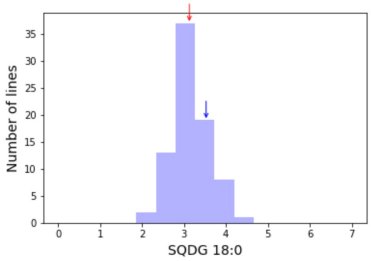

(K) mean: 1.775
std: 0.405

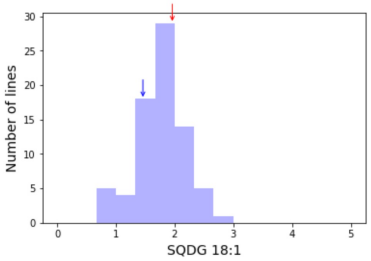

(L) mean: 7.028
std: 1.416

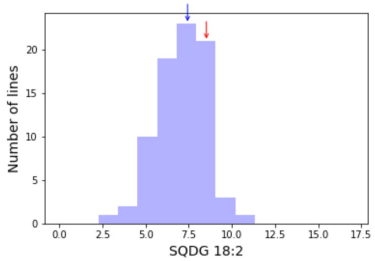

(M) mean: 49.508
std: 4.546

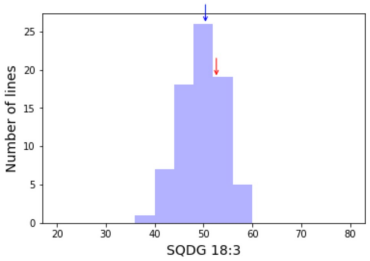

Figure S3.8 (cont'd):

(N) mean: 19.484
std: 1.386

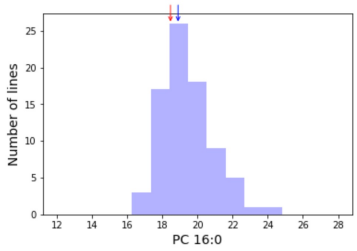

(O) mean: 4.117
std: 1.772

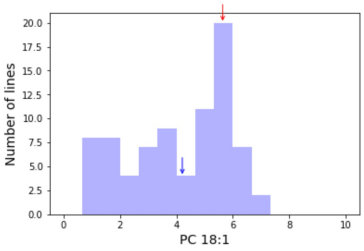

(P) mean: 39.426
std: 1.844

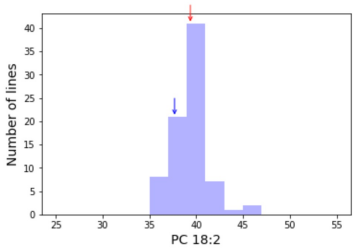

(Q) mean: 33.893
std: 1.812

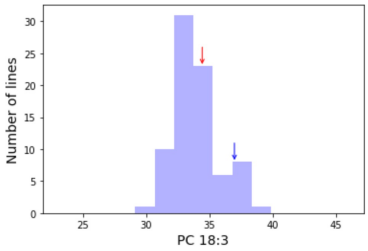

(R) mean: 30.996
std: 1.486

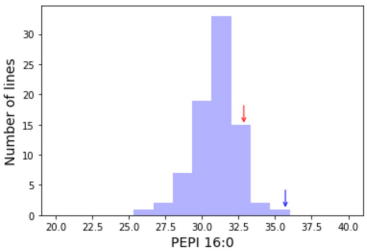

(S) mean: 33.393
std: 1.367

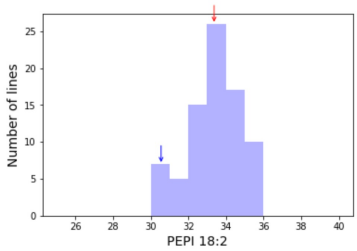

(T) mean: 30.784
std: 1.704

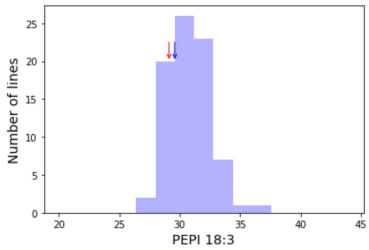

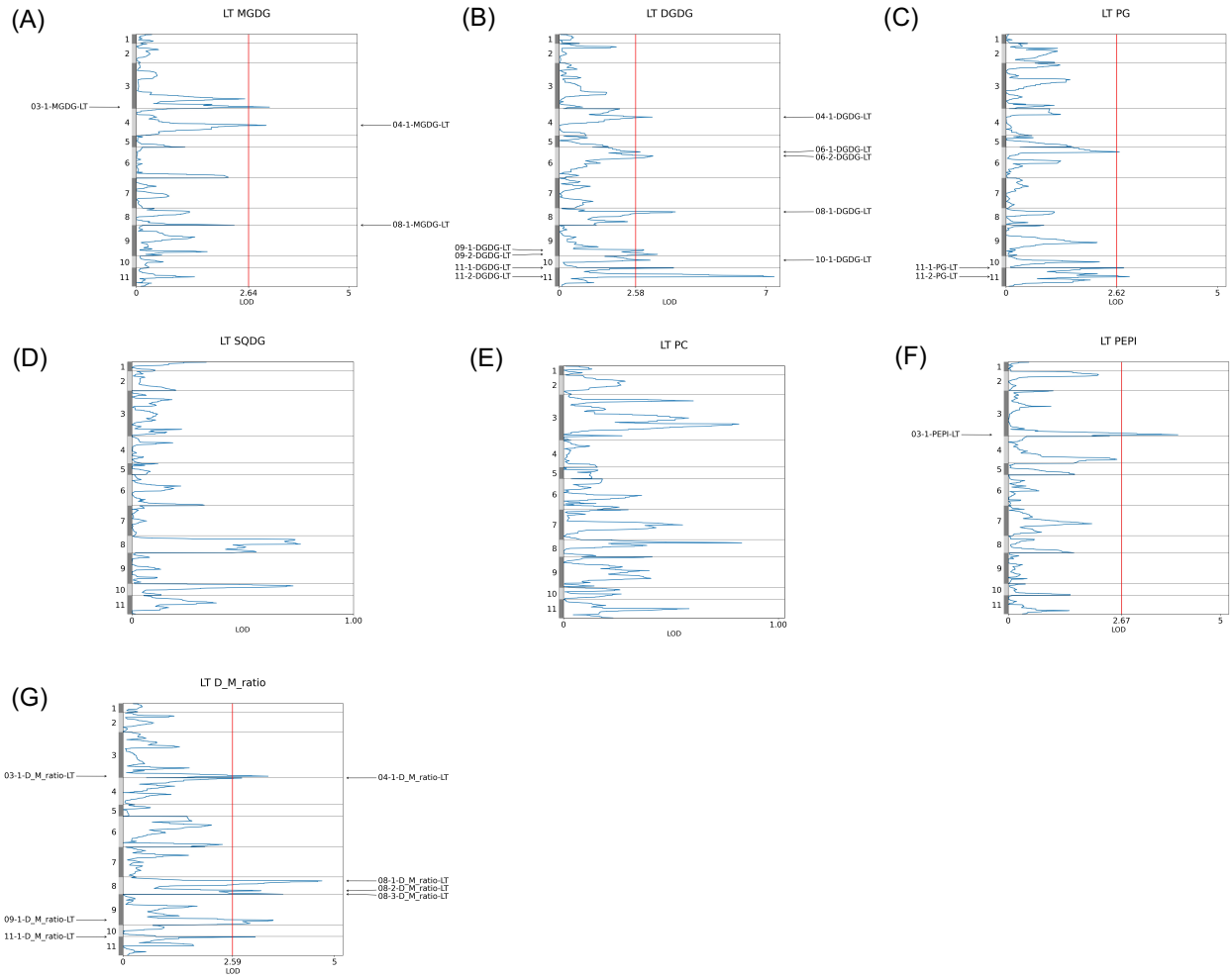

Figure S3.9 QTL analysis of the relative abundance of lipid classes (A-F) and DGDG/MGDG ratio in the chilling condition.
Logarithm of the odds (LOD) score plots of relative abundance of lipid classes. Panel A, MGDG; Panel B, DGDG; Panel C, PG; Panel D, SQDG; Panel E, PC; Panel F, PEPI; Panel G, DGDG/MGDG ratio in the chilling condition measured on the third day of LT. The genetic position is indicated by the y-axis. The significance threshold of 0.05 for each parameter based on 1000 permutations is indicated by the red vertical line. Each QTL named chromosome- index- phenotypes- temperature condition (low temperature, LT) is shown either on the left or right side of the panel with arrows.

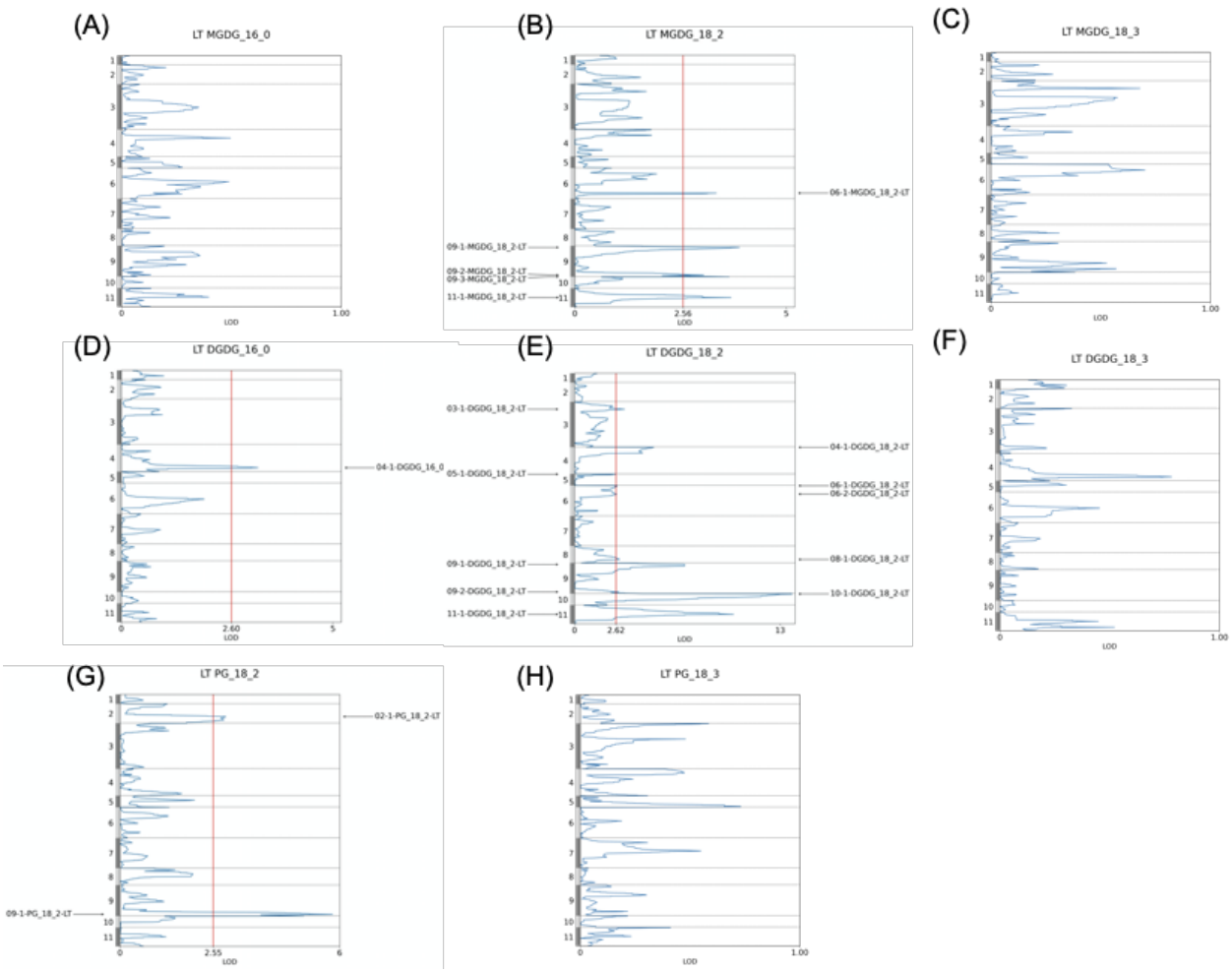

Figure S3.10 QTL analysis of the contents of fatty acids in the chilling condition. Logarithm of the odd (LOD) score plots of the contents of selected fatty acids. Panel A, MGDG 16:0; Panel B, MGDG 18:2; Panel C, MGDG 18:3; Panel D, DGDG 16:0; Panel E, DGDG 18:2; Panel F, DGDG 18:3; Panel G, PG 18:2; Panel H, PG 18:3; Panel I, SQDG 16:0; Panel J, SQDG 18:0; Panel K, SQDG 18:1; Panel L, SQDG 18:2; Panel M, SQDG 18:3; Panel N, PC 16:0; Panel O, PC 18:1; Panel P, PC 18:2; Panel Q, PC 18:3; Panel R, PEPI 16:0; Panel S, PEPI 18:2; Panel T, PEPI 18:3 in the chilling condition measured on the third day of LT. The genetic position is indicated by the y-axis. Significance threshold of 0.05 for each parameter based on 1000 permutations is indicated by the red vertical line. Each QTL named chromosome- index- phenotypes- temperature condition (low temperature, LT) is shown either on the left or right side of the panel with arrows.

Figure S3.10 (cont'd):

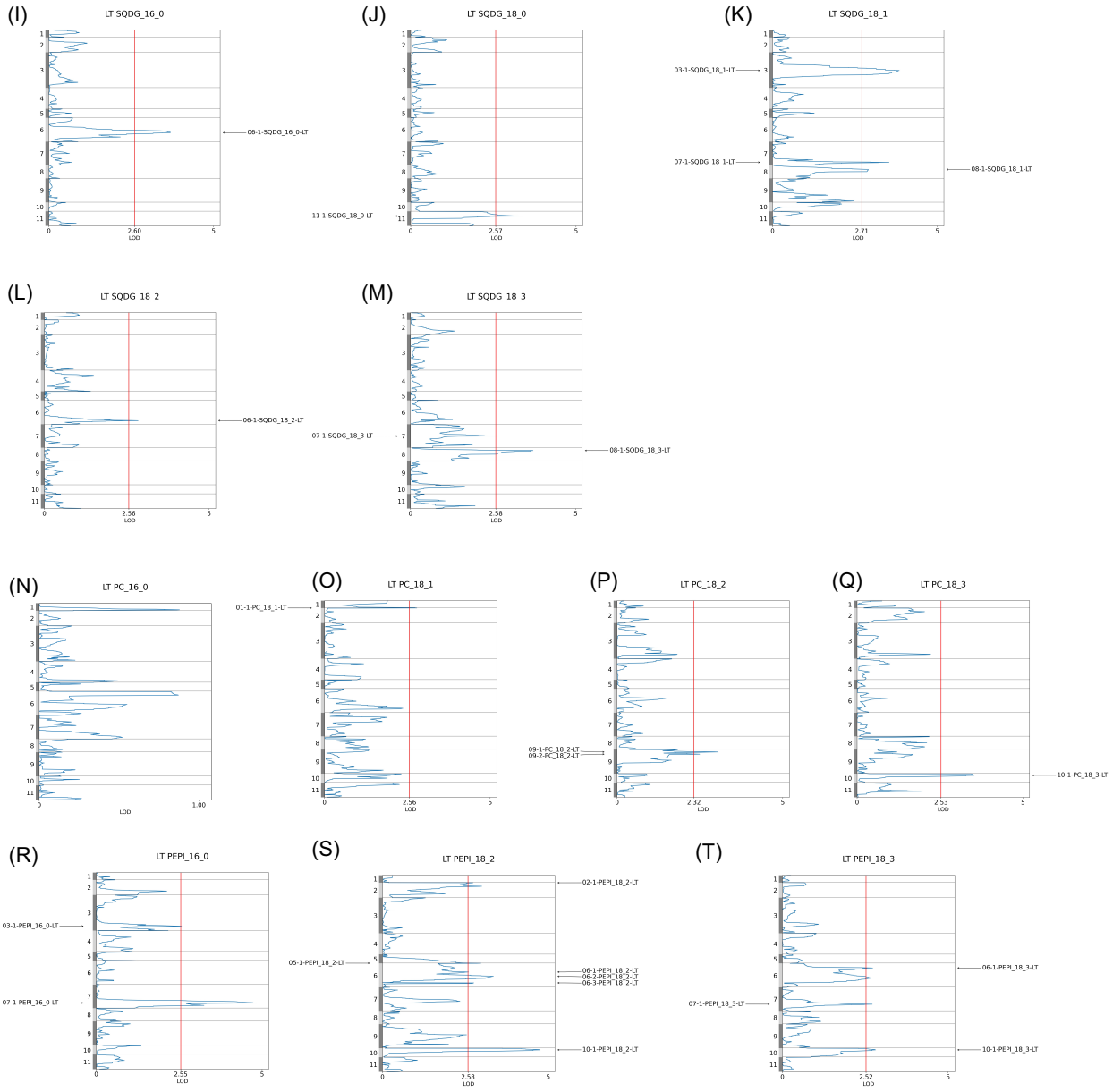

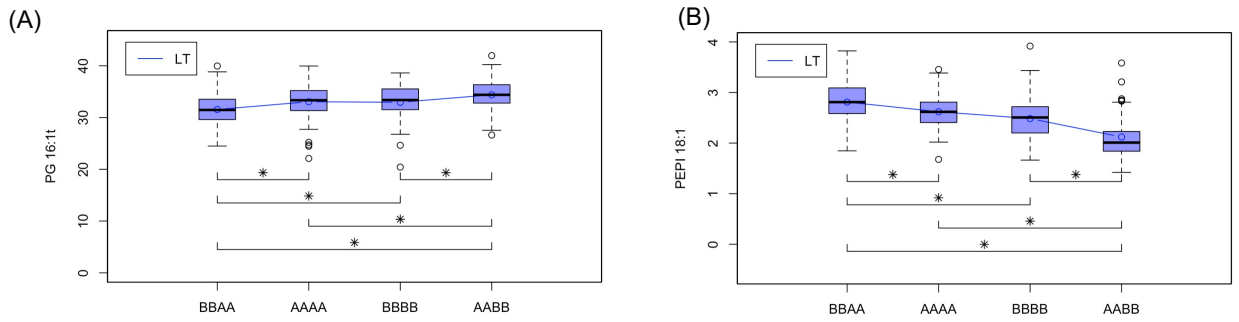

Figure S3.11 Box plots of identified QTLs in Chrs 4 and 9 for PG 16:1t and PEPI 18:1 composition.
Each panel shows mean compositions of PG 16:1t (A) and PEPI 18:1 (B) for genotypes in four allele groups, AABB, BBAA, AAAA and BBBB at identified QTL in Chr 4, 59.64 cM and Chr 9, 86.93 cM. See SI Figure. S3.10 for more detailed description of the nomenclature. Significant differences of fatty acid compositions between groups are indicated for various pairs of allelic groups by the * ($p<0.05$, t-test).

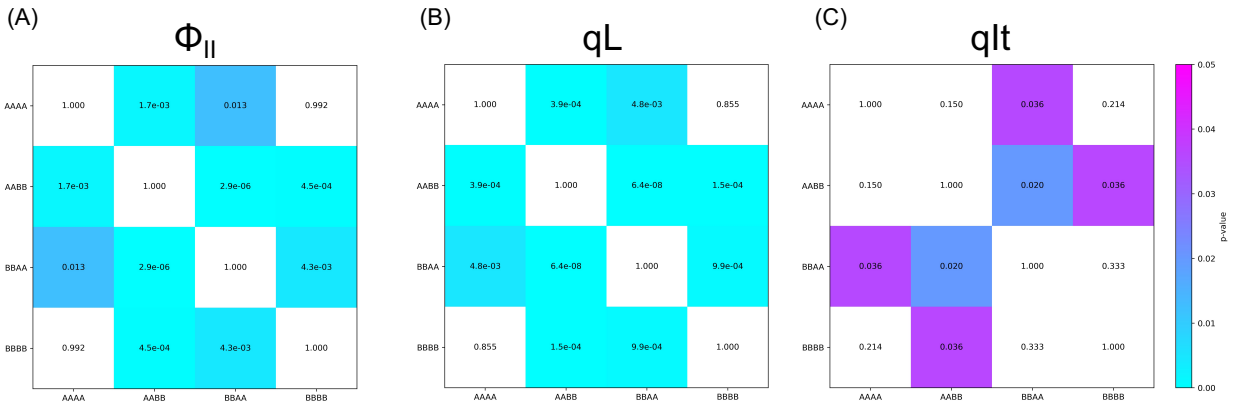

Figure S3.12 Significance matrixes (p-values in each box) of three photosynthetic parameters (A, Φ_{II}; B, qL; C, qlt) for four allele groups shown in Figure 3.6.
Results from Figure 6 were tested for significant differences between groups using t-test. White coloration indicates no significant differences ($p>0.05$) while the gradient of color represents $p < 0.05$, as indicated on the right side of figures.

Table 3.1 List of QTL intervals identified for lipid compositions (lipid classes and fatty acids).

To refer to specific intervals related to different conditions and phenotypes, a standard nomenclature was established to allow comparisons of QTLs that appeared for different parameters, conditions and times that follow the format described in the following: Chromosome number - Index - Phenotype - Temperature, where low temperature is abbreviated as LT. The indexes are numbered with Arabic numerals in the order of genomic loci of identified QTLs in each chromosome for the QTLs for that phenotype.

Phenotype	QTL	Position cM (Max)	Max LOD Score	Flanking markers (bin ID)
LT_D_M_ratio	03-1-D_M_ratio-LT	118.75-120(120)	3.432	2_07401 (459) - 2_28969 (667)
LT_D_M_ratio	04-1-D_M_ratio-LT	0-0.62(0)	2.808	2_03034 (337) - 2_34666 (0)
LT_D_M_ratio	08-1-D_M_ratio-LT	12.93-23.42(15)	4.705	2_08836 (0) - 2_14171 (566)
LT_D_M_ratio	08-2-D_M_ratio-LT	39.6-42.71(40)	3.267	2_35933 (0) - 2_01816 (273)
LT_D_M_ratio	08-3-D_M_ratio-LT	51.88-54.29(54.29)	3.784	2_16563 (588) - 2_11907 (540)
LT_D_M_ratio	09-1-D_M_ratio-LT	78.71-100.54(80)	3.552	2_06016 (0) - 1_1393 (142)
LT_D_M_ratio	11-1-D_M_ratio-LT	0-0(0)	3.128	2_03135 (341) - 2_40245 (0)
LT_DGDG	04-1-DGDG-LT	19.29-22.35(20)	3.129	1_1390 (141) - 2_03479 (349)
LT_DGDG	06-1-DGDG-LT	4.83-5.42(5)	2.727	2_00478 (190) - 2_06634 (441)
LT_DGDG	06-2-DGDG-LT	13.86-18.66(15)	3.153	2_11742 (537) - 2_06302 (430)
LT_DGDG	08-1-DGDG-LT	14.8-19.14(15)	3.909	2_08836 (0) - 2_17117 (594)
LT_DGDG	09-1-DGDG-LT	74.98-78.71(75)	2.846	1_0566 (73) - 2_23951 (640)
LT_DGDG	09-2-DGDG-LT	91.31-98.07(95)	3.306	2_54820 (0) - 2_17422 (597)
LT_DGDG	10-1-DGDG-LT	7.31-10(10)	3.063	2_43080 (696) - 2_03668 (360)
LT_DGDG	11-1-DGDG-LT	0-2.43(0)	3.847	2_03135 (341) - 2_40245 (0)
LT_DGDG	11-2-DGDG-LT	18.12-30(25)	7.238	2_44401 (0) - 2_05408 (413)
LT_DGDG_16_0	04-1-DGDG_16_0-LT	51.05-55.91(55)	3.234	2_28660 (0) - 2_34117 (0)
LT_DGDG_18_2	03-1-DGDG_18_2-LT	18.46-21.48(20)	3.162	1_0057 (14) - 2_08749 (482)
LT_DGDG_18_2	04-1-DGDG_18_2-LT	0-10.58(0)	4.885	2_03034 (337) - 2_12502 (543)
LT_DGDG_18_2	06-1-DGDG_18_2-LT	0-0(0)	2.695	1_1007 (116) - 1_0650 (84)
LT_DGDG_18_2	08-1-DGDG_18_2-LT	39.6-40(40)	2.709	2_26409 (658) - 2_01656 (263)
LT_DGDG_18_2	09-1-DGDG_18_2-LT	0-26.28(5)	6.965	2_03262 (344) - 2_47401 (0)
LT_DGDG_18_2	09-2-DGDG_18_2-LT	95-95.59(95)	2.792	2_20425 (619) - 2_23951 (640)
LT_DGDG_18_2	10-1-DGDG_18_2-LT	0-22.24(0)	13.741	2_00769 (0) - 2_01356 (243)
LT_DGDG_18_2	11-1-DGDG_18_2-LT	7.26-45(30)	10.049	2_26255 (656) - 2_05408 (413)
LT_HMP-PG	07-1-HMP-PG-LT	34.59-35.19(35)	2.615	2_28739 (0) - 2_28739 (0)
LT_MGDG	03-1-MGDG-LT	118.75-120(120)	3.015	2_32543 (0) - 2_21391 (0)
LT_MGDG	04-1-MGDG-LT	34.47-35.07(35)	2.941	2_05775 (419) - 1_0562 (72)
LT_MGDG_18_2	06-1-MGDG_18_2-LT	65-70(65)	3.311	2_07111 (453) - 2_28687 (0)
LT_MGDG_18_2	09-1-MGDG_18_2-LT	3-10.89(5)	3.894	2_03262 (344) - 2_00142 (160)
LT_MGDG_18_2	09-2-MGDG_18_2-LT	93.15-95.59(95)	3.045	2_20425 (619) - 2_23951 (640)
LT_MGDG_18_2	09-3-MGDG_18_2-LT	101.74-104.15(104.15)	3.575	2_17422 (597) - 2_23951 (640)
LT_MGDG_18_2	11-1-MGDG_18_2-LT	19.34-36.51(30)	3.690	2_40688 (0) - 2_06463 (0)
LT_PC_18_1	01-1-PC_18_1-LT	35-35.75(35.75)	2.725	1_0847 (101) - 2_26118 (654)
LT_PC_18_2	09-1-PC_18_2-LT	8.48-11.48(10)	3.035	2_03956 (375) - 2_38670 (0)
LT_PC_18_2	09-2-PC_18_2-LT	19.44-20(20)	2.492	2_03681 (362) - 2_09913 (510)
LT_PC_18_3	10-1-PC_18_3-LT	0-6.7(5)	3.620	2_00769 (0) - 2_01589 (257)

Table 3.1 (cont'd):

LT_PEPI	03-1-PEPI-LT	116.29-122.47(120)	4.023	2_07401 (459) - 2_17764 (600)
LT_PEPI_16_0	03-1-PEPI_16_0-LT	95-95(95)	2.571	1_0707 (94) - 1_0464 (61)
LT_PEPI_16_0	07-1-PEPI_16_0-LT	60-80.9(70)	4.812	2_00233 (172) - 2_06408 (432)
LT_PEPI_18_1	04-1-PEPI_18_1-LT	54.09-64.45(60)	3.417	1_0069 (17) - 2_04962 (402)
LT_PEPI_18_1	06-1-PEPI_18_1-LT	75-75(75)	2.643	2_08255 (468) - 2_05713 (417)
LT_PEPI_18_1	07-1-PEPI_18_1-LT	14.71-15(15)	2.827	2_07479 (460) - 2_01552 (255)
LT_PEPI_18_1	09-1-PEPI_18_1-LT	0-0(0)	2.650	2_03318 (345) - 2_00764 (209)
LT_PEPI_18_1	09-2-PEPI_18_1-LT	75.58-104.15(90)	8.865	2_54820 (0) - 2_00704 (201)
LT_PEPI_18_1	10-1-PEPI_18_1-LT	0-15.24(0)	4.488	2_00769 (0) - 1_0952 (111)
LT_PEPI_18_2	02-1-PEPI_18_2-LT	0-2.4(0)	2.917	2_00017 (150) - 2_08550 (0)
LT_PEPI_18_2	05-1-PEPI_18_2-LT	45-47.05(45)	3.280	2_42402 (695) - 2_37534 (0)
LT_PEPI_18_2	06-1-PEPI_18_2-LT	33.79-45.58(40)	3.314	1_0706 (93) - 2_08255 (468)
LT_PEPI_18_2	06-2-PEPI_18_2-LT	65-66.87(65)	2.764	2_07111 (453) - 2_28687 (0)
LT_PEPI_18_2	10-1-PEPI_18_2-LT	0-10(5)	4.884	1_0960 (113) - 2_01589 (257)
LT_PEPI_18_3	06-1-PEPI_18_3-LT	9.65-10.85(10)	2.809	1_0933 (110) - 2_18750 (610)
LT_PEPI_18_3	06-2-PEPI_18_3-LT	40-41.88(40)	2.564	2_00562 (194) - 2_08827 (487)
LT_PEPI_18_3	07-1-PEPI_18_3-LT	63.83-65.69(65)	2.795	2_04403 (385) - 1_0695 (90)
LT_PEPI_18_3	10-1-PEPI_18_3-LT	2.47-6.7(5)	2.926	2_00769 (0) - 2_10282 (517)
LT_PG	06-1-PG-LT	4.83-5(5)	2.605	1_1007 (116) - 2_00562 (194)
LT_PG	11-1-PG-LT	0-0(0)	2.702	2_03135 (341) - 2_00717 (203)
LT_PG	11-2-PG-LT	23.92-30(25)	2.835	2_44401 (0) - 2_06463 (0)
LT_PG_16_0	07-1-PG_16_0-LT	31-39.39(35)	3.772	2_12704 (545) - 2_42830 (0)
LT_PG_16_1	04-1-PG_16_1-LT	59.04-64.45(64.45)	3.829	2_00148 (161) - 2_04962 (402)
LT_PG_16_1	09-1-PG_16_1-LT	86.93-104.15(95)	5.147	2_20425 (619) - 2_10754 (0)
LT_PG_18_0	03-1-PG_18_0-LT	72.04-80(75)	3.694	2_04499 (387) - 2_08441 (474)
LT_PG_18_0	07-1-PG_18_0-LT	33.99-38.19(35)	2.960	2_11589 (536) - 2_12852 (548)
LT_PG_18_2	02-1-PG_18_2-LT	34.69-46.16(35)	2.889	2_04228 (382) - 2_04763 (396)
LT_PG_18_2	09-1-PG_18_2-LT	90-104.15(95)	5.802	2_00704 (201) - 2_22085 (0)
LT_SQDG_16_0	06-1-SQDG_16_0-LT	38.12-46.82(45)	3.569	2_00810 (211) - 2_49231 (0)
LT_SQDG_18_0	11-1-SQDG_18_0-LT	10.85-15.65(15)	3.366	2_00047 (154) - 2_01687 (264)
LT_SQDG_18_1	03-1-SQDG_18_1-LT	52.89-61.4(55)	3.844	2_00955 (220) - 2_32477 (0)
LT_SQDG_18_1	07-1-SQDG_18_1-LT	79.07-82.17(80)	3.535	2_05014 (405) - 2_15784 (583)
LT_SQDG_18_1	08-1-SQDG_18_1-LT	19.14-25(20)	3.023	2_14171 (566) - 2_49638 (0)
LT_SQDG_18_3	07-1-SQDG_18_3-LT	40-40(40)	2.618	2_04492 (0) - 2_12852 (548)
LT_SQDG_18_3	08-1-SQDG_18_3-LT	12.93-25(15)	3.830	2_14158 (0) - 2_12532 (544)

BIBLIOGRAPHY

BIBLIOGRAPHY

1. Alonso J.M., Stepanova A.N., Leisse T.J., Kim C.J., Chen H., Shinn P., … Ecker J.R. (2003) Genome-wide insertional mutagenesis of *Arabidopsis thaliana*. *Science***301**, 653–657.

2. Anderson J.M. (1986) Photoregulation of the composition, function, and structure of thylakoid membranes. *Annual Review of Plant Physiology***37**, 93–136.

3. Aronsson H., Schöttler M.A., Kelly A.A., Sundqvist C., Dörmann P., Karim S. & Jarvis P. (2008) Monogalactosyldiacylglycerol deficiency in Arabidopsis affects pigment composition in the prolamellar body and impairs thylakoid membrane energization and photoprotection in leaves. *Plant Physiology***148**, 580–592.

4. Babiychuk E., Müller F., Eubel H., Braun H.-P., Frentzen M. &Kushnir S. (2003) Arabidopsis phosphatidylglycerophosphate synthase 1 is essential for chloroplast differentiation, but is dispensable for mitochondrial function. *The Plant Journal: for Cell and Molecular Biology***33**, 899–909.

5. Barkan L., Vijayan P., Carlsson A.S., Mekhedov S. & Browse J. (2006) A suppressor of fab1 challenges hypotheses on the role of thylakoid unsaturation in photosynthetic function. *Plant Physiology***141**, 1012–1020.

6. Broman K.W. & Sen S. (2009) *A Guide to QTL Mapping with R/qtl*. Springer New York, New York, NY.

7. Cook R., Lupette J. & Benning C. (2021) The role of chloroplast membrane lipid metabolism in plant environmental responses. *Cells***10**.

8. Cruz J.A., Savage L.J., Zegarac R., Hall C.C., Satoh-Cruz M., Davis G.A., … Kramer D.M. (2016) Dynamic environmental photosynthetic imaging reveals emergent phenotypes. *Cell Systems***2**, 365–377.

9. Curtis M.D. &Grossniklaus U. (2003) A gateway cloning vector set for high-throughput functional analysis of genes in planta. *Plant Physiology***133**, 462–469.

10. Dörmann P., Hoffmann-Benning S., Balbo I. & Benning C. (1995) Isolation and characterization of an Arabidopsis mutant deficient in the thylakoid lipid digalactosyl diacylglycerol. *The Plant Cell***7**, 1801–1810.

11. Fujii S., Kobayashi K., Nakamura Y. & Wada H. (2014) Inducible knockdown of MONOGALACTOSYLDIACYLGLYCEROL SYNTHASE1 reveals roles of galactolipids in organelle differentiation in Arabidopsis cotyledons. *Plant Physiology***166**, 1436–1449.

12. Gao J., Ajjawi I., Manoli A., Sawin A., Xu C., Froehlich J.E., … Benning C. (2009) FATTY ACID DESATURASE4 of Arabidopsis encodes a protein distinct from characterized fatty acid desaturases. *The Plant Journal: for Cell and Molecular Biology***60**, 832–839.

13. Guo J., Zhang Z., Bi Y., Yang W., Xu Y. & Zhang L. (2005) Decreased stability of photosystem I in dgd1 mutant of Arabidopsis thaliana. *FEBS Letters***579**, 3619–3624.

14. Hagio M., Sakurai I., Sato S., Kato T., Tabata S. & Wada H. (2002) Phosphatidylglycerol is essential for the development of thylakoid membranes in Arabidopsis thaliana. *Plant & Cell Physiology***43**, 1456–1464.

15. Härtel H., Lokstein H., Dörmann P., Grimm B. & Benning C. (1997) Changes in the composition of the photosynthetic apparatus in the galactolipid-deficient dgd1 mutant of Arabidopsis thaliana. *Plant Physiology***115**, 1175–1184.

16. Hölzl G., Witt S., Gaude N., Melzer M., Schöttler M.A. &Dörmann P. (2009) The role of diglycosyl lipids in photosynthesis and membrane lipid homeostasis in Arabidopsis. *Plant Physiology***150**, 1147–1159.

17. Hölzl G., Witt S., Kelly A.A., Zähringer U., Warnecke D., Dörmann P. & Heinz E. (2006) Functional differences between galactolipids and glucolipids revealed in photosynthesis of higher plants. *Proceedings of the National Academy of Sciences of the United States of America***103**, 7512–7517.

18. Horn P.J., Smith M.D., Clark T.R., Froehlich J.E. & Benning C. (2020) PEROXIREDOXIN Q stimulates the activity of the chloroplast 16:1Δ3trans FATTY ACID DESATURASE4. *The Plant Journal: for Cell and Molecular Biology***102**, 718–729.

19. Hugly S. & Somerville C. (1992) A role for membrane lipid polyunsaturation in chloroplast biogenesis at low temperature. *Plant Physiology***99**, 197–202.

20. Huner N.P.A., Öquist G. &Sarhan F. (1998) Energy balance and acclimation to light and cold. *Trends in Plant Science***3**, 224–230.

21. Hurlock A.K., Roston R.L., Wang K. & Benning C. (2014) Lipid trafficking in plant cells. *Traffic***15**, 915–932.

22. Ivanov A.G., Hendrickson L., Krol M., Selstam E., Oquist G., Hurry V. &Huner N.P.A. (2006) Digalactosyl-diacylglycerol deficiency impairs the capacity for photosynthetic intersystem electron transport and state transitions in Arabidopsis thaliana due to photosystem I acceptor-side limitations. *Plant & Cell Physiology***47**, 1146–1157.

23. Kobayashi K., Kondo M., Fukuda H., Nishimura M. &Ohta H. (2007) Galactolipid

synthesis in chloroplast inner envelope is essential for proper thylakoid biogenesis, photosynthesis, and embryogenesis. *Proceedings of the National Academy of Sciences of the United States of America***104**, 17216–17221.

24. Kobayashi K., Narise T., Sonoike K., Hashimoto H., Sato N., Kondo M., … Ohta H. (2013) Role of galactolipid biosynthesis in coordinated development of photosynthetic complexes and thylakoid membranes during chloroplast biogenesis in Arabidopsis. *The Plant Journal: for Cell and Molecular Biology***73**, 250–261.

25. Kunst L., Browse J. & Somerville C. (1989) A mutant of Arabidopsis deficient in desaturation of palmitic Acid in leaf lipids. *Plant Physiology***90**, 943–947.

26. Lonardi S., Muñoz-Amatriaín M., Liang Q., Shu S., Wanamaker S.I., Lo S., … Close T.J. (2019) The genome of cowpea (Vigna unguiculata [L.] Walp.). *The Plant Journal: for Cell and Molecular Biology***98**, 767–782.

27. Lyons J.M. (1973) Chilling Injury in Plants. *Annual Review of Plant Physiology***24**, 445–466.

28. Miquel M., James D., Dooner H. & Browse J. (1993) Arabidopsis requires polyunsaturated lipids for low-temperature survival. *Proceedings of the National Academy of Sciences of the United States of America***90**, 6208–6212.

29. Moellering E.R., Muthan B. & Benning C. (2010) Freezing tolerance in plants requires lipid remodeling at the outer chloroplast membrane. *Science***330**, 226–228.

30. Muchero W., Diop N.N., Bhat P.R., Fenton R.D., Wanamaker S., Pottorff M., … Close T.J. (2009) A consensus genetic map of cowpea [Vigna unguiculata (L) Walp.] and synteny based on EST-derived SNPs. *Proceedings of the National Academy of Sciences of the United States of America***106**, 18159–18164.

31. Murata N. & Nishida I. (1990) Lipids in relation to chilling sensitivity of plants. *Chilling injury of horticultural crops*.

32. Murata N., Sato N., Takahashi N., Hamazaki Y. %J P. & Cell Physiology (1982) Compositions and positional distributions of fatty acids in phospholipids from leaves of chilling-sensitive and chilling-resistant plants. **23**, 1071–1079.

33. Murata N. &Yamaya J. (1984) Temperature-dependent phase behavior of phosphatidylglycerols from chilling-sensitive and chilling-resistant plants. *Plant Physiology***74**, 1016–1024.

34. Murata N. (1983) Molecular Species Composition of Phosphatidylglycerols from Chilling-Sensitive and Chilling-Resistant Plants. *Plant and Cell Physiology***24**, 81–86.

35. Pribil M., Labs M. & Leister D. (2014) Structure and dynamics of thylakoids in land plants. *Journal of Experimental Botany***65**, 1955–1972.

36. Raison J.K. (1973) Temperature-induced phase changes in membrane lipids and their influence on metabolic regulation. pp. 485–512.

37. Reifarth F., Christen G., Seeliger A.G., Dörmann P., Benning C. &Renger G. (1997) Modification of the water oxidizing complex in leaves of the dgd1 mutant of Arabidopsis thaliana deficient in the galactolipid digalactosyldiacylglycerol. *Biochemistry***36**, 11769–11776.

38. Roughan P.G. (1985) Phosphatidylglycerol and chilling sensitivity in plants. *Plant Physiology***77**, 740–746.

39. Selstam E. (2004) Development of Thylakoid Membranes with Respect to Lipids. In *Lipids in photosynthesis: structure, function and genetics*. (eds S. Paul-André & M. Norio), pp. 209–224. Kluwer Academic Publishers, Dordrecht.

40. Shimojima M. &Ohta H. (2011) Critical regulation of galactolipid synthesis controls membrane differentiation and remodeling in distinct plant organs and following environmental changes. *Progress in lipid research***50**, 258–266.

41. Siegenthaler P.-A. & Murata N. (2006) Lipids in Photosynthesis: An Overview. In *Lipids in photosynthesis: structure, function and genetics*. (eds P.-A. Siegenthaler& N. Murata), pp. 1–20. Springer Science & Business Media.

42. Steffen R., Kelly A.A., Huyer J., Dörmann P. &Renger G. (2005) Investigations on the reaction pattern of photosystem II in leaves from Arabidopsis thaliana wild type plants and mutants with genetically modified lipid content. *Biochemistry***44**, 3134–3142.

43. Wang Z. & Benning C. (2011) Arabidopsis thaliana polar glycerolipid profiling by thin layer chromatography (TLC) coupled with gas-liquid chromatography (GLC). *Journal of visualized experiments: JoVE*.

44. Williams W.P. (2004) The physical properties of thylakoid membrane lipids and their relation to photosynthesis. In *Lipids in photosynthesis: structure, function and genetics*. (eds S. Paul-André & M. Norio), pp. 103–118. Kluwer Academic Publishers, Dordrecht.

45. Wolter F.P., Schmidt R. & Heinz E. (1992) Chilling sensitivity of Arabidopsis thaliana with genetically engineered membrane lipids. *The EMBO Journal***11**, 4685–4692.

46. Wu J. & Browse J. (1995) Elevated Levels of High-Melting-Point Phosphatidylglycerols Do Not Induce Chilling Sensitivity in an Arabidopsis

Mutant. *The Plant Cell***7**, 17–27.

47. Wu J., Lightner J. & Warwick N. (1997) Low-temperature damage and subsequent recovery of fab1 mutant Arabidopsis exposed to 2 [deg] C. *Plant Physiology***113**, 347–356.

48. Wu W., Ping W., Wu H., Li M., Gu D. & Xu Y. (2013) Monogalactosyldiacylglycerol deficiency in tobacco inhibits the cytochrome b6f-mediated intersystem electron transport process and affects the photostability of the photosystem II apparatus. *Biochimica et Biophysica Acta***1827**, 709–722.

49. Xu C., Härtel H., Wada H., Hagio M., Yu B., Eakin C. & Benning C. (2002) The pgp1 mutant locus of Arabidopsis encodes a phosphatidylglycerolphosphate synthase with impaired activity. *Plant Physiology***129**, 594–604.

50. Xu Y. &Siegenthaler P.A. (1997) Low Temperature Treatments Induce an Increase in the Relative Content of Both Linolenic and 3-Hexadecenoic Acids in Thylakoid Membrane Phosphatidylglycerol of Squash Cotyledons. *Plant and Cell Physiology***38**, 611–618.

51. Yu B. & Benning C. (2003) Anionic lipids are required for chloroplast structure and function in Arabidopsis. *The Plant Journal: for Cell and Molecular Biology***36**, 762–770.

52. Yu L., Zhou C., Fan J., Shanklin J. & Xu C. (2021) Mechanisms and functions of membrane lipid remodeling in plants. *The Plant Journal: for Cell and Molecular Biology*.

CHAPTER 4

CONCLUDING MARKS AND FUTURE DIRECTIONS

Donghee Hoh

As a growing world population in the face of global climate change, the demand for food is increased, requiring different strategies to alleviate global food insecurity under unpredicted environmental conditions. Natural variations in plants are strategies for the plants to improve in response to environmental stress, including gene drift, natural selection, adaptation of species to changing environments. Exploring natural variation is the way to study how plants adapt and evolve and it could be the avenue to improve photosynthesis. To explore natural variation, we adapted the concept of quantitative genomics, mapping QTL, which has predominantly been used by plant breeders to identify genetic markers for desirable traits, that can be used to introgress multiple desirable traits into elite production lines (Boukar, Fatokun, Huynh, Roberts & Close 2016). In the past, most QTL analyses used bulk or aggregate phenotypes, such as yield or disease symptoms and the lack of specificity in these phenotypes makes it difficult to assess the contributions from individual processes.

To investigate detailed mechanisms of a large number of plants from mapping population, we need high-throughput but detailed photosynthetic phenotyping tools. By taking advantage of the recent development of two photosynthetic phenotyping tools in Kramer Lab, which measure multiple phenotypes simultaneously, and are reproducible (Cruz *et al.* 2016; Kuhlgert*et al.* 2016), I was able to measure detailed photosynthetic responses over the population and map QTL successfully. In this dissertation, we suggest “comparative QTL linkage” approach, which allows us to assess linkages between processes, and thus test specific hypothetical models. By comparing the QTL profiles for the different processes or phenotypes that are interested in, we could define whether genetic diversity in one process is linked to that of another. By “linked” we

mean that it is either controlled by the same genetic loci or is mechanistically related so that one process influences the other.

I demonstrated the feasibility of this new approach in the previous chapters with enlightening mechanistic and genetic bases in response to chilling stress, which is one of the major constraints of photosynthesis, productivity, and geographical distribution of important cultivated crops (Allen & Ort 2001).

In chapter 2, we explored stress-induced photosynthetic responses of a range of related, rapidly measurable photosynthetic processes in a RIL population of cowpea lines. DEPI captures chlorophyll fluorescence images under dynamic environmental conditions without perturbing the plants, which gave us great insight not only efficiency and regulation of PSII but also leaf movements in response to stress-induced conditions. MultispeQ measurements by clamping of the individual leaves, enable us to measure much more detailed photosynthetic responses such as ATP synthase activity, *pmf*, relative CEF, redox states of PSI etc., Combining those two techniques in a natural population, we are able to test models suggested as primary chilling stress by comparing identified QTL intervals.

Under chilling (19^{o}C/13^{o}C day/night temperatures), we found well-defined, colocalized (overlapping) QTL intervals for a range of parameters reflecting the photosynthetic efficiency, photoprotection, photodamage and capture and feedback regulation by control of the thylakoid proton motive force, including with those for photosystem II (PSII) quantum efficiency (Φ_{II}), nonphotochemical quenching (NPQ) in both the qE and qI forms, the redox state of Q_A (q_L), the redox states of photosystem I (PSI), the activity of the thylakoid ATP synthase (*g*H+,) and the light-driven thylakoid

proton motive force (*pmf*) (Figure 2.6)

While we found linkages for the photosynthetic efficiency, photoprotection, photodamage and capture and feedback regulation by control of the thylakoid proton motive force, there are exceptions in ATP synthase activity (*g*H+, Figures 2.2.4E, 2.8C) and PSI overreduction (Y_{NA}). We did observe a general reduction on *g*H+ going from CT to LT (Figure S2.6E), the effect was not significantly different in the two parent lines, nor we did not observe strong linkages to genetic markers, suggesting that modulation of ATP synthase activity did not contribute to the differences in chilling sensitivities, under the RIL population and under our conditions.

The lack of effects on Y_{NA} are interesting in light of the proposal that PSI photodamage, related to over-reduction, is a major factor in chilling-induced photodamage damage in some species, notably *Cucumis sativus (Sonoike 1996)*, and in mutants that lack the ability to activate PCON (Tikkanen*et al.* 2012; Takagi, Takumi, Hashiguchi, Sejima& Miyake 2016; Kanazawa *et al.* 2017). Despite being quite chilling sensitive, we did not see any evidence for PSI over-reduction in cowpea. Instead, we observed strong PCON (Figure S2.6H) which resulted in net oxidation of P700 (Figure S2.6G), preventing the accumulation of electrons on PSI electron acceptors. Consistent with this result, we found no significant differences in the loss of active PSI at LT, as measured by the extent of maximal light-induced absorbance changes at 810 nm, between the two parent lines after either LT or CT exposure ($p>0.7$).

Another exception was NLM, which has been proposed that these may protect against chilling damage to photosynthesis in some species(Huang, Zhang & Cao 2012; Huang, Zhang, Zhang & Hu 2014). We also observed strong induction of NLM

specifically under LT (Figure S2.12C-D), but we did not observe obvious linkages to processes we measured, including long-term changes in NPQt (Figure 2.10B), arguing against strong impact, at least under our conditions. However, we did not observe obvious linkages to processes we measured, including long-term changes in NPQt (Figure. 2.10B), arguing against strong impact, at least under our conditions.

The follow-up biochemical/biophysical assays show that genetic variations impact low temperature tolerance by modulating: 1) redox states of Q_A; 2) the thylakoid *pmf*, through effects on cyclic electron flow; leading to differences in the rates of photodamage to PSII. These processes could be acted by modulating the recombination reactions within PSII that can lead to deleterious singlet O_2 production, which will be a further experiment.

Chapter 3 extends these studies by testing for linkages between photosynthetic processes and thylakoid lipid membrane components, including lipid class and fatty acid (FA) compositions, which have been proposed to be involved in photosynthetic responses to environmental stress. Under low temperature (LT) conditions (19°C/13°C, day/night), quantitative trait loci (QTL) intervals were observed for variations in compositions of specific lipid categories, the ratio of Digalactosyldiacylglycerol (DGDG) to Monogalactosyldiacylglycerol (MGDG), on Chr 9, which overlapped that of the photosynthetic parameter under LT (Figure 3.8). The DGDG/MGDG ratio showed higher average values in the tolerant allele group for the QTL on Chr 9 (Figure 3.8), consistent with a role in chilling responses. MGDG is a non-bilayer forming lipid and DGDG/MGDG ratio affects membrane stability, phase transition, the ability for proteins to insertion (Williams 2004; Shimojima&Ohta 2011). Lipid remodeling under freezing temperatures

is controlled by SENSITIVE TO FREEZING 2 (SFR2), a gene required for freezing tolerance, which acts by transferring galactosyl residues from monogalactolipid to different galactolipid acceptors, forming oligogalactolipids, diacylglycerol and triacylglycerol, leading to the membranes stabilization during freezing conditions (Moellering, Muthan& Benning 2010). Though *sfr2* has not yet been linked to lipid remodeling under chilling (non-freezing) stress, such a role would be consistent with our observation of potential linkages between DGDG/MGDG ratio and photosynthetic responses.

Further, we tested two main hypotheses, 1) the correlation with higher relative levels of unsaturated fatty acids and chilling tolerance, 2) the chilling sensitivity of HMP-PG.

We did not observe QTL intervals for FAs 18:3 of MGDG, DGDG, PG (Figures S3.10C, F and H), suggesting that genetic variations in these components are weak or not linked to specific genetic markers, arguing against roles for 18:3 FA species in controlling the observed genetic variations in photosynthetic responses in our cowpea RIL population. However, we identified QTL intervals for the molecule species of 18:2 FAs of MGDG, DGDG, PG on Chr 9 (Figures S3.10B, E and G), which showed association with photosynthetic parameters (Figure 3.8). Furthermore, compositions of those FAs are positively correlated with the tolerant line (Figure 3.8B), suggesting a potential linkage, as supported by the positive correlation between these FAs and the presence of alleles from the tolerant line in this interval (Figure 3.8B)

Another interesting finding was HMP-PG. HMP-PG is the sum of molecules that contains only PG16:0, PG 16:1t, and PG 18:0 FAs. We identified QTL intervals for PG

16:0, PG 18:0 and HMP-PG in Chr 7 (Figure 3.3), but these did not overlap those for photosynthetic parameters (Figure 3.4), arguing against the models where variations in HMP-PG confer altered chilling stress photosynthetic responses in our cowpea RIL population.

The most striking finding is the composition of the thylakoid-specific FA, PG16:1$^{\Delta 3trans}$ or PG 16:1t showed potential co-associations with the network of photosynthetic parameters observed in chapter 2. We observed the linkages among PG 16:1t and photosynthetic parameters (Φ_{II}, q_L, qIt) (Figures 3.4 A and B), suggesting this composition are genetically/ mechanistically co-linked with photosynthetic regulation under chilling stress.

We also recapitulated this result in a set of *Arabidopsis* FAD4 mutants, showing that PG 16:1t negatively correlated with photosynthetic efficiency by increasing photoinhibition (showing lower Φ_{II} and qL, higher NPQ, qE, qI) at low temperature (Figure 3.7). A recent study showed that PG 16:1t requires the activity of peroxiredoxin-Q, which is activated by H_2O_2 and known to be involved in redox signaling, there is a possibility that the accumulation of PG 16:1t occurs as a result of upstream lesions that result in ROS production and will be needed to further study. To sum, our findings indicate that specific FA and lipid species, rather than bulk unsaturation levels, appear to control photosynthetic responses to LT

Overall, this dissertation proposed a new approach, which is available to test (support or reject) hypothetical models that can be used to identify the mechanistic bases by using natural variations and demonstrated the feasibility of the approach with major findings. The results highlight some advantages of using natural genetic

variations to identify underlying mechanisms. Because classical genetics approaches introduce (typically deleterious) mutations that are not commonly found in natural populations, it can miss variations that have evolved to adapt to specific environments, and thus natural variation would be important for improving crop responses to changing environmental conditions.

More details for genetic bases to predict the candidate genes will be needed to study. Nonetheless, the genetic loci identified with marker information for photosynthetic regulations in response to environmental stress can be immediately used in breeding efforts to improve productivity responses to climate change. I anticipate that this dissertation would be a guiding tool for the improvement of robustness and resilience in plants.

BIBLIOGRAPHY

BIBLIOGRAPHY

1. Boukar O., Fatokun C.A., Huynh B.-L., Roberts P.A. & Close T.J. (2016) Genomic tools in cowpea breeding programs: status and perspectives. *Frontiers in plant science***7**, 757.

2. Cruz J.A., Savage L.J., Zegarac R., Hall C.C., Satoh-Cruz M., Davis G.A., … Kramer D.M. (2016) Dynamic environmental photosynthetic imaging reveals emergent phenotypes. *Cell Systems***2**, 365–377.

3. Huang W., Zhang J.-L., Zhang S.-B. & Hu H. (2014) Evidence for the regulation of leaf movement by photosystem II activity. *Environmental and experimental botany***107**, 167–172.

4. Huang W., Zhang S.-B. & Cao K.-F. (2012) Evidence for leaf fold to remedy the deficiency of physiological photoprotection for photosystem II. *Photosynthesis Research***110**, 185–191.

5. Kanazawa A., Ostendorf E., Kohzuma K., Hoh D., Strand D.D., Sato-Cruz M., … Kramer D.M. (2017) Chloroplast ATP synthase modulation of the thylakoid proton motive force: implications for photosystem I and photosystem II photoprotection. *Frontiers in plant science***8**, 719.

6. Kuhlgert S., Austic G., Zegarac R., Osei-Bonsu I., Hoh D., Chilvers M.I., … Kramer D.M. (2016) MultispeQ Beta: a tool for large-scale plant phenotyping connected to the open PhotosynQ network. *Royal Society Open Science***3**, 160592.

7. Moellering E.R., Muthan B. & Benning C. (2010) Freezing tolerance in plants requires lipid remodeling at the outer chloroplast membrane. *Science***330**, 226–228.

8. Shimojima M. &Ohta H. (2011) Critical regulation of galactolipid synthesis controls membrane differentiation and remodeling in distinct plant organs and following environmental changes. *Progress in lipid research***50**, 258–266.

9. Sonoike K. (1996) Photoinhibition of photosystem I: its physiological significance in the chilling sensitivity of plants. *Plant and Cell Physiology***37**, 239–247.

10. Takagi D., Takumi S., Hashiguchi M., Sejima T. & Miyake C. (2016) Superoxide and Singlet Oxygen Produced within the Thylakoid Membranes Both Cause Photosystem I Photoinhibition. *Plant Physiology***171**, 1626–1634.

11. Tikkanen M., Grieco M., Nurmi M., Rantala M., Suorsa M. &Aro E.-M. (2012) Regulation of the photosynthetic apparatus under fluctuating growth light. *Philosophical Transactions of the Royal Society of London. Series B, Biological Sciences***367**, 3486–3493.

12. Williams W.P. (2004) The physical properties of thylakoid membrane lipids and their relation to photosynthesis. In *Lipids in photosynthesis: structure, function and genetics*. (eds S. Paul-André & M. Norio), pp. 103–118. Kluwer Academic Publishers, Dordrecht.